# Contents

3.1 THE SPACE LATTICE AND UNIT CELLS

The physical structure of solid materials of engineering importance depends mainly on the arrangements of the atoms, ions, or molecules that make up the solid and the bonding forces between them. If the atoms or ions of a solid are arranged in a pattern that repeats itself in three dimensions, they form a solid that has *long-range order* (LRO) and is referred to as a *crystalline solid* or *crystalline material*. Examples of crystalline materials are metals, alloys, and some ceramic materials. In contrast to crystalline materials, there are some materials whose atoms and ions are not arranged in a long-range, periodic, and repeatable manner and possess only *short-range order* (SRO). This means that order exists only in the immediate neighborhood of an atom or a molecule. As an example, liquid water has short-range order in its molecules in which one oxygen atom is covalently bonded to two hydrogen atoms. But this order disappears, as each molecule is bonded to other molecules through weak secondary bonds in a random manner. Materials with only short-range order are classified as *amorphous* (without form) or noncrystalline. A more detailed definition and some examples of amorphous materials are given in Sec. 3.12.

Atomic arrangements in crystalline solids can be described by referring the atoms to the points of intersection of a network of lines in three dimensions. Such

Animation

Tutorial

86   **CHAPTER 3**   Crystal and Amorphous Structure in Materials

(a)   (b)
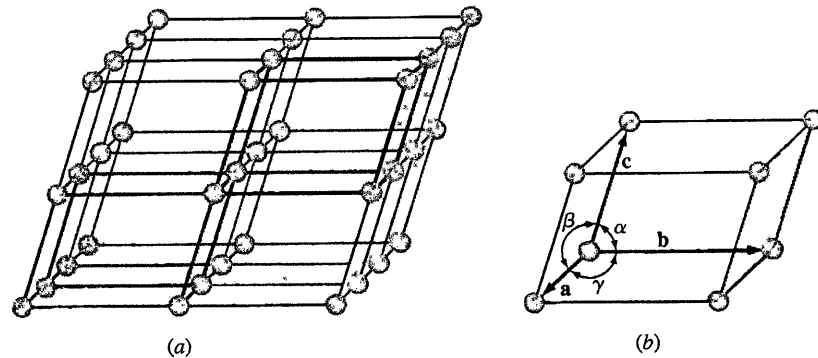
Figure 3.1
(a) Space lattice of ideal crystalline solid. (b) Unit cell showing lattice constants.

a network is called a **space lattice** (Fig. 3.1a), and it can be described as an infinite three-dimensional array of points. Each point in the space lattice has identical surroundings. In an ideal **crystal,** the grouping of **lattice points** about any given point are identical with the grouping about any other lattice point in the crystal lattice. Each space lattice can thus be described by specifying the atom positions in a repeating **unit cell,** such as the one heavily outlined in Fig. 3.1a. The unit cell may be considered the smallest subdivision of the lattice that maintains the characteristics of the overall crystal. A group of atoms organized in a certain arrangement relative to each other and associated with lattice points constitues the **motif** or basis. The crystal structure may then be defined as the collection of lattice and basis. It is important to note that atoms do not necessarily coincide with lattice points. The size and shape of the unit cell can be described by three lattice vectors **a, b,** and **c,** originating from one corner of the unit cell (Fig. 3.1b). The axial lengths a, b, and c and the interaxial angles α, β, and γ are the *lattice constants* of the unit cell.

CHAPTER 3 Crystal and Amorphous Structure in Materials

3.2 CRYSTAL SYSTEMS AND BRAVAIS LATTICES

Tutorial

By assigning specific values for axial lengths and interaxial angles, unit cells of different types can be constructed. Crystallographers have shown that only seven different types of unit cells are necessary to create all space lattices. These crystal systems are listed in Table 3.1.

Many of the seven crystal systems have variations of the basic unit cell. A.J. Bravais[1] showed that 14 standard unit cells could describe all possible lattice networks. These Bravais lattices are illustrated in Fig. 3.2. There are four basic types of unit cells: (1) simple, (2) body-centered, (3) face-centered, and (4) base-centered.

---

[1]August Bravais (1811–1863). French crystallographer who derived the 14 possible arrangements of points in space.

Table 3.1 Classification of space lattices by crystal system

MatVis

Crystal system	Axial lengths and interaxial angles	Space lattice
Cubic	Three equal axes at right angles $a = b = c, \alpha = \beta = \gamma = 90°$	Simple cubic Body-centered cubic Face-centered cubic
Tetragonal	Three axes at right angles, two equal $a = b \neq c, \alpha = \beta = \gamma = 90°$	Simple tetragonal Body-centered tetragonal
Orthorhombic	Three unequal axes at right angles $a \neq b \neq c, \alpha = \beta = \gamma = 90°$	Simple orthorhombic Body-centered orthorhombic Base-centered orthorhombic Face-centered orthorhombic
Rhombohedral	Three equal axes, equally inclined $a = b = c, \alpha = \beta = \gamma \neq 90°$	Simple rhombohedral
Hexagonal	Two equal axes at 120°, third axis at right angles $a = b \neq c, \alpha = \beta = 90°, \gamma = 120°$	Simple hexagonal
Monoclinic	Three unequal axes, one pair not at right angles $a \neq b \neq c, \alpha = \gamma = 90° \neq \beta$	Simple monoclinic Base-centered monoclinic
Triclinic	Three unequal axes, unequally inclined and none at right angles $a \neq b \neq c, \alpha \neq \beta \neq \gamma \neq 90°$	Simple triclinic

In the cubic system there are three types of unit cells: simple cubic, body-centered cubic, and face-centered cubic. In the orthorhombic system all four types are represented. In the tetragonal system there are only two: simple and body-centered. The face-centered tetragonal unit cell appears to be missing but can be constructed from four body-centered tetragonal unit cells. The monoclinic system has simple and base-centered unit cells, and the rhombohedral, hexagonal, and triclinic systems have only one simple type of unit cell.

3.3 PRINCIPAL METALLIC CRYSTAL STRUCTURES

In this chapter, the principal crystal structures of elemental metals will be discussed in detail. In Chap. 11, the principal ionic and covalent crystal structures that occur in ceramic materials will be treated.

Most elemental metals (about 90 percent) crystallize upon solidification into three densely packed crystal structures: **body-centered cubic (BCC)** (Fig. 3.3a), **face-centered cubic (FCC)** (Fig. 3.3b), and **hexagonal close-packed (HCP)** (Fig. 3.3c). The HCP structure is a denser modification of the simple hexagonal crystal structure shown in Fig. 3.2. Most metals crystallize in these dense-packed structures because energy is released as the atoms come closer together and bond more tightly with each other. Thus, the densely packed structures are in lower and more stable energy arrangements.

Tetragonal

Rhombohedral

Monoclinic

Cubic

Hexagonal*

Orthorhombic

Triclinic
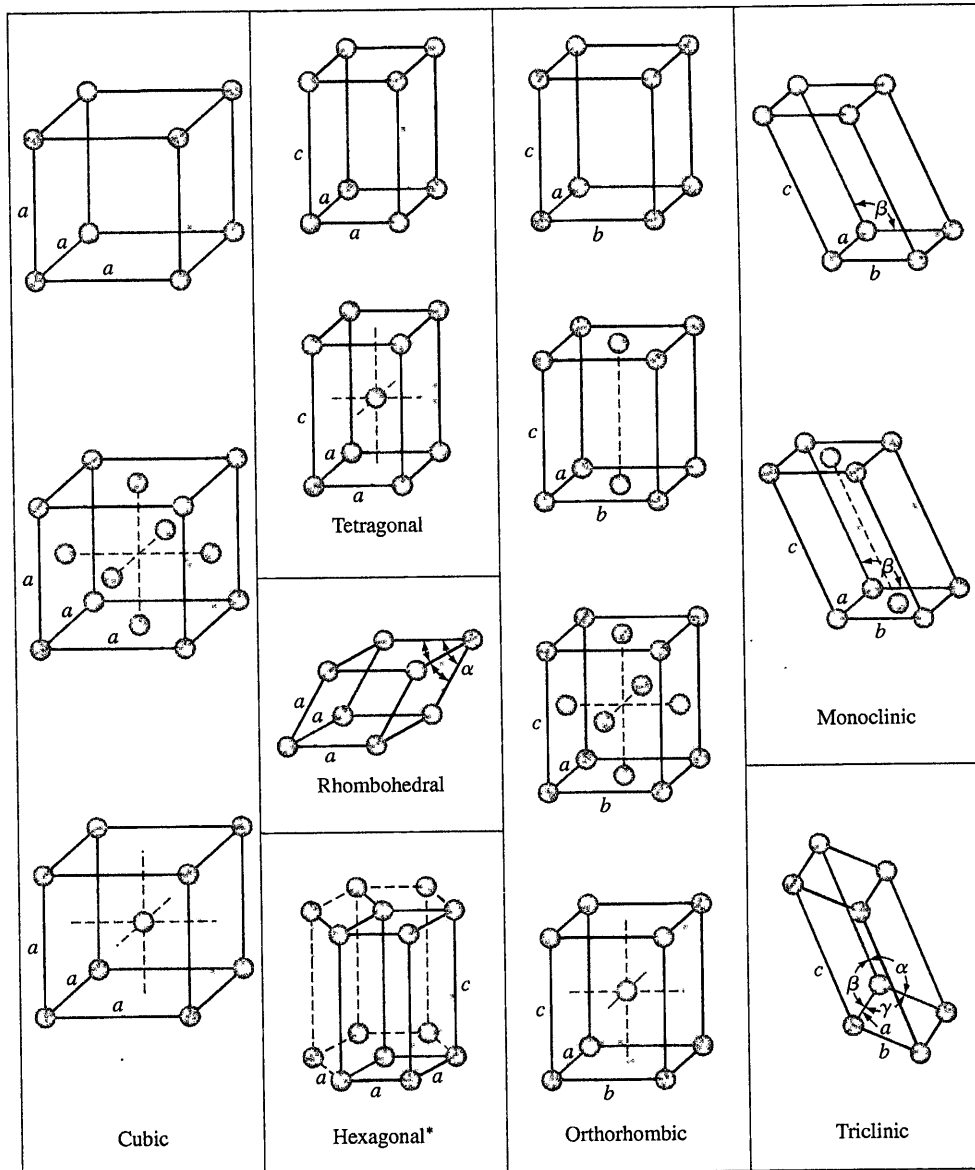
Figure 3.2

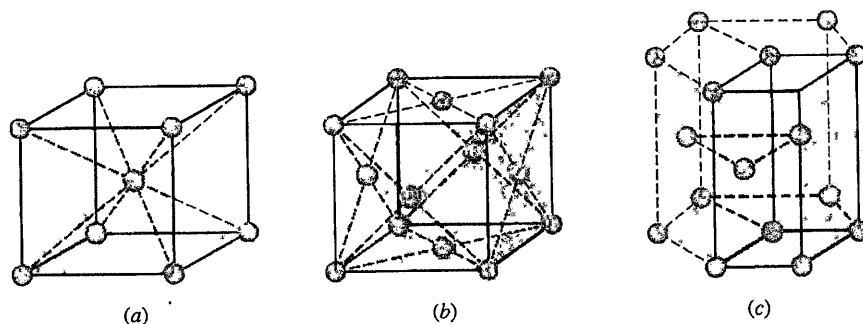The 14 Bravais conventional unit cells grouped according to crystal system. The dots indicate lattice points that, when located on faces or at corners, are shared by other identical lattice unit cells.

(From W.G. Moffatt, G.W. Pearsall, and J.Wulff, The Structure and Properties of Materials, vol. 1: "Structure", Wiley, 1964, p. 47.)

*The unit cell is represented by solid lines.

Tutorial
Animation
MatVis

Figure 3.3
Principal metal crystal structure and unit cells: (*a*) body-centered cubic,
(*b*) face-centered cubic, (*c*) hexagonal close-packed crystal structure (the unit
cell is shown by solid lines).

The extremely small size of the unit cells of crystalline metals that are shown in Fig. 3.3 should be emphasized. The cube side of the unit cell of body-centered cubic iron, for example, at room temperature is equal to 0.287×10^{-9} m, or 0.287 nanometer (nm).[2] Therefore, if unit cells of pure iron are lined up side by side, in 1 mm there will be

$$1 \text{ mm} \times \frac{1 \text{ unit cell}}{0.287 \text{ nm} \times 10^{-6} \text{ mm/nm}} = 3.48 \times 10^{6} \text{ unit cells!}$$

Let us now examine in detail the arrangement of the atoms in the three principal crystal structure unit cells. Although an approximation, we shall consider atoms in these crystal structures to be hard spheres. The distance between the atoms (interatomic distance) in crystal structures can be determined experimentally by X-ray diffraction analysis.[3] For example, the interatomic distance between two aluminum atoms in a piece of pure aluminum at 20°C is 0.2862 nm. The radius of the aluminum atom in the aluminum metal is assumed to be half the interatomic distance, or 0.143 nm. The atomic radii of selected metals are listed in Tables 3.2 to 3.4.

3.3.1 Body-Centered Cubic (BCC) Crystal Structure

First, consider the atomic-site unit cell for the BCC crystal structure shown in Fig. 3.4*a*. In this unit cell, the solid spheres represent the centers where atoms are located and clearly indicate their relative positions. If we represent the atoms in this cell as hard spheres, then the unit cell appears as shown in Fig. 3.4*b*. In this unit cell, we see that the central atom is surrounded by eight nearest neighbors and is said to have a coordination number of 8.

Animation
Tutorial

---

[2]1 nanometer = 10^{-9} meter.

[3]Some of the principles of X-ray diffraction analysis will be studied in Sec. 3.11.

90   **CHAPTER 3**   Crystal and Amorphous Structure in Materials

Table 3.2 Selected metals that have the BCC crystal structure at room temperature (20°C) and their lattice constants and atomic radii

Metal	Lattice constant a (nm)	Atomic radius $R*$ (nm)
Chromium	0.289	0.125
Iron	0.287	0.124
Molybdenum	0.315	0.136
Potassium	0.533	0.231
Sodium	0.429	0.186
Tantalum	0.330	0.143
Tungsten	0.316	0.137
Vanadium	0.304	0.132

*Calculated from lattice constants by using Eq. (3.1), $R = \sqrt{3}a/4$.

Tutorial

Table 3.3 Selected metals that have the FCC crystal structure at room temperature (20°C) and their lattice constants and atomic radii

Metal	Lattice constant a (nm)	Atomic radius $R*$ (nm)
Aluminum	0.405	0.143
Copper	0.3615	0.128
Gold	0.408	0.144
Lead	0.495	0.175
Nickel	0.352	0.125
Platinum	0.393	0.139
Silver	0.409	0.144

*Calculated from lattice constants by using Eq. (3.3), $R = \sqrt{2}a/4$.

Table 3.4 Selected metals that have the HCP crystal structure at room temperature (20°C) and their lattice constants, atomic radii, and c/a ratios

Metal	Lattice constants (nm) a	c	Atomic radius R (nm)	c/a ratio	% deviation from ideality
Cadmium	0.2973	0.5618	0.149	1.890	+15.7
Zinc	0.2665	0.4947	0.133	1.856	+13.6
Ideal HCP				1.633	0
Magnesium	0.3209	0.5209	0.160	1.623	−0.66
Cobalt	0.2507	0.4069	0.125	1.623	−0.66
Zirconium	0.3231	0.5148	0.160	1.593	−2.45
Titanium	0.2950	0.4683	0.147	1.587	−2.81
Beryllium	0.2286	0.3584	0.113	1.568	−3.98

If we isolate a single hard-sphere unit cell, we obtain the model shown in Fig. 3.4c. Each of these cells has the equivalent of two atoms per unit cell. One complete atom is located at the center of the unit cell, and an eighth of a sphere is located at each corner of the cell, making the equivalent of another atom. Thus, there is a total of 1 (at the center) + 8 × $\frac{1}{8}$ (at the corners) = 2 atoms per unit cell. The atoms in the BCC unit cell contact each other across the cube diagonal, as indicated in
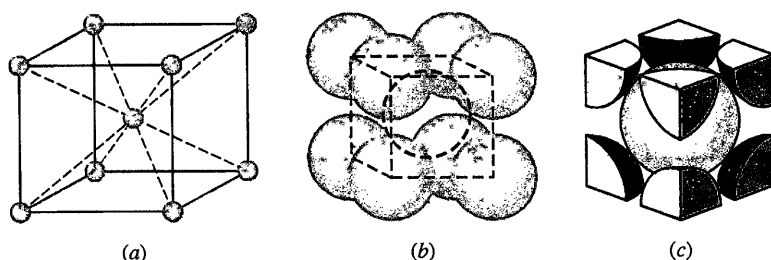
Figure 3.4
BCC unit cells: (*a*) atomic-site unit cell, (*b*) hard-sphere unit cell, and (*c*) isolated unit cell.
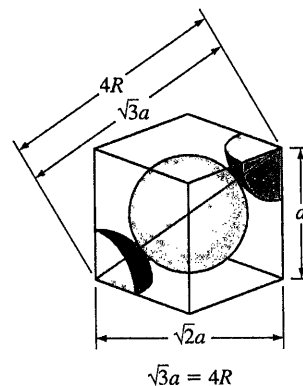
Figure 3.5
BCC unit cell showing relationship between the lattice constant *a* and the atomic radius *R*.

Tutorial

Animation

MatVis

Fig. 3.5, so that the relationship between the length of the cube side *a* and the atomic radius *R* is

$$\sqrt{3}a = 4R \quad \text{or} \quad a = \frac{4R}{\sqrt{3}} \tag{3.1}$$

Iron at 20°C is BCC with atoms of atomic radius 0.124 nm. Calculate the lattice constant *a* for the cube edge of the iron unit cell.

EXAMPLE PROBLEM 3.1

■ **Solution**

From Fig. 3.5 it is seen that the atoms in the BCC unit cell touch across the cube diagonals. Thus, if *a* is the length of the cube edge, then

$$\sqrt{3}a = 4R \tag{3.1}$$

where *R* is the radius of the iron atom. Therefore

$$a = \frac{4R}{\sqrt{3}} = \frac{4(0.124 \text{ nm})}{\sqrt{3}} = 0.2864 \text{ nm} \blacktriangleleft$$

If the atoms in the BCC unit cell are considered to be spherical, an **atomic packing factor** (APF) can be calculated by using the equation

$$\text{APF} = \frac{\text{volume of atoms in unit cell}}{\text{volume of unit cell}} \tag{3.2}$$

92 **CHAPTER 3** Crystal and Amorphous Structure in Materials

Using this equation, the APF for the BCC unit cell (Fig. 3.4c) is calculated to be 68 percent (see Example Problem 3.2). That is, 68 percent of the volume of the BCC unit cell is occupied by atoms and the remaining 32 percent is empty space. The BCC crystal structure is (not a close-packed structure) since the atoms could be packed closer together. Many metals such as iron, chromium, tungsten, molybdenum, and vanadium have the BCC crystal structure at room temperature. Table 3.2 lists the lattice constants and atomic radii of selected BCC metals.

EXAMPLE PROBLEM 3.2	Calculate the atomic packing factor (APF) for the BCC unit cell, assuming the atoms to be hard spheres.

■ **Solution**

$$APF = \frac{\text{volume of atoms in BCC unit cell}}{\text{volume of BCC unit cell}} \qquad (3.2)$$

Tutorial

Since there are two atoms per BCC unit cell, the volume of atoms in the unit cell of radius R is

$$V_{atoms} = (2)(\tfrac{4}{3}\pi R^3) = 8.373R^3$$

The volume of the BCC unit cell is

$$V_{unit\ cell} = a^3$$

where a is the lattice constant. The relationship between a and R is obtained from Fig. 3.5, which shows that the atoms in the BCC unit cell touch each other across the cubic diagonal. Thus

$$\sqrt{3}a = 4R \quad \text{or} \quad a = \frac{4R}{\sqrt{3}} \qquad (3.1)$$

Thus,

$$V_{unit\ cell} = a^3 = 12.32R^3$$

The atomic packing factor for the BCC unit cell is, therefore,

$$APF = \frac{V_{atoms}/\text{unit cell}}{V_{unit\ cell}} = \frac{8.373R^3}{12.32R^3} = 0.68 \blacktriangleleft$$

3.3.2 Face-Centered Cubic (FCC) Crystal Structure

Consider next the FCC lattice-point unit cell of Fig. 3.6a. In this unit cell, there is one lattice point at each corner of the cube and one at the center of each cube face. The hard-sphere model of Fig. 3.6b indicates that the atoms in the FCC crystal structure are packed as close together as possible. The APF for this close-packed structure is 0.74 as compared to 0.68 for the BCC structure, which is not close-packed.

The FCC unit cell as shown in Fig. 3.6c has the equivalent of four atoms per unit cell. The eight corner octants account for one atom ($8 \times \tfrac{1}{8} = 1$), and the six
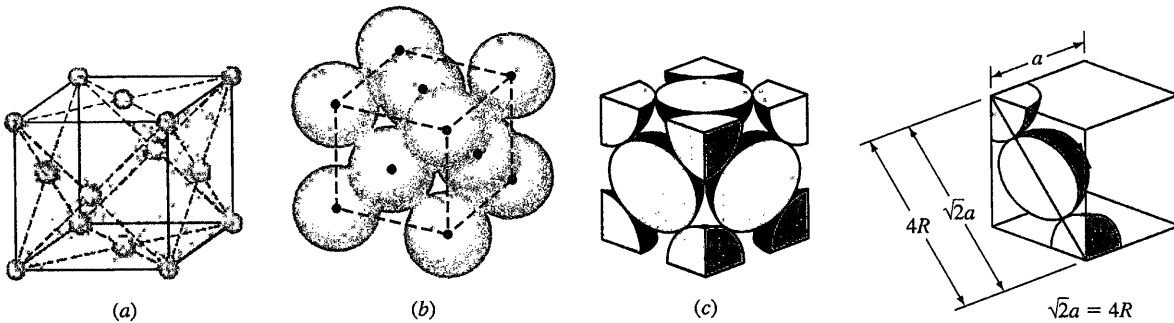
Figure 3.6
FCC unit cells: (a) atomic-site unit cell, (b) hard-sphere unit cell, and (c) isolated unit cell.
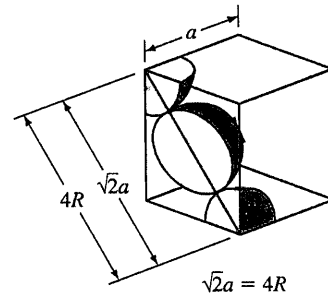

Figure 3.7
FCC unit cell showing relationship between the lattice constant a and atomic radius R. Since the atoms touch across the face diagonals, $\sqrt{2}a = 4R$.

Tutorial
Animation
MatVis

half-atoms on the cube faces contribute another three atoms, making a total of four atoms per unit cell. The atoms in the FCC unit cell contact each other across the cubic face diagonal, as indicated in Fig. 3.7, so that the relationship between the length of the cube side a and the atomic radius R is

$$\sqrt{2}a = 4R \quad \text{or} \quad a = \frac{4R}{\sqrt{2}} \qquad (3.3)$$

The APF for the FCC crystal structure is 0.74, which is greater than the 0.68 factor for the BCC structure. The APF of 0.74 is for the closest packing possible of "spherical atoms." Many metals such as aluminum, copper, lead, nickel, and iron at elevated temperatures (912°C to 1394°C crystallize with the FCC crystal structure. Table 3.3 lists the lattice constants and atomic radii for some selected FCC metals.

3.3.3 Hexagonal Close-Packed (HCP) Crystal Structure

The third common metallic crystal structure is the HCP structure shown in Fig. 3.8a and b. Metals do not crystallize into the simple hexagonal crystal structure shown in Fig. 3.2 because the APF is too low. The atoms can attain a lower energy and a more stable condition by forming the HCP structure of Fig. 3.8b. The APF of the HCP crystal structure is 0.74, the same as that for the FCC crystal structure since in both structures the atoms are packed as tightly as possible. In both the HCP and FCC crystal structures, each atom is surrounded by 12 other atoms, and thus both structures have a coordination number of 12. The differences in the atomic packing in FCC and HCP crystal structures will be discussed in Sec. 3.8.

The isolated HCP unit cell, also called the *primitive cell*, is shown in Fig. 3.8c. The atoms at locations marked "1" on Fig. 3.8c contribute $\frac{1}{6}$ of an atom to the unit cell. The atoms at locations marked "2" contribute $\frac{1}{12}$ of an atom to the unit cell.

(a)   (b)   (c)
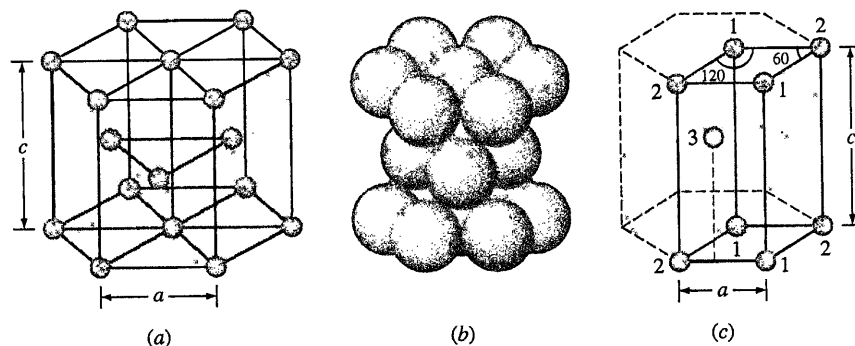
Figure 3.8
HCP crystal structure: (a) schematic of the crystal structure, (b) hard-sphere
model, and (c) isolated unit cell schematic.

Tutorial   *(From F.M. Miller, Chemistry: Structure and Dynamics, McGraw-Hill, 1984, p. 296.*

MatVis   *Reproduced with permission of The McGraw-Hill Companies.)*

Thus, the atoms at the eight corners of the unit cell collectively contribute one atom $(4(\frac{1}{6}) + 4(\frac{1}{12}) = 1)$. The atom at location "3" is centered inside the unit cell but extends slightly beyond the boundary of the cell. The total number of atoms inside an HCP unit cell is therefore 2 (1 at corners and 1 at center). In some text books the HCP unit cell is represented by Fig. 3.8a and is called the "larger cell." In such a case one finds 6 atoms per unit cell. This is mostly for convenience and the true unit cell is presented in Fig. 3.8c by the solid lines. When presenting the topics of crystal directions and planes we will also use the larger cell for convenience, in addition to the primitive cell.

The ratio of the height c of the hexagonal prism of the HCP crystal structure to its basal side a is called the c/a ratio (Fig. 3.8a). The c/a ratio for an ideal HCP crystal structure consisting of uniform spheres packed as tightly together as possible is 1.633. Table 3.4 lists some important HCP metals and their c/a ratios. Of the metals listed, cadmium and zinc have c/a ratios higher than ideality, which indicates that the atoms in these structures are slightly elongated along the c axis of the HCP unit cell. The metals magnesium, cobalt, zirconium, titanium, and beryllium have c/a ratios less than the ideal ratio. Therefore, in these metals the atoms are slightly compressed in the direction along the c axis. Thus, for the HCP metals listed in Table 3.4, there is a certain amount of deviation from the ideal hard-sphere model.

EXAMPLE   a. Calculate the volume of the zinc crystal structure unit cell by using the following
PROBLEM 3.3   data: pure zinc has the HCP crystal structure with lattice constants $a = 0.2665$ nm
                        and $c = 0.4947$ nm.
                    b. Find the volume of the larger cell.

■ Solution

The volume of the zinc HCP unit cell can be obtained by determining the area of the base of the unit cell and then multiplying this by its height (Fig. EP3.3).

a. The area of the base of the unit cell is area $ABDC$ of Fig. EP3.3a and b. This total area consists of the areas of six equilateral triangles of area ABC of Fig. EP3.3b. From Fig. EP3.3c,

$$\text{Area of triangle } ABC = \tfrac{1}{2}(\text{base})(\text{height})$$
$$= \tfrac{1}{2}(a)(a \sin 60°) = \tfrac{1}{2}a^2 \sin 60°$$

From Fig. EP3.3b,

$$\text{Total area of HCP base, area } ABDC = (2)(\tfrac{1}{2}a^2 \sin 60°)$$
$$= a^2 \sin 60°$$

From Fig. EP3.3a,

$$\text{Volume of zinc HCP unit cell} = (a^2 \sin 60°)(c)$$
$$= (0.2665 \text{ nm})^2(0.8660)(0.4947 \text{ nm})$$
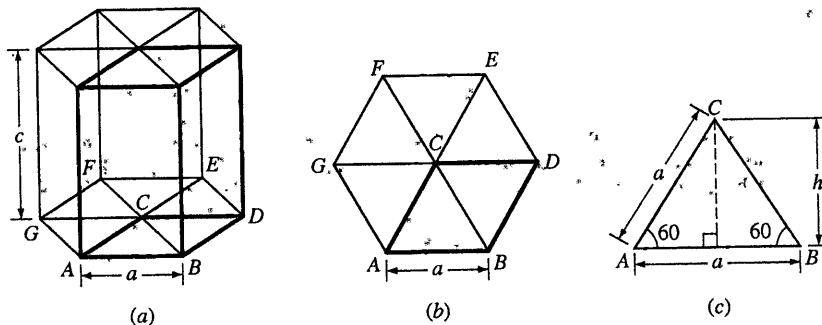$$= 0.0304 \text{ nm}^3 \blacktriangleleft$$

Figure EP3.3
Diagrams for calculating the volume of an HCP unit cell. (a) HCP unit cell.
(b) Base of HCP unit cell. (c) Triangle ABC removed from base of unit cell.

b. From Fig. EP3.3a,

$$\text{Volume of the "large" zinc HCP cell} = 3(\text{volume of the unit cell or primitive cell})$$
$$= 3(0.0304) = 0.0913 \text{ nm}^3$$

3.8 COMPARISON OF FCC, HCP, AND BCC CRYSTAL STRUCTURES

3.8.1 FCC and HCP Crystal Structures

As previously pointed out, both the HCP and FCC crystal structures are close-packed structures. That is, their atoms, which are considered approximate "spheres," are packed together as closely as possible so that an atomic packing factor of 0.74 is attained.[6] The (111) planes of the FCC crystal structure shown in Fig. 3.17a have the identical packing arrangement as the (0001) planes of the HCP crystal structure shown in Fig. 3.17b. However, the three-dimensional FCC and HCP crystal structures are not identical because there is a difference in the stacking arrangement of their atomic planes, which can best be described by considering the stacking of hard spheres representing atoms. As a useful analogy, one can imagine the stacking of planes of equal-sized marbles on top of each other, minimizing the space between the marbles.

Consider first a plane of close-packed atoms designated the *A* plane, as shown in Fig. 3.18. Note that there are two different types of empty spaces or voids between

---

[6]As pointed out in Sec. 3.3, the atoms in the HCP structure deviate to varying degrees from ideality. In some HCP metals, the atoms are elongated along the *c* axis, and in other cases, they are compressed along the *c* axis (see Table 3.4).
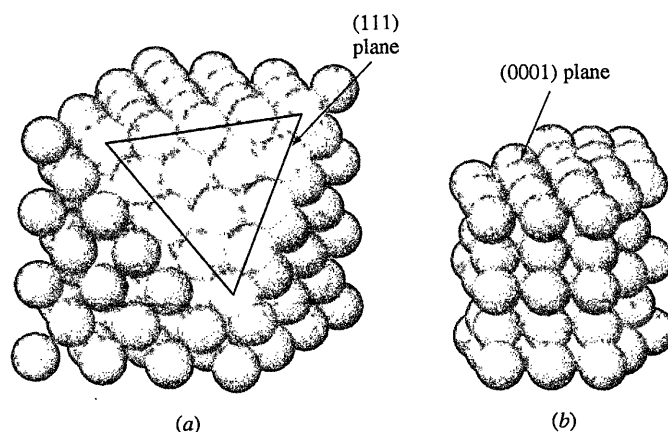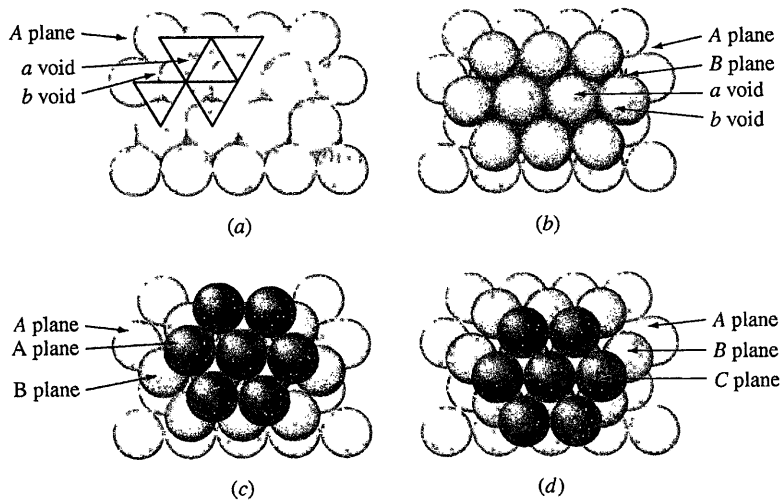

(a)   (b)

Figure 3.17
Comparison of the (*a*) FCC crystal structure showing a close-packed (111) plane and (*b*) a HCP crystal structure showing the close-packed (0001) plane.
(From W.G. Moffatt, G.W. Pearsall, and J. Wulff, The Structure and Properties of Materials, vol. 1: "Structure", Wiley, 1964, p. 51.)

(a)   (b)

(c)   (d)

Animation

Figure 3.18
Formation of the HCP and FCC crystal structures by the stacking
of atomic planes. (a) A plane showing the a and b voids. (b) B plane
placed in a voids of plane A. (c) Third plane placed in b voids of
B plane, making another A plane and forming the HCP crystal
structure. (d) Third plane placed in the a voids of B plane, making
a new C plane and forming the FCC crystal structure.
(*Ander, P.; Sonnessa, A.J., Principles of Chemistry, 1st ed., © 1965, Reprinted by
permission of Pearson Education, Inc., Upper Saddle River, NJ.*)

the atoms. The voids pointing to the top of the page are designated a voids and those
pointing to the bottom of the page, b voids. A second plane of atoms can be placed
over the a or b voids, and the same three-dimensional structure will be produced.
Let us place plane B over the a voids, as shown in Fig. 3.18b. Now if a third plane
of atoms is placed over plane B to form a closest-packed structure, it is possible to
form two different close-packed structures. One possibility is to place the atoms of
the third plane in the b voids of the B plane. Then the atoms of this third plane will
lie directly over those of the A plane and thus can be designated another A plane
(Fig. 3.18c). If subsequent planes of atoms are placed in this same alternating stack-
ing arrangement, then the stacking sequence of the three-dimensional structure pro-
duced can be denoted by ABABAB . . . Such a stacking sequence leads to the HCP
crystal structure (Fig. 3.17b).

The second possibility for forming a simple close-packed structure is to
place the third plane in the a voids of plane B (Fig. 3.18d). This third plane is
designated the C plane since its atoms do not lie directly above those of the
B plane or the A plane. The stacking sequence in this close-packed structure
is thus designated ABCABCABC . . . and leads to the FCC structure shown in
Fig. 3.17a.
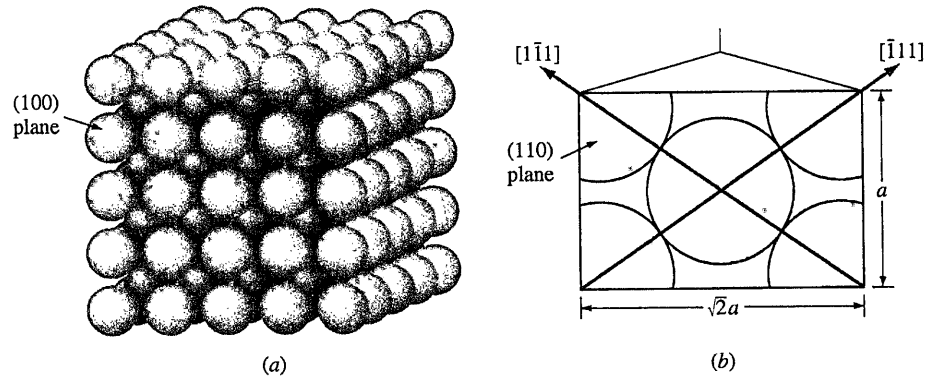
Figure 3.19
BCC crystal structure showing (a) the (100) plane and (b) a section of the (110) plane. Note that this is not a close-packed structure but that the diagonals have close-packed directions.
(*From W.G. Moffatt, G.W. Pearsall, and J. Wulff, The Structure and Properties of Materials, vol. 1: "Structure", Wiley, 1964, p. 51.*)

3.8.2 BCC Crystal Structure

The BCC structure is not a close-packed structure and hence does not have close-packed planes like the {111} planes in the FCC structure and the {0001} planes in the HCP structure. The most densely packed planes in the BCC structure are the {110} family of planes of which the (110) plane is shown in Fig. 3.19b. However, the atoms in the BCC structure do have close-packed directions along the cube diagonals, which are the ⟨111⟩ directions.

3.9 VOLUME, PLANAR, AND LINEAR DENSITY UNIT-CELL CALCULATIONS

3.9.1 Volume Density

Using the hard-sphere atomic model for the crystal structure unit cell of a metal and a value for the atomic radius of the metal obtained from X-ray diffraction analysis, a value for the **volume density** of a metal can be obtained by using the equation

$$\text{Volume density of metal} = \rho_v = \frac{\text{mass/unit cell}}{\text{volume/unit cell}} \tag{3.5}$$

In Example Problem 3.11 a value of 8.98 Mg/m^3 (8.98 g/cm^3) is obtained for the density of copper. The handbook experimental value for the density of copper is 8.96 Mg/m^3 (8.96 g/cm^3). The slightly lower density of the experimental value could be attributed to the absence of atoms at some atomic sites (vacancies), line defects,

and mismatch where grains meet (grain boundaries). These crystalline defects are discussed in Chap. 4. Another cause of the discrepancy could also be due to the atoms not being perfect spheres.

Copper has an FCC crystal structure and an atomic radius of 0.1278 nm. Assuming the atoms to be hard spheres that touch each other along the face diagonals of the FCC unit cell as shown in Fig. 3.7, calculate a theoretical value for the density of copper in mega-grams per cubic meter. The atomic mass of copper is 63.54 g/mol.

EXAMPLE PROBLEM 3.11

■ Solution

For the FCC unit cell, $1\,\overline{2}a = 4R$, where a is the lattice constant of the unit cell and R is the atomic radius of the copper atom. Thus,

$$a = \frac{4R}{\sqrt{2}} = \frac{(4)(0.1278 \text{ nm})}{\sqrt{2}} = 0.361 \text{ nm}$$

$$\text{Volume density of copper} = \rho_v = \frac{\text{mass/unit cell}}{\text{volume/unit cell}} \tag{3.5}$$

In the FCC unit cell, there are four atoms/unit cell. Each copper atom has a mass of $(63.54 \text{ g/mol})/(6.02 \times 10^{23} \text{ atoms/mol})$. Thus, the mass m of Cu atoms in the FCC unit cell is

$$m = \frac{(4 \text{ atoms})(63.54 \text{ g/mol})}{6.02 \times 10^{23} \text{ atoms/mol}} \left(\frac{10^{-6} \text{ Mg}}{g} \right) = 4.22 \times 10^{-28} \text{ Mg}$$

The volume V of the Cu unit cell is

$$V = a^3 = \left(0.361 \text{ nm} \times \frac{10^{-9} \text{ m}}{\text{nm}} \right)^3 = 4.70 \times 10^{-29} \text{ m}^3$$

Thus, the density of copper is

$$\rho_v = \frac{m}{V} = \frac{4.22 \times 10^{-28} \text{ Mg}}{4.70 \times 10^{-29} \text{ m}^3} = 8.98 \text{ Mg/m}^3 \quad (8.98 \text{ g/cm}^3) \blacktriangleleft$$

3.9.2 Planar Atomic Density

Sometimes it is important to determine the atomic densities on various crystal planes. To do this a quantity called the **planar atomic density** is calculated by using the relationship

$$\text{Planar atomic density} = \rho_p = \frac{\text{equiv. no. of atoms whose centers are intersected by selected area}}{\text{selected area}} \tag{3.6}$$

For convenience the area of a plane that intersects a unit cell is usually used in these calculations, as shown, for example, in Fig. 3.20 for the (110) plane in a BCC unit
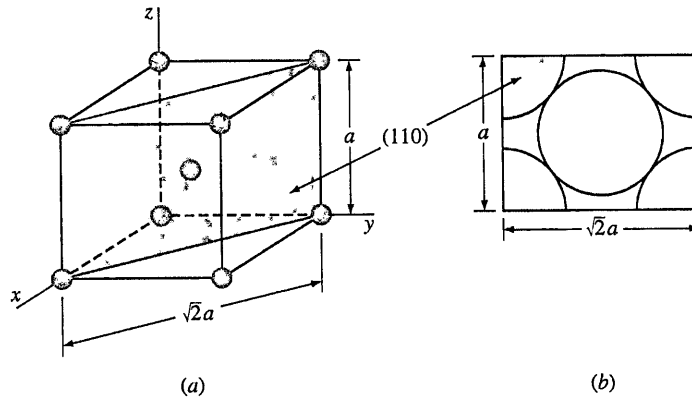
Figure 3.20
(a) A BCC atomic-site unit cell showing a shaded (110) plane.
(b) Areas of atoms in BCC unit cell cut by the (110) plane.

cell. In order for an atom area to be counted in this calculation, the plane of interest must intersect the center of an atom) In Example Problem 3.12 the (110) plane intersects the centers of five atoms, but the equivalent of only two atoms is counted since only one-quarter of each of the four corner atoms is included in the area inside the unit cell.

EXAMPLE PROBLEM 3.12

Calculate the planar atomic density ρ_p on the (110) plane of the α iron BCC lattice in atoms per square millimeter. The lattice constant of α iron is 0.287 nm.

■ **Solution**

$$\rho_p = \frac{\text{equiv. no. of atoms whose centers are intersected by selected area}}{\text{selected area}} \tag{3.6}$$

The equivalent number of atoms intersected by the (110) plane in terms of the surface area inside the BCC unit cell is shown in Fig. 3.22 and is

1 atom at center $+ 4 \times \frac{1}{4}$ atoms at four corners of plane $= 2$ atoms

The area intersected by the (110) plane inside the unit cell (selected area) is

$$(\sqrt{2}a)(a) = \sqrt{2}a^2$$

Thus, the planar atomic density is

$$\rho_p = \frac{2 \text{ atoms}}{\sqrt{2}(0.287 \text{ nm})^2} = \frac{17.2 \text{ atoms}}{\text{nm}^2}$$

$$= \frac{17.2 \text{ atoms}}{\text{nm}^2} \times \frac{10^{12} \text{ nm}^2}{\text{mm}^2}$$

$$= 1.72 \times 10^{13} \text{ atoms/mm}^2 \blacktriangleleft$$

3.9.3 Linear Atomic Density

Sometimes it is important to determine the atomic densities in various directions in crystal structures. To do this a quantity called the **linear atomic density** is calculated by using the relationship

$$\text{Linear atomic density} = \rho_l = \frac{\frac{\text{no. of atomic diam. intersected by selected}}{\text{length of line in direction of interest}}}{\text{selected length of line}}$$

$$(3.7)$$

Example Problem 3.13 shows how the linear atomic density can be calculated in the [110] direction in a pure copper crystal lattice.

Calculate the linear atomic density ρ_l in the [110] direction in the copper crystal lattice in atoms per millimeter. Copper is FCC and has a lattice constant of 0.361 nm.

EXAMPLE PROBLEM 3.13

■ Solution
The atoms whose centers the [110] direction intersects are shown in Fig. EP3.13. We shall select the length of the line to be the length of the face diagonal of the FCC unit cell, which is $\sqrt{2}a$. The number of atomic diameters intersected by this length of line are $\frac{1}{2} + 1 + \frac{1}{2} = 2$ atoms. Thus using Eq. 3.7, the linear atomic density is

$$\rho_l = \frac{2 \text{ atoms}}{\sqrt{2}a} = \frac{2 \text{ atoms}}{\sqrt{2}(0.361 \text{ nm})} = \frac{3.92 \text{ atoms}}{\text{nm}}$$

$$= \frac{3.92 \text{ atoms}}{\text{nm}} \times \frac{10^6 \text{ nm}}{\text{mm}}$$

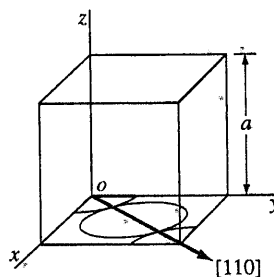$$= 3.92 \times 10^6 \text{ atoms/mm} \blacktriangleleft$$

Figure EP3.13
Diagram for calculating the atomic linear density in the [110] direction in an FCC unit cell.

3.10 POLYMORPHISM OR ALLOTROPY

Many elements and compounds exist in more than one crystalline form under different conditions of temperature and pressure. This phenomenon is termed **polymorphism,** or *allotropy*. Many industrially important metals such as iron, titanium, and cobalt undergo allotropic transformations at elevated temperatures at atmospheric pressure. Table 3.5 lists some selected metals that show allotropic transformations and the structure changes that occur.

Iron exists in both BCC and FCC crystal structures over the temperature range from room temperature to its melting point at 1539°C as shown in Fig. 3.21. Alpha (α) iron exists from −273°C to 912°C and has the BCC crystal structure. Gamma (γ)

Table 3.5 Allotropic crystalline forms of some metals

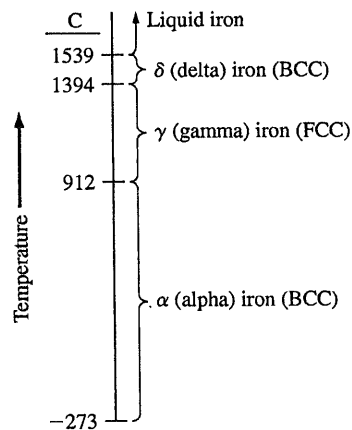| Metal	Crystal structure at room temperature	At other temperatures
Ca	FCC	BCC (> 447°C)
Co	HCP	FCC (> 427°C)
Hf	HCP	BCC (> 1742°C)
Fe	BCC	FCC (912–1394°C)
		BCC (> 1394°C)
Li	BCC	HCP (< −193°C)
Na	BCC	HCP (< −233°C)
Tl	HCP	BCC (> 234°C)
Ti	HCP	BCC (> 883°C)
Y	HCP	BCC (> 1481°C)
Zr	HCP	BCC (> 872°C)

Figure 3.21
Allotropic crystalline forms of iron over temperature ranges at atmospheric pressure

iron exists from 912°C to 1394°C and has the FCC crystal structure. Delta (δ) iron exists from 1394°C to 1539°C which is the melting point of iron. The crystal structure of δ iron is also BCC but with a larger lattice constant than α iron.

Calculate the theoretical volume change accompanying a polymorphic transformation in a pure metal from the FCC to BCC crystal structure. Assume the hard-sphere atomic model and that there is no change in atomic volume before and after the transformation.

EXAMPLE PROBLEM 3.14

■ Solution

In the FCC crystal structure unit cell, the atoms are in contact along the face diagonal of the unit cell, as shown in Fig. 3.7. Hence,

$$\sqrt{2}a = 4R \quad \text{or} \quad a = \frac{4R}{\sqrt{2}} \tag{3.3}$$

In the BCC crystal structure unit cell, the atoms are in contact along the body diagonal of the unit cell as shown in Fig. 3.5. Hence,

$$\sqrt{3}a = 4R \quad \text{or} \quad a = \frac{4R}{\sqrt{3}} \tag{3.1}$$

The volume per atom for the FCC crystal lattice, since it has four atoms per unit cell, is

$$V_{\text{FCC}} = \frac{a^3}{4} = \left(\frac{4R}{\sqrt{2}}\right)^3\left(\frac{1}{4}\right) = 5.66R^3$$

The volume per atom for the BCC crystal lattice, since it has two atoms per unit cell, is

$$V_{\text{BCC}} = \frac{a^3}{2} = \left(\frac{4R}{\sqrt{3}}\right)^3\left(\frac{1}{2}\right) = 6.16R^3$$

The change in volume associated with the transformation from the FCC to BCC crystal structure, assuming no change in atomic radius, is

$$\frac{\Delta V}{V_{\text{FCC}}} = \frac{V_{\text{BCC}} - V_{\text{FCC}}}{V_{\text{FCC}}}$$

$$= \left(\frac{6.16R^3 - 5.66R^3}{5.66R^3}\right)100\% = +8.8\% \blacktriangleleft$$

4.1 SOLIDIFICATION OF METALS

The solidification of metals and alloys is an important industrial process since most metals are melted and then cast into a semifinished or finished shape. Figure 4.1 shows a large, semicontinuously[2] cast aluminum ingot that will be further fabricated into aluminum alloy flat products. It illustrates the large scale on which the casting process (solidification) of metals is sometimes carried out.

In general, the solidification of a metal or alloy can be divided into the following steps:

1. The formation of stable **nuclei** in the melt (nucleation) (Fig. 4.2a)
2. The growth of nuclei into crystals (Fig. 4.2b) and the formation of a grain structure (Fig. 4.2c)

---

[2]A semicontinuously cast ingot is produced by solidifying molten metal (e.g., aluminum or copper alloys) in a mold that has a movable bottom block (see Fig. 4.8) that is slowly lowered as the metal is solidified. The prefix *semi-* is used since the maximum length of the ingot produced is determined by the depth of the pit into which the bottom block is lowered.

138 **CHAPTER 4** Solidification and Crystalline Imperfections

Animation

Figure 4.1
Large, semicontinuously cast aluminum alloy ingot being removed from casting pit. Ingots of this type are subsequently hot- and cold-rolled into plate or sheet.
(*Courtesy of Reynolds Metals Co.*)

(*a*) (*b*) (*c*)

Virtual Lab
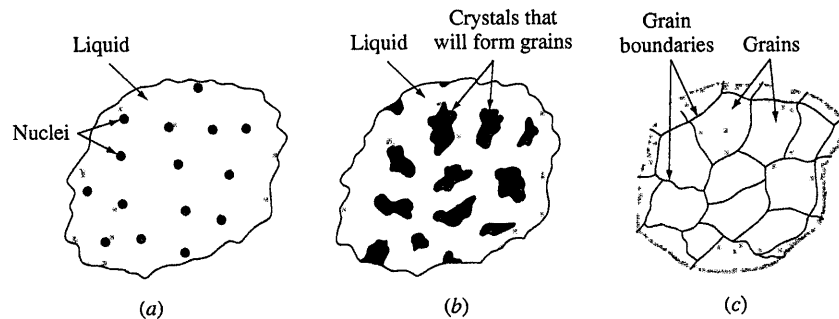
Figure 4.2
Schematic illustration showing the several stages in the solidification of metals: (*a*) formation of nuclei, (*b*) growth of nuclei into crystals, and (*c*) joining together of crystals to form grains and associated grain boundaries. Note that the grains are randomly oriented.

Figure 4.3
A grain grouping parted from an arc-cast titanium alloy ingot under the blows of a hammer. The grouping has preserved the true bonding facets of the individual grains of the original cast structure. (Magnification $\frac{1}{6}\times$.)
(After W. Rostoker and J.R. Dvorak, "Interpretation of Metallographic Structures," Academic, 1965, p. 7.)

The shapes of some real grains formed by the solidification of a titanium alloy are shown in Fig. 4.3. The shape that each grain acquires after solidification of the metal depends on many factors, of which thermal gradients are important. The grains shown in Fig. 4.3 are *equiaxed* since their growth is about equal in all directions.

4.1.1 The Formation of Stable Nuclei in Liquid Metals

The two main mechanisms by which the nucleation of solid particles in liquid metal occurs are homogeneous nucleation and heterogeneous nucleation.

Homogeneous Nucleation Homogeneous nucleation is considered first since it is the simplest case of nucleation. **Homogeneous nucleation** in a liquid melt occurs when the metal itself provides the atoms needed to form a nuclei. Let us consider the case of a pure metal solidifying. When a pure liquid metal is cooled below its equilibrium freezing temperature to a sufficient degree, many homogeneous nuclei are created by slow-moving atoms bonding together. Homogeneous nucleation usually requires a considerable amount of undercooling, which may be as much as several hundred degrees Celsius for some metals (see Table 4.1). For a nucleus to be stable so that it can grow into a crystal, it must reach a *critical size*. A cluster of atoms bonded together that is less than the critical size is called an **embryo,** and one that is larger than the critical size is called a *nucleus.* Because of their instability, embryos are continuously being formed and redissolved in the molten metal due to the agitation of the atoms.

Energies Involved in Homogeneous Nucleation In the homogeneous nucleation of a solidifying pure metal, two kinds of energy changes must be considered: (1) the *volume (or bulk) free energy* released by the liquid-to-solid transformation and (2) *the surface energy* required to form the new solid surfaces of the solidified particles.

140   **CHAPTER 4**   Solidification and Crystalline Imperfections

Table 4.1 Values for the freezing temperature, heat of fusion, surface energy, and maximum undercooling for selected metals

| Metal | Freezing temp. | | Heat of fusion (J/cm³) | Surface energy (J/cm²) | Maximum undercooling, observed ($\Delta T[°C]$) |
	°C	K			
Pb	327	600	280	33.3×10^{-7}	80
Al	660	933	1066	93×10^{-7}	130
Ag	962	1235	1097	126×10^{-7}	227
Cu	1083	1356	1826	177×10^{-7}	236
Ni	1453	1726	2660	255×10^{-7}	319
Fe	1535	1808	2098	204×10^{-7}	295
Pt	1772	2045	2160	240×10^{-7}	332

Source: B. Chalmers, "Solidification of Metals," Wiley, 1964.
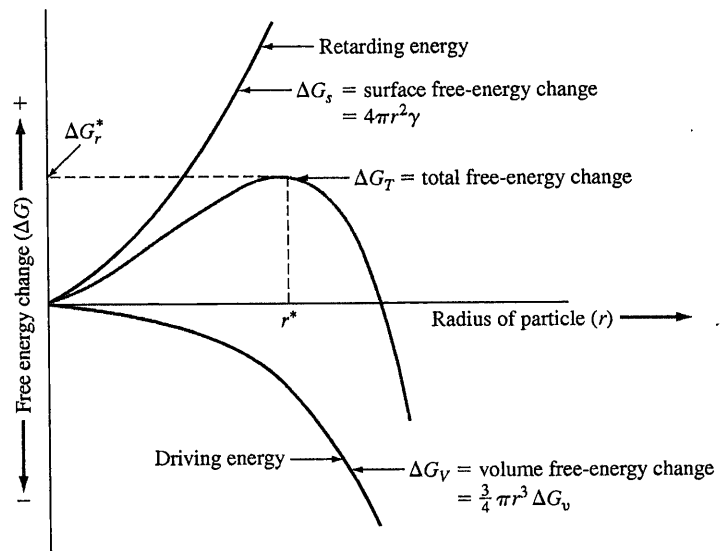
Figure 4.4
Free-energy change ΔG versus radius of embryo or nucleus created by the solidifying of a pure metal. If the radius of the particle is greater than r^* a stable nucleus will continue to grow.

When a pure liquid metal such as lead is cooled below its equilibrium freezing temperature, the driving energy for the liquid-to-solid transformation is the difference in the volume (bulk) free energy ΔG_v of the liquid and that of the solid. If ΔG_v is the change in free energy between the liquid and solid per unit volume of metal, then the free-energy change for a *spherical nucleus* of radius r is $\frac{4}{3}\pi r^3 \Delta G_v$ since the volume of a sphere is $\frac{4}{3}\pi r^3$. The change in volume free energy versus radius of an

embryo or nucleus is shown schematically in Fig. 4.4 as the lower curve and is a negative quantity since energy is released by the liquid-to-solid transformation.

However, there is an opposing energy to the formation of embryos and nuclei, the energy required to form the surface of these particles. The energy needed to create a surface for these spherical particles, ΔG_s, is equal to the specific surface free energy of the particle, γ, times the area of the surface of the sphere, or $4\pi r^2 \gamma$, where $4\pi r^2$ is the surface area of a sphere. This retarding energy ΔG_s for the formation of the solid particles is shown graphically in Fig. 4.4 by an upward curve in the positive upper half of the figure. The total free energy associated with the formation of an embryo or nucleus, which is the sum of the volume free-energy and surface free-energy changes, is shown in Fig. 4.4 as the middle curve. In equation form, the total free-energy change for the formation of a spherical embryo or nucleus of radius r formed in a freezing pure metal is

$$\Delta G_T = \tfrac{4}{3}\pi r^3 \, \Delta G_v + 4\pi r^2 \gamma \qquad (4.1)$$

where ΔG_T = total free-energy change
$\quad\quad r$ = radius of embryo or nucleus
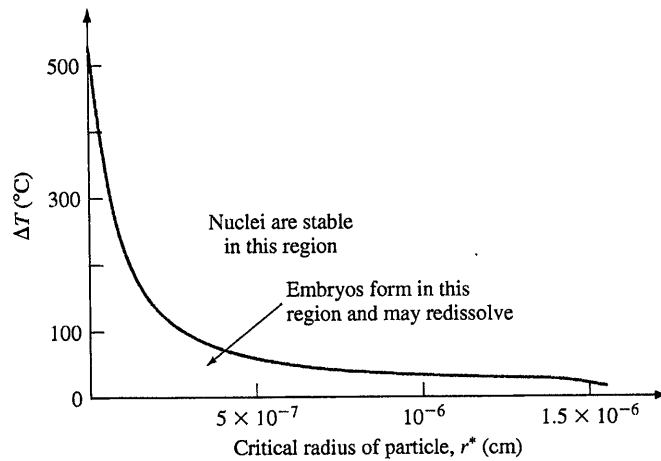$\quad \Delta G_v$ = volume free energy
$\quad\quad \gamma$ = specific surface free energy

In nature, a system can change spontaneously from a higher- to a lower-energy state. In the case of the freezing of a pure metal, if the solid particles formed upon freezing have radii less than the **critical radius** r^*, the energy of the system will be lowered if they redissolve. These small embryos can, therefore, redissolve in the liquid metal. However, if the solid particles have radii greater than r^*, the energy of the system will be lowered when these particles (nuclei) grow into larger particles or crystals (Fig. 4.2b). When r reaches the critical radius r^*, ΔG_T has its maximum value of ΔG^* (Fig. 4.4).

A relationship among the size of the critical nucleus, surface free energy, and volume free energy for the solidification of a pure metal can be obtained by differentiating Eq. 4.1. The differential of the total free energy ΔG_T with respect to r is zero when $r = r^*$ since the total free energy versus radius of the embryo or nucleus plot is then at a maximum and the slope $d(\Delta G_T)/dr = 0$. Thus,

$$\frac{d(\Delta G_T)}{dr} = \frac{d}{dr}\left(\frac{4}{3}\pi r^3 \Delta G_v + 4\pi r^2 \gamma\right)$$

$$\frac{12}{3}\pi r^{*2} \, \Delta G_V + 8\pi r^* \gamma = 0 \qquad (4.1a)$$

$$r^* = -\frac{2\gamma}{\Delta G_v}.$$

Critical Radius versus Undercooling The greater the degree of undercooling ΔT below the equilibrium melting temperature of the metal, the greater the change in

142   **CHAPTER 4**   Solidification and Crystalline Imperfections

Figure 4.5
Critical radius of copper nuclei versus degree of
undercooling ΔT.
(*From B. Chalmers, Principles of Solidification, Wiley, 1964.*)

volume free energy ΔG_V. However, the change in free energy due to the surface energy ΔG_s does not change much with temperature. Thus, the critical nucleus size is determined mainly by ΔG_V. Near the freezing temperature, the critical nucleus size must be infinite since ΔT approaches zero. As the amount of undercooling increases, the critical nucleus size decreases. Figure 4.5 shows the variation in critical nucleus size for copper as a function of undercooling. The maximum amount of undercooling for homogeneous nucleation in the pure metals listed in Table 4.1 is from 327°C to 1772°C. The critical-sized nucleus is related to the amount of undercooling by the relation

$$r^* = \frac{2\gamma T_m}{\Delta H_f \Delta T}$$

(4.2)

where r^* = critical radius of nucleus

γ = surface free energy

ΔH_f = latent heat of fusion

ΔT = amount of undercooling at which nucleus is formed

Example Problem 4.1 shows how a value for the number of atoms in a critical nucleus can be calculated from experimental data.

EXAMPLE PROBLEM 4.1	a. Calculate the critical radius (in centimeters) of a homogeneous nucleus that forms when pure liquid copper solidifies. Assume ΔT (undercooling) $= 0.2T_m$. Use data from Table 4.1.
	b. Calculate the number of atoms in the critical-sized nucleus at this undercooling.

■ **Solution**

a. Calculation of critical radius of nucleus:

$$r^* = \frac{2\gamma T_m}{\Delta H_f \Delta T}$$

(4.2)

$$\Delta T = 0.2 T_m = 0.2(1083°C + 273) = (0.2 \times 1356\ K) = 271\ K$$

$$\gamma = 177 \times 10^{-7}\ J/cm^2 \quad \Delta H_f^° = 1826\ J/cm^3 \quad T_m = 1083°C = 1356\ K$$

$$r^* = \frac{2(177 \times 10^{-7}\ J/cm^2)(1356\ K)}{(1826\ J/cm^3)(271\ K)} = 9.70 \times 10^{-8}\ cm\ \blacktriangleleft$$

b. Calculation of number of atoms in critical-sized nucleus:

Vol. of critical-sized nucleus $= \frac{4}{3}\pi r^{*3} = \frac{4}{3}\pi(9.70 \times 10^{-8}\ cm)^3$

$$= 3.82 \times 10^{-21}\ cm^3$$

Vol. of unit cell of Cu $(a = 0.361\ nm) = a^3 = (3.61 \times 10^{-8}\ cm)^3$

$$= 4.70 \times 10^{-23}\ cm^3$$

Since there are four atoms per FCC unit cell,

$$\text{Volume/atom} = \frac{4.70 \times 10^{-23}\ cm^3}{4} = 1.175 \times 10^{-23}\ cm^3$$

Thus, the number of atoms per homogeneous critical nucleus is,

$$\frac{\text{Volume of nucleus}}{\text{Volume/atom}} = \frac{3.82 \times 10^{-21}\ cm^3}{1.175 \times 10^{-23}\ cm^3} = 325\ \text{atoms}\ \blacktriangleleft$$

Heterogeneous Nucleation Heterogeneous nucleation is nucleation that occurs in a liquid on the surfaces of its container, insoluble impurities, and other structural material that lower the critical free energy required to form a stable nucleus. Since large amounts of undercooling do not occur during industrial casting operations and usually range between 0.1°C and 10°C, the nucleation must be heterogeneous and not homogeneous.

For heterogeneous nucleation to take place, the solid nucleating agent (impurity solid or container) must be wetted by the liquid metal. Also the liquid should solidify easily on the nucleating agent. Figure 4.6 shows a nucleating agent (substrate) that is wetted by the solidifying liquid, creating a low contact angle θ between the solid metal and the nucleating agent. Heterogeneous nucleation takes place on the nucleating agent because the surface energy to form a stable nucleus is lower on this material than in the pure liquid itself (homogeneous nucleation). Since the surface energy is lower for heterogeneous nucleation, the total free-energy change for the formation of a stable nucleus will be lower and the critical size of the nucleus will be smaller. Thus, a much smaller amount of undercooling is required to form a stable nucleus produced by heterogeneous nucleation.

θ = contact angle

Liquid

γ_{SL}

Solid γ_{na-S} θ

θ

γ_{na-L}
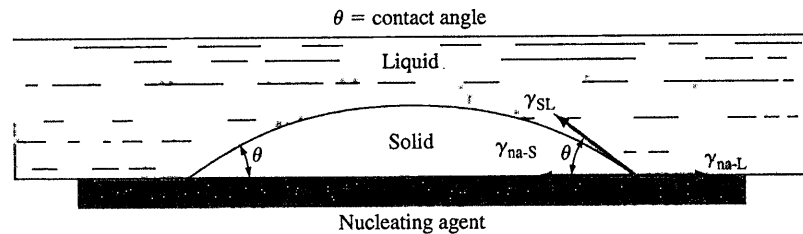
Nucleating agent

Figure 4.6
Heterogeneous nucleation of a solid on a nucleating agent. na =
nucleating agent, SL = solid-liquid, S = solid, L = liquid; θ =
contact angle.
*(From J.H. Brophy, R.M. Rose and J. Wulff, The Structure and Properties of Materials,
vol. II: "Thermodynamics of Structure," Wiley, 1964, p. 105.)*

4.1.2 Growth of Crystals in Liquid Metal and Formation of a Grain Structure

After stable nuclei have been formed in a solidifying metal, these nuclei grow into crystals, as shown in Fig. 4.2b. In each solidifying crystal, the atoms are arranged in an essentially regular pattern, but the orientation of each crystal varies (Fig. 4.2b). When solidification of the metal is finally completed, the crystals join together in different orientations and form crystal boundaries at which changes in orientation take place over a distance of a few atoms (Fig. 4.2c). Solidified metal containing many crystals is said to be *polycrystalline*. The crystals in the solidified metal are called **grains,** and the surfaces between them, *grain boundaries*.

The number of nucleation sites available to the freezing metal will affect the grain structure of the solid metal produced. If relatively few nucleation sites are available during solidification, a coarse, or large-grain, structure will be produced. If many nucleation sites are available during solidification, a fine-grain structure will result. Almost all engineering metals and alloys are cast with a fine-grain structure since this is the most desirable type for strength and uniformity of finished metal products.

When a relatively pure metal is cast into a stationary mold without the use of *grain refiners,*[3] two major types of grain structures are usually produced:

1. Equiaxed grains
2. Columnar grains

If the nucleation and growth conditions in the liquid metal during solidification are such that the crystals can grow about equally in all directions, **equiaxed grains** will be produced. Equiaxed grains are commonly found adjacent to a cold mold wall, as shown in Fig. 4.7. Large amounts of undercooling near the wall create a relatively high concentration of nuclei during solidification, a condition necessary to produce the equiaxed gain structure.

---

[3]A grain refiner is a material added to a molten metal to attain finer grains in the final grain structure.
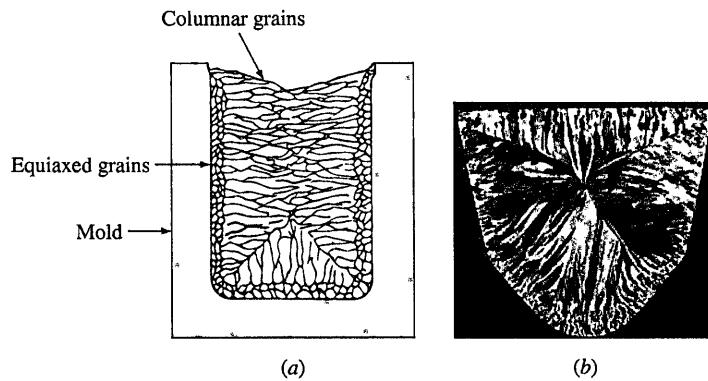
Figure 4.7
(*a*) Schematic drawing of a solidified metal grain structure
produced by using a cold mold. (*b*) Transverse section through
an ingot of aluminum alloy 1100 (99.0% Al) cast by the Properzi
method (a wheel and belt method). Note the consistency with
which columnar grains have grown perpendicular to each
mold face.
(*After "Metals Handbook," vol. 8, 8th ed., American Society for Metals,
1973, p. 164.*)

Columnar grains are long, thin, coarse grains created when a metal solidifies
rather slowly in the presence of a steep temperature gradient. Relatively few nuclei
are available when columnar grains are produced. Equiaxed and columnar grains are
shown in Fig. 4.7*a*. Note that in Fig. 4.7*b* the columnar grains have grown perpendi-
cular to the mold faces since large thermal gradients were present in those directions.

4.1.3 Grain Structure of Industrial Castings

In industry, metals and alloys are cast into various shapes. If the metal is to be fur-
ther fabricated after casting, large castings of simple shapes are produced first and
then fabricated further into semifinished products. For example, in the aluminum
industry, common shapes for further fabrication are sheet ingots (Fig. 4.1), which
have rectangular cross sections, and extrusion[4] ingots, which have circular cross sec-
tions. For some applications, the molten metal is cast into essentially its final shape
as, for example, an automobile piston (see Fig. 6.3).

The large aluminum alloy sheet ingot in Fig. 4.1 was cast by a direct-chill semi-
continuous casting process. In this casting method, the molten metal is cast into a
mold with a movable bottom block that is slowly lowered after the mold is filled

---

[4]*Extrusion* is the process of converting a metal ingot into lengths of uniform cross section by forcing solid
plastic metal through a die or orifice of the desired cross-sectional outline.
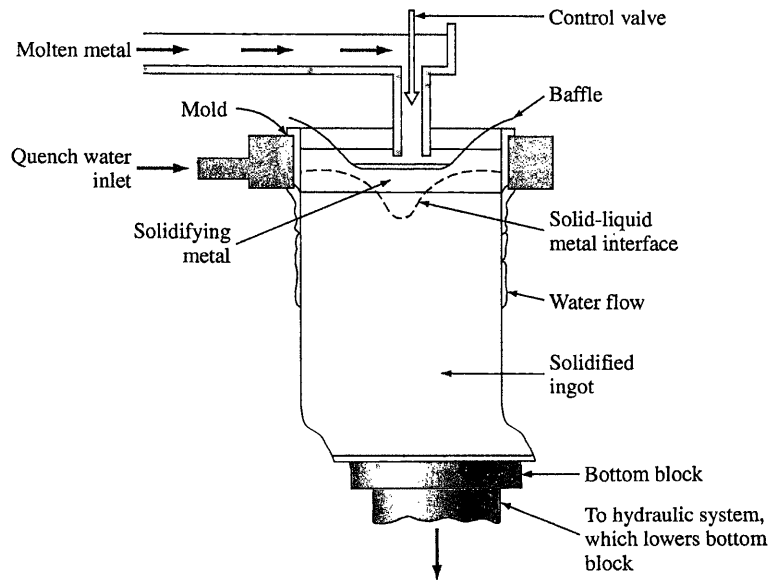
Figure 4.8
Schematic of an aluminum alloy ingot being cast in a direct-chill
semicontinuous casting unit.

(Fig. 4.8). The mold is water-cooled by a water box, and water is also sprayed down the sides of the solidified surface of the ingot. In this way, large ingots about 15 ft long can be cast continuously, as shown in Fig. 4.1. In the steel industry, about 60 percent of the metal is cast into stationary molds, with the remaining 40 percent being continuously cast, as shown in Fig. 4.9.

To produce cast ingots with a fine grain size, grain refiners are usually added to the liquid metal before casting. For aluminum alloys, small amounts of grain refining elements such as titanium, boron, or zirconium are included in the liquid metal just before the casting operation so that a fine dispersion of heterogeneous nuclei will be available during solidification. Figure 4.10 shows the effect of using a grain refiner while casting 6-in.-diameter aluminum extrusion ingots. The ingot section cast without the grain refiner has large columnar grains (Fig. 4.10a), and the section cast with the grain refiner has a fine, equiaxed grain structure (Fig. 4.10b).

150   **CHAPTER 4** Solidification and Crystalline Imperfections

4.3 METALLIC SOLID SOLUTIONS

Although very few metals are used in the pure or nearly pure state, a few are used in the nearly pure form. For example, high-purity copper of 99.99 percent purity is used for electronic wires because of its very high electrical conductivity. High-purity aluminum (99.99% Al) (called *superpure aluminum*) is used for decorative purposes because it can be finished with a very bright metallic surface. However, most engineering metals are combined with other metals or nonmetals to provide increased strength, higher corrosion resistance, or other desired properties.

A *metal alloy,* or simply an **alloy,** is a mixture of two or more metals or a metal (metals) and a nonmetal (nonmetals). Alloys can have structures that are relatively simple, such as that of cartridge brass, which is essentially a binary alloy (two metals) of 70 wt% Cu and 30 wt% Zn. On the other hand, alloys can be extremely complex, such as the nickel-base superalloy Inconel 718 used for jet engine parts, which has about 10 elements in its nominal composition.

The simplest type of alloy is that of the solid solution. A **solid solution** is a *solid* that consists of two or more elements atomically dispersed in a single-phase structure. In general there are two types of solid solutions: *substitutional* and *interstitial.*
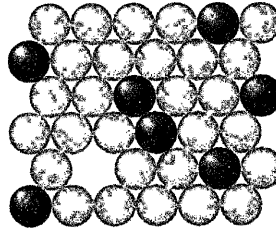
Figure 4.14
Substitutional solid
solution. The dark circles
represent one type of
atom and the light
another. The plane of
atoms is a (111) plane
in an FCC crystal lattice.

4.3.1 Substitutional Solid Solutions

In **substitutional solid solutions** formed by two elements, solute atoms can substitute for parent solvent atoms in a crystal lattice. Figure 4.14 shows a (111) plane in an FCC crystal lattice in which some solute atoms of one element have substituted for solvent atoms of the parent element. The crystal structure of the parent element or solvent is unchanged, but the lattice may be distorted by the presence of the solute atoms, particularly if there is a significant difference in atomic diameters of the solute and solvent atoms.

The fraction of atoms of one element that can dissolve in another can vary from a fraction of an atomic percent to 100 percent. The following conditions, known as *Hume–Rothery rules*, are favorable for extensive solid solubility of one element in another:

1. The diameters of the atoms of the elements must not differ by more than about 15 percent.
2. The crystal structures of the two elements must be the same.
3. There should be no appreciable difference in the electronegativities of the two elements so that compounds will not form.
4. The two elements should have the same valence.

If the atomic diameters of the two elements that form a solid solution differ, there will be a distortion of the crystal lattice. Since the atomic lattice can only sustain a limited amount of contraction or expansion, there is a limit in the difference in atomic diameters that atoms can have and still maintain a solid solution with the same kind of crystal structure. When the atomic diameters differ by more than about 15 percent, the "size factor" becomes unfavorable for extensive solid solubility.

152   **CHAPTER 4** Solidification and Crystalline Imperfections

EXAMPLE PROBLEM 4.2	Using the data in the following table, predict the relative degree of atomic solid solubility of the following elements in copper:

a. Zinc   d. Nickel
b. Lead   e. Aluminum
c. Silicon   f. Beryllium

Use the scale very high, 70%–100%; high, 30%–70%; moderate, 10%–30%; low, 1%–10%; and very low, <1%.

Element	Atom radius (nm)	Crystal structure	Electro-negativity	Valence
Copper	0.128	FCC	1.8	+2
Zinc	0.133	HCP	1.7	+2
Lead	0.175	FCC	1.6	+2, +4
Silicon	0.117	Diamond cubic	1.8	+4
Nickel	0.125	FCC	1.8	+2
Aluminum	0.143	FCC	1.5	+3
Beryllium	0.114	HCP	1.5	+2

■ **Solution**

A sample calculation for the atomic radius difference for the Cu–Zn system is

$$\text{Atomic radius difference} = \frac{\text{final radius} - \text{initial radius}}{\text{initial radius}}(100\%)$$

$$= \frac{R_{Zn} - R_{Cu}}{R_{Cu}}(100\%) \qquad (4.3)$$

$$= \frac{0.133 - 0.128}{0.128}(100\%) = +3.9\%$$

System	Atomic radius difference (%)	Electronegativity difference	Predicted relative degree of solid solubility	Observed maximum solid solubility (at %)
Cu–Zn	+3.9	0.1	High	38.3
Cu–Pb	+36.7	0.2	Very low	0.1
Cu–Si	−8.6	0	Moderate	11.2
Cu–Ni	−2.3	0	Very high	100
Cu–Al	+11.7	0.3	Moderate	19.6
Cu–Be	−10.9	0.3	Moderate	16.4

The predictions can be made principally on the atomic radius difference. In the case of the Cu–Si system, the difference in the crystal structures is important. There is very little electronegativity difference for all these systems. The valences are all the same except for Al and Si. In the final analysis, the experimental data must be referred to.

If the solute and solvent atoms have the same crystal structure, then extensive solid solubility is favorable. If the two elements are to show complete solid solubility in all proportions, then both elements must have the same crystal structure. Also, there cannot be too great a difference in the electronegativities of the two elements forming solid solutions, or else the highly electropositive element will lose electrons, the highly electronegative element will acquire electrons, and compound formation will result. Finally, if the two solid elements have the same valence, solid solubility will be favored. If there is a shortage of electrons between the atoms, the binding between them will be upset, resulting in conditions unfavorable for solid solubility.

4.3.2 Interstitial Solid Solutions

In interstitial solutions the solute atoms fit into the spaces between the solvent or parent atoms. These spaces or voids are called *interstices*. **Interstitial solid solutions** can form when one atom is much larger than another. Examples of atoms that can form interstitial solid solutions due to their small size are hydrogen, carbon, nitrogen, and oxygen.

An important example of an interstitial solid solution is that formed by carbon in FCC γ iron that is stable between 912°C and 1394°C. The atomic radius of γ iron is 0.129 nm and that of carbon is 0.075 nm, and so there is an atomic radius difference of 42 percent. However, in spite of this difference, a maximum of 2.08 percent of the carbon can dissolve interstitially in iron at 1148°C. Figure 4.15 illustrates this schematically by showing distortion around the carbon atoms in the γ iron lattice.

The radius of the largest interstitial hole in FCC γ iron is 0.053 nm (see Example Problem 4.3), and since the atomic radius of the carbon atom is 0.075 nm, it is not surprising that the maximum solid solubility of carbon in γ iron is only 2.08 percent. The radius of the largest interstitial void in BCC α iron is only 0.036 nm, and as a result, just below 723°C, only 0.025 percent of the carbon can be dissolved interstitially.
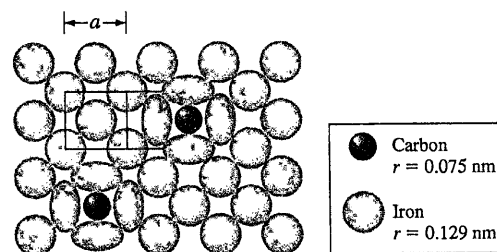

Figure 4.15
Schematic illustration of an interstitial solid solution of carbon in FCC γ iron just above 912°C showing a (100) plane. Note the distortion of the iron atoms (0.129 nm radius) around the carbon atoms (0.075 nm radius), fitting into voids of 0.053 nm radius.
(*From p. 113 in L. H. Van Vlack, Elements of Materials Science and Engineering, 4th ed.*)

154   **CHAPTER 4** Solidification and Crystalline Imperfections

EXAMPLE PROBLEM 4.3	Calculate the radius of the largest interstitial void in the FCC γ iron lattice. The atomic radius of the iron atom is 0.129 nm in the FCC lattice, and the largest interstitial voids occur at the $(\frac{1}{2}, 0, 0)$, $(0, \frac{1}{2}, 0)$, $(0, 0, \frac{1}{2})$, etc., -type positions.

■ Solution

Figure EP4.3 shows a (100) FCC lattice plane on the yz plane. Let the radius of an iron atom be R and that of the interstitial void at the position $(0, \frac{1}{2}, 0)$ be r. Then, from Fig. EP4.3,

$$2R + 2r = a \tag{4.4}$$

Also from Fig. 4.15b,

$$(2R)^2 = (\tfrac{1}{2}a)^2 + (\tfrac{1}{2}a)^2 = \tfrac{1}{2}a^2 \tag{4.5}$$

Solving for a gives

$$2R = \frac{1}{\sqrt{2}}a \qquad \text{or} \qquad a = 2\sqrt{2}R \tag{4.6}$$

Combining Eqs. 4.4 and 4.6 gives

$$2R + 2r = 2\sqrt{2}R$$
$$r = (\sqrt{2} - 1)R = 0.414R$$
$$= (0.414)(0.129 \text{ nm}) = 0.053 \text{ nm} \blacktriangleleft$$
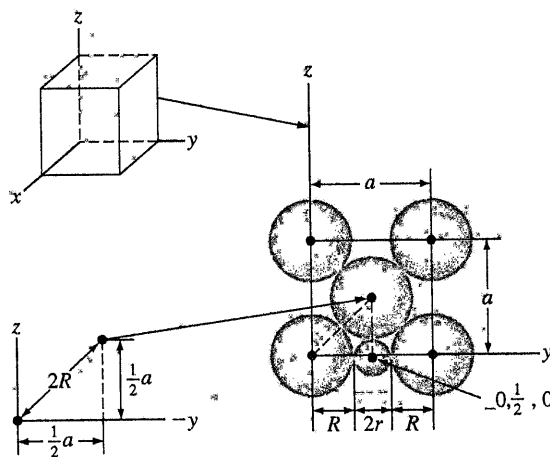

Figure EP4.3
(100) plane of the FCC lattice containing an interstitial atom at the $(0, \frac{1}{2}, 0)$ position coordinate.

4.4 CRYSTALLINE IMPERFECTIONS

In reality, crystals are never perfect and contain various types of imperfections and defects that affect many of their physical and mechanical properties, which in turn affect many important engineering properties of materials such as the cold formability of alloys, the electronic conductivity of semiconductors, the rate of migration of atoms in alloys, and the corrosion of metals.

Crystal lattice imperfections are classified according to their geometry and shape. The three main divisions are (1) zero-dimensional or point defects, (2) one-dimensional or line defects (dislocations), and (3) two-dimensional defects, that include external surfaces, grain boundaries, twins, low-angle boundaries, high-angle boundaries, twists, stacking faults, voids, and precipitates. Three-dimensional macroscopic or bulk defects could also be included. Examples of these defects are pores, cracks, and foreign inclusions.

4.4.1 Point Defects

The simplest point defect is the vacancy, an atom site from which an atom is missing (Fig. 4.16a). **Vacancies** may be produced during solidification as a result of local disturbances during the growth of crystals, or they may be created by atomic rearrangements in an existing crystal due to atomic mobility. In metals the equilibrium concentration of vacancies rarely exceeds about 1 in 10,000 atoms. Vacancies are equilibrium defects in metals, and their energy of formation is about 1 eV.

Additional vacancies in metals can be introduced by plastic deformation, rapid cooling from higher temperatures to lower ones to entrap the vacancies, and by bombardment with energetic particles such as neutrons. Nonequilibrium vacancies have a tendency to cluster, causing divacancies or trivacancies to form. Vacancies can move by exchanging positions with their neighbors. This process is important in the
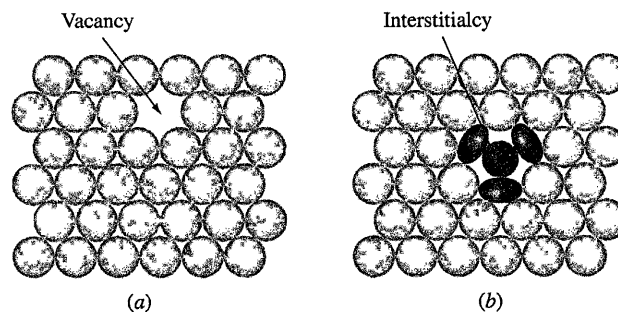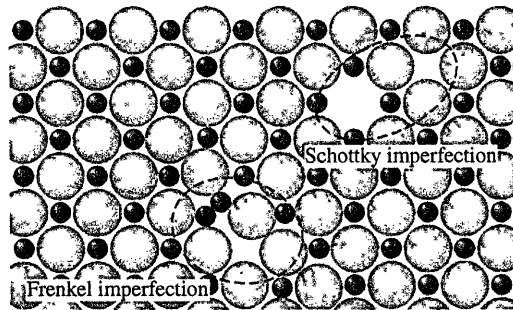

Figure 4.16
(a) Vacancy point defect. (b) Self-interstitial, or interstitialcy, point defect in a close-packed solid-metal lattice.

Figure 4.17
Two-dimensional representation of an ionic crystal illustrating a Schottky defect and a Frenkel defect.
(*From Wulff et al., Structure and Properties of Materials, Vol. I: "Structure," Wiley, 1964, p. 78.*)

migration or diffusion of atoms in the solid state, particularly at elevated temperatures where atomic mobility is greater.

Sometimes an atom in a crystal can occupy an interstitial site between surrounding atoms in normal atom sites (Fig. 4.16b). This type of point defect is called a **self-interstitial,** or **interstitialcy.** These defects do not generally occur naturally because of the structural distortion they cause, but they can be introduced into a structure by irradiation.

In ionic crystals point defects are more complex due to the necessity to maintain electrical neutrality. When two oppositely charged ions are missing from an ionic crystal, a cation-anion divacancy is created that is known as a **Schottky imperfection** (Fig. 4.17). If a positive cation moves into an interstitial site in an ionic crystal, a cation vacancy is created in the normal ion site. This vacancy-interstitialcy pair is called a **Frenkel**[6] **imperfection** (Fig. 4.17). The presence of these defects in ionic crystals increases their electrical conductivity.

Impurity atoms of the substitutional or interstitial type are also point defects and may be present in metallic or covalently bonded crystals. For example, very small amounts of substitutional impurity atoms in pure silicon can greatly affect its electrical conductivity for use in electronic devices. Impurity ions are also point defects in ionic crystals.

4.4.2 Line Defects (Dislocations)

Line imperfections, or **dislocations,** in crystalline solids are defects that cause lattice distortion centered around a line. Dislocations are created during the solid-

---

[6]Yakov Ilyich Frenkel (1894–1954). Russian physicist who studied defects in crystals. His name is associated with the vacancy-interstitialcy defect found in some ionic crystals.

(a) (b)
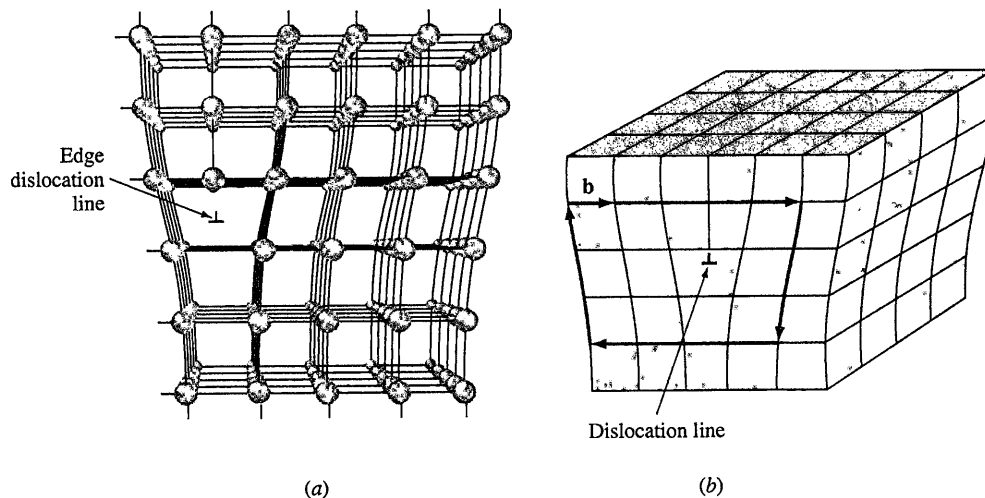
Figure 4.18
(a) Positive edge dislocation in a crystalline lattice. A linear defect occurs in the region just above the inverted "tee," ⊥, where an extra half plane of atoms has been wedged in.

Animation

(*After A.G. Guy, "Essentials of Materials Science," McGraw-Hill, 1976, p. 153.*)
(b) Edge dislocation that indicates the orientation of its Burgers or slip vector **b**.
(*Eisenstadt, M., Introduction to Mechanical Properties of Materials: An Ecological Approach, 1st ed., © 1971. Reprinted by permission of Pearson Education, Inc., Upper Saddle River, NJ.*)

ification of crystalline solids. They are also formed by the permanent or plastic deformation of crystalline solids, vacancy condensation, and atomic mismatch in solid solutions.

The two main types of dislocations are the *edge* and *screw types*. A combination of the two gives *mixed dislocations,* which have edge and screw components. An edge dislocation is created in a crystal by the insertion of an extra half plane of atoms, as shown in Fig. 4.18a just above the symbol ⊥. The inverted "tee," ⊥, indicates a positive edge dislocation, whereas the upright "tee," ⊤, indicates a negative edge dislocation.

The displacement distance of the atoms around the dislocation is called the *slip* or *Burgers vector* **b** and is *perpendicular* to the edge-dislocation line (Fig. 4.18b). Dislocations are nonequilibrium defects, and they store energy in the distorted region of the crystal lattice around the dislocation. The edge dislocation has a region of compressive strain at the extra half plane and a region of tensile strain below the extra half plane of atoms (Fig. 4.19a).

The screw dislocation can be formed in a perfect crystal by applying upward and downward shear stresses to regions of a perfect crystal that have been separated by a cutting plane, as shown in Fig. 4.20a. These shear stresses introduce a region of distorted crystal lattice in the form of a spiral ramp of distorted atoms or screw dislocation (Fig. 4.20b). The region of distorted crystal is not well
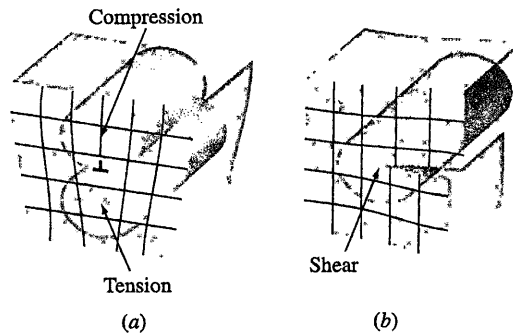
Figure 4.19
Strain fields surrounding (a) an edge
dislocation and (b) a screw dislocation.
*(From Wulff et al., Structure and Properties of Materials,
Vol. III, H.W. Hayden, L.G. Moffatt, and J. Wulff,
"Mechanical Behavior," Wiley, 1965, p. 69.)*
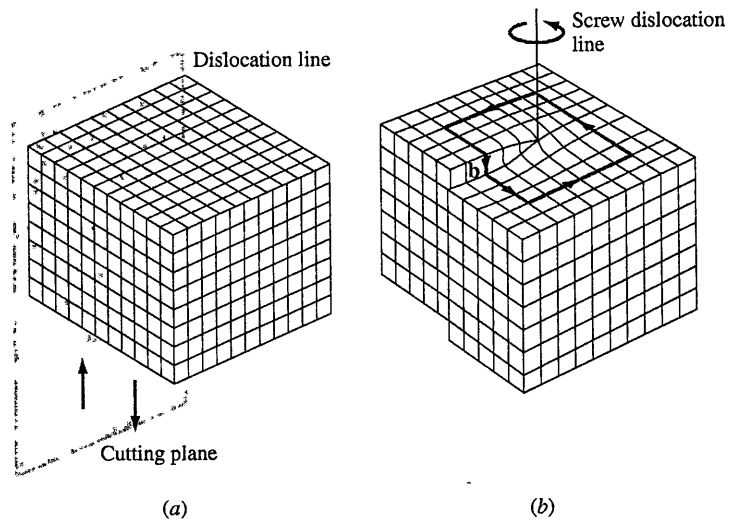
Figure 4.20
Formation of a screw dislocation. (a) A perfect crystal is sliced
by a cutting plane, and up and down shear stresses are applied
parallel to the cutting plane to form the screw dislocation in (b).
(b) A screw dislocation is shown with its slip or Burgers vector **b**
parallel to the dislocation line.
*(Eisenstadt, M., Introduction to Mechanical Properties of Materials: An
Ecological Approach, 1st ed., © 1971. Reprinted by permission of Pearson
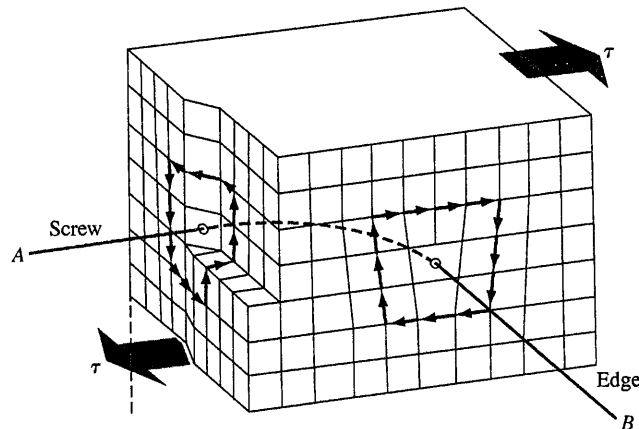Education, Inc., Upper Saddle River, NJ.)*

Figure 4.21
Mixed dislocation in a crystal. Dislocation line *AB* is pure
screw type where it enters the crystal on left and pure
edge type where it leaves the crystal on right.
(*From Wulff et al., Structure and Properties of Materials, Vol. III,
H.W. Hayden, L.G. Moffatt, and J. Wulff, "Mechanical Properties",
Wiley, 1965, p. 65.*)

defined and is at least several atoms in diameter. A region of shear strain is created
around the screw dislocation in which energy is stored (Fig. 4.19*b*). The slip or
Burgers vector of the screw dislocation is *parallel* to the dislocation line, as shown
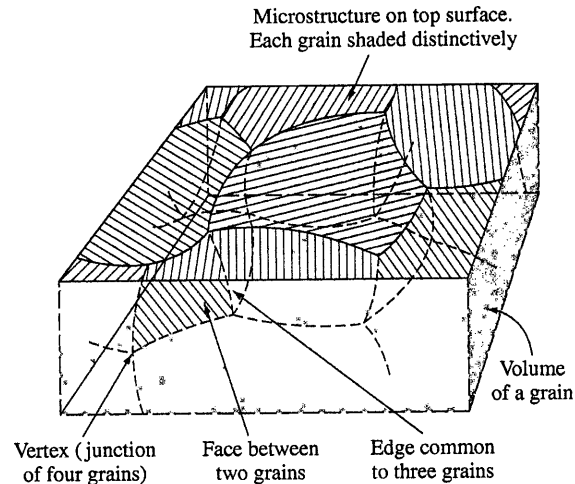in Fig. 4.20*b*.

Most dislocations in crystals are of the mixed type, having edge and screw com-
ponents. In the curved dislocation line *AB* in Fig. 4.21, the dislocation is of the pure
screw type at the left where it enters the crystal and of the pure edge type on the
right where it leaves the crystal. Within the crystal, the dislocation is of the mixed
type, with edge and screw components.

4.4.3 Planar Defects

Planar defects include external surfaces, **grain boundaries, twins, low-angle
boundaries, high-angle boundaries, twists,** and **stacking faults.** The free or exter-
nal surface of any material is the most common type of planar defect. External sur-
faces are considered defects because the atoms on the surface are bonded to other
atoms only on one side. Therefore, the surface atoms have a lower number of neigh-
bors. As a result, these atoms have a higher state of energy when compared to the
atoms positioned inside the crystal with an optimal number of neighbors. The higher
energy associated with the atoms on the surface of a material makes the surface sus-
ceptible to erosion and reaction with elements in the environment. This point further
illustrates the importance of defects in the behavior of materials.

160   CHAPTER 4 Solidification and Crystalline Imperfections

Microstructure on top surface.
Each grain shaded distinctively

Volume
of a grain

Vertex (junction   Face between   Edge common
of four grains)   two grains   to three grains
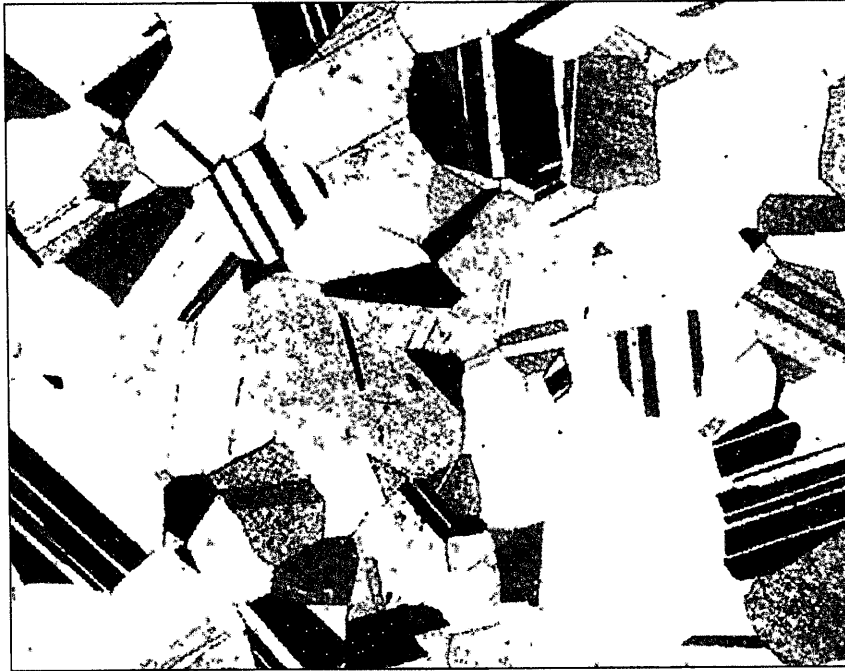
Figure 4.22
Sketch showing the relation of the two-dimensional
microstructure of a crystalline material to the
underlying three-dimensional network. Only
portions of the total volume and total face of any
one grain are shown.
*(After A.G. Guy, "Essentials of Materials Science,"
McGraw-Hill, 1976.)*

Grain boundaries are surface imperfections in polycrystalline materials that separate grains (crystals) of different orientations. In metals, grain boundaries are created during solidification when crystals formed from different nuclei grow simultaneously and meet each other (Fig. 4.2). The shape of the grain boundaries is determined by the restrictions imposed by the growth of neighboring grains. Grain-boundary surfaces of an approximately equiaxed grain structure are shown schematically in Fig. 4.22 and of real grains in Fig. 4.3.

The grain boundary itself is a narrow region between two grains of about two to five atomic diameters in width and is a region of atomic mismatch between adjacent grains. The atomic packing in grain boundaries is lower than within the grains because of the atomic mismatch. Grain boundaries also have some atoms in strained positions that raise the energy of the grain-boundary region.

The higher energy of the grain boundaries and their more open structure make them a more favorable region for the nucleation and growth of precipitates (see Sec. 9.5). The lower atomic packing of the grain boundaries also allows for more rapid diffusion of atoms in the grain boundary region. At ordinary temperatures, grain boundaries also restrict plastic flow by making it difficult for the movement of dislocations in the grain boundary region.

Figure 4.23
Twin boundaries in the grain structure of brass.
(*Figure from A.G. Guy, Essentials of Materials Science, McGraw-Hill, 1976.*)

Virtual Lab

Twins or *twin boundaries* are another example of a two-dimensional defect. A twin is defined as a region in which a mirror image of the structure exists across a plane or a boundary. Twin boundaries form when a material is permanently or plastically deformed (*deformation twin*). They can also appear during the recrystallization process in which atoms reposition themselves in a deformed crystal (*annealing twin*), but this happens only in some FCC alloys. A number of annealing twins formed in the microstructure of brass are shown in Fig. 4.23. As the name indicates, twin boundaries form in pairs. Similar to dislocations, twin boundaries tend to strengthen a material. A more detailed explanation of twin boundaries is given in Sec. 6.5.

When an array of edge dislocations are oriented in a crystal in a manner that seems to misorient or tilt two regions of a crystal (Fig. 4.24a), a two-dimensional defect called a *small-angle tilt boundary* is formed. A similar phenomenon can occur when a network of screw dislocations create a small-angle twist boundary (Fig 4.24b). The misorientation angle θ for a small-angle boundary is generally less than 10 degrees. As the density of dislocations in small-angle boundaries (tilt or twist) increases, the misorientation angle θ becomes larger. If θ exceeds 20 degrees, the boundary is no longer characterized as a small-angle boundary but
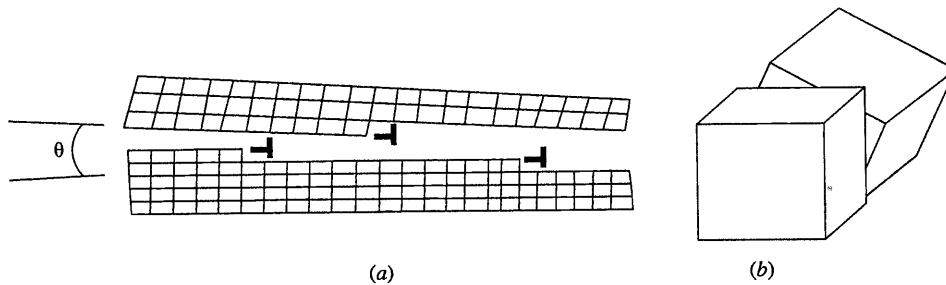
Figure 4.24
(a) Edge dislocations in an array forming a small-angle tilt boundary. (b) Schematic of a small-angle twist boundary.

is considered a general grain boundary. Similar to dislocations and twins, small-angle boundaries are regions of high energy due to local lattice distortions and tend to strengthen a metal.

In Sec. 3.8, we discussed formation of FCC and HCP crystal structures by the stacking of atomic planes. It was noted that the stacking sequence *ABABAB* . . . leads to the formation of an HCP crystal structure while the sequence *ABCABCABC* . . . leads to the FCC structure. Sometimes during the growth of a crystalline material, collapse of a vacancy cluster, or interaction of dislocations, one or more of the stacking planes may be missing, giving rise to another two-dimensional defect called a *stacking fault* or a *piling-up fault*. Stacking faults *ABCABAACBABC* and *ABAABBAB* are typical in FCC and HCP crystals, respectively. The bold-faced planes indicate the faults. Stacking faults also tend to strengthen the material.

It is important to note that, generally speaking, of the two-dimensional defects discussed here, grain boundaries are most effective in strengthening a metal; however stacking faults, twin boundaries, and small-angle boundaries often also serve a similar purpose. The reason why these defects tend to strengthen a metal will be discussed in more detail in Chap. 6.

4.4.4 Volume Defects

Volume or *three-dimensional defects* form when a cluster of point defects join to form a three-dimensional void or a pore. Conversely, a cluster of impurity atoms may join to form a three-dimensional precipitate. The size of a volume defect may range from a few nanometers to centimeters or sometimes larger. Such defects have a tremendous effect or influence on the behavior and performance of the material. Finally, the concept of a three-dimensional or volume defect may be extended to an amorphous region within a polycrystalline material. Such materials were briefly discussed in Chap. 3 and will be more extensively discussed in future chapters.

6.2 STRESS AND STRAIN IN METALS

In the first section of this chapter, we briefly examined most of the principal methods by which metals are processed into semifinished wrought and cast products. Let us now investigate how the mechanical properties of strength and ductility are evaluated for engineering applications.

6.2.1 Elastic and Plastic Deformation

When a piece of metal is subjected to a uniaxial tensile force, deformation of the metal occurs. If the metal returns to its original dimensions when the force is removed, the metal is said to have undergone **elastic deformation.** The amount of elastic deformation a metal can undergo is small, since during elastic deformation the metal atoms are displaced from their original positions but not to the extent that they take up new positions. Thus, when the force on a metal that has been elastically deformed is removed, the metal atoms return to their original positions and the metal takes back its original shape. If the metal is deformed to such an extent that it cannot fully recover its original dimensions, it is said to have undergone *plastic deformation.* During plastic deformation, the metal atoms are *permanently* displaced from their original positions and take up new positions. The ability of some metals to be extensively plastically deformed without fracture is one of the most useful engineering properties of metals. For example, the extensive plastic deformability of steel enables automobile parts such as fenders, hoods, and doors to be stamped out mechanically without the metal fracturing.

Virtual Lab

226   **CHAPTER 6** Mechanical Properties of Metals I

6.2.2 Engineering Stress and Engineering Strain

Engineering Stress   Let us consider a cylindrical rod of length l_0 and cross-sectional area A_0 subjected to a uniaxial tensile force F, as shown in Fig. 6.13. By definition, the **engineering stress** σ on the bar is equal to the average uniaxial tensile force F on the bar divided by the original cross-sectional area A_0 of the bar. Thus,

$$\text{Engineering stress } \sigma = \frac{F \text{ (average uniaxial tensile force)}}{A_0 \text{ (original cross-sectional area)}} \tag{6.3}$$

The units for engineering stress are:

   U.S. customary: pounds force per square inch (lb_f/in.^{2}, or psi);

   lb_f = pounds force

   SI: newtons per square meter (N/m^2) or pascals (Pa), where $1 \text{ N/m}^2 = 1 \text{ Pa}$

The conversion factors for psi to pascals are

$$1 \text{ psi} = 6.89 \times 10^3 \text{ Pa}$$

$$10^6 \text{ Pa} = 1 \text{ megapascal} = 1 \text{ MPa}$$

$$1000 \text{ psi} = 1 \text{ ksi} = 6.89 \text{ MPa}$$

EXAMPLE PROBLEM 6.4

A 0.500-in.-diameter aluminum bar is subjected to a force of 2500 lb_f. Calculate the engineering stress in pounds per square inch (psi) on the bar.

■ **Solution**

$$\sigma = \frac{\text{force}}{\text{original cross-sectional area}} = \frac{F}{A_0}$$

$$= \frac{2500 \text{ lb}_f}{(\pi/4)(0.500 \text{ in})^2} \doteq 12{,}700 \text{ lb}_f/\text{in.}^2 \blacktriangleleft$$

EXAMPLE PROBLEM 6.5

A 1.25-cm-diameter bar is subjected to a load of 2500 kg. Calculate the engineering stress on the bar in megapascals (MPa).

■ **Solution**

The load on the bar has a mass of 2500 kg. In SI units, the force on the bar is equal to the mass of the load times the acceleration of gravity (9.81 m/s^2), or

$$F = ma \doteq (2500 \text{ kg})(9.81 \text{ m/s}^2) = 24{,}500 \text{ N}$$

The diameter d of the bar = 1.25 cm = 0.0125 m. Thus, the engineering stress on the bar is

$$\sigma = \frac{F}{A_0} = \frac{F}{(\pi/4)(d^2)} = \frac{24{,}500 \text{ N}}{(\pi/4)(0.0125 \text{ m})^2}$$

$$= (2.00 \times 10^8 \text{ Pa})\left(\frac{1 \text{ MPa}}{10^6 \text{ Pa}}\right) = 200 \text{ MPa} \blacktriangleleft$$
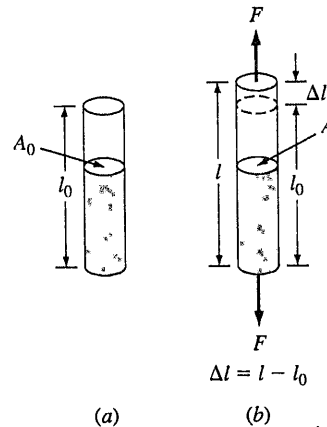
Figure 6.13
Elongation of a cylindrical
metal rod subjected to a
uniaxial tensile force F.
(a) The rod with no force on
it; and (b) the rod subjected
to a uniaxial tensile force F,
which elongates the rod from
length l_0 to l.

Engineering Strain When a uniaxial tensile force is applied to a rod, such as that shown in Fig. 6.13, it causes the rod to be elongated in the direction of the force. Such a displacement is called *strain*. By definition, **engineering strain,** which is caused by the action of a uniaxial tensile force on a metal sample, is the ratio of the change in length of the sample in the direction of the force divided by the original length of sample considered. Thus, the engineering strain for the metal bar shown in Fig. 6.13 (or for a similar-type metal sample) is

$$\text{Engineering strain } \epsilon = \frac{l - l_0}{l_0} = \frac{\Delta l \,(\text{change in length of sample})}{l_0 \,(\text{original length of sample})} \qquad \textbf{(6.4)}$$

where l_0 = original length of sample and l = new length of sample after being extended by a uniaxial tensile force. In most cases, engineering strain is determined by using a small length, usually 2 in., called the *gage length,* within a much longer, for example, 8 in., sample (see Example Problem 6.6).

Virtual Lab

The *units for engineering strain* ϵ are:

U.S. customary: inches per inch (in./in.)

SI: meters per meter (m/m)

Thus, engineering strain has *dimensionless units.* In industrial practice, it is common to convert engineering strain into *percent strain* or *percent elongation:*

% engineering strain = engineering strain $\times$ 100% = % elongation

---

EXAMPLE PROBLEM 6.6

A sample of commercially pure aluminum 0.500 in. wide, 0.040 in. thick, and 8 in. long that has gage markings 2.00 in. apart in the middle of the sample is strained so that the gage markings are 2.65 in. apart (Fig. 6.14). Calculate the engineering strain and the percent engineering strain elongation that the sample undergoes.

■ **Solution**

$$\text{Engineering strain } \epsilon = \frac{l - l_0}{l_0} = \frac{2.65 \text{ in.} - 2.00 \text{ in.}}{2.00 \text{ in.}} = \frac{0.65 \text{ in.}}{2.00 \text{ in.}} = 0.325 \blacktriangleleft$$

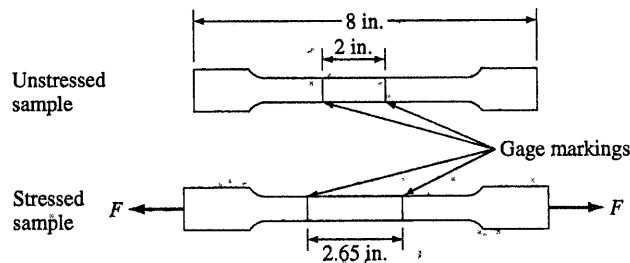$$\% \text{ elongation} = 0.325 \times 100\% = 32.5\% \blacktriangleleft$$

Figure 6.14
Flat tensile specimen before and after testing.

6.2.3 Poisson's Ratio

A longitudinal elastic deformation of a metal produces an accompanying lateral dimensional change. As shown in Fig. 6.15b, a tensile stress σ_z produces an axial strain $+\epsilon_z$ and lateral contractions of $-\epsilon_x$ and $-\epsilon_y$. For isotropic behavior,[4] ϵ_x and ϵ_y are equal. The ratio

$$\nu = -\frac{\epsilon \text{ (lateral)}}{\epsilon \text{ (longitudinal)}} = -\frac{\epsilon_x}{\epsilon_z} = -\frac{\epsilon_y}{\epsilon_z} \tag{6.5}$$

is called *Poisson's ratio*. For ideal materials, $\nu = 0.5$. However, for real materials, Poisson's ratio typically ranges from 0.25 to 0.4, with an average of about 0.3. Table 6.1 lists ν values for some metals and alloys.

6.2.4 Shear Stress and Shear Strain

Until now we have discussed the elastic and plastic deformation of metals and alloys under uniaxial tension stresses. Another important method by which a metal can be deformed is under the action of a **shear stress.** The action of a simple shear stress couple (shear stresses act in pairs) on a cubic body is shown in Fig. 6.15c, where a shearing force S acts over an area A. The shear stress τ is related to the shear force S by

$$\tau \text{ (shear stress)} = \frac{S \text{ (shear force)}}{A \text{ (area over which shear force acts)}} \tag{6.6}$$

---

[4]*Isotropic:* exhibiting properties with the same values when measured along axes in all directions.

(a) Unstressed body

S = shear force

(b) Body under tensile stress   (c) Body under shear stress

Virtual Lab
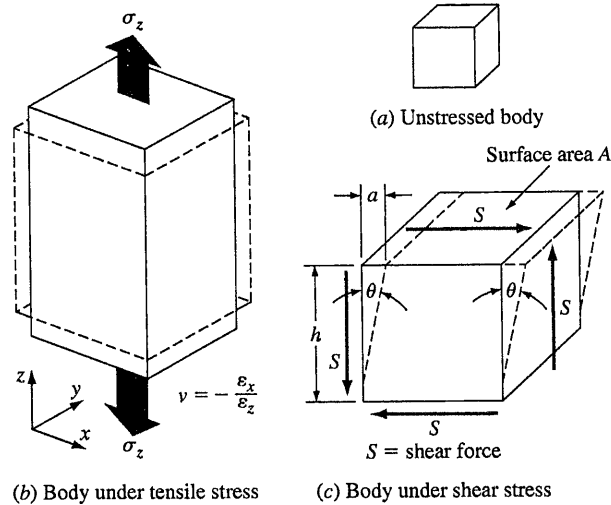
Figure 6.15
(a) Unstressed cubic body. (b) Cubic body subjected
to tensile stress. The ratio of the elastic contraction
perpendicular to the extension is designated Poisson's
ratio v. (c) Cubic body subjected to pure shear forces S
acting over surface areas A. The shear stress τ acting
on the body is equal to S/A.

Table 6.1 Typical room-temperature values of elastic constants for isotropic materials

Material	Modulus of elasticity, 10^6 psi (GPa)	Shear modulus, 10^6 psi (GPa)	Poisson's ratio
Aluminum alloys	10.5 (72.4)	4.0 (27.5)	0.31
Copper	16.0 (110)	6.0 (41.4)	0.33
Steel (plain carbon and low-alloy)	29.0 (200)	11.0 (75.8)	0.33
Stainless steel (18-8)	28.0 (193)	9.5 (65.6)	0.28
Titanium	17.0 (117)	6.5 (44.8)	0.31
Tungsten ·	58.0 (400)	22.8 (157)	0.27

Source: G. Dieter, "Mechanical Metallurgy," 3rd ed., McGraw-Hill, 1986.

The units for shear stress are the same as for uniaxial tensile stress:

  U.S. customary: pounds force per square inch ($lb_f/in.^2$, or psi)

  SI: newtons per square meter (N/m^2) or pascals (Pa)

  The **shear strain** γ is defined in terms of the amount of the shear displacement
a in Fig. 6.15c divided by the distance h over which the shear acts, or

$$\gamma = \frac{a}{h} = \tan \theta \qquad\qquad (6.7)$$

230   **CHAPTER 6** Mechanical Properties of Metals I

For pure elastic shear, the proportionality between shear and stress is

$$\tau = G\gamma \qquad (6.8)$$

where G is the elastic modulus.

We will be concerned with shear stresses when we discuss the plastic deformation of metals in Sec. 6.5.

6.3 THE TENSILE TEST AND THE ENGINEERING STRESS-STRAIN DIAGRAM

The *tensile test* is used to evaluate the strength of metals and alloys. In this test, a metal sample is pulled to failure in a relatively short time at a constant rate. Figure 6.16 is a picture of a modern tensile testing machine, and Fig. 6.17 illustrates schematically how the sample is tested in tension.

The force (load) on the specimen being tested is measured by the load cell while the strain is obtained from the extensometer attached to the specimen (Fig. 6.18) and the data is collected in a computer-control software package.

Virtual Lab

Figure 6.16
Modern tensile testing machine. The force (load) on the specimen is measured by the load cell while the strain is measured by the clip-on extensometer. The data is collected and analyzed by computer-controlled software.
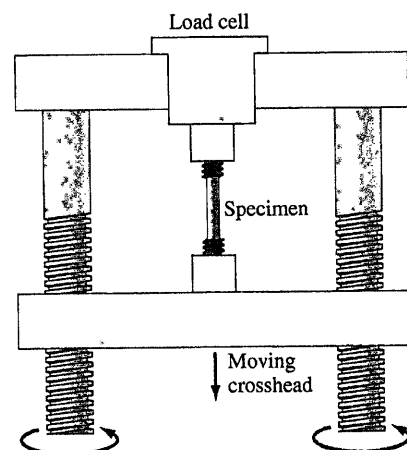(*Courtesy of the Instron® Corporation.*)

Figure 6.17
Schematic illustration showing how the tensile machine of Fig. 6.16 operates. Note, however, that the crosshead of the machine in Fig. 6.16 moves up.
(*From H.W. Hayden, W.G. Moffatt and J. Wulff, The Structure and Properties of Materials, vol. III, "Mechanical Behavior," Wiley, 1965, Fig. 1.1, p. 2.*)

The types of samples used for the tensile test vary considerably. For metals with a thick cross section such as plate, a 0.50-in.-diameter round specimen is commonly used (Fig. 6.19*a*). For metal with thinner cross sections such as sheet, a flat specimen is used (Fig. 6.19*b*). A 2-in. gage length within the specimen is the most commonly used gage length for tensile tests.
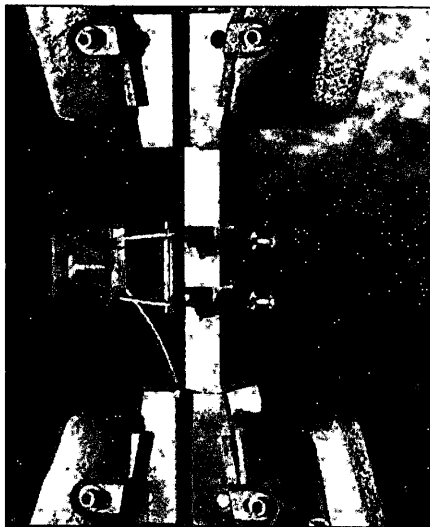
Figure 6.18
Close-up of the tensile machine extensometer that measures the strain that the sample undergoes during the tensile test. The extensometer is attached to the sample by small spring clamps.
(*Courtesy of the Instron Corporation.*)

Virtual Lab

(*a*)

(*b*)

Figure 6.19
Examples of the geometrical shape of commonly used tension test specimens. (*a*) Standard round tension test specimen with 2-in. gage length. (*b*) Standard rectangular tension test specimen with 2-in. gage length.
(*From H.E. McGannon (ed.), "The Making, Shaping, and Treating of Steel," 9th ed., United States Steel, 1971, p. 1220. Courtesy of United States Steel Corporation.*)
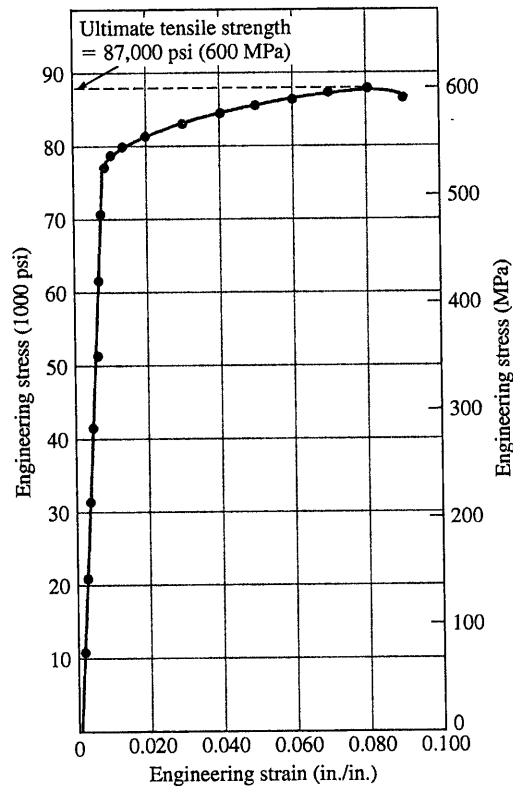
Figure 6.20
Engineering stress-strain diagram for a
high-strength aluminum alloy (7075-T6). The
specimens for the diagram were taken from
⅝-in. plate and had a 0.50-in. diameter with a
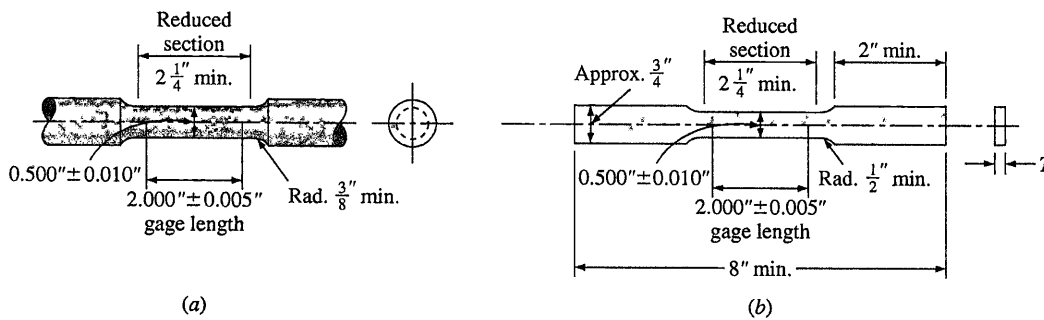2-in. gage length.
(*Courtesy of Aluminum Company of America.*)

Virtual Lab

The force data obtained from the chart paper for the tensile test can be converted to engineering stress data, and a plot of engineering stress versus engineering strain can be constructed. Figure 6.20 shows an **engineering stress-strain diagram** for a high-strength aluminum alloy.

6.3.1 Mechanical Property Data Obtained from the Tensile Test and the Engineering Stress-Strain Diagram

The mechanical properties of metals and alloys that are of engineering importance for structural design and can be obtained from the engineering tensile test are:

1. Modulus of elasticity
2. Yield strength at 0.2 percent offset

3. Ultimate tensile strength
4. Percent elongation at fracture
5. Percent reduction in area at fracture

Modulus of Elasticity In the first part of the tensile test, the metal is deformed elastically. That is, if the load on the specimen is released, the specimen will return to its original length. For metals, the maximum elastic deformation is usually less than 0.5 percent. In general, metals and alloys show a linear relationship between stress and strain in the elastic region of the engineering stress-strain diagram, which is described by Hooke's law:[5]

$$\sigma \text{ (stress)} = E\epsilon \text{ (strain)} \qquad \textbf{(6.9)}$$

or

$$E = \frac{\sigma \text{ (stress)}}{\epsilon \text{ (strain)}} \quad \text{(units of psi or Pa)}$$

Virtual Lab

where E is the **modulus of elasticity,** or *Young's modulus.*[6]

The modulus of elasticity is related to the bonding strength between the atoms in a metal or alloy. Table 6.1 lists the elastic moduli for some common metals. Metals with high elastic moduli are relatively stiff and do not deflect easily. Steels, for example, have high elastic moduli values of 30×10^6 psi (207 GPa),[7] whereas aluminum alloys have lower elastic moduli of about 10 to 11×10^6 psi (69 to 76 GPa). Note that in the elastic region of the stress-strain diagram, the modulus does not change with increasing stress.

Yield Strength The **yield strength** is a very important value for use in engineering structural design since it is the strength at which a metal or alloy shows significant plastic deformation. Because there is no definite point on the stress-strain curve where elastic strain ends and plastic strain begins, the yield strength is chosen to be that strength when a definite amount of plastic strain has occurred. For American engineering structural design, the yield strength is chosen when 0.2 percent plastic strain has taken place, as indicated on the engineering stress-strain diagram of Fig. 6.21.

The 0.2 percent yield strength, also called the *0.2 percent offset yield strength,* is determined from the engineering stress-strain diagram, as shown in Fig. 6.21. First, a line is drawn parallel to the elastic (linear) part of the stress-strain plot at 0.002 in./in. (m/m) strain, as indicated on Fig. 6.21. Then at the point where this line intersects the upper part of the stress-strain curve, a horizontal line is drawn to the stress axis. The 0.2 percent offset yield strength is the stress where the horizontal line intersects the stress axis, and in the case of the stress-strain

[5]Robert Hooke (1635–1703). English physicist who studied the elastic behavior of solids.

[6]Thomas Young (1773–1829). English physicist.

[7]SI prefix G = giga = 10^9.
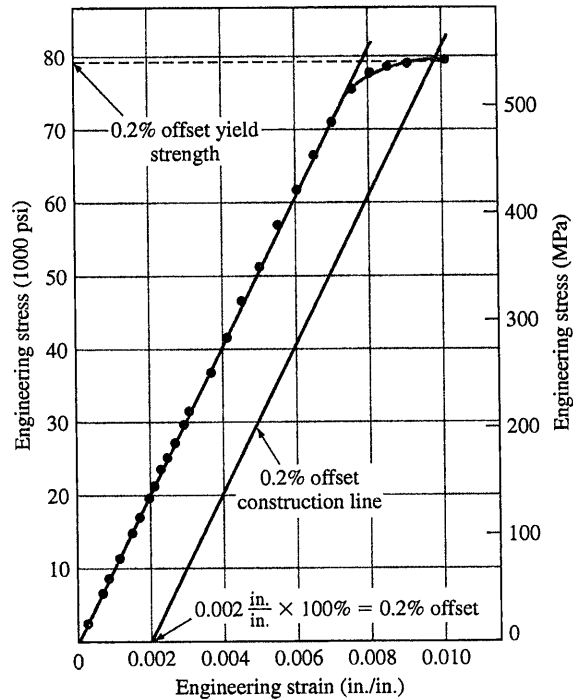
Figure 6.21
Linear part of engineering stress-strain diagram of
Fig. 6.22 expanded on the strain axis to make a
more accurate determination of the 0.2 percent
offset yield stress.
(*Courtesy of Aluminum Company of America.*)

Virtual Lab

curve of Fig. 6.21, the yield strength is 78,000 psi. It should be pointed out that the 0.2 percent offset yield strength is arbitrarily chosen, and thus the yield strength could have been chosen at any other small amount of permanent deformation. For example, a 0.1 percent offset yield strength is commonly used in the United Kingdom.

Ultimate Tensile Strength The **ultimate tensile strength** (UTS) is the maximum strength reached in the engineering stress-strain curve. If the specimen develops a localized decrease in cross-sectional area (commonly called *necking*) (Fig. 6.22), the engineering stress will decrease with further strain until fracture occurs since the engineering stress is determined by using the *original* cross-sectional area of the specimen. The more ductile a metal is, the more the specimen will neck before fracture and hence the more the decrease in the stress on the

stress-strain curve beyond the maximum stress. For the high-strength aluminum alloy whose stress-strain curve is shown in Fig. 6.20, there is only a small decrease in stress beyond the maximum stress because this material has relatively low ductility.

An important point to understand with respect to engineering stress-strain diagrams is that the metal or alloy continues to increase in stress up to the stress at fracture. It is only because we use the original cross-sectional area to determine engineering stress that the stress on the engineering stress-strain diagram decreases at the latter part of the test.

The ultimate tensile strength of a metal is determined by drawing a horizontal line from the maximum point on the stress-strain curve to the stress axis. The stress where this line intersects the stress axis is called the *ultimate tensile strength,* or sometimes just the *tensile strength.* For the aluminum alloy of Fig. 6.20, the ultimate tensile strength is 87,000 psi.

The ultimate tensile strength is not used much in engineering design for ductile alloys since too much plastic deformation takes place before it is reached. However, the ultimate tensile strength can give some indication of the presence of defects. If the metal contains porosity or inclusions, these defects may cause the ultimate tensile strength of the metal to be lower than normal.

Percent Elongation   The amount of elongation that a tensile specimen undergoes during testing provides a value for the ductility of a metal. Ductility of metals is most commonly expressed as percent elongation, starting with a gage length usually of 2 in. (5.1 cm) (Fig. 6.19). In general, the higher the ductility (the more deformable the metal is), the higher the percent elongation. For example, a sheet of 0.062-in. (1.6-mm) commercially pure aluminum (alloy 1100-0) in the soft condition has a high percent elongation of 35 percent, whereas the same thickness of the high-strength aluminum alloy 7075-T6 in the fully hard condition has a percent elongation of only 11 percent.

As previously mentioned, during the tensile test an extensometer can be used to continuously measure the strain of the specimen being tested. However, the percent elongation of a specimen after fracture can be measured by fitting the fractured specimen together and measuring the final elongation with calipers.

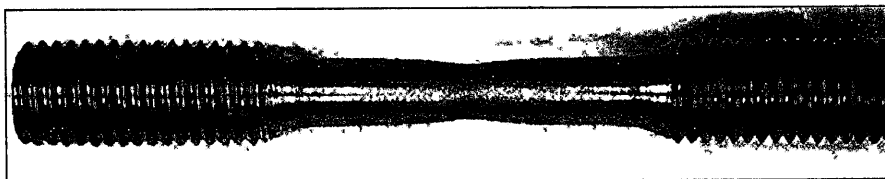
Figure 6.22
Necking in a mild-steel round specimen. The specimen was originally uniformly cylindrical. After being subjected to uniaxial tension forces up to almost fracture, the specimen decreased in cross section, or "necked" in the middle.

The percent elongation can then be calculated from the equation

$$\% \text{ elongation} = \frac{\text{final length* } - \text{ initial length*}}{\text{initial length}} \times 100\%$$

$$= \frac{l - l_0}{l_0} \times 100\% \quad \text{(6.10)}$$

Virtual Lab

The percent elongation at fracture is of engineering importance not only as a measure of ductility but also as an index of the quality of the metal. If porosity or inclusions are present in the metal or if damage due to overheating the metal has occurred, the percent elongation of the specimen tested may be decreased below normal.

Percent Reduction in Area The ductility of a metal or alloy can also be expressed in terms of the percent reduction in area. This quantity is usually obtained from a tensile test using a specimen 0.50 in. (12.7 mm) in diameter. After the test, the diameter of the reduced cross section at the fracture is measured. Using the measurements of the initial and final diameters, the percent reduction in area can be determined from the equation

$$\% \text{ reduction in area} = \frac{\text{initial area } - \text{ final area}}{\text{initial area}} \times 100\%$$

$$= \frac{A_0 - A_f}{A_0} \times 100\% \quad \text{(6.11)}$$

EXAMPLE PROBLEM 6.7

A 0.500-in.-diameter round sample of a 1030 carbon steel is pulled to failure in a tensile testing machine. The diameter of the sample was 0.343 in. at the fracture surface. Calculate the percent reduction in area of the sample.

■ **Solution**

$$\% \text{ reduction in area} = \frac{A_0 - A_f}{A_0} \times 100\% = \left(1 - \frac{A_f}{A_0}\right)(100\%)$$

$$= \left[1 - \frac{(\pi/4)(0.343 \text{ in.})^2}{(\pi/4)(0.500 \text{ in.})^2}\right](100\%)$$

$$= (1 - 0.47)(100\%) = 53\% \blacktriangleleft$$

The percent reduction in area, like the percent elongation, is a measure of the ductility of the metal and is also an index of quality. The percent reduction in area may be decreased if defects such as inclusions and/or porosity are present in the metal specimen.

---

*The initial length is the length between the gage marks on the specimen before testing. The final length is the length between these same gage marks after testing when the fractured surface of the specimen is fitted together (see Example Problem 6.6).

6.3.2 Comparison of Engineering Stress-Strain Curves for Selected Alloys

Engineering stress-strain curves for selected metals and alloys are shown in Fig. 6.23. Alloying a metal with other metals or nonmetals and heat treatment can greatly affect the tensile strength and ductility of metals. The stress-strain curves of Fig. 6.23 show a great variation in ultimate tensile strength. Elemental magnesium has a UTS of 35 ksi (1 ksi = 1000 psi), whereas SAE 1340 steel water-quenched and tempered at 700°F (370°C) has a UTS of 240 ksi.

6.3.3 True Stress and True Strain

The engineering stress is calculated by dividing the applied force F on a tensile test specimen by its original cross-sectional area A_0 (Eq. 6.3). Since the cross-sectional area of the test specimen changes continuously during a tensile test, the engineering stress calculated is not precise. During the tensile test, after necking of the sample occurs (Fig. 6.22), the engineering stress decreases as the strain increases, leading to a maximum engineering stress in the engineering stress-
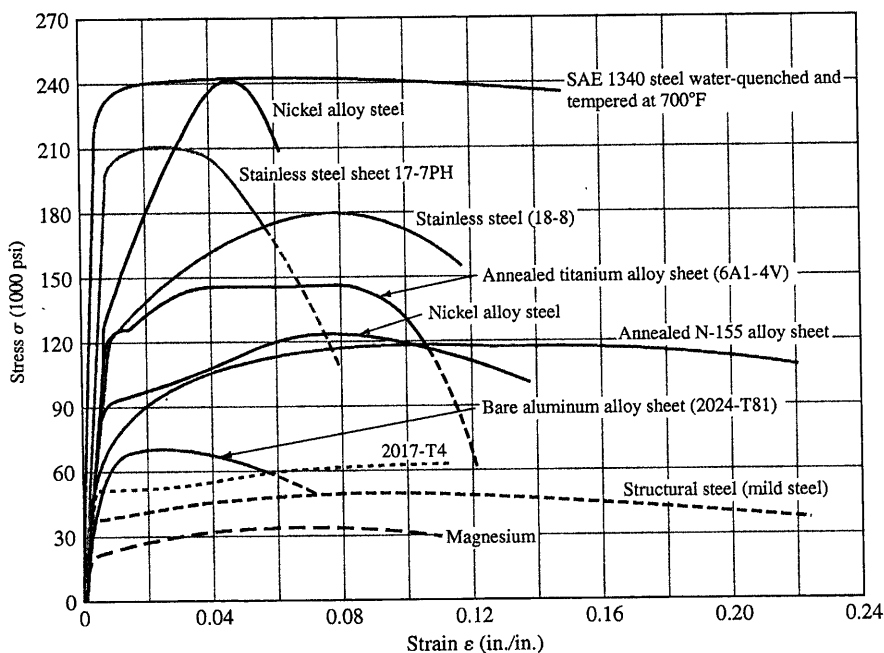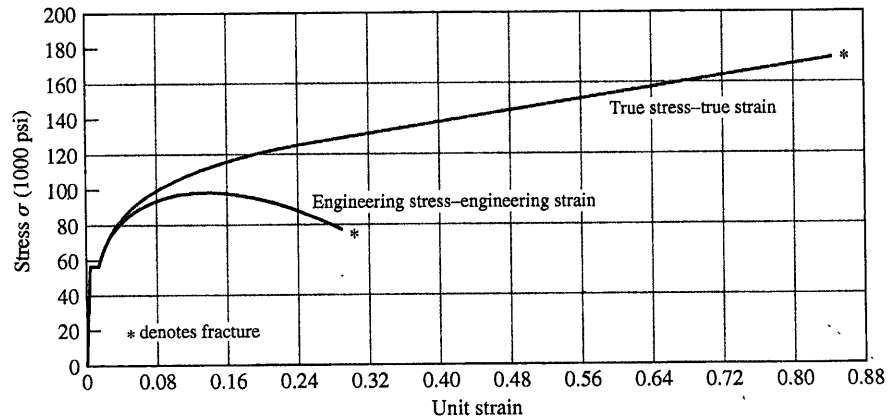

Figure 6.23
Engineering stress-strain curves for selected metals and alloys.
(*Marin, Mechanical Behavior of Engineering Materials, 1st ed., 1962. Adapted by permission of Pearson Education, Inc., Upper Saddle River, NJ.*)

Figure 6.24

Comparison of the true stress–true strain curve with the engineering (nominal) stress-strain diagram for a low-carbon steel.

(From H.E. McGannon (ed.), The Making, Shaping, and Treating of Steel, 9th ed., United States Steel, 1971. Courtesy of United States Steel Corporation.)

Virtual Lab

strain curve (Fig. 6.24). Thus, once necking begins during the tensile test, the true stress is higher than the engineering stress. We define the true stress and true strain by the following:

$$\text{True stress } \sigma_t = \frac{F \text{ (average uniaxial force on the test sample)}}{A_i \text{ (instantaneous minimum cross-sectional area of sample)}} \tag{6.12}$$

$$\text{True strain } \epsilon_t = \int_{l_0}^{l_i} \frac{dl}{l} = \ln \frac{l_i}{l_0} \tag{6.13}$$

where l_0 is the original gage length of the sample and l_i is the instantaneous extended gage length during the test. If we assume constant volume of the gage-length section of the test specimen during the test, then $l_0 A_0 = l_i A_i$ or

$$\frac{l_i}{l_0} = \frac{A_0}{A_i} \quad \text{and} \quad \epsilon_t = \ln \frac{l_i}{l_0} = \ln \frac{A_0}{A_i} \tag{6.14}$$

Figure 6.24 compares engineering stress-strain and true stress-strain curves for a low-carbon steel.

Engineering designs are not based on true stress at fracture since as soon as the yield strength is exceeded, the material starts to deform. Engineers use instead the 0.2 percent offset engineering yield stress for structural designs with the proper safety factors. However, for research, sometimes the true stress-strain curves are needed.

Compare the engineering stress and strain with the true test and strain for the tensile test of a low-carbon steel that has the following test values.

**EXAMPLE
PROBLEM 6.8**

Load applied to specimen = $17,000$ lb$_f$ Initial specimen diameter = 0.500 in.

        Diameter of specimen under $17,000$ lb$_f$ load = 0.472 in.

■ **Solution**

$$\text{Area at start } A_0 = \frac{\pi}{4}d^2 = \frac{\pi}{4}(0.500 \text{ in.})^2 = 0.196 \text{ in.}^2$$

$$\text{Area under load } A_i = \frac{\pi}{4}(0.472 \text{ in.})^2 = 0.175 \text{ in.}^2$$

Assuming no volume change during extension, $A_0 l_0 = A_i l_i$ or $l_i/l_0 = A_0/A_i$.

$$\text{Engineering stress} = \frac{F}{A_0} = \frac{17,000 \text{ lb}_f}{0.196 \text{ in.}^2} = 86,700 \text{ psi} \blacktriangleleft$$

$$\text{Engineering strain} = \frac{\Delta l}{l} = \frac{l_i - l_0}{l_0} = \frac{A_0}{A_i} - 1 = \frac{0.196 \text{ in.}^2}{0.175 \text{ in.}^2} - 1 = 0.12$$

$$\text{True stress} = \frac{F}{A_i} = \frac{17,000 \text{ lb}_f}{0.175 \text{ in.}^2} = 97,100 \text{ psi} \blacktriangleleft$$

$$\text{True strain} = \ln\frac{l_i}{l_0} = \ln\frac{A_0}{A_i} = \ln\frac{0.196 \text{ in.}^2}{0.175 \text{ in.}^2} = \ln 1.12 = 0.113$$

6.4 HARDNESS AND HARDNESS TESTING

Hardness is a measure of the resistance of a metal to permanent (plastic) deformation. The hardness of a metal is measured by forcing an indenter into its surface. The indenter material, which is usually a ball, pyramid, or cone, is made of a material much harder than the material being tested. For example, hardened steel, tungsten carbide, or diamond are commonly used materials for indenters. For most standard hardness tests a known load is applied slowly by pressing the indenter at 90° into the metal surface being tested [Fig. 6.25b (2)]. After the indentation has been made, the indenter is withdrawn from the surface [Fig. 6.25b (3)]. An empirical hardness number is then calculated or read off a dial (or digital display), which is based on the cross-sectional area or depth of the impression.

Table 6.2 lists the types of indenters and types of impressions associated with four common hardness tests: Brinell, Vickers, Knoop, and Rockwell. The hardness number for each of these tests depends on the shape of the indentation and the applied load. Figure 6.25 shows a modern Rockwell hardness tester, which has a digital readout display.

The hardness of a metal depends on the ease with which it plastically deforms. Thus a relationship between hardness and strength for a particular metal can be determined empirically. The hardness test is much simpler than the tensile test and can

Indenter

Surface of specimen

(1) Indenter above specimen surface

Load

t

(2) Indenter under set load penetrates specimen surface

t

(3) Indenter is removed from specimen surface leaving indentation.

(a)

(b)

Virtual Lab
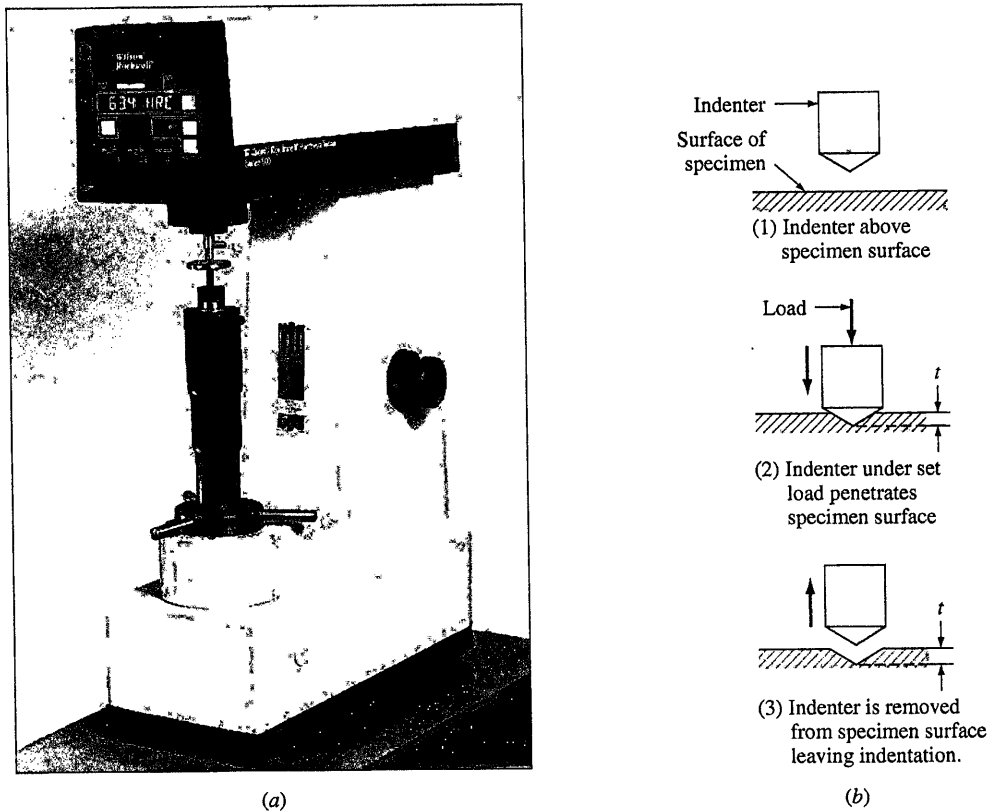
Figure 6.25
(a) A Rockwell hardness tester.
(*Courtesy of the Page-Wilson Co.*)
(b) Steps in the measurement of hardness with a diamond-cone indenter. The depth t determines the hardness of the material. The lower the value of t, the harder the material.

be nondestructive (i.e., the small indentation of the indenter may not be detrimental to the use of an object). For these reasons, the hardness test is used extensively in industry for quality control.

6.5 PLASTIC DEFORMATION OF METAL SINGLE CRYSTALS
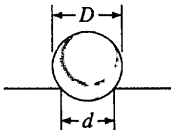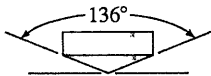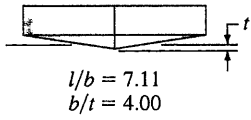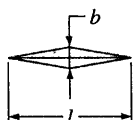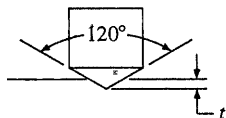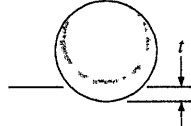
6.5.1 Slipbands and Slip Lines on the Surface of Metal Crystals

Let us first consider the permanent deformation of a rod of a zinc single crystal by stressing it beyond its elastic limit. An examination of the zinc crystal after the deformation shows that step markings appear on its surface, which are called

Table 6.2 Hardness tests

Test	Indenter	Shape of indentation		Load	Formula for hardness number
		Side view	Top view		
Brinell	10 mm sphere of steel or tungsten carbide			P	$BHN = \dfrac{2P}{\pi D(D - \sqrt{D^2 - d^2})}$
Vickers	Diamond pyramid	136°	d_1 d_1	P	$VHN = \dfrac{1.72P}{d_1^2}$
Knoop microhardness	Diamond pyramid	$l/b = 7.11$ $b/t = 4.00$	b l	P	$KHN = \dfrac{14.2P}{l^2}$
Rockwell A C D	Diamond cone	120°		60 kg $R_A =$ 150 kg $R_C =$ 100 kg $R_D =$	100–500f
B F G	$\frac{1}{16}$-in.-diameter steel sphere			100 kg $R_B =$ 60 kg $R_F =$ 150 kg $R_G =$ 100 kg $R_E =$	130–500f
E	$\frac{1}{8}$-in.-diameter steel sphere				

Source: After H.W. Hayden, W.G. Moffatt, and J. Wulff, "The Structure and Properties of Materials," vol. III, Wiley, 1965, p. 12.

slipbands (Fig. 6.26*a* and *b*). The slipbands are caused by the slip or shear deformation of metal atoms on specific crystallographic planes called *slip planes*. The deformed zinc single-crystal surface illustrates the formation of slipbands very clearly since **slip** in these crystals is restricted primarily to slip on the HCP basal planes (Fig. 6.26*c* and *d*).

In single crystals of ductile FCC metals like copper and aluminum, slip occurs on multiple slip planes, and as a result the slipband pattern on the surface of these metals when they are deformed is more uniform (Fig. 6.27). A closer examination of the slipped surface of metals at high magnification shows that slip has occurred
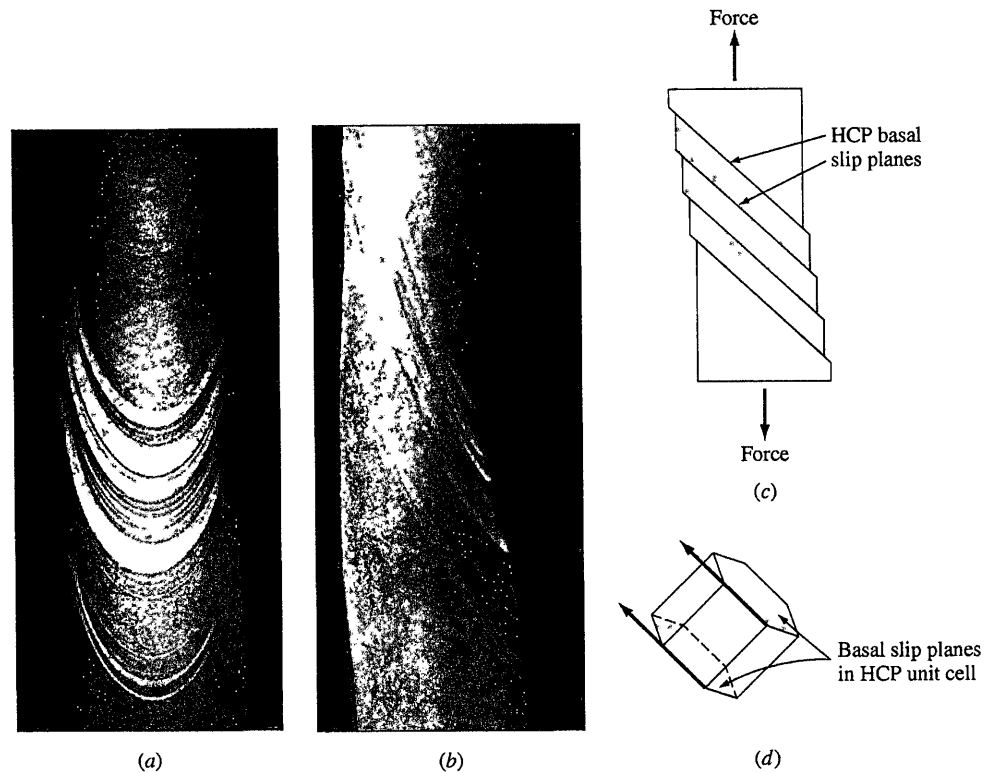
Figure 6.26
Plastically deformed zinc single crystal showing slipbands: (*a*) front view of real crystal, (*b*) side view of real crystal, (*c*) schematic side view indicating HCP basal slip planes in crystal, and (*d*) HCP unit cell indicating basal slip planes.
(*Zinc single-crystal photos courtesy of Prof. Earl Parker of the University of California at Berkeley.*)

on many slip planes within the slipbands (Fig. 6.28). These fine steps are called *slip lines* and are usually about 50 to 500 atoms apart, whereas slipbands are commonly separated by about 10,000 atom diameters. Unfortunately, the terms "slipband" and "slip line" are often used interchangeably.

6.5.2 Plastic Deformation in Metal Crystals by the Slip Mechanism

Figure 6.29 shows a possible atomic model for the slippage of one block of atoms over another in a perfect metal crystal. Calculations made from this model determine that the strength of metal crystals should be about 1000 to 10,000 times greater than their observed shear strengths. Thus, this mechanism for atomic slip in large real metal crystals must be incorrect.

6.5 Plastic Deformation of Metal Single Crystals

243
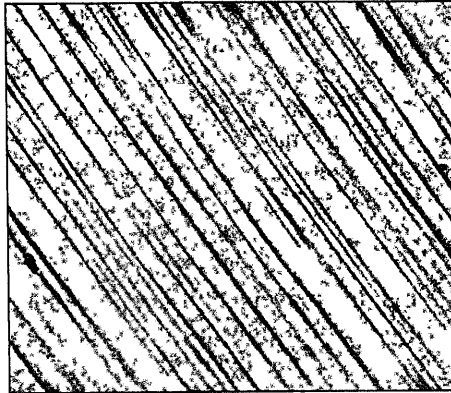
Figure 6.27
Slipband pattern on surface of copper
single crystal after 0.9 percent
deformation. (Magnification 100×.)
[*After F.D. Rosi. Trans. AIME,* **200:***1018 (1954).*]

(a)   *(b)*   *(c)*
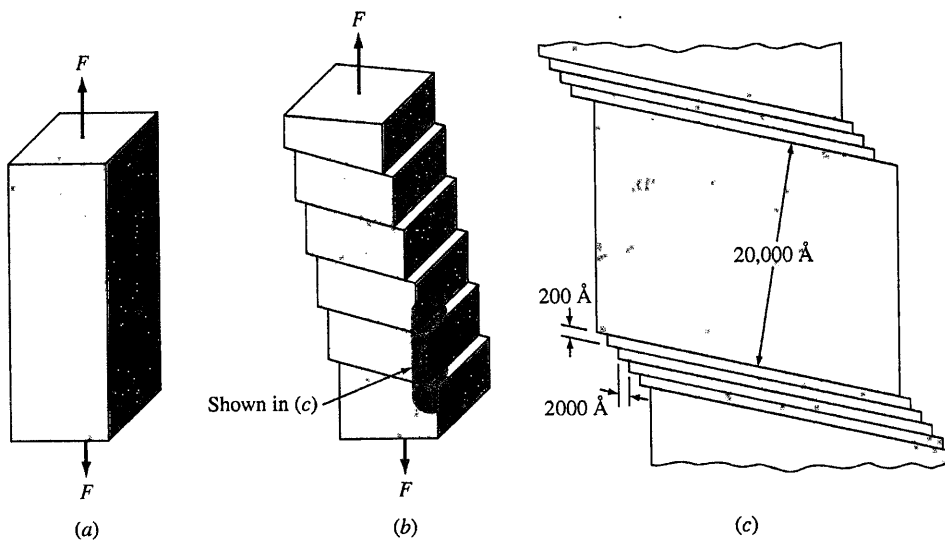
Figure 6.28
The formation of slipbands during plastic deformation. (*a*) A single crystal under a
tensile force. (*b*) Slipbands appear when the applied stress exceeds the yield stress.
Blocks of crystal slide past each other. (*c*) The shaded region of (*b*) has been
magnified. Slip occurs on a large number of closely packed slip planes that are parallel.
This region is called a *slipband* and appears as a line at lower magnification.

Animation

(*Eisenstadt, M., "Introduction to Mechanical Properties of Materials: An Ecological Approach," 1st ed.,
1971. Reprinted by permission of Pearson Education, Inc., Upper Saddle River, NJ.*)

244   **CHAPTER 6**   Mechanical Properties of Metals I

In order for large metal crystals to deform at their observed low shear strengths, a high density of crystalline imperfections known as *dislocations* must be present. These dislocations are created in large numbers ($\sim 10^6$ cm/cm^3) as the metal solidifies, and when the metal crystal is deformed, many more are created so that a highly deformed crystal may contain as high as 10^{12} cm/cm^3 of dislocations. Figure 6.30 shows schematically how an *edge dislocation* can produce a unit of slip under a low *shear stress*. A relatively small amount of stress is required for slip by this process since only a small group of atoms slips over each other at any instant.

An analogous situation to the movement of a dislocation in a metal crystal under a shear stress can be envisaged by the movement of a carpet with a ripple in it across a very large floor. Moving the carpet by pulling on one end may be impossible because of the friction between the floor and the carpet. However, by putting a ripple in the carpet (analogous to a dislocation in a metal crystal), the carpet may be moved by pushing the ripple in the carpet one step at a time across the floor (Fig. 6.30*d*).

Dislocations in real crystals can be observed in the transmission electron microscope in thin metal foils and appear as lines due to the atomic disarray at the dislocations that interfere with the transmission path of the electron beam of the microscope. Figure 6.31 shows a cellular wall pattern of dislocations created by lightly deforming an aluminum sample. The cells are relatively free from dislocations but are separated by walls of high dislocation density.

6.5.3 Slip Systems

Dislocations produce atomic displacements on specific crystallographic slip planes and in specific crystallographic slip directions. The slip planes are usually the most densely packed planes, which are also the farthest separated. Slip is favored on close-packed planes since a lower shear stress for atomic displacement is required than for
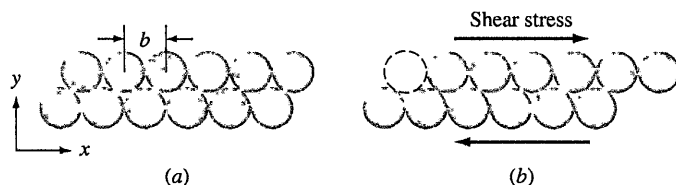
Figure 6.29
Large groups of atoms in large metal crystals do *not* slide over each other simultaneously during plastic shear deformation, as indicated in this figure, since the process requires too much energy. A lower-energy process involving the slippage of a small group of atoms takes place instead.

Interleaved atomic plane

1   2

Edge
dislocation
line

⊥

(a) An edge dislocation, pictured as formed
by an extra half plane of atoms.

Shear stress

1   2

x

⊥

←— *d* —→

(b) A low stress causes a shift of atomic bonds
to free a new interleaved plane.

Shear stress

Unit step
of slip

(c) Repetition of this process causes the
dislocation to move across the crystal.

"Ripple in rug" is analogous to
an edge dislocation in a metal crystal

Force

Rug on floor   Edge dislocation

(d)
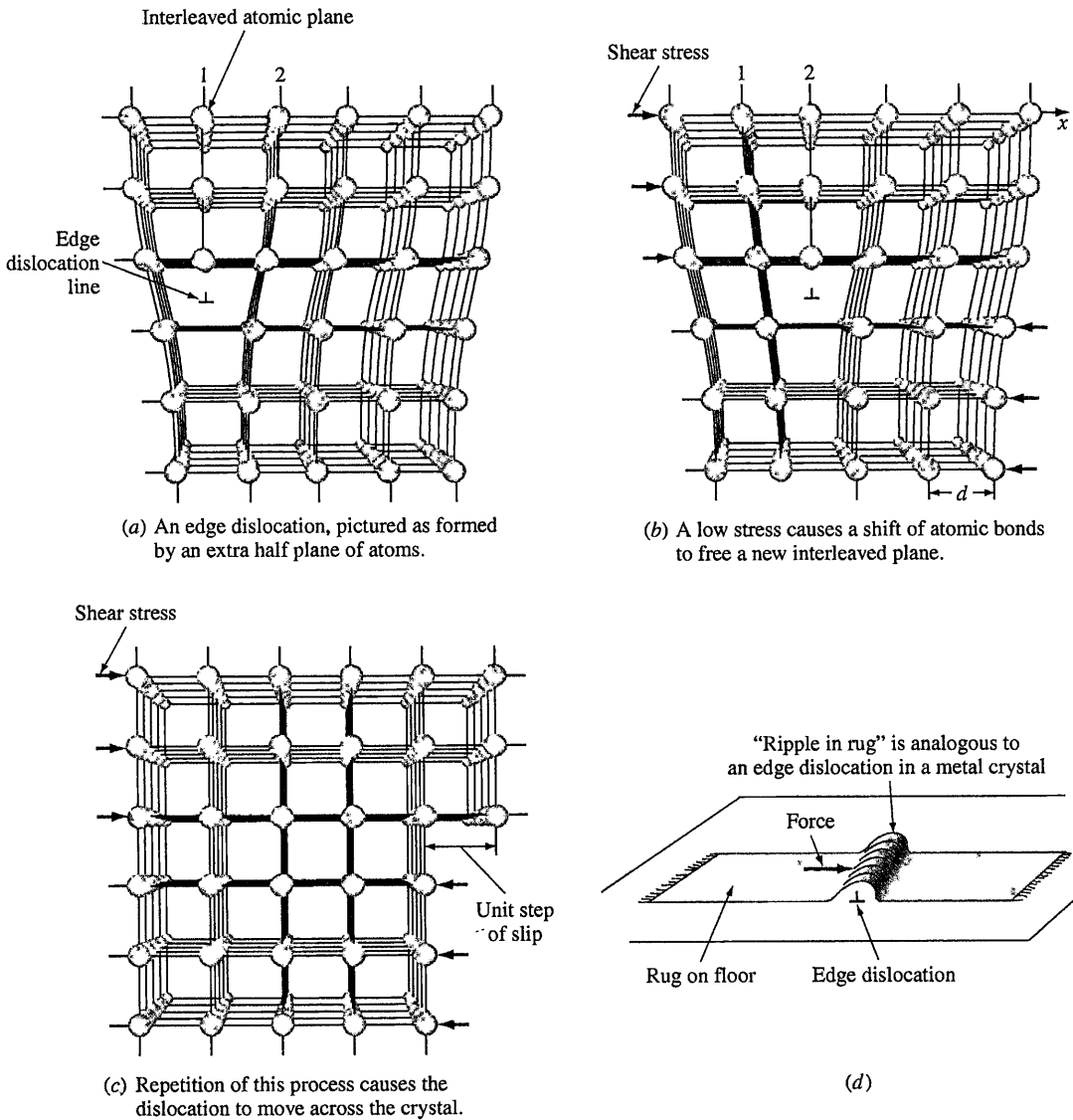
Figure 6.30

Schematic illustration of how the motion of an edge dislocation produces a unit step of slip under
a low shear stress. (a) An edge dislocation, pictured as formed by an extra half plane of atoms.
(b) A low stress causes a shift of atomic bonds to free a new interleaved plane. (c) Repetition of
this process causes the dislocation to move across the crystal. This process requires less energy
than the one depicted in Fig. 6.28.

Animation

(From A.G. Guy, "Essentials of Materials Science," McGraw-Hill, 1976, p. 153.)

(d) The "ripple in the rug" analogy. A dislocation moves through a metal crystal during plastic
deformation in a manner similar to a ripple that is pushed along a carpet lying on a floor. In both
cases, a small amount of relative movement is caused by the passage of the dislocation or ripple,
and hence a relatively low amount of energy is expended in this process.
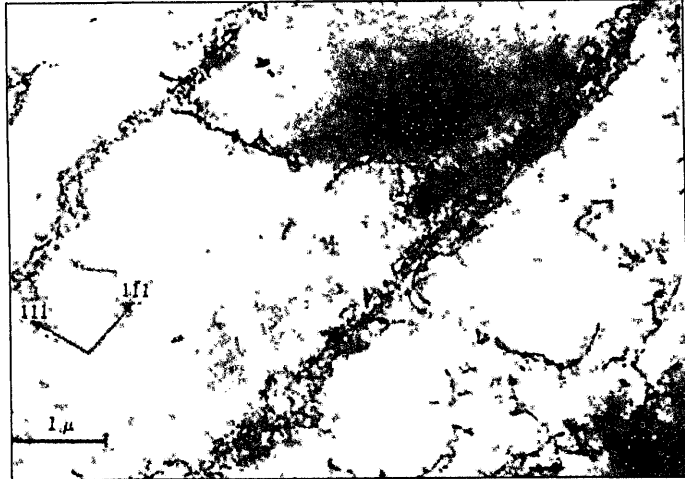
Figure 6.31
Dislocation cell structure in a lightly deformed aluminum sample as revealed by transmission electron microscopy. The cells are relatively free from dislocations but are separated by walls of high dislocation density.
(After P.R. Swann, in G. Thomas and J. Washburn, [eds.], "Electron Microscopy and Strength of Crystals," Wiley, 1963, p. 133.)

(a)

(b)
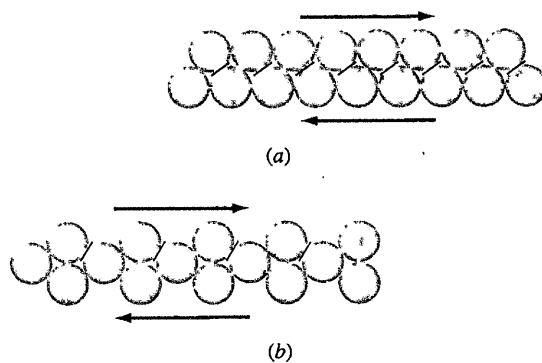
Figure 6.32
Comparison of atomic slip on (a) a close-packed plane and (b) a non–close-packed plane. Slip is favored on the close-packed plane because less force is required to move the atoms from one position to the next closest one, as indicated by the slopes of the bars on the atoms. Note that dislocations move one atomic slip step at a time.
(From A.H. Cottrell, The Nature of Metals, "Materials," Scientific American, September 1967, p. 48. Illustration © Enid Kotschnig. Reproduced by permission of Enid Kotschnig.)

less densely packed planes (Fig. 6.32). However, if slip on the close-packed planes is restricted due to local high stresses, for example, then planes of lower atomic packing can become operative. Slip in the close-packed directions is also favored since less energy is required to move the atoms from one position to another if the atoms are closer together.

A combination of a slip plane and a slip direction is called a **slip system.** Slip in metallic structures occurs on a number of slip systems that are characteristic for each crystal structure. Table 6.3 lists the predominant slip planes and slip directions for FCC, BCC, and HCP crystal structures.
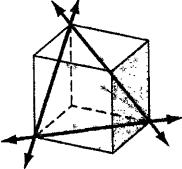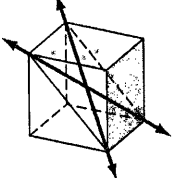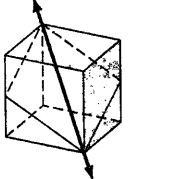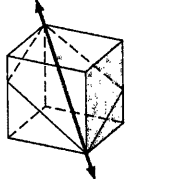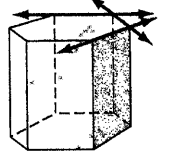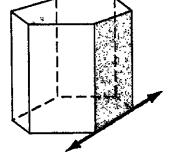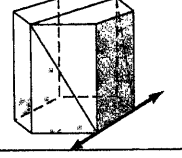
For metals with the FCC crystal structure, slip takes place on the close-packed {111} octahedral planes and in the ⟨1̄10⟩ close-packed directions. There are eight {111} octahedral planes in the FCC crystal structure (Fig. 6.33). The (111) type planes at opposite faces of the octahedron that are parallel to each other are considered the same type of (111) slip plane. Thus, there are only four different types of (111) slip planes in the FCC crystal structure. Each (111)-type plane contains three [1̄10]-type slip directions. The reverse directions are not considered different slip directions. Thus, for the FCC lattice there are 4 slip planes × 3 slip directions = 12 slip systems (Table 6.3).

The BCC structure is *not* a close-packed structure and does not have a predominant plane of highest atomic packing like the FCC structure. The {110} planes

(a)

(b)
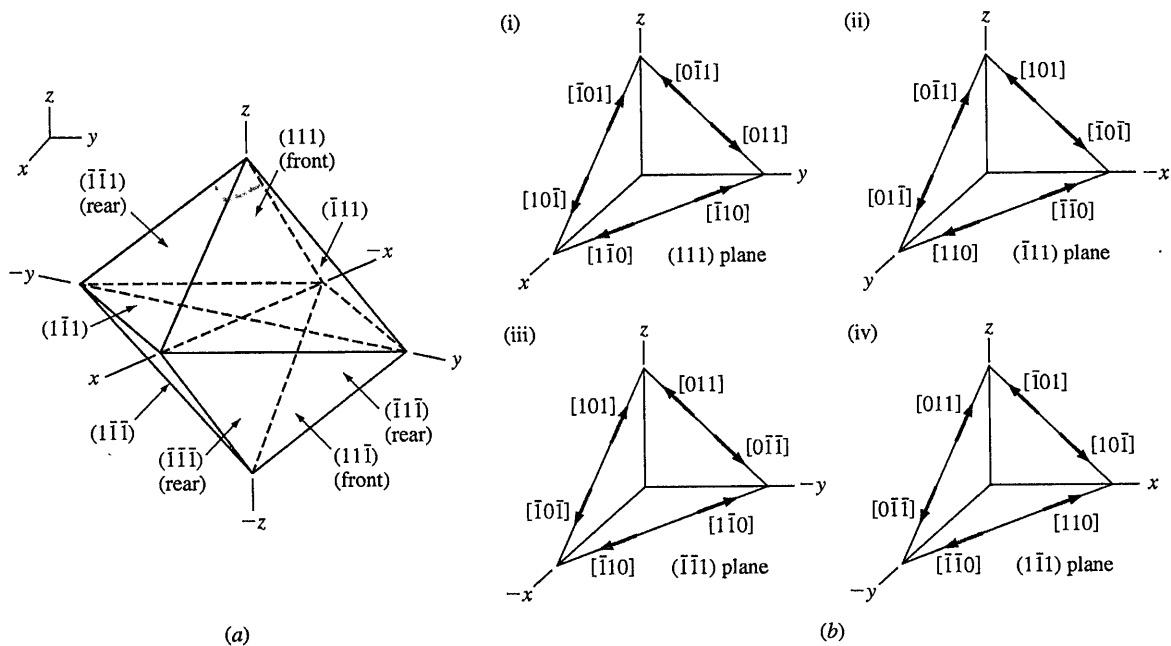
Figure 6.33

Slip planes and directions for the FCC crystal structure. (a) Only four of the eight {111} octahedral planes are considered slip planes since planes opposite each other are considered the same slip plane. (b) For each slip plane there are three ⟨1̄10⟩ slip directions since opposite directions are considered as only one slip direction. Note that slip directions are only shown for the upper four slip planes of the octahedral FCC planes. Thus, there are 4 slip planes × 3 slip directions, giving a total of 12 slip systems for the FCC crystal structure.

Table 6.3 Slip systems observed in crystal structures

Structure	Slip plane	Slip direction	Number of slip systems	
FCC: Cu, Al, Ni, Pb, Au, Ag, γFe, . . .	{111}	$\langle 1\bar{1}0 \rangle$	$4 \times 3 = 12$	
BCC: αFe, W, Mo, β brass	{110}	$\langle \bar{1}11 \rangle$	$6 \times 2 = 12$	
αFe, Mo, W, Na	{211}	$\langle \bar{1}11 \rangle$	$12 \times 1 = 12$	
αFe, K	{321}	$\langle \bar{1}11 \rangle$	$24 \times 1 = 24$	
HCP: Cd, Zn, Mg, Ti, Be, . . .	{0001}	$\langle 11\bar{2}0 \rangle$	$1 \times 3 = 3$	
Ti (prism planes)	{10$\bar{1}$0}	$\langle 11\bar{2}0 \rangle$	$3 \times 1 = 3$	
Ti, Mg (pyramidal planes)	{10$\bar{1}$1}	$\langle 11\bar{2}0 \rangle$	$6 \times 1 = 6$	

Source: After H.W. Hayden, W.G. Moffatt, and J. Wulff, "The Structure and Properties of Materials," vol. III, Wiley, 1965, p. 100.

have the highest atomic density, and slip commonly takes place on these planes. However, slip in BCC metals also occurs on {112} and {123} planes. Since the slip planes in the BCC structure are not close-packed as in the case of the FCC structure, higher shear stresses are necessary for slip in BCC than in FCC metals. The slip direction in BCC metals is always of the $\langle \bar{1}11\rangle$ type. Since there are six (110)-type slip planes of which each can slip in two [$\bar{1}11$] directions, there are $6 \times 2 = 12$ {110}$\langle \bar{1}11\rangle$ slip systems.

In the HCP structure, the basal plane (0001) is the closest-packed plane and is the common slip plane for HCP metals such as Zn, Cd, and Mg that have high c/a ratios (Table 6.3). However, for HCP metals such as Ti, Zr, and Be that have low c/a ratios, slip also occurs commonly on prism {10$\bar{1}$0} and pyramidal {10$\bar{1}$1} planes. In all cases, the slip direction remains $\langle 11\bar{2}0\rangle$. The limited number of slip systems in HCP metals restricts their ductilities.

6.5.4 Critical Resolved Shear Stress for Metal Single Crystals

The stress required to cause slip in a pure-metal single crystal depends mainly on the crystal structure of the metal, its atomic bonding characteristics, the temperature at which it is deformed, and the orientation of the active slip planes with respect to the shear stresses. Slip begins within the crystal when the shear stress on the slip plane in the slip direction reaches a required level called the *critical resolved shear stress, τ_c.* Essentially, this value is the yield stress of a single crystal and is equivalent to the yield stress of a polycrystalline metal or alloy determined by a stress-strain tensile test curve.

Table 6.4 lists values for the critical resolved shear stresses of some pure-metal single crystals at room temperature. The HCP metals Zn, Cd, and Mg have low critical resolved shear stresses ranging from 0.18 to 0.77 MPa. The HCP metal titanium,

Table 6.4 Room-temperature slip systems and critical resolved shear stress for metal single crystals

Metal	Crystal structure	Purity (%)	Slip plane	Slip direction	Critical shear stress (MPa)
Zn	HCP	99.999	(0001)	[11$\bar{2}$0]	0.18
Mg	HCP	99.996	(0001)	[11$\bar{2}$0]	0.77
Cd	HCP	99.996	(0001)	[11$\bar{2}$0]	0.58
Ti	HCP	99.99	(1010)	[11$\bar{2}$0]	13.7
		99.9	(1010)	[11$\bar{2}$0]	90.1
Ag	FCC	99.99	(111)	[1$\bar{1}$0]	0.48
		99.97	(111)	[1$\bar{1}$0]	0.73
		99.93	(111)	[1$\bar{1}$0]	1.3
Cu	FCC	99.999	(111)	[1$\bar{1}$0]	0.65
		99.98	(111)	[1$\bar{1}$0]	0.94
Ni	FCC	99.8	(111)	[1$\bar{1}$0]	5.7
Fe	BCC	99.96	(110)	[$\bar{1}$11]	27.5
			(112)		
			(123)		
Mo	BCC	. . .	(110)	[$\bar{1}$11]	49.0

Source: After G. Dieter, "Mechanical Metallurgy," 2nd ed., McGraw-Hill, 1976, p. 129.

on the other hand, has a very high τ_c of 13.7 MPa. It is believed that some covalent bonding mixed with metallic bonding is partly responsible for this high value of τ_c. Pure FCC metals such as Ag and Cu have low τ_c values of 0.48 and 0.65 MPa, respectively, because of their multiple slip systems.

6.5.5 Schmid's Law

The relationship between a uniaxial stress acting on a cylinder of a pure metal single crystal and the resulting resolved shear stress produced on a slip system within the cylinder can be derived as follows. Consider a uniaxial tensile stress σ acting on a metal cylinder, as shown in Fig. 6.34. Let A_0 be the area normal to the axial force F, and A_1 the area of the slip plane or shear area on which the resolved shear force F_r is acting. We can orient the slip plane and slip direction by defining the angles ϕ and λ. ϕ is the angle between the uniaxial force F and the normal to the slip plane area A_1, and λ is the angle between the axial force and the slip direction.

In order for dislocations to move in the slip system, a sufficient resolved shear stress acting in the slip direction must be produced by the applied axial force. The resolved shear stress is

$$\tau_r = \frac{\text{shear force}}{\text{shear area (slip plane area)}} = \frac{F_r}{A_1} \qquad (6.15)$$
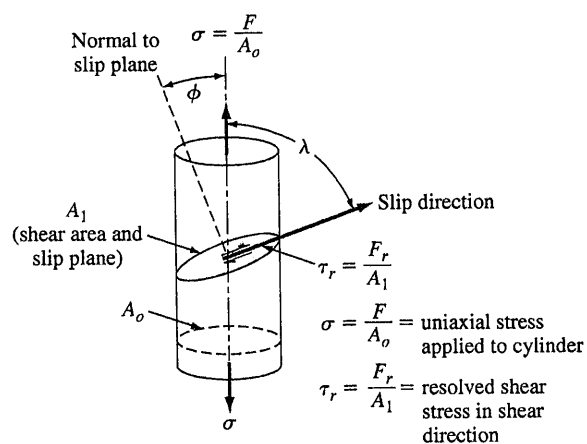
Figure 6.34
Axial stress σ can produce a resolved shear stress τ_r and cause dislocation motion in slip plane A_1 in the slip direction.

6.5 Plastic Deformation of Metal Single Crystals   **251**

The resolved shear force F_r is related to the axial force F by $F_r = F \cos \lambda$. The area of the slip plane (shear area) $A_1 = A_0/\cos \phi$. By dividing the shear force $F \cos \lambda$ by the shear area $A_0/\cos \phi$, we obtain

$$\tau_r = \frac{F \cos \lambda}{A_0/\cos \phi} = \frac{F}{A_0} \cos \lambda \cos \phi = \sigma \cos \lambda \cos \phi \qquad (6.16)$$

which is called *Schmid's law.* Let us now consider an example problem to calculate the resolved shear stress when a slip system is acted upon by an axial stress.

Calculate the resolved shear stress on the (111) [0$\bar{1}$1] slip system of a unit cell in an FCC nickel single crystal if a stress of 13.7 MPa is applied in the [001] direction of a unit cell.

**EXAMPLE
PROBLEM 6.9**

■ Solution

By geometry, the angle λ between the applied stress and the slip direction is 45°, as shown in Fig. EP6.9a. In the cubic system, the direction indices of the normal to a crystal plane are the same as the Miller indices of the crystal plane. Therefore, the normal to the (111) plane that is the slip plane is the [111] direction. From Fig. EP6.9b,

$$\cos \phi = \frac{a}{\sqrt{3}a} = \frac{1}{\sqrt{3}} \quad \text{or} \quad \phi = 54.74°$$

$$\tau_r = \sigma \cos \lambda \cos \phi = (13.7 \, \text{MPa})(\cos 45°)(\cos 54.74°) = 5.6 \, \text{MPa} \blacktriangleleft$$

(a)   (b)
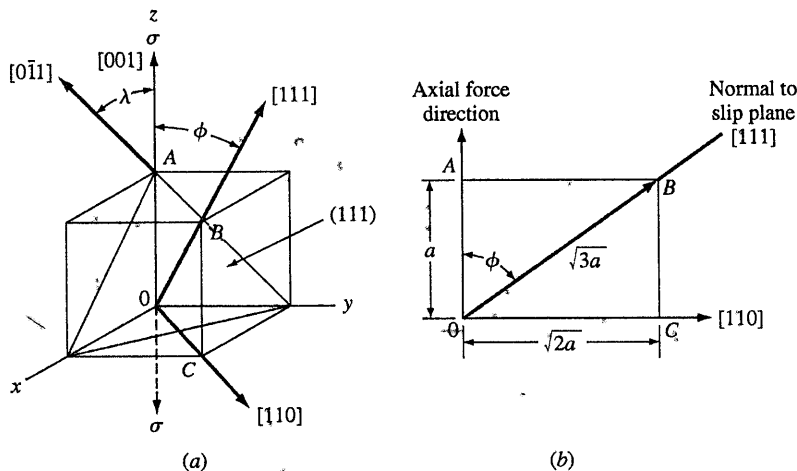
Figure EP6.9
An FCC unit cell is acted upon by a [001] tensile stress producing a resolved shear stress on the (111) [0$\bar{1}$1] slip system.

6.5.6 Twinning

A second important plastic deformation mechanism that can occur in metals is **twinning.** In this process a part of the atomic lattice is deformed so that it forms a mirror image of the undeformed lattice next to it (Fig. 6.35). The crystallographic plane of symmetry between the undeformed and deformed parts of the metal lattice is called the *twinning plane*. Twinning, like slip, occurs in a specific direction called the *twinning direction*. However, in slip the atoms on one side of the slip plane all move equal distances (Fig. 6.30), whereas in twinning the atoms move distances proportional to their distance from the twinning plane (Fig. 6.35). Figure 6.36 illustrates the basic difference between slip and twinning on the surface of a metal after deformation. Slip leaves a series of steps (lines) (Fig. 6.36*a*), whereas twinning leaves small but well-defined regions of the crystal deformed (Fig. 6.36*b*). Figure 6.37 shows some deformation twins on the surface of titanium metal.

Virtual Lab

Twinning only involves a small fraction of the total volume of the metal crystal, and so the amount of overall deformation that can be produced by twinning is small. However, the important role of twinning in deformation is that the lattice orientation changes that are caused by twinning may place new slip systems into favorable orientation with respect to the shear stress and thus enable additional slip to occur. Of the three major metallic unit-cell structures (BCC, FCC, and HCP), twinning is most important for the HCP structure because of its small number of slip systems. However, even with the assistance of twinning, HCP metals like zinc and magnesium are still less ductile than the BCC and FCC metals that have more slip systems.
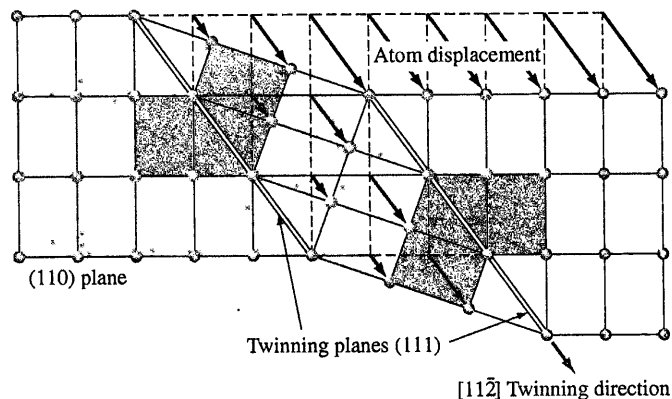
Figure 6.35
Schematic diagram of the twinning process in an FCC lattice.
(From H.W. Hayden, W.G. Moffatt and J. Wulff, "The Structure and Properties of Materials," vol. III, Wiley, 1965, p. 111.)

6.5 Plastic Deformation of Metal Single Crystals

253
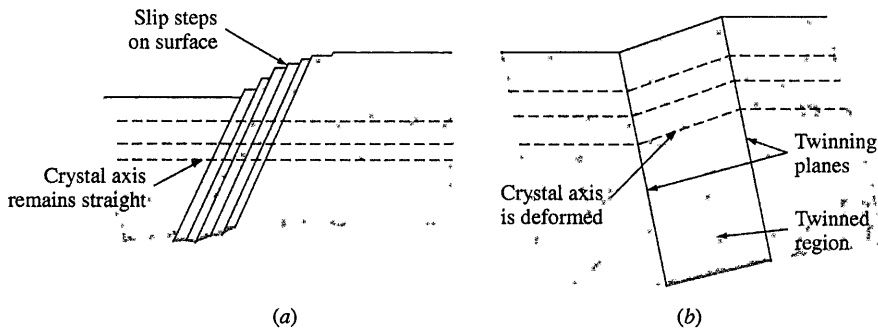
Figure 6.36
Schematic diagram of surfaces of a deformed metal after (a) slip and (b) twinning.
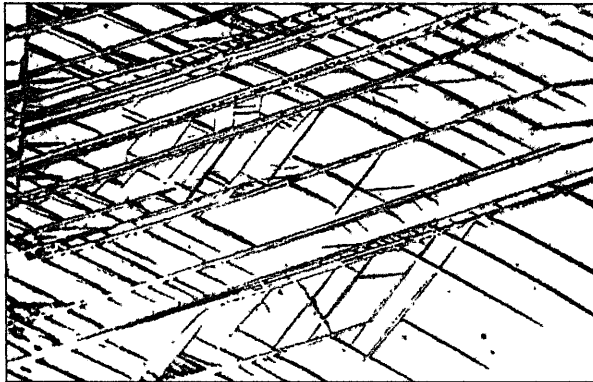
Figure 6.37
Deformation twins in unalloyed (99.77%) titanium.
(Magnification 150×.)
[After F.D. Rosi, C.A. Dube, and B.H. Alexander, Trans. AIME, 197:259 (1953).]

Deformation twinning is observed at room temperature for the HCP metals. Twinning is found in the BCC metals such as Fe, Mo, W, Ta, and Cr in crystals that were deformed at very low temperatures. Twinning has also been found in some of these BCC metal crystals at room temperature when they have been subjected to very high strain rates. The FCC metals show the least tendency to form deformation twins. However, deformation twins can be produced in some FCC metals if the stress level is high enough and the temperature sufficiently low. For example, copper crystals deformed at 4 K at high stress levels can form deformation twins.

6.6 PLASTIC DEFORMATION OF POLYCRYSTALLINE METALS

6.6.1 Effect of Grain Boundaries on the Strength of Metals

Almost all engineering alloys are polycrystalline. Single-crystal metals and alloys are used mainly for research purposes and only in a few cases for engineering applications.[8] Grain boundaries strengthen metals and alloys by acting as barriers to dislocation movement except at high temperatures, where they become regions of weakness. For most applications where strength is important, a fine grain size is desirable, and so most metals are fabricated with a fine grain size. In general, at room temperature, fine-grained metals are stronger, harder, tougher, and more susceptible to strain hardening. However, they are less resistant to corrosion and creep (deformation under constant load at elevated temperatures; see Sec. 7.4). A fine grain size also results in a more uniform and isotropic behavior of materials. In Sec. 4.5, the ASTM grain size number and a method to determine the average grain diameter of a metal using metallography techniques were discussed. These parameters allow us to make a relative comparison of grain density and therefore grain boundary density in metals. Accordingly, for two components made of the same alloy, the component that has a larger ASTM grain size number or a smaller average grain diameter is stronger. The relationship between strength and grain size is of great importance to engineers. The well known *Hall–Petch equation,* Eq. 6.16, is an empirical (based on experimental measurements and not on theory) equation that relates the yield strength of a metal, σ_y, to its average grain diameter d as follows:

$$\sigma_y = \sigma_0 + k/(d)^{1/2} \qquad (6.17)$$

where σ_0 and k are constants related to the material of interest. A similar effect exists between hardness (Vickers microhardness test) and grain size. The equation clearly shows that as grain diameter decreases, the yield strength of the material increases. Considering that the conventional grain diameters may range from a few hundred microns to a few microns, one may expect a significant change in strength through grain refinement. The values for σ_0 and k for selected materials are given in Table 6.5. It is important to note that the Hall–Petch equation does not apply to (1) extremely coarse or extremely fine grain sizes and (2) metals used at elevated temperatures.

Figure 6.38 compares the tensile stress-strain curves for single-crystal and polycrystalline unalloyed copper at room temperature. At all strains, the polycrystalline copper is stronger than the single-crystal copper. At 20 percent strain, the tensile strength of the polycrystalline copper is 40 ksi (276 MPa) as compared to 8 ksi (55 MPa) for single-crystal copper.

---

[8]Single-crystal turbine blades have been developed for use in gas turbine engines to avoid grain boundary cracking at high temperatures and stresses. See F.L. Ver Snyder and M.E. Shank, *Mater. Sci. Eng.,* **6:**213–247(1970).

Table 6.5 Hall–Petch relationship constants for selected materials

	σ_0 (MPa)	k (MPa·m$^{1/2}$)
Cu	25	0.11
Ti	80	0.40
Mild steel	70	0.74
Ni$_3$Al	300	1.70

Source: www.tf.uni-kiel.de/matwis/matv/pdf/chap_3_3.pdf
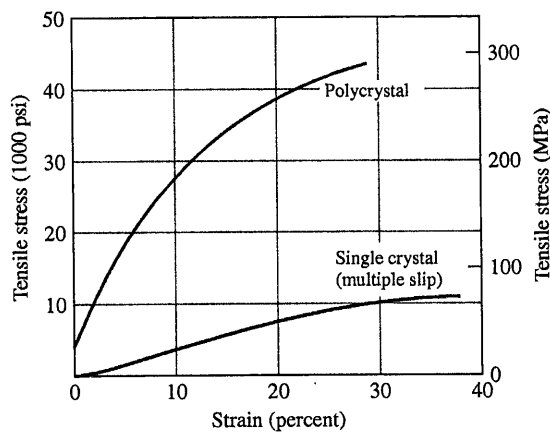
Figure 6.38
Stress-strain curves for single-crystal and polycrystalline copper. The single crystal is oriented for multiple slip. The polycrystal shows higher strength at all strains.
(*After M. Eisenstadt, "Introduction to Mechanical Properties of Materials," Macmillan, 1971, p. 258.*)

During the plastic deformation of metals, dislocations moving along on a particular slip plane cannot go directly from one grain into another in a straight line. As shown in Fig. 6.39, slip lines change directions at grain boundaries. Thus, each grain has its own set of dislocations on its own preferred slip planes, which have different orientations from those of neighboring grains. As the number of grains increases and grain diameter becomes smaller, dislocations within each grain can travel a smaller distance before they encounter the grain boundary, at which point their movement is terminated (dislocation pileup). It is for this reason that
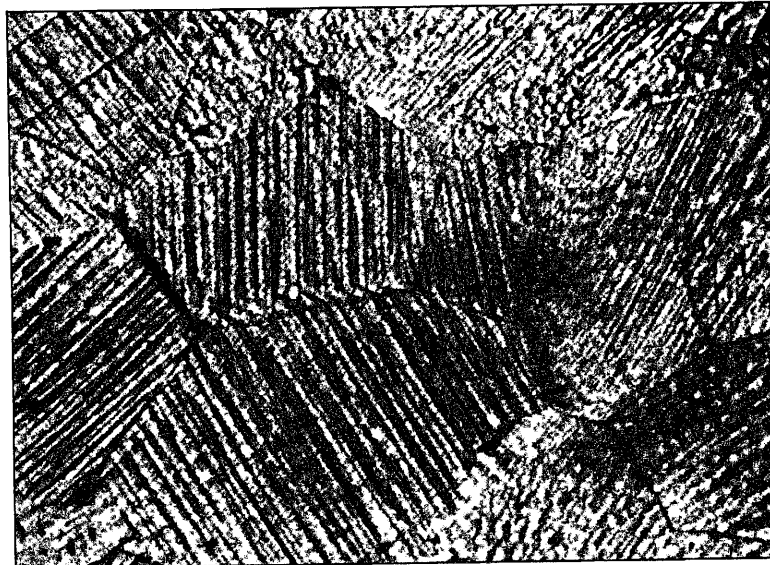
Figure 6.39
Polycrystalline aluminum that has been plastically deformed. Note that
the slipbands are parallel within a grain but are discontinuous across
the grain boundaries. (Magnification 60×.)
(*After G.C. Smith, S. Charter, and S. Chiderley of Cambridge University.*)

fine-grained materials possess a higher strength. Figure 6.40 shows clearly a high-angle grain boundary that is acting as a barrier to dislocation movement and has caused dislocations to pile up at the grain boundary.

6.6.2 Effect of Plastic Deformation on Grain Shape and Dislocation Arrangements

Grain Shape Changes with Plastic Deformation Let us consider the plastic deformation of annealed samples[9] of unalloyed copper that have an equiaxed grain structure. Upon cold plastic deformation, the grains are sheared relative to each other by the generation, movement, and rearrangement of dislocations. Figure 6.41 shows the microstructures of samples of unalloyed copper sheet that was cold-rolled to reductions of 30 and 50 percent. Note that with increased cold rolling the grains are more elongated in the rolling direction as a consequence of dislocation movements.

---

[9]Samples in the annealed conditions have been plastically deformed and then reheated to such an extent that a grain structure in which the grains are approximately equal in all directions (equiaxed) is produced.
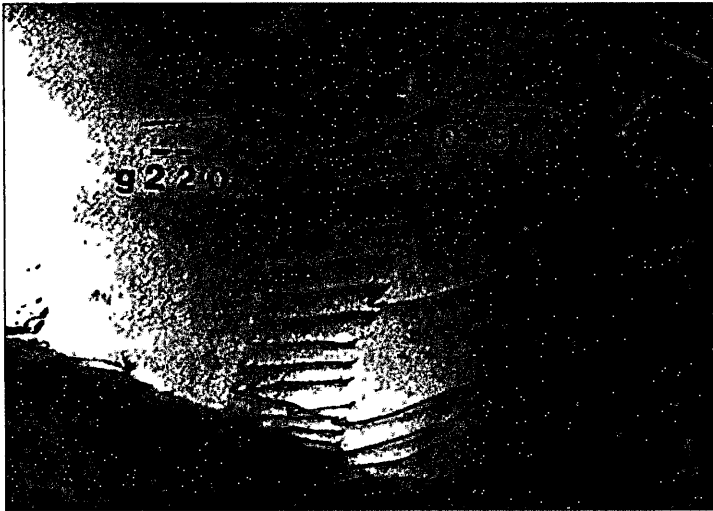
Figure 6.40
Dislocations piled up against a grain boundary as observed with a
transmission electron microscope in a thin foil of stainless steel.
(Magnification 20,000×.)
[*After Z. Shen, R.H. Wagoner, and W.A.T. Clark, Scripta Met., 20: 926 (1986).*]
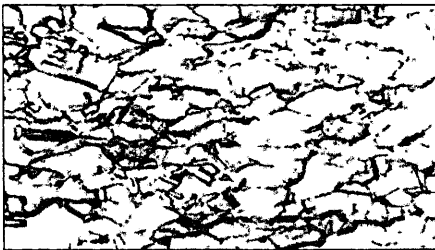
(*a*)

(*b*)

Figure 6.41
Optical micrographs of deformation structures of unalloyed copper that was cold-rolled
to reductions of (*a*) 30 percent and (*b*) 50 percent. (Etch: potassium dichromate;
magnification 300×.)
(*After J.E. Boyd in "Metals Handbook," vol. 8: "Metallography, Structures, and Phase Diagrams," 8th ed.,
American Society for Metals, 1973, p. 221. Reprinted with permission from ASM International. All rights
reserved. www.asminternational.org.*)

Dislocation Arrangement Changes with Plastic Deformation   The dislocations in
the unalloyed copper sample after 30 percent plastic deformation form cell-like con-
figurations with clear areas in the centers of the cells (Fig. 6.42*a*). With increased

258   **CHAPTER 6** Mechanical Properties of Metals I

(a)   (b)
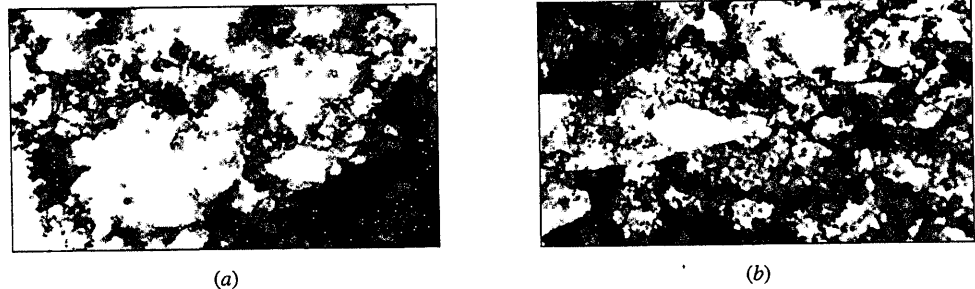
Figure 6.42
Transmission electron micrographs of deformation structures of unalloyed copper that
was cold-rolled to reductions of (a) 30 percent and (b) 50 percent. Note that these
electron micrographs correspond to the optical micrographs of Fig. 6.41. (Thin-foil
specimens, magnification 30,000×.)
*(After J.E. Boyd in "Metals Handbook," vol. 8: "Metallography, Structures, and Phase Diagrams," 8th ed.,
American Society for Metals, 1973, p. 221. Reprinted with permission from ASM International. All rights
reserved. www.asminternational.org.)*

cold plastic deformation to 50 percent reduction, the cell structure becomes denser
and elongated in the direction of rolling (Fig. 6.42b).

6.6.3 Effect of Cold Plastic Deformation on Increasing the Strength of Metals

As shown by the electron micrographs of Fig. 6.42, the dislocation density increases
with increased cold deformation. The exact mechanism by which the dislocation den-
sity is increased by cold working is not completely understood. New dislocations are
created by the cold deformation and must interact with those already existing. As
the dislocation density increases with deformation, it becomes more and more diffi-
cult for the dislocations to move through the existing "forest of dislocations," and
thus the metal work or strain hardens with increased cold deformation.

When ductile metals such as copper, aluminum, and α iron that have been
annealed are cold-worked at room temperature, they strain-harden because of the dis-
location interaction just described. Figure 6.43 shows how cold working at room
temperature increases the tensile strength of unalloyed copper from about 30 ksi
(200 MPa) to 45 ksi (320 MPa) with 30 percent cold work. Associated with the increase
in tensile strength, however, is a decrease in elongation (ductility), as observed in
Fig. 6.43. With 30 percent cold work, the elongation of unalloyed copper decreases
from about 52 to 10 percent elongation.

Cold working or **strain hardening** is one of the most important methods for
strengthening some metals. For example, pure copper and aluminum can be strength-
ened significantly only by this method. Thus, cold-drawn unalloyed copper wire can
be produced with different strengths (within certain limitations) by varying the
amount of strain hardening.

Figure 6.43
Percent cold work versus tensile strength and
elongation for unalloyed oxygen-free copper.
Cold work is expressed as a percent reduction in
cross-sectional area of the metal being reduced.

We wish to produce a 0.040-in.-thick sheet of oxygen-free copper with a tensile strength of 45 ksi. What percent cold work must the metal be given? What must the starting thickness of the metal be before cold rolling?

EXAMPLE PROBLEM 6.10

■ **Solution**

From Fig. 6.43, the percent cold work must be 25 percent. Thus, the starting thickness must be

$$\frac{x - 0.040 \text{ in.}}{x} = 0.25$$

$$x = 0.053 \text{ in.} \blacktriangleleft$$

6.7 SOLID-SOLUTION STRENGTHENING OF METALS

Another method besides cold working by which the strength of metals can be increased is **solid-solution strengthening.** The addition of one or more elements to a metal can strengthen it by the formation of a solid solution. The structure of *substitutional* and *interstitial solid solutions* has already been discussed in Sec. 4.3 and should be referred to for review. When substitutional (solute) atoms are mixed in the solid state with those of another metal (solvent), stress fields are created around each

CHAPTER 6 Mechanical Properties of Metals I

solute atom. These stress fields interact with dislocations and make their movement more difficult, and thus the solid solution becomes stronger than the pure metal.

Two important factors in solid-solution strengthening are:

1. *Relative-size factor.* Differences in atomic size of solute and solvent atoms affect the amount of solid-solution strengthening because of the crystal lattice distortions produced. Lattice distortions make dislocation movement more difficult and hence strengthen the metallic solid solution.

2. *Short-range order.* Solid solutions are rarely random in atomic mixing, and some kind of short-range order or clustering of like atoms takes place. As a result, dislocation movement is impeded by different bonding structures.

In addition to these factors, there are others that also contribute to solid-solution strengthening but will not be dealt with in this book.

As an example of solid-solution strengthening, let us consider a solid solution alloy of 70 wt % Cu and 30 wt % Zn (cartridge brass). The tensile strength of unalloyed copper with 30 percent cold work is about 48 ksi (330 MPa) (Fig. 6.43). However, the tensile strength of the 70 wt % Cu–30 wt % Zn alloy with 30 percent cold work is about 72 ksi (500 MPa) (Fig. 6.44). Thus, solid-solution strengthening in this case produced an increase in strength in the copper of about 24 ksi (165 MPa). On the other hand, the ductility of the copper by the 30 percent zinc addition after 30 percent cold work was reduced from about 65 to 10 percent (Fig. 6.44).
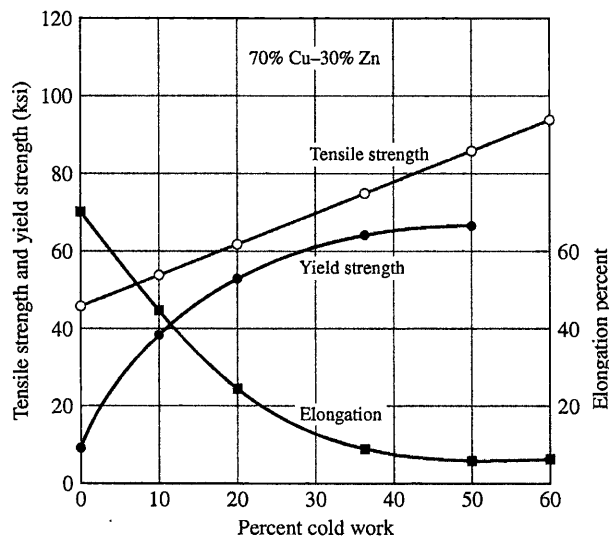
Figure 6.44
Percent cold work versus tensile strength and elongation for 70 wt % Cu–30 wt % Zn alloy. Cold work is expressed as a percent reduction in cross-sectional area of the metal being reduced (see Eq. 6.2).

6.8 RECOVERY AND RECRYSTALLIZATION OF PLASTICALLY DEFORMED METALS

In previous sections the effect of plastic deformation on the mechanical properties and microstructural features of metals was discussed. When metal-forming processes such as rolling, forging, extrusion, and others are performed cold, the work material has many dislocations and other defects, and the grains are stretched and deformed; as a result, the worked metal is significantly stronger but less ductile. Many times the reduced ductility of the cold-worked metal is undesirable, and a softer metal is required. To achieve this, the cold-worked metal is heated in a furnace. If the metal is reheated to a sufficiently high temperature for a long enough time, the cold-worked metal structure will go through a series of changes called (1) **recovery,** (2) **recrystallization,** and (3) **grain growth.** Figure 6.45 shows these structural changes schematically as the temperature of the metal is increased along with the corresponding changes in mechanical properties. This reheating treatment that softens a cold-worked metal is called **annealing,** and the terms *partial anneal* and *full anneal* are often used to refer to degrees of softening. Let us now examine these structural changes in more detail, starting with the heavily cold-worked metal structure.
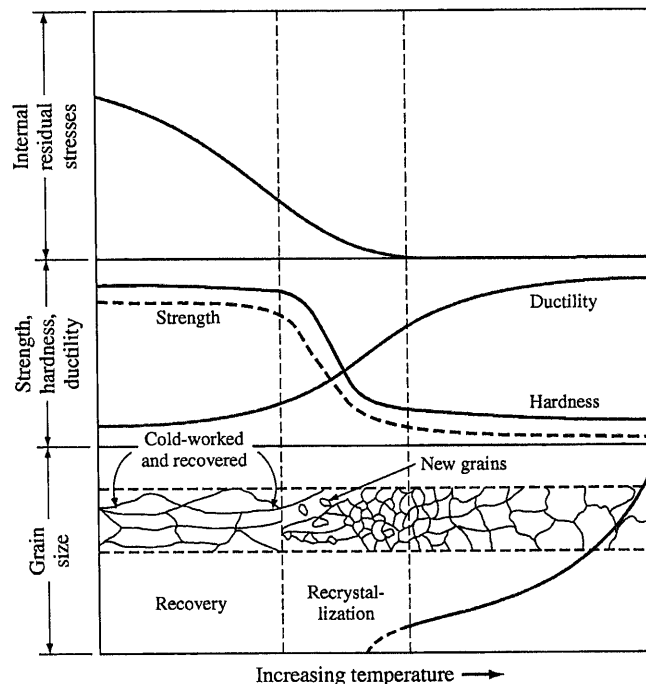
Figure 6.45
Effect of annealing on the structure and mechanical property changes of a cold-worked metal.
(*Adapted from Z.D. Jastrzebski, "The Nature and Properties of Engineering Materials," 2nd ed., Wiley, 1976, p. 228.*)

6.8.1 Structure of a Heavily Cold-Worked Metal before Reheating

When a metal is heavily cold-worked, much of the strain energy expended in the plastic deformation is stored in the metal in the form of dislocations and other imperfections such as point defects. Thus a strain-hardened metal has a higher internal energy than an unstrained one. Figure 6.46a shows the microstructure (100×) of an Al−0.8% Mg alloy sheet that has been cold-worked with 85 percent reduction. Note that the grains are greatly elongated in the rolling direction. At higher magnification (20,000×), a thin-foil transmission electron micrograph

(a)

(b)

(b)
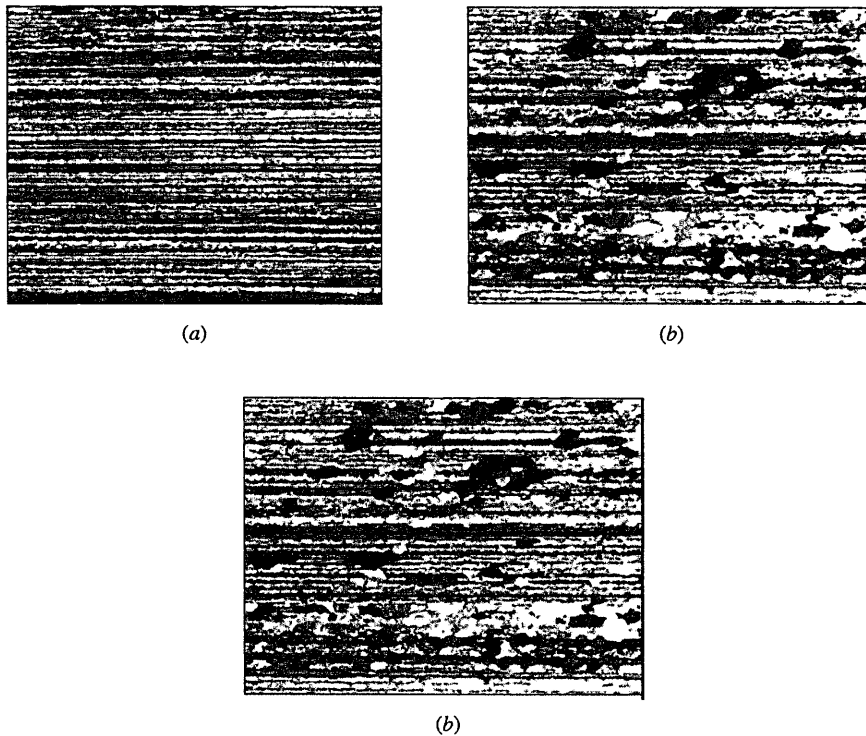
Figure 6.46
Aluminum alloy 5657 (0.8% Mg) sheet showing microstructures after cold rolling 85 percent and subsequent reheating (optical micrographs at 100× viewed under polarized light). (a) Cold-worked 85 percent; longitudinal section. Grains are greatly elongated. (b) Cold-worked 85 percent and stress-relieved at 302ºC (575ºF) for 1 h. Structure shows onset of recrystallization, which improves the formability of the sheet. (c) Cold-worked 85 percent and annealed at 316ºC (600ºF) for 1 h. Structure shows recrystallized grains and bands of unrecrystallized grains.

(After "Metals Handbook," vol. 7, 8th ed., American Society for Metals, 1972, p. 243. Reprinted with permission from ASM International. All rights reserved. www.asminternational.org.)

(a)

(b)

(c)
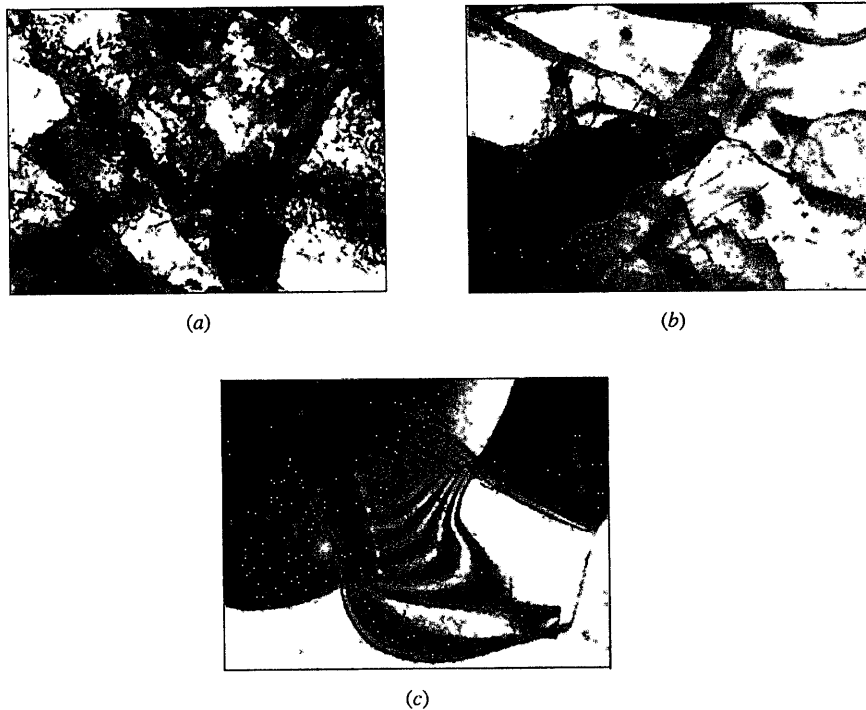
Figure 6.47
Aluminum alloy 5657 (0.8% Mg) sheet showing microstructures after cold rolling 85 percent and subsequent reheating. The microstructures shown in this figure were obtained by using thin-foil transmission electron microscopy. (Magnified 20,000×.) (a) Sheet was cold-worked 85 percent; micrograph shows dislocation tangles and banded cells (subgrains) caused by cold working extensively. (b) Sheet was cold-worked 85 percent and subsequently stress-relieved at 302ºC (575ºF) for 1 h. Micrograph shows dislocation networks and other low-angle boundaries produced by polygonization.
(c) Sheet was cold-worked 85 percent and annealed at 316ºC (600ºF) for 1 h. Micrograph shows recrystallized structure and some subgrain growth.
(*After "Metals Handbook," vol. 7, 8th ed., American Society for Metals, 1972, p. 243. Reprinted with permission from ASM International. All rights reserved. www.asminternational.org.*)

(Fig. 6.47) shows the structure to consist of a cellular network with cell walls of high dislocation density. A fully cold-worked metal has a density of approximately 10^{12} dislocation lines/cm^2.

6.8.2 Recovery

When a cold-worked metal is heated in the recovery temperature range that is just below the recrystallization temperature range, internal stresses in the metal are relieved (Fig. 6.45). During recovery, sufficient thermal energy is supplied to allow
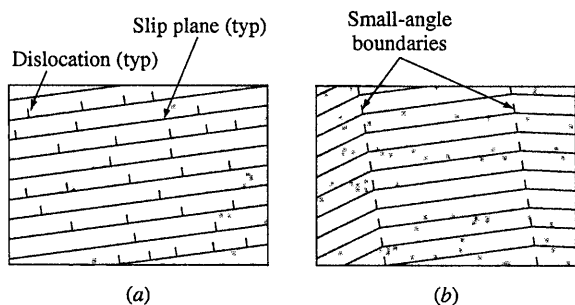
Figure 6.48
Schematic representation of polygonization in a deformed metal. (*a*) Deformed metal crystal showing dislocations piled up on slip planes. (*b*) After recovery heat treatment, dislocations move to form small-angle grain boundaries.
(*After L.E. Tanner and I.S. Servi, in "Metals Handbook," vol. 8, 8th ed., American Society for Metals, 1973, p. 222.*)
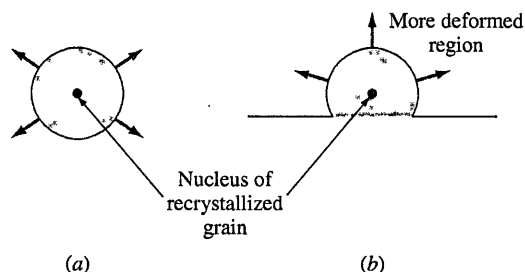
Figure 6.49
Schematic model of the growth of a recrystallized grain during the recrystallization of a metal. (*a*) Isolated nucleus expanded by growth within a deformed grain. (*b*) Original high-angle grain boundary migrating into a more highly deformed region of metal.

the dislocations to rearrange themselves into lower-energy configurations (Fig. 6.48). Recovery of many cold-worked metals (such as pure aluminum) produces a subgrain structure with low-angle grain boundaries, as shown in Fig. 6.48*b*. This recovery process is called *polygonization*, and often it is a structural change that precedes recrystallization. The internal energy of the recovered metal is lower than that of the cold-worked state since many dislocations are annihilated or moved into lower-energy configurations by the recovery process. During recovery the strength of a cold-worked metal is reduced only slightly but its ductility is usually significantly increased (Fig. 6.45).

6.8.3 Recrystallization

Upon heating a cold-worked metal to a sufficiently high temperature, new strain-free grains are nucleated in the recovered metal structure and begin to grow (Fig. 6.46*b*), forming a recrystallized structure. After a long enough time at a temperature at which recrystallization takes place, the cold-worked structure is completely replaced with a recrystallized grain structure, as shown in Fig. 6.46*c*.

Primary recrystallization occurs by two principal mechanisms: (1) an isolated nucleus can expand with a deformed grain (Fig. 6.49*a*) or (2) an original high-angle grain boundary can migrate into a more highly deformed region of the metal (Fig. 6.49*b*). In either case, the structure on the concave side of the moving boundary is strain-free and has a relatively low internal energy, whereas the structure on the convex side of the moving interface is highly strained with a high dislocation density and high internal energy. Grain boundary movement is therefore

away from the boundary's center of curvature. Thus, the growth of an expanding new grain during primary recrystallization leads to an overall decrease in the internal energy of the metal by replacing deformed regions with strain-free regions.

The tensile strength of a cold-worked metal is greatly decreased and its ductility increased by an annealing treatment that causes the metal structure to be recrystallized. For example, the tensile strength of a 0.040-in. (1-mm) sheet of 85% Cu–15% Zn brass that had been cold-rolled to 50 percent reduction was decreased from 75 to 45 ksi (520 to 310 MPa) by annealing 1 h at 400°C (Fig. 6.50a). The

(a)

(b)
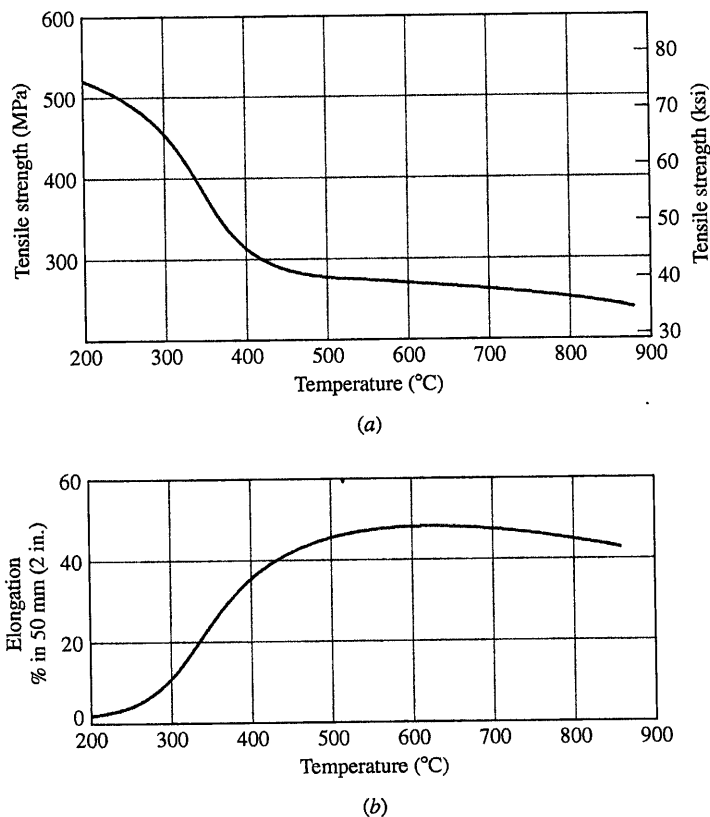
Figure 6.50
Effect of annealing temperature on (a) the tensile strength and (b) elongation of a 50 percent cold-rolled 85% Cu–15% Zn, 0.040-in. (1 mm) thick sheet. (Annealing time was 1 h at temperature.)
(After "Metals Handbook," vol. 2, 9th ed., American Society for Metals, 1979, p. 320.)
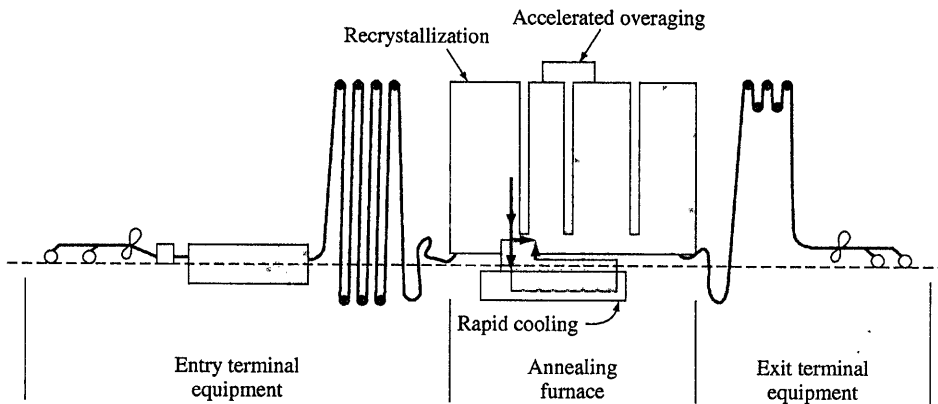
Figure 6.51
Continuous annealing schematic diagram.
(*After W.L. Roberts, "Flat Processing of Steel," Marcel Dekker, 1988.*)

ductility of the sheet, on the other hand, was increased from 3 to 38 percent with the annealing treatment (Fig. 6.50*b*). Figure 6.51 shows a schematic diagram of a continuous annealing process for sheet steel.

Important factors that affect the recrystallization process in metals and alloys are (1) amount of prior deformation of the metal, (2) temperature, (3) time, (4) initial grain size, and (5) composition of the metal or alloy. The recrystallization of a metal can take pace over a range of temperatures, and the range is dependent to some extent on the variables just listed. Thus, one cannot refer to the recrystallization temperature of a metal in the same sense as the melting temperature of a pure metal. The following generalizations can be made about the recrystallization process:

1. A minimum amount of deformation of the metal is necessary for recrystallization to be possible.

2. The smaller the degree of deformation (above the minimum), the higher the temperature needed to cause recrystallization.

3. Increasing the temperature for recrystallization decreases the time necessary to complete it (see Fig. 6.52).

4. The final grain size depends mainly on the degree of deformation. The greater the degree of deformation, the lower the annealing temperature for recrystallization and the smaller the recrystallized grain size.

5. The larger the original grain size, the greater the amount of deformation required to produce an equivalent recrystallization temperature.

6. The recrystallization temperature decreases with increasing purity of the metal. Solid-solution alloying additions always increase the recrystallization temperature.
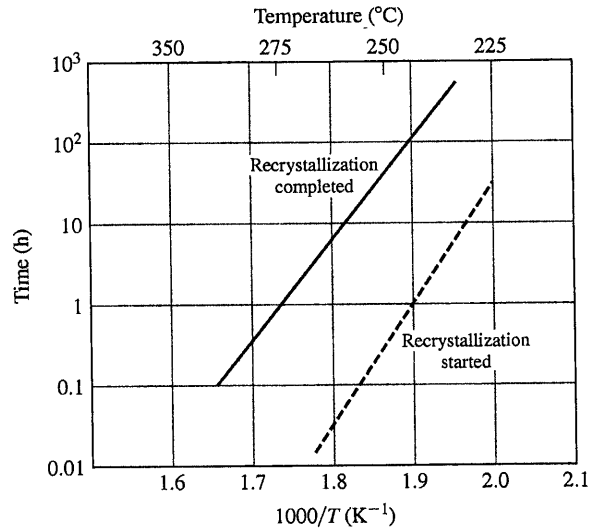
Figure 6.52

Time-temperature relations for the recrystallization
of 99.0% Al cold-worked 75 percent. The solid line
is for recrystallization finished and the dashed line
for recrystallization started. Recrystallization in
this alloy follows an Arrhenius-type relationship of
ln t versus $1/T(\text{K}^{-1})$.

*(After "Aluminum," vol. 1, American Society for Metals,
1967, p. 98.)*

If it takes 9.0×10^3 min to recrystallize a piece of copper at 88°C and 200 min at 135°C,
what is the activation energy for the process, assuming the process obeys the Arrhenius
rate equation and the time to recrystallize $= Ce^{-Q/RT}$, where $R = 8.314$ J/(mol · K) and T
is in kelvins?

**EXAMPLE
PROBLEM 6.11**

■ **Solution**

$t_1 = 9.0 \times 10^3$ min; $T_1 = 88°C + 273 = 361$ K

$t_2 = 200$ min; $T_2 = 135°C + 273 = 408$ K

$$t_1 = Ce^{Q/RT_1} \quad \text{or} \quad 9.0 \times 10^3 \text{ min} = Ce^{Q/R(361 \text{ K})} \qquad (6.17)$$

$$t_2 = Ce^{Q/RT_2} \quad \text{or} \quad 200 \text{ min} \qquad = Ce^{Q/R(408 \text{ K})} \qquad (6.18)$$

Dividing Eq. 6.17 by 6.18 gives

$$45 = \exp\left[\frac{Q}{8.314}\left(\frac{1}{361} - \frac{1}{408}\right)\right]$$

$$\ln 45 = \frac{Q}{8.314}(0.00277 - 0.00245) = 3.80$$

$$Q = \frac{3.80 \times 8.314}{0.000319} = 99{,}038 \text{ J/mol or } 99.0 \text{ kJ/mol} \blacktriangleleft$$

Phase Diagrams
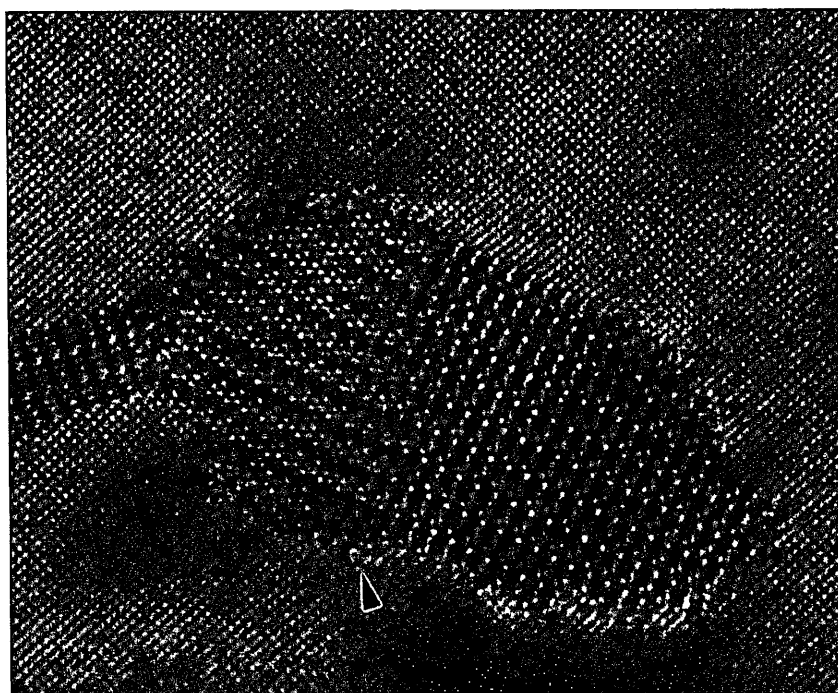
(*After W.M. Rainforth, 'Opportunities and pitfalls in characterization of nanoscale features,' Materials Science and Technology, vol. 16 (2000) 1349–1355.*)

Precipitation hardening or age hardening is a heat-treatment process used to produce a mixture of uniformly distributed hard phases in a soft matrix. The precipitated phase interferes with the movement of dislocations and, as a result, strengthens the alloy. The chapter-opening figure is a high-resolution electron microscope image of the Al_2CuMg phase in an aluminum matrix.[1]

A **phase** in a material is a region that differs in its microstructure and/or composition from another region. *Phase diagrams* are graphical representations of what phases are present in a materials system at various temperatures, pressures, and compositions. Most phase diagrams are constructed by using equilibrium conditions[2] and are used by engineers and scientists to understand and predict many aspects of the behavior of materials. ■

---

[1] http://www.shef.ac.uk/uni/academic/D-H/em/research/centres/sorbcent.html

[2] **Equilibrium phase diagrams** are determined by using slow cooling conditions. In most cases, equilibrium is approached but never fully attained.

LEARNING OBJECTIVES

By the end of this chapter, students will be able to . . .

1. Describe equilibrium, phase, and degrees of freedom for a materials system.

2. Describe the application of Gibbs rule in a material system.

3. Describe cooling curves and phase diagrams and the type of information that may be extracted from them.

4. Describe a binary isomorphous phase diagram and be able to draw a generic diagram showing all phase regions and relevant information.

5. Be able to apply tie line and lever rule to phase diagrams in order to determine the phase composition and phase fraction in a mixture.

6. Describe nonequilibrium solidification of metals and explain the general differences in microstructure when compared to equilibrium solidification.

7. Describe a binary eutectic phase diagram and be able to draw a generic diagram showing all phase regions and relevant information.

8. Describe the microstructure evolution during equilibrium cooling as metal solidifies at various regions of the phase diagram.

9. Define various invariant reactions.

10. Define intermediate phase compounds and intermetallics.

11. Describe ternary phase diagrams.

8.1 PHASE DIAGRAMS OF PURE SUBSTANCES

A pure substance such as water can exist in solid, liquid, or vapor phases, depending on the conditions of temperature and pressure. An example familiar to everyone of two phases of a pure substance in **equilibrium** is a glass of water containing ice cubes. In this case, solid and liquid water are two separate and distinct phases that are separated by a phase boundary, the surface of the ice cubes. During the boiling of water, liquid water and water vapor are two phases in equilibrium. A graphical representation of the phases of water that exist under different conditions of temperature and pressure is shown in Fig. 8.1.

Animation

In the *pressure-temperature (PT)* phase diagram of water, there exists a *triple point* at low pressure (4.579 torr) and low temperature (0.0098°C) where solid, liquid, and vapor phases of water coexist. Liquid and vapor phases exist along the vaporization line and liquid and solid phases along the freezing line, as shown in Fig. 8.1. These lines are two-phase equilibrium lines.

Pressure-temperature equilibrium phase diagrams also can be constructed for other pure substances. For example, the equilibrium *PT* phase diagram for pure iron is shown in Fig. 8.2. One major difference with this phase diagram is that there are three separate and distinct *solid phases:* alpha (α) Fe, gamma (γ) Fe, and delta (δ) Fe. Alpha and delta iron have BCC crystal structures, whereas gamma iron has an FCC structure. The
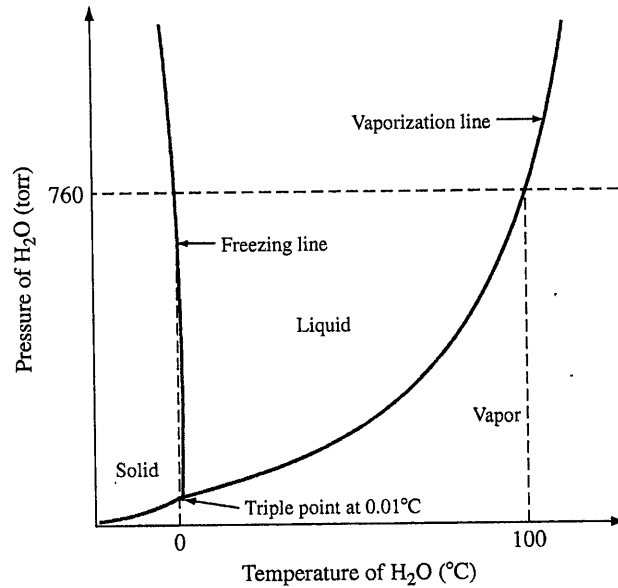
Figure 8.1
Approximate *PT* equilibrium phase diagram for pure water. (The axes of the diagram are distorted to some extent.)
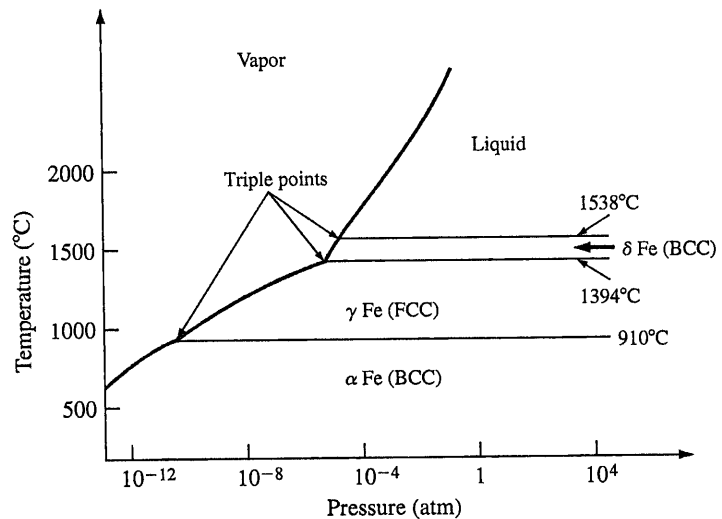
Figure 8.2
Approximate *PT* equilibrium phase diagram for pure iron.
(From W.G. Moffatt, G.W. Pearsall, and J. Wulff, "The Structure and Properties of Materials," vol. 1: "Structure," Wiley, 1964, p. 151.)

phase boundaries in the solid state have the same properties as the liquid and solid phase boundaries. For example, under equilibrium conditions, alpha and gamma iron can exist at a temperature of 910°C and 1 atm pressure. Above 910°C only single-phase gamma exists, and below 910°C only single-phase alpha exists (Fig. 8.2). There are also three

triple points in the iron PT diagram where three different phases coexist: (1) liquid, vapor, and δFe, (2) vapor, δFe, and γFe, and (3) vapor, γFe, and αFe.

8.2 GIBBS PHASE RULE

From thermodynamic considerations, J.W. Gibbs[3] derived an equation that computes the number of phases that can coexist in equilibrium in a chosen system. This equation, called **Gibbs phase rule,** is

$$P + F = C + 2 \qquad\qquad (8.1)$$

where P = number of phases that coexist in a chosen system

$\quad\ \ C$ = **number of components** in the system

$\quad\ \ F$ = degrees of freedom

Usually a component C is an element, compound, or solution in the system). F, the **degrees of freedom,** is the number of variables (pressure, temperature, and composition) that can be changed independently without changing the number of phases in equilibrium in the chosen system.

Let us consider the application of Gibbs phase rule to the PT phase diagram of pure water (Fig. 8.1). At the triple point, three phases coexist in equilibrium, and since there is one component in the **system** (water), the number of degrees of freedom can be calculated:

$$P + F = C + 2$$

$$3 + F = 1 + 2$$

or

$$F = 0 \qquad \text{(zero degrees of freedom)}$$

Since none of the variables (temperature or pressure) can be changed and still keep the three phases in balance, the triple point is called an *invariant point.*

Consider next a point along the liquid-solid freezing curve of Fig. 8.1. At any point along this line two phases will coexist. Thus, from the phase rule,

$$2 + F = 1 + 2$$

or

$$F = 1 \qquad \text{(one degree of freedom)}$$

This result tells us that there is one degree of freedom, and thus one variable (T or P) can be changed independently and still maintain a system with two coexisting phases. Thus, if a particular pressure is specified, there is only one temperature at which both liquid and solid phases can coexist. For a third case, consider a point on the water PT phase diagram inside a single phase. Then there will be only one phase present ($P = 1$), and substituting into the phase-rule equation gives

$$1 + F = 1 + 2$$

---

[3]Josiah Willard Gibbs (1839–1903). American physicist. He was a professor of mathematical physics at Yale University and made great contributions to the science of thermodynamics, which included the statement of the phase rule for multiphase systems.

CHAPTER 8 Phase Diagrams

or

$$F = 2 \qquad \text{(two degrees of freedom)}$$

This result tells us that two variables (temperature and pressure) can be varied independently and the system will still remain a single phase.

Most binary phase diagrams used in materials science are temperature composition diagrams in which pressure is kept constant, usually at 1 atm. In this case, we have the condensed phase rule, which is given by

$$P + F = C + 1 \qquad\qquad\qquad (8.1a)$$

Equation 8.1a will apply to all subsequent binary phase diagrams discussed in this chapter.

8.3 COOLING CURVES

Cooling curves can be used to determine phase transition temperatures for both pure metals and alloys. A **cooling curve** is obtained by recording the temperature of a material versus time as it cools (from a temperature at which it is molten through solidification and finally to room temperature.) The cooling curve for a pure metal is shown in Fig. 8.3. If the metal is allowed to cool under equilibrium conditions (slow cooling), its temperature drops continuously along line AB of the curve. At the melting point (freezing temperature) solidification begins and the cooling curve becomes flat (horizontal segment BC, also called a **plateau** or **region of thermal arrest**) and remains flat until solidification is complete. In region BC, the metal is in the form of a mixture of solid and liquid phases. As point C is approached, the weight fraction of solid in the mixture grows until solidification is complete. The temperature remains constant because there is a balance between the heat lost by the metal through the mold and the latent heat supplied by the solidifying metal. Simply stated, the latent heat keeps the mixture at the freezing temperature until complete solidification is achieved.)After solidification is complete at C, the cooling curve will again show a drop in temperature with time (segment CD of the curve).
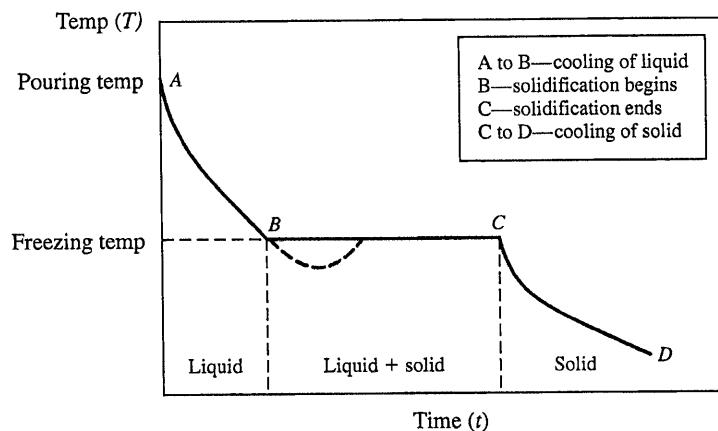
Figure 8.3
The cooling curve for a pure metal.
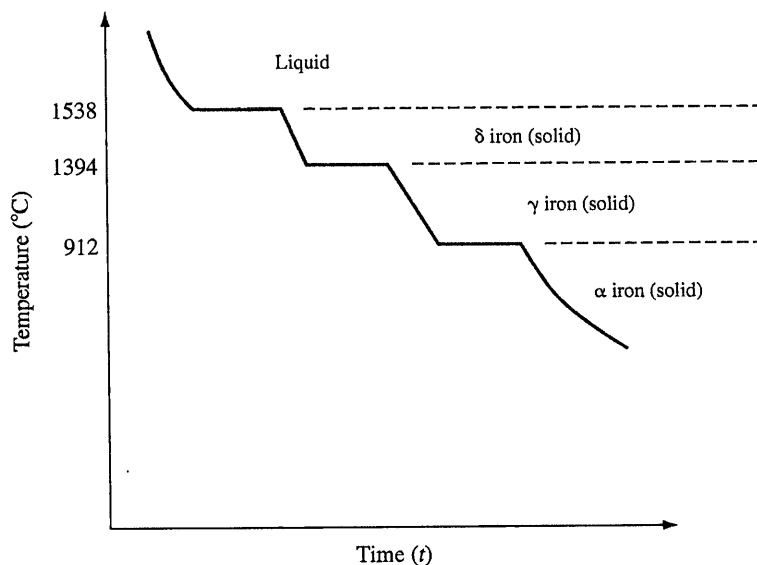
Figure 8.4
Cooling curve for pure iron at a pressure of 1 atm.

As discussed in the sections on the solidification of pure metals in Chap. 4, a degree of undercooling (cooling below the freezing temperature) is required for the formation of solid nuclei. The undercooling will appear on the cooling curve as a drop below the freezing temperature as shown in Fig. 8.3.

The cooling curve may also provide information regarding the solid state phase transformation in metals. An example of such a cooling curve would be that of pure iron. The pure iron cooling curve under atmospheric pressure conditions ($P = 1$ atm) shows a freezing temperature of 1538°C at which point a high-temperature solid of BCC structure is formed called δ iron (Fig. 8.4). Upon additional cooling, at a temperature of approximately 1394°C, the cooling curve shows a second plateau. At this temperature, a solid-solid phase transformation of BCC δ ferrite to an FCC solid called γ iron (polymorphic transformation, see Sec. 3.10) takes place. With further cooling, a second solid-solid phase transformation takes place at a temperature of 912°C. In this transformation, the FCC γ iron reverts back to a BCC iron structure called α iron. This solid-solid transformation has important technological implications in steel-processing industries and will be discussed in Chap. 9.

8.4 BINARY ISOMORPHOUS ALLOY SYSTEMS

Let us now consider a mixture or alloy of two metals instead of pure substances. A mixture of two metals is called a *binary alloy* and constitutes a *two-component* system since each metallic element in an alloy is considered a separate component. Thus, pure copper is a one-component system, whereas an alloy of copper and nickel is a two-component system. Sometimes a compound in an alloy is also considered a separate component. For example, plain-carbon steels containing mainly iron and iron carbide are considered two-component systems.

CHAPTER 8 Phase Diagrams

In some binary metallic systems, the two elements are completely soluble in each other in both the liquid and solid states. In these systems, only a single type of crystal structure exists for all compositions of the components, and therefore they are called **isomorphous systems.** In order for the two elements to have complete solid solubility in each other, they usually satisfy one or more of the following conditions formulated by Hume-Rothery[4] and known as the Hume-Rothery solid solubility rules:

1. The size of the atoms of each of the two elements must not differ by more than 15 percent.
2. The elements should not form compounds with each other, i.e., there should be no appreciable difference in the electronegativities of the two elements.
3. The crystal structure of each element of the solid solution must be the same.
4. The elements should have the same valence.

The Hume-Rothery rules are not all applicable for every pair of elements that shows complete solid solubility.

An important example of an isomorphous binary alloy system is the copper-nickel system. A phase diagram of this system with temperature as the ordinate and chemical composition in weight percent as the abscissa is shown in Fig. 8.5. This diagram has been determined for slow cooling or equilibrium conditions at atmospheric pressure and does not apply to alloys that have been rapidly cooled through the solidification temperature range. The area above the upper line in the diagram, called the **liquidus,** corresponds to the region of stability of the liquid phase, and the area below the lower line, or **solidus,** represents the region of stability for the solid phase. The region between the liquidus and solidus represents a two-phase region where both the liquid and solid phases coexist.

For the binary isomorphous phase diagram of Cu and Ni, according to the Gibbs phase rule ($F = C - P + 1$), at the melting point of the pure components, the number of components C is 1 (either Cu or Ni) and the number of phases available P is 2 (liquid or solid), resulting in a degree of freedom of 0 ($F = 1 - 2 + 1 = 0$). These points are referred to as *invariant points* ($F = 0$). This means that any change in temperature will change the microstructure either into solid or liquid. Accordingly, in the single-phase regions (liquid or solid), the number of components, C, is 2 and the number of phases available, P, is 1, resulting in a degree of freedom of 2 ($F = 2 - 1 + 1 = 2$). This means that we can maintain the microstructure of the system in this region by varying either the temperature or composition independently. In the two-phase region, the number of components, C, is 2 and the number of phases available, P, is 2, resulting in a degree of freedom of 1 ($F = 2 - 2 + 1 = 1$). This means that only one variable (either temperature or composition) can be changed independently while maintaining the two-phase structure of the system. If the temperature is changed, the phase composition will also change.

---

[4]William Hume-Rothery (1899–1968). English metallurgist who made major contributions to theoretical and experimental metallurgy and who spent years studying alloy behavior. His empirical rules for solid solubility in alloys were based on his alloy design work.
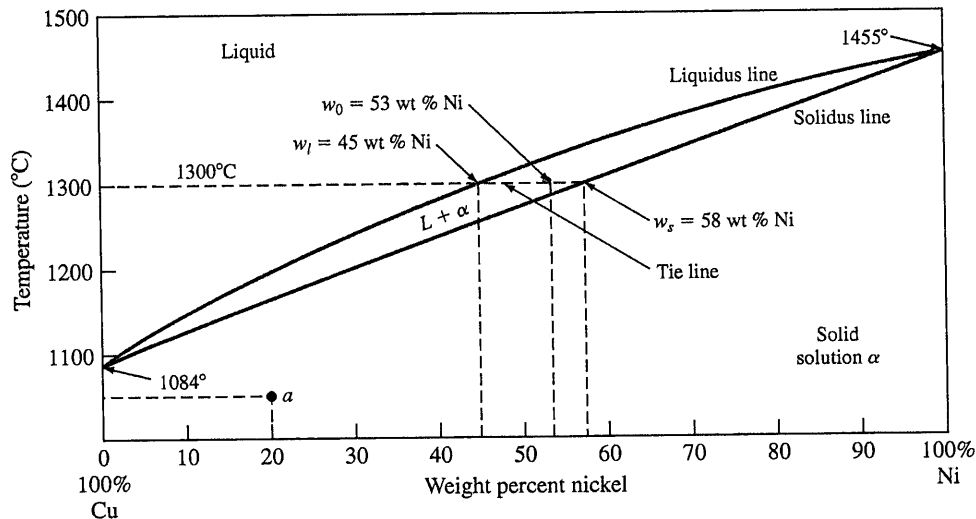
Figure 8.5

The copper-nickel phase diagram. Copper and nickel have complete liquid solubility and complete solid solubility. Copper-nickel solid solutions melt over a range of temperatures rather than at a fixed temperature, as is the case for pure metals.

(*Adapted from "Metals Handbook," vol. 8, 8th ed., American Society for Metals, 1973, p. 294.*)

In the single-phase region of solid solution α, both the temperature and the composition of the alloy must be specified in order to locate a point on the phase diagram. For example, the temperature 1050°C and 20 percent Ni specify the point a on the Cu-Ni phase diagram of Fig. 8.5. The microstructure of solid solution α at this temperature and composition appears the same as that of a pure metal, i.e., the only observable feature in the optical microscope will be grain boundaries. However, because the alloy is a solid solution of 20 percent Ni in copper, the alloy will have higher strength and electrical resistivity than pure copper.

In the region between the liquidus and solidus lines, both liquid and solid phases exist. The amount of each phase present depends on the temperature and chemical composition of the alloy. Let us consider an alloy of 53 wt % Ni–47 wt % Cu at 1300°C in Fig. 8.5. Since this alloy contains both liquid and solid phases at 1300°C, neither of these phases can have the average composition of 53% Ni–47% Cu. The compositions of the liquid and solid phases at 1300°C can be determined by drawing a horizontal *tie line* at 1300°C from the liquidus line to the solidus line and then dropping vertical lines to the horizontal composition axis. The composition of the liquid phase (w_l) at 1300°C is 45 wt % Ni and that of the solid phase (w_s) is 58 wt % Ni, as indicated by the intersection of the dashed vertical lines with the composition axis.

Binary equilibrium phase diagrams for components that are completely soluble in each other in the solid state can be constructed from a series of liquid-solid cooling curves, as shown for the Cu-Ni system in Fig. 8.6. As discussed in the previous section, the cooling curves for pure metals show horizontal thermal arrests at their freezing points, as shown for pure copper and nickel in Fig. 8.6a at AB and CD. Binary solid solutions exhibit slope changes in their cooling curves at the liquidus and

CHAPTER 8   Phase Diagrams

(a)

(b)
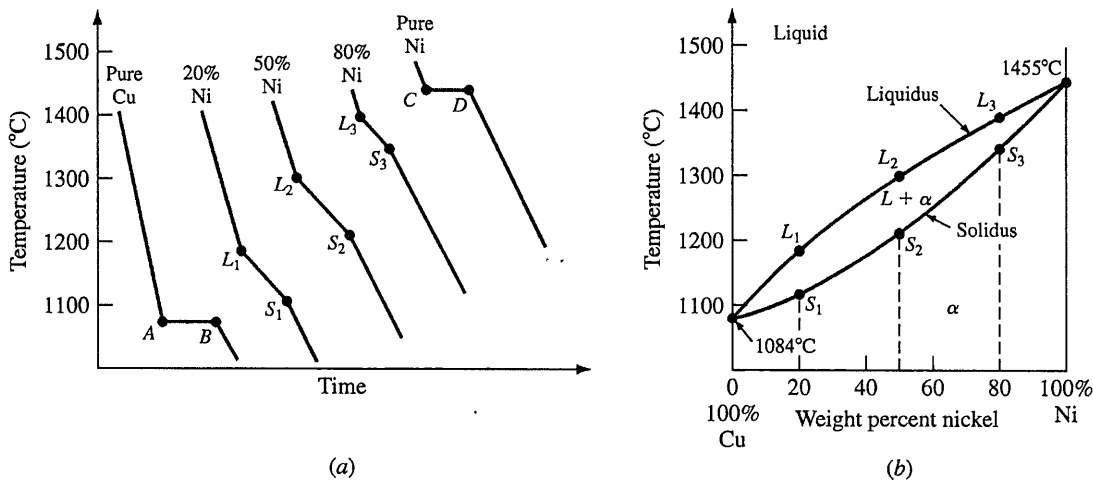
Figure 8.6
Construction of the Cu–Ni equilibrium phase diagram from liquid-solid cooling curves.
(a) Cooling curves and (b) equilibrium phase diagram.
(*From "Metals Handbook," vol. 8, 8th ed., American Society for Metals, 1973, p. 294. Used by permission of ASM International.*)

solidus lines, as shown in Fig. 8.6a at compositions of 80% Cu–20% Ni, 50% Cu–50% Ni, and 20% Cu–80% Ni. The slope changes at L_1, L_2, and L_3 in Fig. 8.6a correspond to the liquidus points L_1, L_2, and L_3 of Fig. 8.6b. Similarly, the slope changes of S_1, S_2, and S_3 of Fig. 8.6a correspond to the points S_1, S_2, and S_3 on the solidus line of Fig. 8.6b. Further accuracy in the construction of the Cu-Ni phase diagram can be attained by determining more cooling curves at intermediate alloy compositions.

The cooling curve for metal alloys in an isomorphous system does not contain the thermal arrest region that one observes in the solidification of a pure metal. Instead, solidification begins at a specific temperature and ends at a lower temperature as presented by L and S symbols in Fig. 8.6. As a result, unlike pure metals, alloys solidify over a range of temperatures. Thus, when we refer to the freezing temperature of a metal alloy, we are speaking of the temperature at which the solidification process is complete.

8.5 THE LEVER RULE

The weight percentages of the phases in any two-phase region of a binary equilibrium phase diagram can be calculated by using the **lever rule.** For example, by using the lever rule, the weight percent liquid and weight percent solid for any particular temperature can be calculated for any average alloy composition in the two-phase liquid-plus-solid region of the binary copper-nickel phase diagram of Fig. 8.5.

To derive the lever-rule equations, let us consider the binary equilibrium phase diagram of two elements A and B that are completely soluble in each other, as shown in Fig. 8.7. Let x be the alloy composition of interest and its weight fraction of B in A be w_0. Let T be the temperature of interest, and let us construct a **tie line** (LS) at temperature T from the liquidus at point L to the solidus line at point S, forming the tie line LOS. At temperature T, the alloy x consists of a mixture of liquid of w_l weight fraction of B and solid of w_s weight fraction of B.
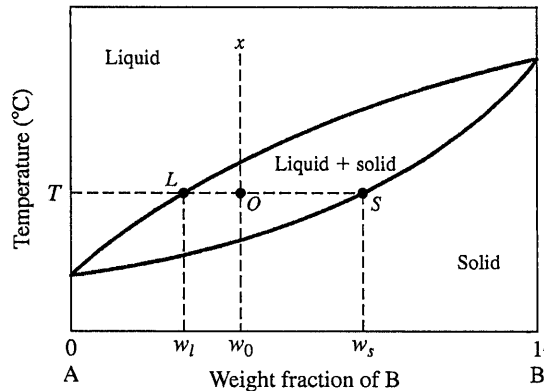
Figure 8.7
Binary phase diagram of two metals A and
B completely soluble in each other being
used to derive the lever-rule equations. At
temperature T, the composition of the liquid
phase is w_l and that of the solid is w_s.

The lever-rule equations can be derived by using weight balances. One equation
for the derivation of the lever-rule equations is obtained from the fact that the sum
of the weight fraction of the liquid phase, X_l, and the weight fraction of the solid
phase, X_s, must equal 1. Thus,

$$X_l + X_s = 1 \tag{8.2}$$

or
$$X_l = 1 - X_s \tag{8.2a}$$

and
$$X_s = 1 - X_l \tag{8.2b}$$

A second equation for the derivation of the lever rule can be obtained by a
weight balance of B in the alloy as a whole and the sum of B in the two separate
phases. Let us consider 1 g of the alloy, and make this weight balance:

$$
\begin{array}{ccc}
\text{Grams of B in} & = & \text{Grams of B in} \quad + \quad \text{Grams of B in} \\
\text{two-phase mixture} & & \text{liquid phase} \qquad\quad \text{solid phase}
\end{array}
$$

$$
\overbrace{(1\text{ g})(1)}^{\substack{\text{Grams of two-}\\ \text{phase mixture}}}\left(\frac{\%w_0}{100}\right) = \overbrace{(1\text{ g})(X_l)}^{\substack{\text{Grams of liquid}\\ \text{phase}}}\left(\frac{\%w_l}{100}\right) + \overbrace{(1\text{ g})(X_s)}^{\substack{\text{Grams of}\\ \text{solid}}}\left(\frac{\%w_s}{100}\right)
$$

Wt fraction of   Wt fraction of   Wt fraction of
phase mixture   liquid phase   solid phase

Average wt fraction   Wt fraction of B   Wt fraction of B
of B in phase mixture   in liquid phase   in solid phase

$$\tag{8.3}$$

332   **CHAPTER 8** Phase Diagrams

Thus, $$w_0 = X_l w_l + X_s w_s \tag{8.4}$$

combined with $$X_l = 1 - X_s \tag{8.2a}$$

gives $$w_0 = (1 - X_s)\, w_l + X_s w_s$$

or $$w_0 = w_l - X_s w_l + X_s w_s$$

Rearranging, $$X_s w_s - X_s w_l = w_0 - w_l$$

$$\boxed{\text{Wt fraction of solid phase} = X_s = \frac{w_0 - w_l}{w_s - w_l}} \tag{8.5}$$

Similarly, $$w_0 = X_l w_l + X_s w_s \tag{8.4}$$

combined with $$X_s = 1 - X_l \tag{8.2b}$$

gives $$\boxed{\text{Wt fraction of liquid phase} = X_l = \frac{w_s - w_0}{w_s - w_l}} \tag{8.6}$$

Equations 8.5 and 8.6 are the lever-rule equations. Effectively, the lever-rule equations state that to calculate the weight fraction of one phase of a two-phase mixture, one must use the segment of the tie line that is on the opposite side of the alloy of interest and is farthest away from the phase for which the weight fraction is being calculated. The ratio of this line segment of the tie line to the total tie line provides the weight fraction of the phase being determined. Thus, in Fig. 8.7, the weight fraction of the liquid phase is the ratio OS/LS, and the weight fraction of the solid phase is the ratio LO/LS.

Weight fractions can be converted to weight percentages by multiplying by 100 percent. Example Problem 8.1 shows how the lever rule can be used to determine the weight percentage of a phase in a binary alloy at a particular temperature.

EXAMPLE PROBLEM 8.1

Derive the lever rule for the case shown in Fig. EP8.1.

■ Solution

To derive the lever rule, let us consider the binary equilibrium diagram of two elements A and B that are completely soluble in each other, as shown in Fig. EP8.1. Let x be the alloy composition of interest and its weight fraction of B in A be w_0. Let T be the temperature of interest, and let us construct a tie line from the solidus line at point S forming the tie line SOL. From the solution of these equations:

The weight fraction of the liquid phase would equal

$$\frac{w_0 - w_s}{w_l - w_s} = \frac{SO}{LS}$$

The weight fraction of the solid phase would equal

$$\frac{w_l - w_0}{w_l - w_s} = \frac{OL}{LS}$$

This problem is illustrated in Example Problem 8.3 at 1200°C.
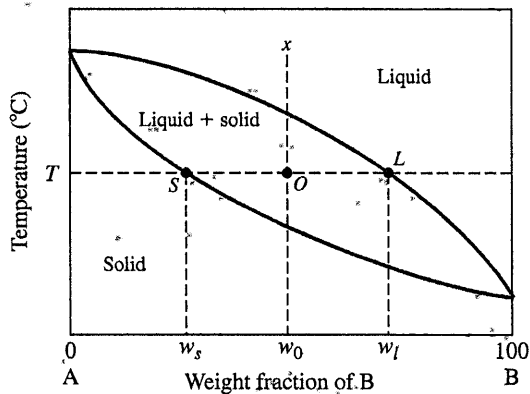
Figure EP8.1

A copper-nickel alloy contains 47 wt % Cu and 53 wt % Ni and is at 1300°C. Use Fig. 8.5 and answer the following:

EXAMPLE PROBLEM 8.2

a. What is the weight percent of copper in the liquid and solid phases at this temperature?
b. What weight percent of this alloy is liquid, and what weight percent is solid?

■ Solution

a. From Fig. 8.5 at 1300°C, the intersection of the 1300°C tie line with the liquidus gives 55 wt % Cu in the liquid phase and the intersection of the solidus of the 1300°C tie line gives 42 wt % Cu in the solid phase.
b. From Fig. 8.5 and using the lever rule on the 1300°C tie line,

$$w_0 = 53\% \ Ni \qquad w_l = 45\% \ Ni \qquad w_s = 58\% \ Ni$$

$$\text{Wt fraction of liquid phase} = X_l = \frac{w_s - w_0}{w_s - w_l}$$

$$= \frac{58 - 53}{58 - 45} = \frac{5}{13} = 0.38$$

$$\text{Wt \% of liquid phase} = (0.38)(100\%) = 38\% \blacktriangleleft$$

$$\text{Wt fraction of solid phase} = X_s = \frac{w_0 - w_l}{w_s - w_l}$$

$$= \frac{53 - 45}{58 - 45} = \frac{8}{13} = 0.62$$

$$\text{Wt \% of solid phase} = (0.62)(100\%) = 62\% \blacktriangleleft$$

EXAMPLE PROBLEM 8.3

Calculate the percent liquid and solid for the Ag-Pd phase diagram shown in Fig. EP8.3 at 1200°C and 70 wt % Ag. Assume $W_l = 74$ without Ag and $W_s = 64$ without Ag.

■ **Solution**

$$W(\%) \text{ liquid} = \frac{70 - 64}{74 - 64} = \frac{6}{10} = 60\%$$

$$W(\%) \text{ solid} = \frac{74 - 70}{74 - 64} = \frac{4}{10} = 40\%$$
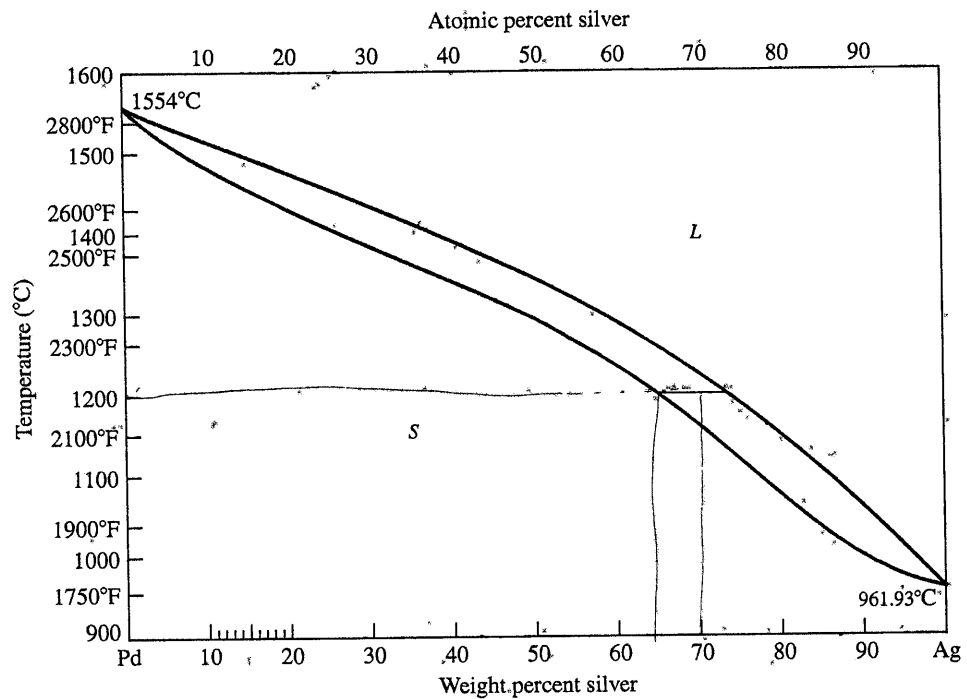
Figure EP8.3
The Ag-Pd equilibrium phase diagram.

8.6 NONEQUILIBRIUM SOLIDIFICATION OF ALLOYS

The phase diagram for the Cu-Ni system previously referred to was constructed by using very slow cooling conditions approaching equilibrium. That is, when the Cu-Ni alloys were cooled through the two-phase liquid + solid regions, the compositions of the liquid and solid phases had to readjust continuously by solid-state diffusion as the temperature was lowered. Since atomic diffusion is very slow in the solid state, an extensive period of time is required to eliminate concentration
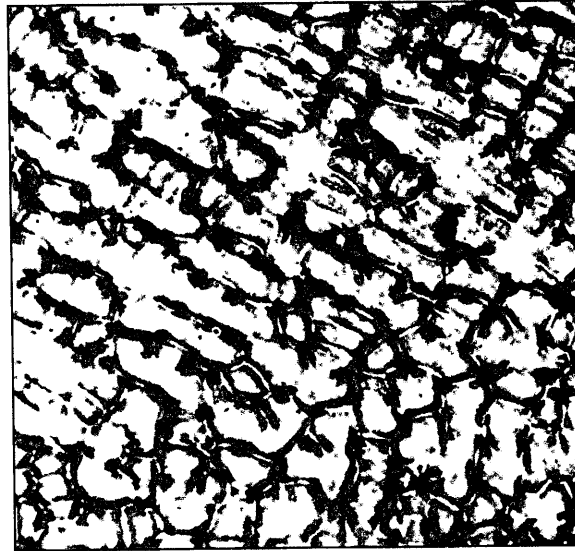
Figure 8.8
The microstructure of an as-cast 70% Cu–30%
Ni alloy showing a cored structure.
(*After W.G. Moffat et al., "Structure and Properties of
Materials," vol. I, Wiley, 1964, p. 177.*)

gradients. Thus, the as-cast microstructures of slowly solidified alloys usually have a **cored structure** (Fig. 8.8) caused by regions of different chemical composition.

The copper-nickel alloy system provides a good example to describe how such a cored structure originates. Consider an alloy of 70% Ni–30% Cu that is cooled from a temperature T_0 at a rapid rate (Fig. 8.9). The first solid forms at temperature T_1 and has the composition α_1 (Fig. 8.9). Upon further rapid cooling to T_2, additional layers of composition α_2 will form without much change in the composition of the solid primarily solidified. The overall composition at T_2 lies somewhere between α_1 and α_2 and will be designated α'_2. Since the tie line $\alpha'_2 L_2$ is longer than $\alpha_2 L_2$, there will be more liquid and less solid in the rapidly cooled alloy than if it were cooled under equilibrium conditions to the same temperature. Thus, solidification has been delayed at that temperature by the rapid cooling.

As the temperature is lowered to T_3 and T_4, the same processes occur and the average composition of the alloy follows the *nonequilibrium solidus* $\alpha_1 \alpha'_2 \alpha'_3 \cdots$. At T_6 the solid freezing has less copper than the original composition of the alloy, which is 30 percent Cu. At temperature T_7 the average composition of the alloy is 30 percent Cu, and freezing is complete. Regions in the microstructure of the alloy will thus consist of compositions varying from α_1 to α'_7 as the cored structure forms during solidification (Fig. 8.10). Figure 8.8 shows a cored microstructure of rapidly solidified 70% Cu–30% Ni alloy.

Most as-cast microstructures are cored to some extent and thus have composition gradients. In many cases, this structure is undesirable, particularly if the alloy

CHAPTER 8 Phase Diagrams
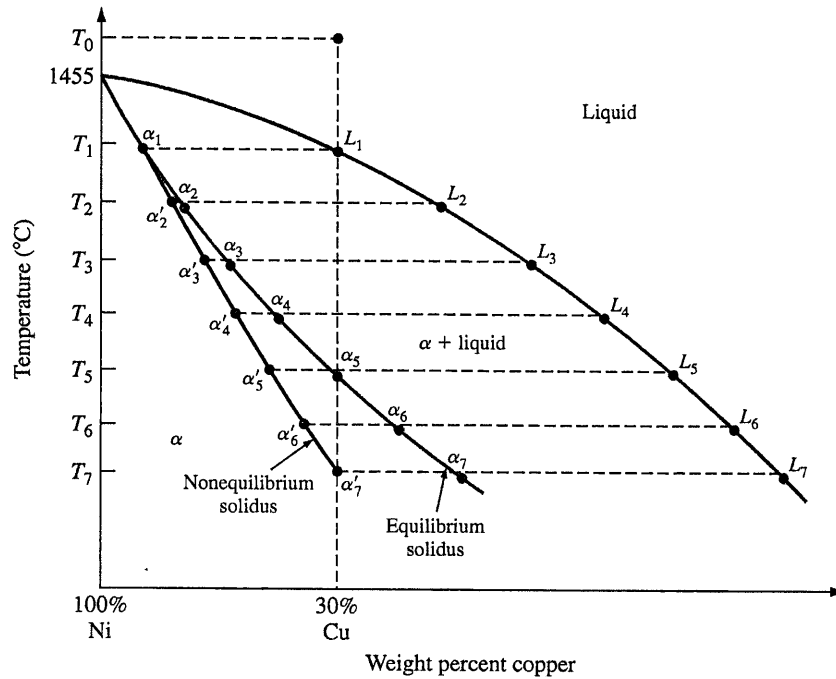
Figure 8.9

Nonequilibrium solidification of a 70% Ni–30% Cu alloy. This phase diagram has been distorted for illustrative purposes. Note the nonequilibrium solidus α_1 to α'_7. The alloy is not completely solidified until the nonequilibrium solidus reaches α'_7 at T_7.
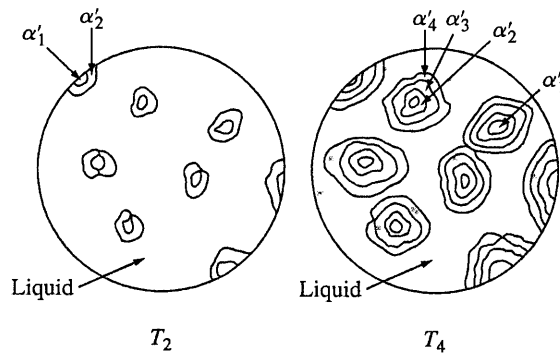
Figure 8.10

Schematic microstructures at temperature T_2 and T_4 of Fig. 8.9 for the nonequilibrium solidification of a 70% Ni–30% Cu alloy illustrating the development of a cored structure.

(a) (b)
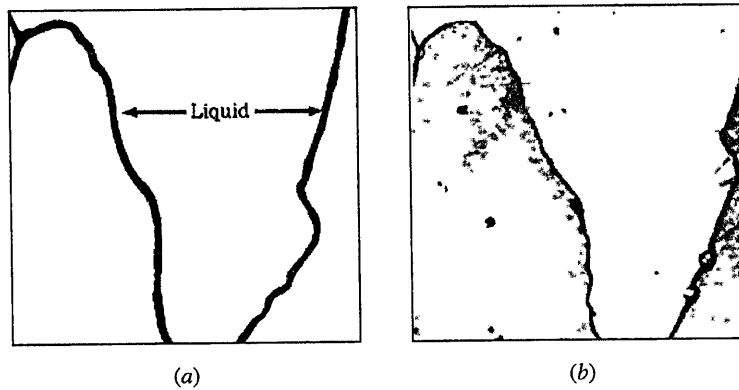
Figure 8.11
Liquation in a 70% Ni–30% Cu alloy. Heating only slightly
above the solidus temperature so that melting just begins,
produces a liquated structure such as shown in (*a*). In (*b*) the
grain-boundary region was slightly melted, and then upon
subsequent freezing, the melted zone became copper-rich and
caused the grain boundaries to appear as broad dark lines.
(Courtesy of F. Rhines.)

is to be subsequently worked. To eliminate the cored structure, as-cast ingots or castings are heated to elevated temperatures to accelerate solid-state diffusion. This process is called **homogenization** since it produces a homogeneous structure in the alloy. The homogenizing heat treatment must be carried out at a temperature that is lower than the lowest-melting solid in the as-cast alloy or else melting will occur. For homogenizing the 70% Ni–30% Cu alloy just discussed, a temperature just below T_7 indicated in Fig. 8.9 should be used. If the alloy is overheated, localized melting or *liquation* may take place. If the liquid phase forms a continuous film along the grain boundaries, the alloy will lose strength and may break up during subsequent working. Figure 8.11 shows liquation in the microstructure of a 70% Ni–30% Cu alloy.

8.7 BINARY EUTECTIC ALLOY SYSTEMS

Many binary alloy systems have components that have limited solid solubility in each other as, for example, in the lead-tin system (Fig. 8.12). The regions of restricted solid solubility at each end of the Pb-Sn diagram are designated as alpha and beta phases and are called *terminal solid solutions* since they appear at the ends of the diagram. The alpha phase is a lead-rich solid solution and can dissolve in solid solution a maximum of 19.2 wt % Sn at 183°C. The beta phase is a tin-rich solid solution and can dissolve a maximum of 2.5 wt % Pb at 183°C. As the temperature is decreased below 183°C, the maximum solid solubility of the solute elements decreases according to the **solvus** lines of the Pb-Sn phase diagram.

In simple binary eutectic systems like the Pb-Sn one, there is a specific alloy composition known as the **eutectic composition** that freezes at a lower temperature than all other compositions. This low temperature, which corresponds to the lowest temperature at which the liquid phase can exist when cooled slowly, is called the **eutectic temperature.** In the Pb-Sn system, the eutectic composition (61.9 percent Sn and 38.1 percent Pb) and the eutectic temperature (183°C) determine a point on the phase diagram called the **eutectic point.** When liquid of eutectic composition is slowly cooled to the eutectic temperature, the single liquid phase transforms simultaneously into two solid forms (solid solutions α and β). This transformation is known as the **eutectic reaction** and is written as

$$\text{Liquid} \xrightarrow[\text{cooling}]{\text{eutectic temperature}} \alpha \text{ solid solution} + \beta \text{ solid solution} \qquad (8.7)$$
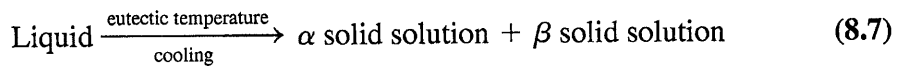
The eutectic reaction is called an **invariant reaction** since it occurs under equilibrium conditions at a specific temperature and alloy composition that cannot be
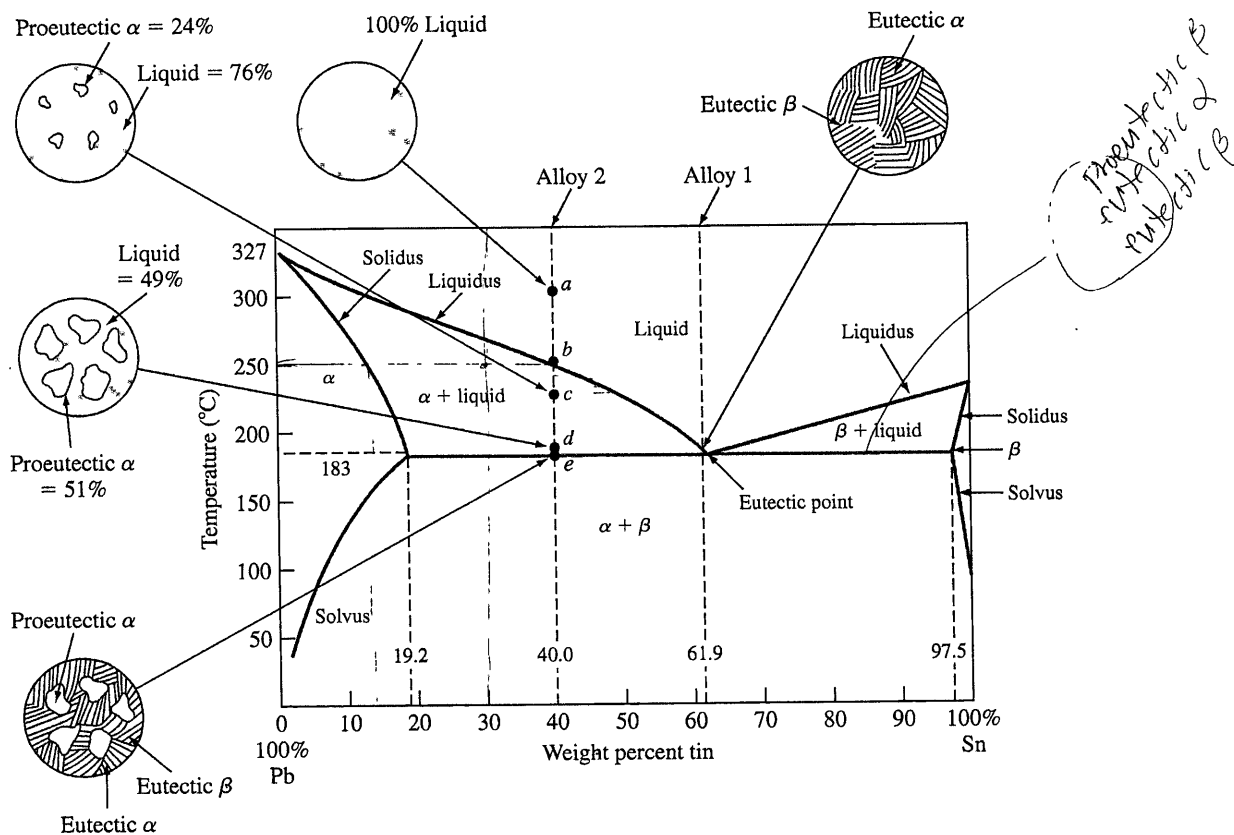
Figure 8.12
The lead-tin equilibrium phase diagram. This diagram is characterized by the limited solid solubility of each terminal phase (α and β). The eutectic invariant reaction at 61.9% Sn and 183°C is the most important feature of this system. At the eutectic point, α (19.2% Sn), β (97.5% Sn), and liquid (61.9% Sn) can coexist.

varied (according to Gibbs rule, $F = 0$). During the progress of the eutectic reaction, the liquid phase is in equilibrium with the two solid solutions α and β, and thus during a eutectic reaction, three phases coexist and are in equilibrium. Since three phases in a binary phase diagram can only be in equilibrium at one temperature, a horizontal thermal arrest appears at the eutectic temperature in the cooling curve of an alloy of eutectic composition.

Slow cooling of a Pb-Sn alloy of eutectic composition. Consider the slow cooling of a Pb-Sn alloy (alloy 1 of Fig. 8.12) of eutectic composition (61.9 percent Sn) from 200°C to room temperature. During the cooling period from 200°C to 183°C, the alloy remains liquid. At 183°C, which is the eutectic temperature, all the liquid solidifies by the eutectic reaction and forms a eutectic mixture of solid solutions α (19.2 percent Sn) and β (97.5 percent Sn) according to the reaction

$$\text{Liquid (61.9\% Sn)} \xrightarrow[\text{cooling}]{183°C} \alpha \,(19.2\% \text{ Sn}) + \beta \,(97.5\% \text{ Sn}). \qquad (8.8)$$
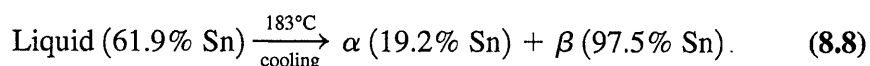
After the eutectic reaction has been completed, upon cooling the alloy from 183°C to room temperature, there is a decrease in solid solubility of solute in the α and β solid solutions, as indicated by the solvus lines. However, since diffusion is slow at the lower temperatures, this process does not normally reach equilibrium, and thus solid solutions α and β can still be distinguished at room temperature, as shown in the microstructure of Fig. 8.13a.

Compositions to the left of the eutectic point are called **hypoeutectic,** Fig. 8.13b. Conversely, compositions to the right of the eutectic point are called **hypereutectic,** Fig. 8.13d.

Slow cooling of a 60% Pb–40% Sn alloy. Next consider the slow cooling of a 40% Sn–60% Pb alloy (alloy 2 of Fig. 8.12) from the liquid state at 300°C to room temperature. As the temperature is lowered from 300°C (point a), the alloy will remain liquid until the liquidus line is intersected at point b at about 245°C. At this temperature, solid solution α containing 12 percent Sn will begin to precipitate from the liquid. The first solid to form in this type of alloy is called **primary** or **proeutectic** *alpha.* The term proeutectic alpha is used to distinguish this constituent from the alpha that forms later by the eutectic reaction.

As the liquid cools from 245°C to slightly above 183°C through the two-phase liquid + alpha region of the phase diagram (points b to d), the composition of the solid phase (alpha) follows the solidus and varies from 12 percent Sn at 245°C to 19.2 percent Sn at 183°C. Likewise, the composition of the liquid phase varies from 40 percent Sn at 245°C to 61.9 percent Sn at 183°C. These composition changes are possible since the alloy is cooling very slowly and atomic diffusion occurs to equalize compositional gradients. At the eutectic temperature (183°C) all the remaining liquid solidifies by the eutectic reaction (Eq. 8.8). After the eutectic reaction is completed, the alloy consists of proeutectic alpha and a eutectic mixture of alpha (19.2 percent Sn) and beta (97.5 percent Sn). Further cooling below 183°C to room temperature

(a)

(b)

(c)

(d)
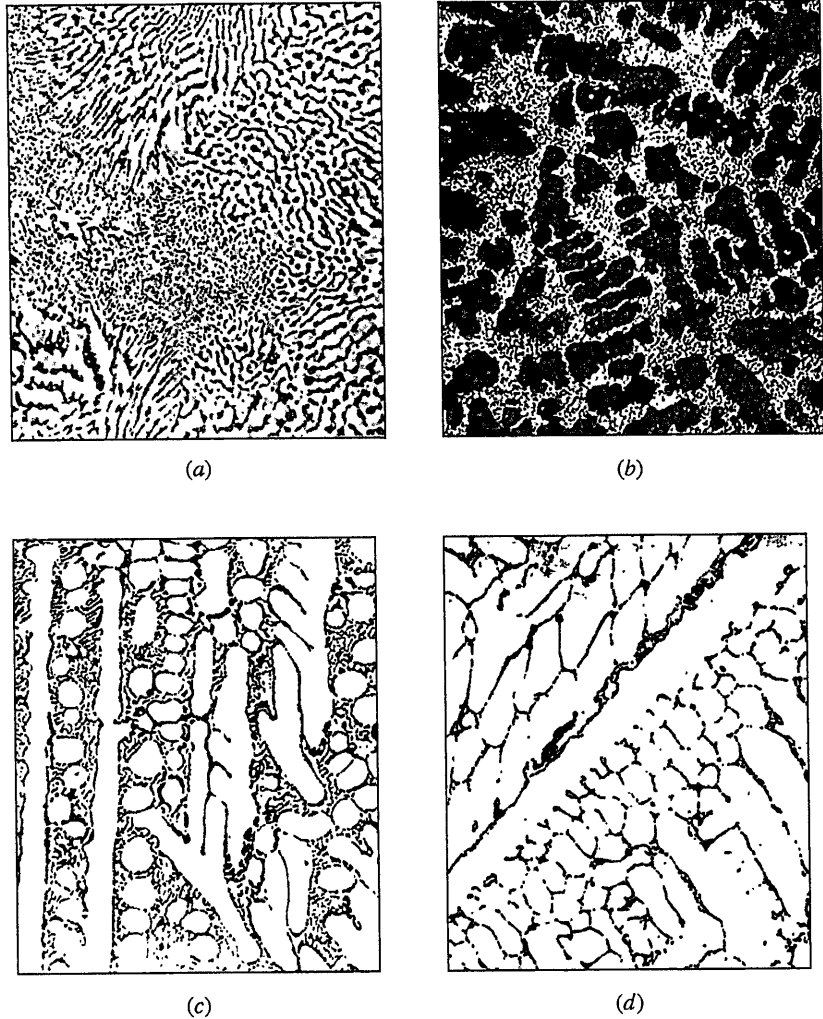
Figure 8.13
Microstructures of slowly cooled Pb–Sn alloys: (a) eutectic
composition (63% Sn–37% Pb), (b) 40% Sn–60% Pb, (c) 70%
Sn–30% Pb, (d) 90% Sn–10% Pb. (Magnification 75×.)
(*From J. Nutting and R.G. Baker, "Microstructure of Metals," Institute of Metals,
London, 1965, p. 19.*)

lowers the tin content of the alpha phase and the lead content of the beta
phase. However, at the lower temperatures the diffusion rate is much lower,
and equilibrium is not attained. Figure 8.13b shows the microstructure of a
40% Sn–60% Pb alloy that has been slowly cooled. Note the dark-etching
dendrites of the lead-rich alpha phase surrounded by eutectic. Figure 8.14
shows a cooling curve for a 60% Pb–40% Sn alloy. Note that a slope change
occurs at the liquidus at 245°C and a horizontal thermal arrest appears dur-
ing the freezing of the eutectic.
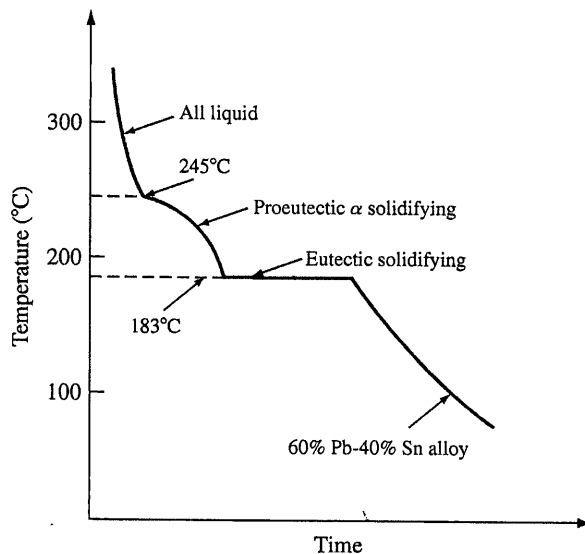
Figure 8.14
Schematic temperature-time cooling curve for a
60% Pb–40% Sn alloy.

Make phase analyses of the equilibrium (ideal) solidification of lead-tin alloys at the following points in the lead-tin phase diagram of Fig. 8.12:

a. At the eutectic composition just below 183°C (eutectic temperature).
b. The point c at 40% Sn and 230°C.
c. The point d at 40% Sn and 183°C + ΔT.
d. The point e at 40% Sn and 183°C − ΔT.

■ **Solution**

a. At the eutectic composition (61.9 percent Sn) just below 183°C:

Phases present:	alpha	beta
Compositions of phases:	19.2% Sn in alpha phase	97.5% Sn in beta phase
Amounts of phases:	Wt % alpha phase*	Wt % beta phase*
	$= \dfrac{97.5 - 61.9}{97.5 - 19.2}(100\%)$	$= \dfrac{61.9 - 19.2}{97.5 - 19.2}(100\%)$
	$= 45.5\%$	$= 54.5\%$

---

*Note that in the lever-rule calculations one uses the ratio of the tie-line segment that is *farthest away* from the phase for which the weight percent is being determined to the whole tie line.

b.   The point c at 40 percent Sn and 230°C:

Phases present:	liquid	alpha
Compositions of phases:	48% Sn in liquid phase.	15% Sn in alpha phase
Amounts of phases:	Wt % liquid phase $$= \frac{40 - 15}{48 - 15}(100\%)$$ $$= 76\%$$	Wt % alpha phase $$= \frac{48 - 40}{48 - 15}(100\%)$$ $$= 24\%$$

c.   The point d at 40 percent Sn and 183°C + ΔT:

Phases present:	liquid	alpha
Compositions of phases:	61.9% Sn in liquid phase	19.2% Sn in alpha phase
Amounts of phases:	Wt % liquid phase $$= \frac{40 - 19.2}{61.9 - 19.2}(100\%)$$ $$= 49\%$$	Wt % alpha phase $$= \frac{61.9 - 40}{61.9 - 19.2}(100\%)$$ $$= 51\%$$

d.   The point e at 40 percent Sn and 183°C − ΔT:

Phases present:	alpha	beta
Compositions of phases:	19.2% Sn in alpha phase	97.5% Sn in beta phase
Amounts of phases:	Wt % alpha phase $$= \frac{97.5 - 40}{97.5 - 19.2}(100\%)$$ $$= 73\%$$	Wt % beta phase $$= \frac{40 - 19.2}{97.5 - 19.2}(100\%)$$ $$= 27\%$$

One kilogram of an alloy of 70 percent Pb and 30 percent Sn is slowly cooled from 300°C. Refer to the lead-tin phase diagram of Fig. 8.12 and calculate the following:

EXAMPLE PROBLEM 8.5

a. The weight percent of the liquid and proeutectic alpha at 250°C.
b. The weight percent of the liquid and proeutectic alpha just above the eutectic temperature (183°C) and the weight in kilograms of these phases.
c. The weight in kilograms of alpha and beta formed by the eutectic reaction.

■ Solution

a. From Fig. 8.12 at 250°C,

$$\text{Wt \% liquid*} = \frac{30 - 12}{40 - 12}(100\%) = 64\% \blacktriangleleft$$

$$\text{Wt \% proeutectic } \alpha^* = \frac{40 - 30}{40 - 12}(100\%) = 36\% \blacktriangleleft$$

b. The weight percent liquid and proeutectic alpha just above the eutectic temperature, $183°C + \Delta T$, is

$$\text{Wt \% liquid} = \frac{30 - 19.2}{61.9 - 19.2}(100\%) = 25.3\% \blacktriangleleft$$

$$\text{Wt \% proeutectic } \alpha = \frac{61.9 - 30.0}{61.9 - 19.2}(100\%) = 74.7\% \blacktriangleleft$$

$$\text{Weight of liquid phase} = 1 \text{ kg} \times 0.253 = 0.253 \text{ kg} \blacktriangleleft$$

$$\text{Weight of proeutectic } \alpha = 1 \text{ kg} \times 0.747 = 0.747 \text{ kg} \blacktriangleleft$$

c. At $183°C - \Delta T$,

$$\text{Wt \% total } \alpha \text{ (proeutectic } \alpha + \text{ eutectic } \alpha) = \frac{97.5 - 30}{97.5 - 19.2}(100\%)$$

$$= 86.2\%$$

$$\text{Wt \% total } \beta \text{ (eutectic } \beta) = \frac{30 - 19.2}{97.5 - 19.2}(100\%)$$

$$= 13.8\%$$

$$\text{Wt total } \alpha = 1 \text{ kg} \times 0.862 = 0.862 \text{ kg}$$

$$\text{Wt total } \beta = 1 \text{ kg} \times 0.138 = 0.138 \text{ kg}$$

The amount of proeutectic alpha will remain the same before and after the eutectic reaction. Thus,

$$\text{Wt of } \alpha \text{ created by eutectic reaction} = \text{total } \alpha - \text{proeutectic } \alpha$$

$$= 0.862 \text{ kg} - 0.747 \text{ kg}$$

$$= 0.115 \text{ kg} \blacktriangleleft$$

$$\text{Wt of } \beta \text{ created by eutectic reaction} = \text{total } \beta$$

$$= 0.138 \text{ kg} \blacktriangleleft$$

*See note in Example Problem 8.4.

EXAMPLE PROBLEM 8.6	A lead-tin (Pb-Sn) alloy contains 64 wt % proeutectic α and 36 wt % eutectic $\alpha + \beta$ at 183°C $- \Delta T$. Calculate the average composition of this alloy (see Fig. 8.12):

■ Solution

Let x be the wt % Sn in the unknown alloy. Since this alloy contains 64 wt % proeutectic α, the alloy must be hypoeutectic, and x will therefore lie between 19.2 and 61.9 wt % Sn, as indicated in Fig. EP8.6. At 183°C $+ \Delta T$, using Fig. EP8.6 and the lever rule gives

$$\% \text{ proeutectic } \alpha = \frac{61.9 - x}{61.9 - 19.2}(100\%) = 64\%$$

or

$$61.9 - x = 0.64(42.7) = 27.3$$

$$x = 34.6\%$$

Thus, the alloy consists of 34.6 percent Sn and 65.4 percent Pb. ◀ Note that we use the lever-rule calculation above the eutectic temperature, since the percentage of the proeutectic α remains the same just above and just below the eutectic temperature.
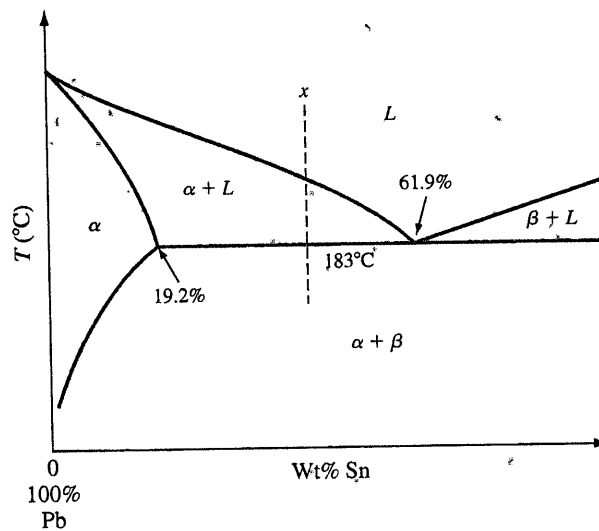
Figure EP8.6

Lead-rich end of the Pb–Sn phase diagram.

In a binary eutectic reaction, the two solid phases ($\alpha + \beta$) can have various morphologies. Figure 8.15 shows schematically some varied eutectic structures. The shape that will be created depends on many factors. Of prime importance is a minimization of free energy at the $\alpha - \beta$ interfaces. An important factor that determines the eutectic shape is the manner in which the two phases (α and β) nucleate and
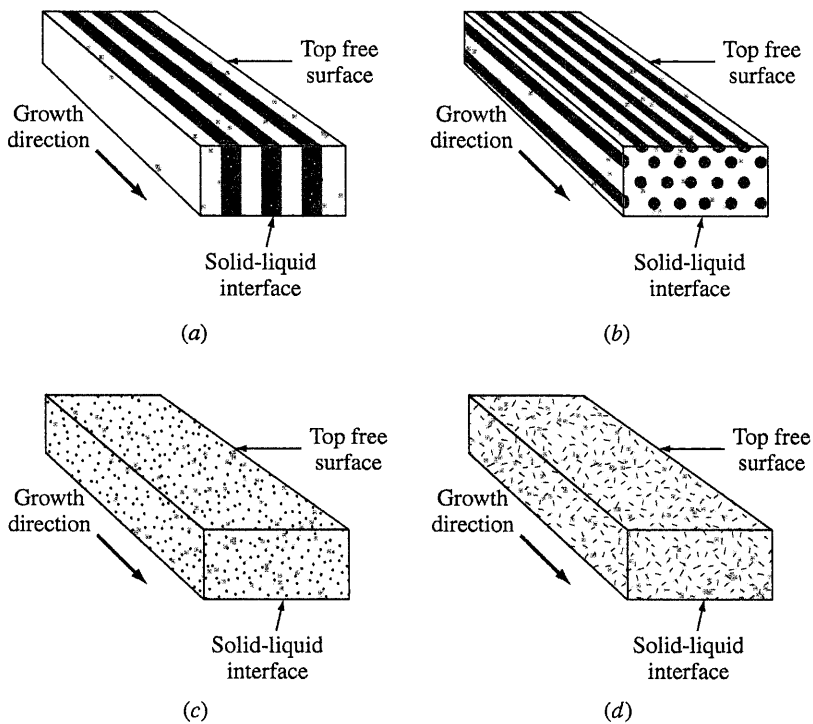
Figure 8.15

Schematic illustration of various eutectic structures: (*a*) lamellar,
(*b*) rodlike, (*c*) globular, (*d*) acicular.

(*After W.C. Winegard, "An Introduction to the Solidification of Metals," Institute of Metals, London, 1964.*)

grow. For example, rod- and plate-type eutectics form when repeated nucleation of the two phases is not required in certain directions. An example of a *lamellar eutectic structure* formed by a Pb-Sn eutectic reaction is shown in Fig. 8.16. Lamellar eutectic structures are very common. A mixed irregular eutectic structure found in the Pb-Sn system is shown in Fig. 8.13*a*.

8.13 SUMMARY

Phase diagrams are graphical representations of what phases are present in an alloy (or ceramic) system at various temperatures, pressures, and compositions. Phase diagrams are constructed using the information gathered from cooling curves. Cooling curves are time temperature plots generated for various alloy compositions and provide information about phase transition temperatures. In this chapter, the emphasis has been placed on temperature-composition binary equilibrium phase diagrams. These diagrams tell us which phases are present at different compositions and temperatures for slow cooling or heating conditions that approach equilibrium. In two-phase regions of these diagrams, the chemical compositions of each of the two phases is indicated by the intersection of the isotherm with the phase boundaries. The weight fraction of each phase in a two-phase region can be determined by using the lever rule along an isotherm (tie line at a particular temperature).

In binary equilibrium *isomorphous phase diagrams,* the two components are completely soluble in each other in the solid state, and so there is only one solid phase. In binary equilibrium alloy (ceramic) phase diagrams, *invariant reactions* involving three phases in equilibrium often occur. The most common of these reactions are:

1. Eutectic reaction: $L \to \alpha + \beta$
2. Eutectoid reaction: $\alpha \to \beta + \gamma$
3. Peritectic reaction: $\alpha + L \to \beta$
4. Peritectoid reaction: $\alpha + \beta \to \gamma$
5. Monotectic reaction: $L_1 \to \alpha + L_2$

In many binary equilibrium phase diagrams, intermediate phase(s) and/or compounds are present. The intermediate phases have a range of compositions, whereas the intermediate compounds have only one composition. If the components are both metal, the intermediate compound is called an *intermetallic.*

During the rapid solidification of many alloys, compositional gradients are created and *cored* structures are produced. A cored structure can be eliminated by homogenizing the cast alloy for long times at high temperatures just below the melting temperature of the lowest melting phase in the alloy. If the cast alloy is overheated slightly so that melting occurs at the grain boundaries, a *liquated* structure is produced. This type of structure is undesirable since the alloy loses strength and may break up during subsequent working.

8.14 DEFINITIONS

Sec. 8.1

Phase: a physically homogeneous and distinct portion of a material system.

Equilibrium: a system is said to be in equilibrium if no macroscopic changes take place with time.

Equilibrium phase diagram: a graphical representation of the pressures, temperatures, and compositions for which various phases are stable at equilibrium. In materials science, the most common phase diagrams involve temperature versus composition.

Sec. 8.2

System: a portion of the universe that has been isolated so that its properties can be studied.

Gibbs phase rule: the statement that at equilibrium the number of phases plus the degrees of freedom equals the number of components plus 2. $P + F = C + 2$. In the condensed form with pressure ≈ 1 atm, $P + F = C + 1$.

Degrees of freedom F: the number of variables (temperature, pressure, and composition) that can be changed *independently* without changing the phase or phases of the system.

Number of components of a phase diagram: the number of elements or compounds that make up the phase-diagram system. For example, the Fe-Fe_3C system is a two-component system; the Fe-Ni system is also a two-component system.

Sec. 8.3

Cooling curve: plots of temperature vs time acquired during solidification of a metal. It provides phase change information as the temperature is lowered.

Thermal arrest: a region of the cooling curve for a pure metal where temperature does not change with time (plateau), representing the freezing temperature.

Sec. 8.4

Isomorphous system: a phase diagram in which there is only one solid phase, i.e., there is only one solid-state structure.

CHAPTER 8 Phase Diagrams

Liquidus: the temperature at which liquid starts to solidify under equilibrium conditions.

Solidus: the temperature during the solidification of an alloy at which the last of the liquid phase solidifies.

Sec. 8.5

Lever rule: the weight percentages of the phases in any two-phase region of a binary phase diagram can be calculated using this rule if equilibrium conditions prevail.

Tie line: a horizontal working line drawn at a particular temperature between two phase boundaries (in a binary phase diagram) to be used to apply the lever rule. Vertical lines are drawn from the intersection of the tie line with the phase boundaries to the horizontal composition line. A vertical line is also drawn from the tie line to the horizontal line at the intersection point of the tie line with the alloy of interest to use with the lever rule.

Sec. 8.6

Cored structure: a type of microstructure that occurs during rapid solidification or non-equilibrium cooling of a metal.

Homogenization: a heat treatment process given to a metal to remove undesirable cored structures.

Sec. 8.7

Solvus: a phase boundary below the isothermal liquid + proeutectic solid phase boundary and between the terminal solid solution and two-phase regions in a binary eutectic phase diagram.

Eutectic composition: the composition of the liquid phase that reacts to form two new solid phases at the eutectic temperature.

Eutectic temperature: the temperature at which a eutectic reaction takes place.

Eutectic point: the point determined by the eutectic composition and temperature.

Eutectic reaction (in a binary phase diagram): a phase transformation in which all the liquid phase transforms on cooling into two solid phases isothermally.

Hypoeutectic composition: one that is to the left of the eutectic point.

Hypereutectic composition: one that is to the right of the eutectic point.

Primary phase: a solid phase that forms at a temperature above that of an invariant reaction and is still present after the invariant reaction is completed.

Proeutectic phase: a phase that forms at a temperature above the eutectic temperature.

Sec. 8.8

Peritectic reaction (in a binary phase diagram): a phase transformation in which, upon cooling, a liquid phase combines with a solid phase to produce a new solid phase.

Sec. 8.9

Monotectic reaction (in a binary phase diagram): a phase transformation in which, upon cooling, a liquid phase transforms into a solid phase and a new liquid phase (of different composition than the first liquid phase).

Sec. 8.10

Invariant reactions: those reactions in which the reacting phases have fixed temperature and composition. The degree of freedom, *F*, is zero at these reaction points.

Sec. 8.11

Terminal phase: a solid solution of one component in another for which one boundary of the phase field is a pure component.

Intermediate phase: a phase whose composition range is between those of the terminal phases.

8.15 PROBLEMS

Answers to problems marked with an asterisk are given at the end of the book.

Knowledge and Comprehension Problems

8.1 Define (a) a phase in a material and (b) a phase diagram.

8.2 In the pure water pressure-temperature equilibrium phase diagram (Fig. 8.1), what phases are in equilibrium for the following conditions: (a) along the freezing line, (b) along the vaporization line, and (c) at the triple point.

8.3 How many triple points are there in the pure iron pressure-temperature equilibrium phase diagram of Fig. 8.2? What phases are in equilibrium at each of the triple points?

8.4 Write the equation for Gibbs phase rule and define each of the terms.

8.5 Refer to the pressure-temperature equilibrium phase diagram for pure water (Fig. 8.1) and answer the following:

(a) How many degrees of freedom are there at the triple point?

(b) How many degrees of freedom are there along the freezing line?

8.6 (a) What is a cooling curve? (b) What type of information may be extracted from a cooling curve? (c) Draw a schematic of a cooling curve for a pure metal and one for an alloy. Discuss the differences.

8.7 What is a binary isomorphous alloy system?

8.8 What are the four Hume-Rothery rules for the solid solubility of one element in another?

8.9 Describe how the liquidus and solidus of a binary isomorphous phase diagram can be determined experimentally.

8.10 Explain how a cored structure is produced in a 70% Cu–30% Ni alloy.

8.11 How can the cored structure in a 70% Cu–30% Ni alloy be eliminated by heat treatment?

8.12 Explain what is meant by the term *liquation*. How can a liquated structure be produced in an alloy? How can it be avoided?

8.13 Describe the mechanism that produces the phenomenon of *surrounding* in a peritectic alloy that is rapidly solidified through the peritectic reaction.

8.14 Can coring and surrounding occur in a peritectic-type alloy that is rapidly solidified? Explain.

8.15 What is a monotectic invariant reaction? How is the monotectic reaction in the copper-lead system important industrially?

8.16 Write equations for the following invariant reactions: eutectic, eutectoid, peritectic, and peritectoid. How many degrees of freedom exist at invariant reaction points in binary phase diagrams?

8.17 How are eutectic and eutectoid reactions similar? What is the significance of the −*oid* suffix?

8.18 Distinguish between (a) a terminal phase and (b) an intermediate phase.

8.19 Distinguish between (a) an intermediate phase and (b) an intermediate compound.

8.20 What is the difference between a congruently melting compound and an incongruently melting one?

Application and Analysis Problems

*8.21 Consider an alloy containing 70 wt % Ni and 30 wt % Cu (see Fig. 8.5).

(a) At 1350°C, make a phase analysis assuming equilibrium conditions. In the phase analysis, include the following:

(i) What phases are present?

(ii) What is the chemical composition of each phase?

(iii) What amount of each phase is present?

(b) Make a similar phase analysis at 1500°C.

(c) Sketch the microstructure of the alloy at each of these temperatures by using circular microscopic fields.

8.22 Consider the binary eutectic copper-silver phase diagram in Fig. P8.22. Make phase analyses of an 88 wt % Ag–12 wt % Cu alloy at the temperatures (a) 1000°C, (b) 800°C, (c) 780°C + ΔT, and (d) 780°C − ΔT. In the phase analyses, include:

(i) The phases present

(ii) The chemical compositions of the phases

(iii) The amounts of each phase

(iv) Sketch the microstructure by using 2-cm diameter circular fields.

8.23 If 500 g of a 40 wt % Ag–60 wt % Cu alloy is slowly cooled from 1000°C to just below 780°C (see Fig. P8.22):

(a) How many grams of liquid and proeutectic alpha are present at 850°C?

(b) How many grams of liquid and proeutectic alpha are present at 780°C + ΔT?

(c) How many grams of alpha are present in the eutectic structure at 780°C − ΔT?

(d) How many grams of beta are present in the eutectic structure at 780°C − ΔT?
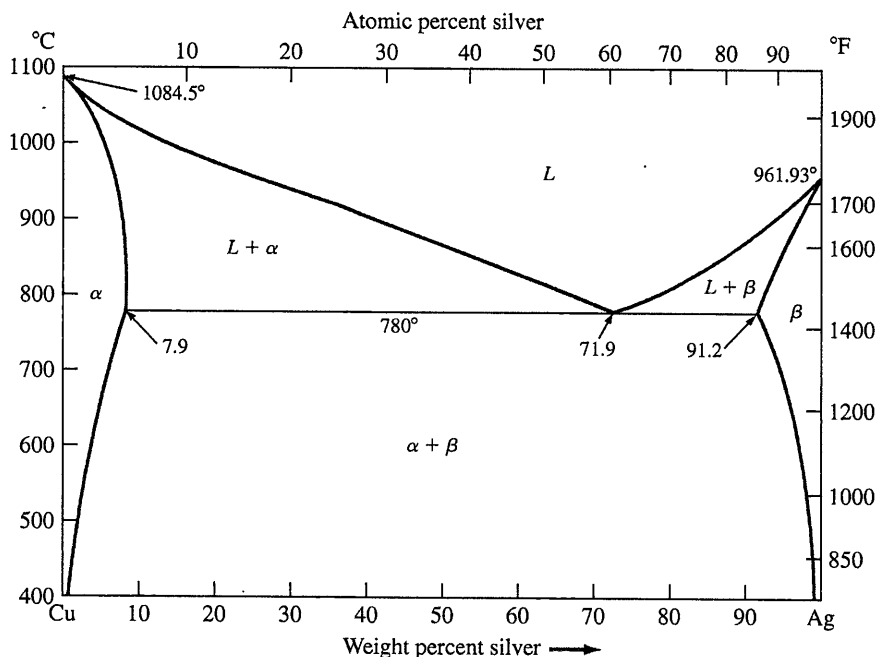
Figure P8.22
The copper-silver phase diagram.
(After "Metals Handbook," vol. 8, 8th ed., American Society for Metals, 1973, p. 253.)

8.24 A lead-tin (Pb–Sn) alloy consists of 60 wt % proeutectic β and 60 wt % eutectic $\alpha + \beta$ at 183°C $- \Delta T$. Calculate the average composition of this alloy (see Fig. 8.12).

8.25 A Pb–Sn alloy (Fig. 8.12) contains 40 wt % β and 60 wt % α at 50°C. What is the average composition of Pb and Sn in this alloy?

*8.26 An alloy of 30 wt % Pb– 70 wt % Sn is slowly cooled from 250°C to 27°C (see Fig. 8.12).

  (a) Is this alloy hypoeutectic or hypereutectic?

  (b) What is the composition of the first solid to form?

  (c) What are the amounts and compositions of each phase that is present at 183°C $+ \Delta T$?

  (d) What is the amount and composition of each phase that is present at 183°C $- \Delta T$?

  (e) What are the amounts of each phase present at room temperature?

8.27 Consider the binary peritectic iridium-osmium phase diagram of Fig. P8.27. Make phase analyses of a 70 wt % Ir–30 wt % Os at the temperatures (a) 2600°C, (b) 2665°C $+ \Delta T$, and (c) 2665°C $- \Delta T$. In the phase analyses include:

  (i) The phases present

  (ii) The chemical compositions of the phases

  (iii) The amounts of each phase

  (iv) Sketch the microstructure by using 2 cm diameter circular fields.

8.28 Consider the binary peritectic iridium-osmium phase diagram of Fig. P8.27. Make phase analyses of a 40 wt % Ir–60 wt % Os at the temperatures (a) 2600°C, (b) 2665°C $+ \Delta T$, (c) 2665°C $- \Delta T$, and (d) 2800°C. Include in the phase analyses the four items listed in Prob. 8.20.

8.29 Consider the binary peritectic iridium-osmium phase diagram of Fig. P8.27. Make phase analyses of a 70 wt % Ir–30 wt % Os at the temperatures (a) 2600°C, (b) 2665°C $+ \Delta T$, and (c) 2665°C $- \Delta T$. In the phase analyses include:

  (i) The phases present

  (ii) The chemical compositions of the phases

  (iii) The amounts of each phase

  (iv) Sketch the microstructure by using 2-cm diameter circular fields.
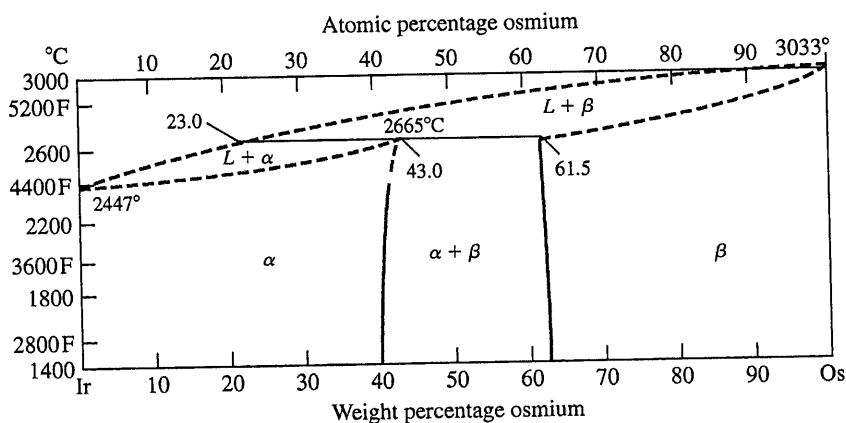
Figure P8.27
The iridium-osmium phase diagram.
(*From "Metals Handbook," vol. 8, 8th ed., American Society for Metals, 1973, p. 425. Used by permission of ASM International.*)

CHAPTER 8   Phase Diagrams

Atomic percent nickel
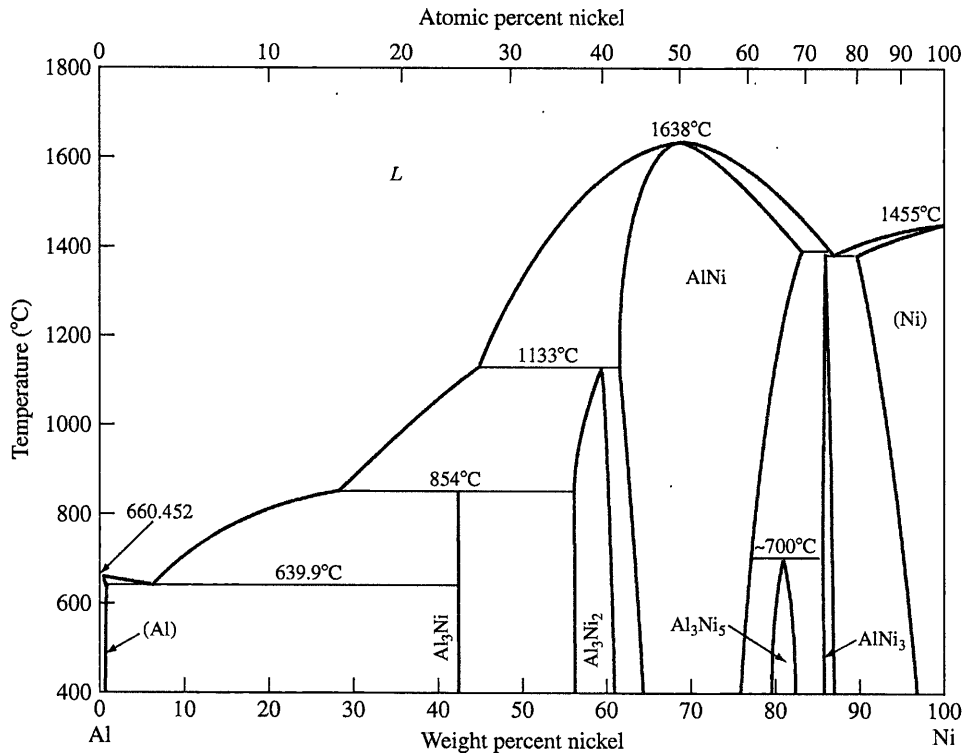
Figure P8.39
Aluminum-nickel phase diagram.
(*From "Metals Handbook", vol. 8, 8th ed., American Society for Metals, 1973, p. 253. Used by permission of ASM International.*)

*8.30   In the copper-lead (Cu-Pb) system (Fig. 8.24) for an alloy of Cu–10 wt % Pb, determine the amounts and compositions of the phases present at (*a*) 1000°C, (*b*) 955°C + ΔT, (*c*) 955°C − ΔT, and (*d*) 200°C.

8.31   For an alloy of Cu–70 wt % Pb (Fig. 8.24), determine the amounts and compositions in weight percent of the phases present at (*a*) 955°C + ΔT, (*b*) 955°C − ΔT, and (*c*) 200°C.

8.32   What is the average composition (weight percent) of a Cu-Pb alloy that contains 30 wt % L_1 and 70 wt % α at 955°C + ΔT?

8.33   Consider an Fe–4.2 wt % Ni alloy (Fig. 8.17) that is slowly cooled from 1550°C to 1450°C. What weight percent of the alloy solidifies by the peritectic reaction?

*8.34   Consider an Fe–5.0 wt % Ni alloy (Fig. 8.17) that is slowly cooled from 1550°C to 1450°C. What weight percent of the alloy solidifies by the peritectic reaction?

8.35   Determine the weight percent and composition in weight percent of each phase present in an Fe–4.2 wt % Ni alloy (Fig. 8.17) at 1517°C + ΔT.

8.36   Determine the composition in weight percent of the alloy in the Fe–Ni system (Fig. 8.17) that will produce a structure of 40 wt % δ and 60 wt % γ just below the peritectic temperature.

8.37   Draw, schematically, the liquidus and the solidus lines for Cu-Zn diagram (Fig. 8.26). Show all the critical zinc contents and temperatures. Which one of these temperatures should be important to metal-forming processes? Why?
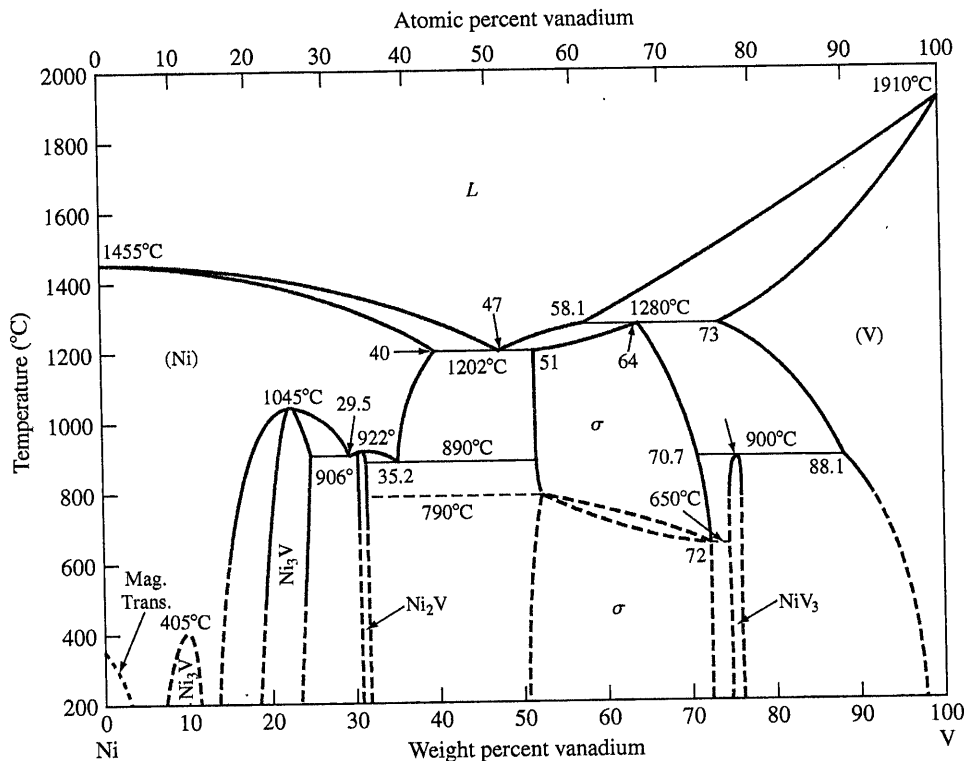
Figure P8.40
Nickel-vanadium phase diagram.
(*From "Metals Handbook," vol. 8, 8th ed., American Society for Metals, 1973, p. 332. Used by permission of ASM International.*)

*8.38 Consider the Cu-Zn phase diagram of Fig. 8.26.

    (a) What is the maximum solid solubility in weight percent of Zn in Cu in the terminal solid solution α?

    (b) Identify the intermediate phases in the Cu-Zn phase diagram.

    (c) Identify the three-phase invariant reactions in the Cu-Zn diagram.

        (i) Determine the composition and temperature coordinates of the invariant reactions.

        (ii) Write the equations for the invariant reactions.

        (iii) Name the invariant reactions.

8.39 Consider the aluminum-nickel phase diagram of Fig. P8.39. For this phase diagram:

    (a) Determine the coordinates of the composition and temperature of the invariant reactions.

    (b) Write the equations for the three-phase invariant reactions and name them.

    (c) Label the two-phase regions in the phase diagram.

8.40 Consider the nickel-vanadium phase diagram of Fig. P8.40. For this phase diagram, repeat questions of Prob. 8.38.

8.41 Consider the titanium-aluminum phase diagram of Fig. P8.41. For this phase diagram, repeat the questions of Prob. 8.38.

8.42 What is the composition of point y in Fig. EP8.9?
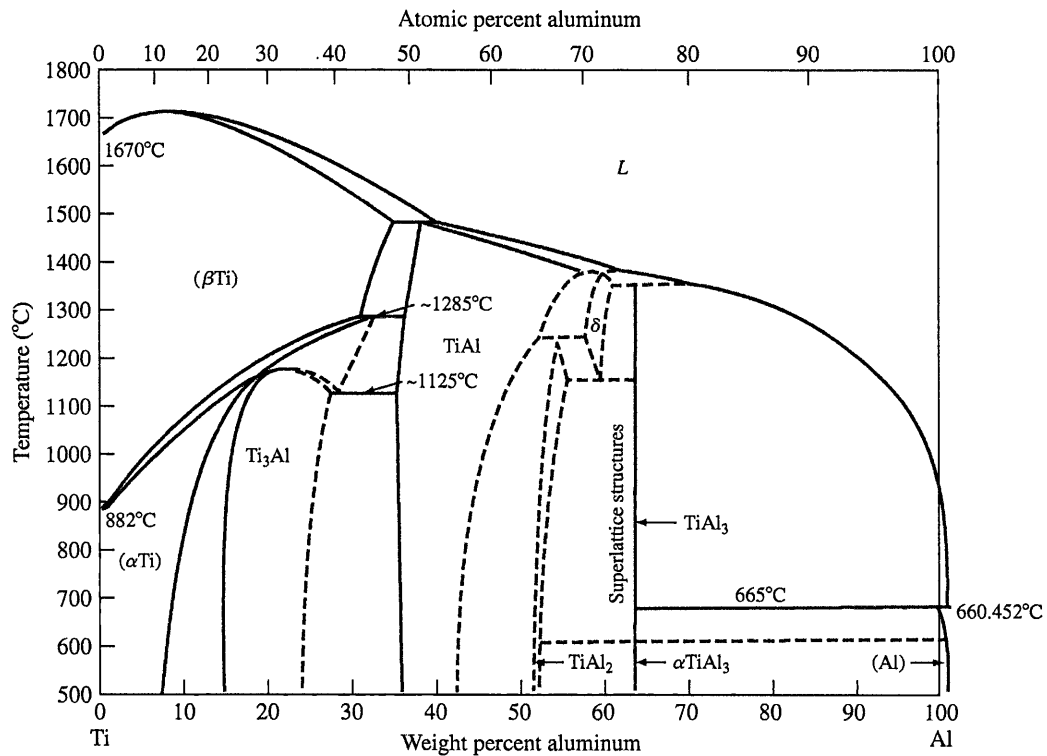
Figure P8.41
Titanium-aluminum phase diagram.
(*From "Binary Phase Diagrams," ASM Int., 1986, p. 142. Used by permission of ASM International.*)

Synthesis and Evaluation Problems

*8.43 In Fig. 8.12, determine the degree of freedom, F, according to Gibbs rule at the following points:

(*a*) At the melting point of pure tin.

(*b*) Inside the α region.

(*c*) Inside the α + liquid region

(*d*) Inside the α + β region

(*e*) At the eutectic point

8.44 In the Pb-Sn phase diagram (Fig. 8.12) answer the following questions:

(*a*) What is α (explain in detail including atomic structure? What is β?

(*b*) What the maximum solubility of Sn in α? At what temperature?

(*c*) What happens to the α in part (*b*) if it is cooled to room temperature?

(*d*) What is the maximum solubility of Sn in liquid metal at the lowest possible temperature? What is that temperature?

(*e*) What is the solubility limit of Sn in α when liquid is present? (This will be a range.)

8.45 Based on the Cu – Ag phase diagram in Fig. P8.22, draw the approximate cooling curve for the following alloys with approximate temperatures and explanations:
(*i*) Pure Cu, (*ii*) Cu – 10wt% Ag (*iii*) Cu – 71.9 wt% Ag (*iv*) Cu – 91.2 wt% Ag

8.46 Based on the Pd – Ag phase diagram in Fig. EP 8.3, draw the approximate cooling curve for the following alloys with approximate temperatures and explanations:
(*i*) Pure Pd, (*ii*) Pd – 30wt% Ag (*iii*) Pd – 70 wt% Ag (*iv*) Pure Ag

8.47 A number of elements along with their crystal structures and atomic radii are listed in the following table. Which pairs might be expected to have complete solid solubility in each other?

	Crystal structure	Atomic radius (nm)		Crystal structure	Atomic radius (nm)
Silver	FCC	0.144	Lead	FCC	0.175
Palladium	FCC	0.137	Tungsten	BCC	0.137
Copper	FCC	0.128	Rhodium	FCC	0.134
Gold	FCC	0.144	Platinum	FCC	0.138
Nickel	FCC	0.125	Tantalum	BCC	0.143
Aluminum	FCC	0.143	Potassium	BCC	0.231
Sodium	BCC	0.185	Molybdenum	BCC	0.136

8.48 Derive the lever rule for the amount in weight percent of each phase in two-phase regions of a binary phase diagram. Use a phase diagram in which two elements are completely soluble in each other.

8.49 Based on the Al – Ni phase diagram given in Fig. P8.39, how many grams of Ni should be alloyed with 100 grams of Al to synthesize an alloy of liquidus temperature of approximately 640°C?

8.50 An Al-10 wt % Ni alloy, Fig. P8.39, is completely liquid at 800°C. How many grams of Ni can you add to this alloy at 800°C without creating a solid phase?

8.51 Based on the Al_2O_3-SiO_2 phase diagram in Fig. 8.27, the wt% of phases present for Al_2O_3 – 55 wt% SiO_2 over the 1900 to 1500°C temperature range (use 100°C increments).

8.52 (*a*) Design a Cu-Ni alloy that will be completely solid at 1200°C (use Fig. 8.5).
(*b*) Design a Cu-Ni alloy that will exist at a completely molten state at 1300°C and becomes completely solid at 1200°C.

8.53 (*a*) Design a Pb-Sn alloy that will have a 50-50 solid and liquid phase fraction at 184°C. (*b*) How many grams of each component should you use to produce 100 grams of the overall alloy? (Use Fig. 8.12.)

8.54 Given that Pb and Sn have similar tensile strengths, design a Pb-Sn alloy that when cast would be the strongest alloy (use Fig. 8.12). Explain your reasons for your choice.

*8.55 Consider the sugar-water phase diagram shown in Fig. P8.55. (*a*) What wt% sugar can you dissolve in water at room temperature? (*b*) What wt% sugar can you dissolve in water at 100°C? (*c*) What would you call the solid curve?
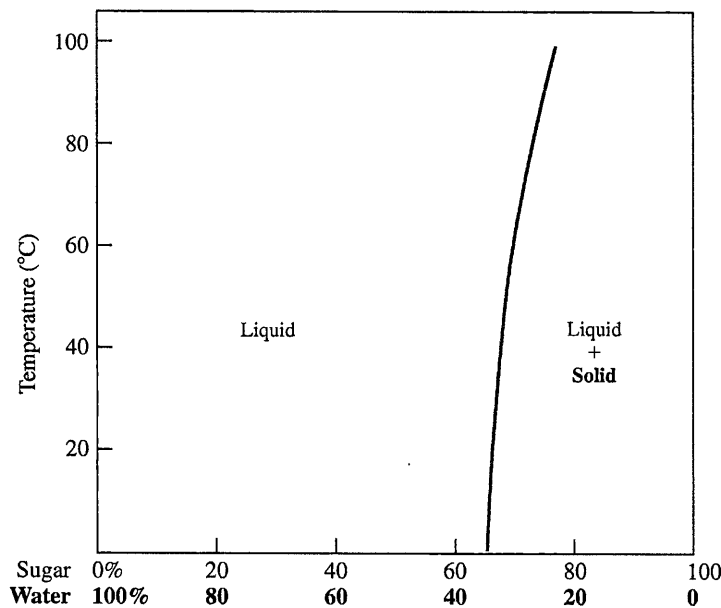
Figure P8.55

8.56 In Fig. P8.55, if 60 grams of water and 140 grams of sugar are mixed and stirred at a temperature of 80°C, (*a*) will this result in a single phase solution or a mixture? (*b*) What will happen if the solution/mixture in part (*a*) is slowly cooled to room temperature?

8.57 In Fig. P8.55, if 30 grams of water and 170 grams of sugar are mixed and stirred at a temperature of 30°C, (*a*) will this result in a single phase solution or a mixture? (*b*) If it's a mixture, how many grams of solid sugar will exist in the mixture? (*c*) How many grams of sugar (solid and dissolved) will exist in the mixture?

8.58 At 80°C, if the wt% of sugar is 80%, (*a*) what phases exist? (*b*) What is the weight fraction of each phase? (*c*) What is the wt% of water?

8.59 (*a*) Based on the phase diagram in Fig. P8.59, explain why city workers throw rock salt on icy roads. (*b*) Based on the same diagram, suggest a process that would produce almost pure water from seawater (3wt% salt).

*8.60 Referring to Fig. P8.59, explain what happens as 5wt% salt solution is cooled from room temperature to −30°C. Give information regarding phases available and the compositional changes in each phase.

8.61 Referring to Fig. P8.59, (*a*) explain what happens as 23wt% salt solution is cooled from room temperature to −30°C. Give information regarding phases available and the compositional changes in each phase. (*b*) What would you call this reaction? Can you write a transformation equation for this reaction?

8.62 Using Fig. P8.39, explain what the phase diagram is showing when the overall alloy composition is Al − 43wt% Ni (below 854°C)? Why is there a vertical line at that point in the phase diagram? Verify that the formula for the compound is Al_3Ni. What do you call such a compound?
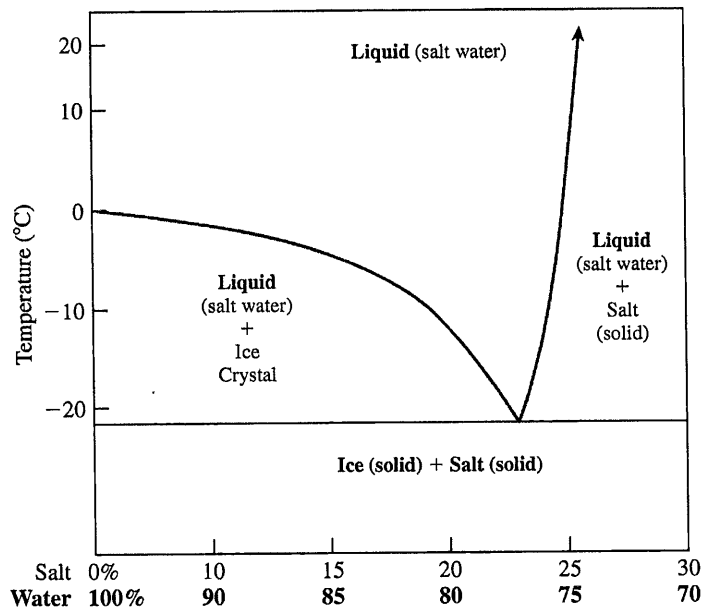
Figure P8.59

8.63 Using Fig. P8.39, explain why, according to the diagram, the intermetallic Al_3Ni is represented by a single vertical line while intermetallics Al_3Ni_2 and Al_3Ni_5 are represented by a region.

8.64 (*a*) In the Ti-Al phase diagram, Fig. P8.41, what phases are available at an overall alloy composition of Ti – 63 wt% Al at temperatures below 1300°C? (*b*) What is the significance of the vertical line at that alloy composition? (*c*) Verify the formula next to the vertical line. (*d*) Compare the melt temperature of this compound to that of Ti and Al. What is your conclusion?

9.2 THE IRON-CARBON SYSTEM

Iron-carbon alloys containing from a very small amount (about 0.03 percent) to about 1.2 percent carbon, 0.25 to 1.00 percent manganese, and minor amounts of other elements[3] are termed *plain-carbon steels*. However, for purposes of this section of the book, plain-carbon steels will be treated as essentially iron-carbon binary alloys. The effects of other elements in steels will be dealt with in later sections.

9.2.1 The Iron–Iron-Carbide Phase Diagram

The phases present in very slowly cooled iron-carbon alloys at various temperatures and compositions of iron with up to 6.67 percent carbon are shown in the Fe-Fe$_3$C phase diagram of Fig. 9.6. This phase diagram is not a true equilibrium diagram since the compound iron carbide (Fe$_3$C) that is formed is not a true equilibrium phase. Under certain conditions, Fe$_3$C, which is called **cementite,** can decompose into the more stable phases of iron and carbon (graphite). However, for most practical conditions, Fe$_3$C is very stable and will therefore be treated as an equilibrium phase.

9.2.2 Solid Phases in the Fe-Fe$_3$C Phase Diagram

The Fe-Fe$_3$C diagram contains the following solid phases: α ferrite, austenite (γ), cementite (Fe$_3$C), and δ ferrite.

α **ferrite.** This phase is an interstitial solid solution of carbon in the BCC iron crystal lattice. As indicated by the Fe-Fe$_3$C phase diagram, carbon is only slightly soluble in α ferrite, reaching a maximum solid solubility of 0.02 percent at 723°C. The solubility of carbon in α ferrite decreases to 0.005 percent at 0°C.

Austenite (γ). The interstitial solid solution of carbon in γ iron is called *austenite*. Austenite has an FCC crystal structure and a much higher solid solubility for carbon than α ferrite. The solid solubility of carbon in austenite is a maximum of 2.08 percent at 1148°C and decreases to 0.8 percent at 723°C (Fig. 9.6).

Cementite (Fe$_3$C). The intermetallic compound Fe$_3$C is called *cementite*. Cementite has negligible solubility limits and a composition of 6.67 percent C and 93.3 percent Fe. Cementite is a hard and brittle compound.

δ **ferrite.** The interstitial solid solution of carbon in δ iron is called δ *ferrite*. It has a BCC crystal structure like α ferrite but with a greater lattice constant. The maximum solid solubility of carbon in δ ferrite is 0.09 percent at 1465°C.

---

[3]Plain-carbon steels also contain impurities of silicon, phosphorus, and sulfur as well as others.
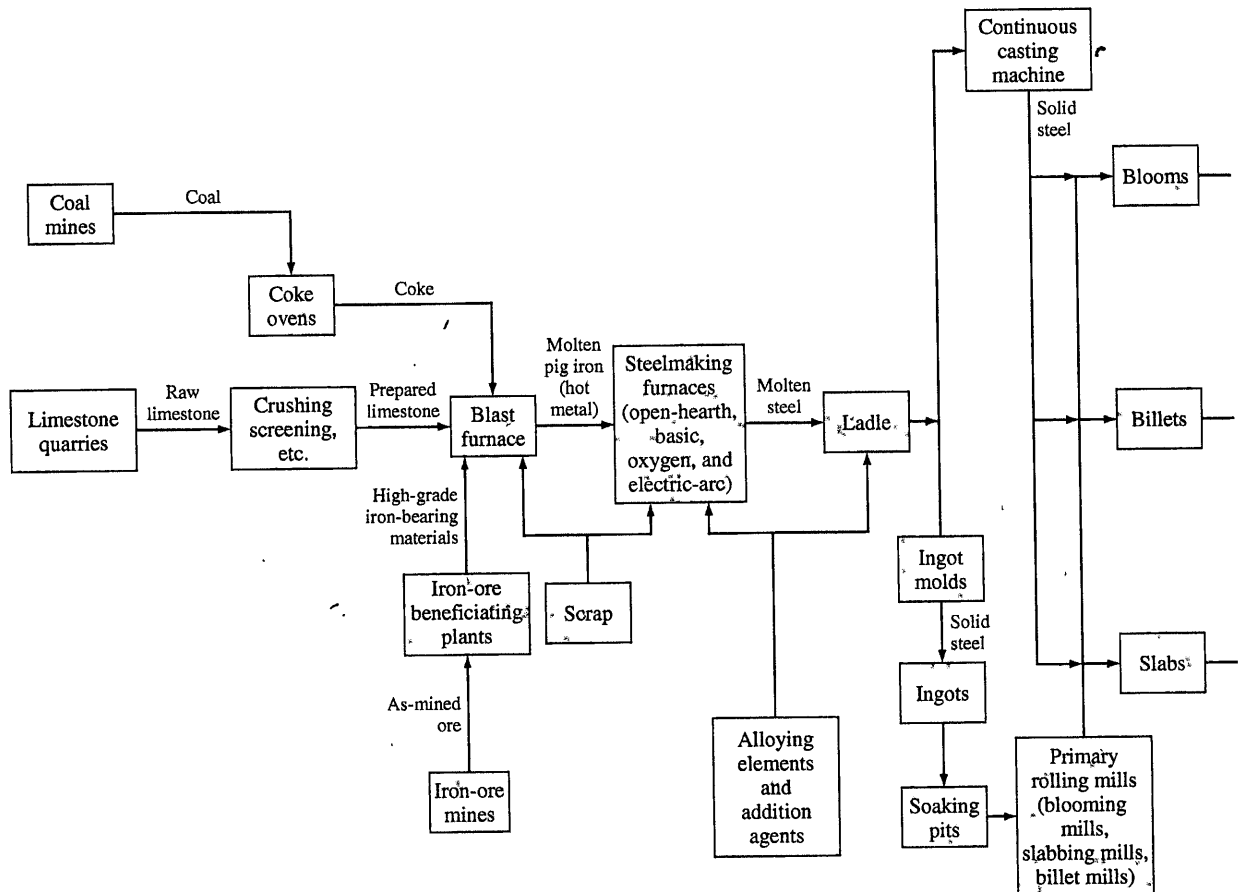
Figure 9.5
Flow diagram showing the principal process steps involved in converting raw materials into the major product forms, excluding coated products.
[*From H.E. McGannon (ed.), "The Making, Shaping, and Treating of Steel," 9th ed., United States Steel, 1971, p. 2. Courtesy of United States Steel Corporation.*]

9.2.3 Invariant Reactions in the Fe-Fe₃C Phase Diagram

Peritectic Reaction   At the peritectic reaction point, liquid of 0.53 percent C combines with δ ferrite of 0.09 percent C to form γ austenite of 0.17 percent C. This reaction, which occurs at 1495°C, can be written as

$$\text{Liquid (0.53\% C)} + \delta\,(0.09\%\,\text{C}) \xrightarrow{1495°C} \gamma\,(0.17\%\,\text{C})$$
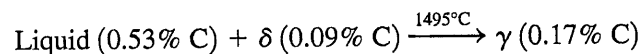
δ Ferrite is a high-temperature phase and so is not encountered in plain-carbon steels at lower temperatures.

Eutectic Reaction   At the eutectic reaction point, liquid of 4.3 percent forms γ austenite of 2.08 percent C and the intermetallic compound Fe₃C (cementite),

Some product forms (not to same scale)

Beams   Angles   Tees   Zees   Channels   Piling

Standard rails   Crane rails   Joint bars

Bars

Round   Square   Hexagonal   Octagonal   Flat   Triangular   Half round

Wire and wire products   Wire   Wire rope   Nails   Wire fabric

Pipe and tubes

Note: Other tubular products include electric-welded, large-diameter pipe made from plates, and electric-resistance-welded (ERW) pipe made from hot-rolled and cold-rolled strip.

Plates

Hot-rolled sheets and strip

Hot-rolled breakdowns in coil form   Cold-rolled sheets and strip (including black plate)   Sheets   Coils

Heating furnaces — Structural mills — Structural shapes

Rail mills — Rails and joint bars

Bar mills

Heating furnaces — Rod mills — Rods — Wire mills

Seamless pipe and tube mills

Heating furnaces — Skelp mills — Skelp — Continuous butt-weld pipe mill

Plate mills

Hot-strip mills — Cold reduction mills

Figure 9.5 (continued)

which contains 6.67 percent C. This reaction, which occurs at 1148°C, can be written as

$$\text{Liquid } (4.3\% \text{ C}) \xrightarrow{1148°C} \gamma \text{ austenite } (2.08\% \text{ C}) + \text{Fe}_3\text{C } (6.67\% \text{ C})$$
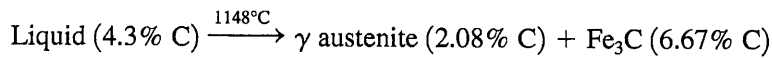
This reaction is not encountered in plain-carbon steels because their carbon contents are too low.

Eutectoid Reaction   At the eutectoid reaction point, solid austenite of 0.8 percent C produces α ferrite with 0.02 percent C and Fe_3C (cementite) that contains 6.67 percent C. This reaction, which occurs at 723°C, can be written as

$$\gamma \text{ austenite } (0.8\% \text{ C}) \xrightarrow{723°C} \alpha \text{ ferrite } (0.02\% \text{ C}) + \text{Fe}_3\text{C } (6.67\% \text{ C})$$
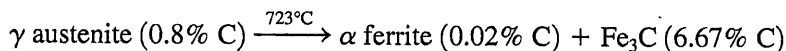
This eutectoid reaction, which takes place completely in the solid state, is important for some of the heat treatments of plain-carbon steels.
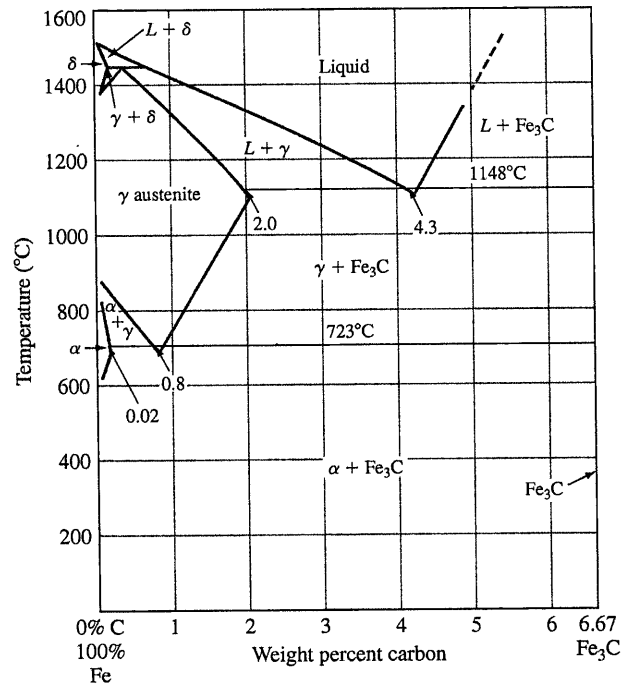
Figure 9.6
The iron–iron-carbide phase diagram.

A plain-carbon steel that contains 0.8 percent C is called a **eutectoid steel** since an all-eutectoid structure of α ferrite and Fe_3C is formed when austenite of this composition is slowly cooled below the eutectoid temperature. If a plain-carbon steel contains less than 0.8 percent C, it is termed a **hypoeutectoid steel,** and if the steel contains more than 0.8 percent C, it is designated a **hypereutectoid steel.**

9.2.4 Slow Cooling of Plain-Carbon Steels

Eutectoid Plain-Carbon Steels If a sample of a 0.8 percent (eutectoid) plain-carbon steel is heated to about 750°C and held for a sufficient time, its structure will become homogeneous austenite. This process is called **austenitizing.** If this eutectoid steel is then cooled very slowly to just above the eutectoid temperature, its structure will remain austenitic, as indicated in Fig. 9.7 at point a. Further cooling to the eutectoid temperature or just below it will cause the entire structure to transform from austenite to a lamellar structure of alternate plates of α ferrite and cementite (Fe_3C). Just below the eutectoid temperature, at point b in Fig. 9.7, the lamellar structure will appear as shown in Fig. 9.8. This eutectoid structure is called **pearlite** since it resembles mother-of-pearl. Since the solubility of carbon in α ferrite and Fe_3C changes very little from 723°C to room temperature, the pearlite structure will remain essentially unchanged in this temperature interval.
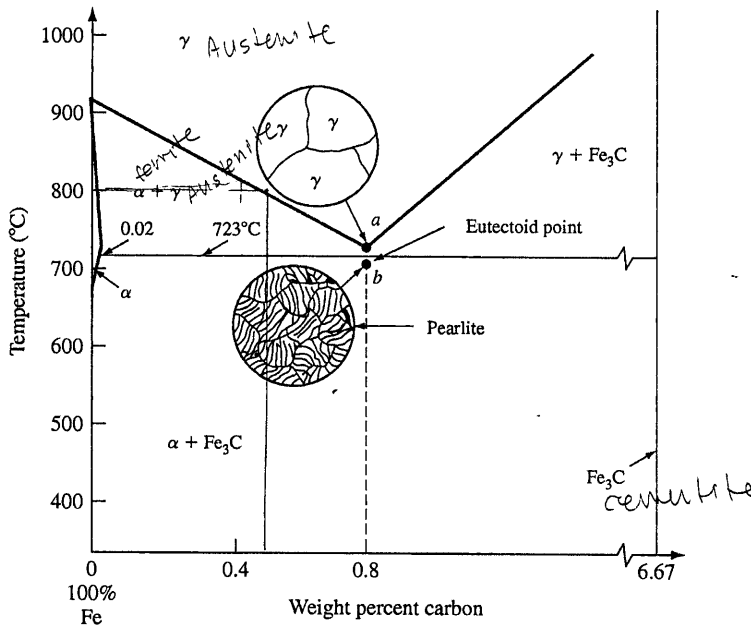
Figure 9.7
Transformation of a eutectoid steel (0.8 percent C) with slow cooling.
(From W.F. Smith, "Structure and Properties of Engineering Alloys," 2d ed., McGraw-Hill, 1993, p. 8. Reproduced with permission of The McGraw-Hill Companies.)

Figure 9.8
Microstructure of a slowly cooled eutectoid steel. The microstructure consists of lamellar eutectoid pearlite. The dark etched phase is cementite, and the white phase is ferrite. (Etch: picral; magnification 650×.)   Virtual Lab
(United States Steel Corporation, as presented in "Metals Handbook," vol. 8, 8th ed., American Society for Metals, 1973, p. 188.)

EXAMPLE PROBLEM 9.1

A 0.80 percent C eutectoid plain-carbon steel is slowly cooled from 750°C to a temperature just slightly below 723°C. Assuming that the austenite is completely transformed to α ferrite and cementite:

a. Calculate the weight percent eutectoid ferrite formed.
b. Calculate the weight percent eutectoid cementite formed.

■ **Solution**

Referring to Fig. 9.6, we first draw a tie line just below 723°C from the α ferrite phase boundary to the Fe_3C phase boundary and indicate the 0.80 percent C composition on the tie line as shown in the following figure:
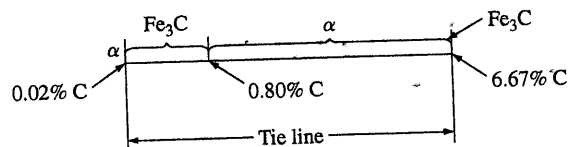
a. The weight fraction of ferrite is calculated from the ratio of the segment of the tie line to the right of 0.80 percent C over the whole length of the tie line. Multiplying by 100 percent gives the weight percent ferrite:

$$\text{Wt \% ferrite} = \frac{6.67 - 0.80}{6.67 - 0.02} \times 100\% = \frac{5.87}{6.65} \times 100\% = 88.3\% \blacktriangleleft$$

b. The weight percent cementite is calculated in a similar way by using the ratio of the segment of the tie line to the left of 0.80 percent C over the length of the whole tie line and multiplying by 100 percent:

$$\text{Wt \% cementite} = \frac{0.80 - 0.02}{6.67 - 0.02} \times 100\% = \frac{0.78}{6.65} \times 100\% = 11.7\% \blacktriangleleft$$

Hypoeutectoid Plain-Carbon Steels   If a sample of a 0.4 percent C plain-carbon steel (hypoeutectoid steel) is heated to about 900°C (point a in Fig. 9.9) for a sufficient time, its structure will become homogeneous austenite. Then, if this steel is slowly cooled to temperature b in Fig. 9.9 (about 775°C), **proeutectoid[4] ferrite** will nucleate and grow mostly at the austenitic grain boundaries. If this alloy is slowly cooled from temperature b to c in Fig. 9.9, the amount of proeutectoid ferrite formed will continue to increase until about 50 percent of the austenite is transformed. While the steel is cooling from b to c, the carbon content of the remaining austenite will be increased from 0.4 to 0.8 percent. At 723°C, if very slow cooling conditions prevail, the remaining austenite will transform isothermally

[4]The prefix *pro-* means "before," and thus the term *proeutectoid ferrite* is used to distinguish this constituent, which forms earlier, from eutectoid ferrite, which forms by the eutectoid reaction later in the cooling.
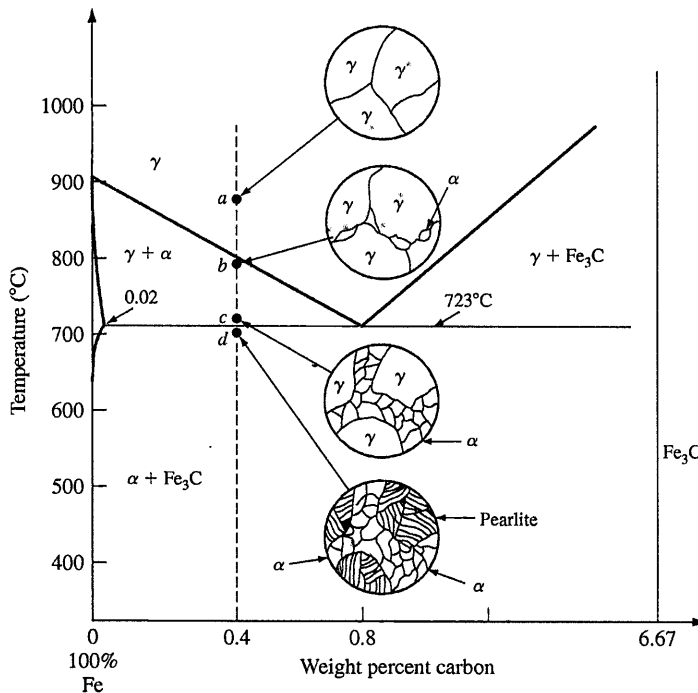
Figure 9.9
Transformation of a 0.4 percent C hypoeutectoid plain-carbon
steel with slow cooling.

(*From W.F. Smith, "Structure and Properties of Engineering Alloys," 2d ed.,
McGraw-Hill, 1993, p. 10. Reproduced with permission of The McGraw-Hill
Companies.*)

into pearlite by the eutectoid reaction austenite → ferrite + cementite. The α ferrite in the pearlite is called **eutectoid ferrite** to distinguish it from the proeutectoid ferrite that forms first above 723°C. Figure 9.10 is an optical micrograph of the structure of a 0.35 percent C hypoeutectoid steel that was austenitized and slowly cooled to room temperature.

---

a. A 0.40 percent C hypoeutectoid plain-carbon steel is slowly cooled from 940°C to a temperature just slightly above 723°C.

    (i)   Calculate the weight percent austenite present in the steel.

    (ii) Calculate the weight percent proeutectoid ferrite present in the steel.

b. A 0.40 percent C hypoeutectoid plain-carbon steel is slowly cooled from 940°C to a temperature just slightly below 723°C.

    (i)   Calculate the weight percent proeutectoid ferrite present in the steel.

    (ii)   Calculate the weight percent eutectoid ferrite and weight percent eutectoid cementite present in the steel.

**EXAMPLE
PROBLEM 9.2**

384 **CHAPTER 9** Engineering Alloys

■ **Solution**

Referring to Fig. 9.6 and using tie lines:

a. (i) Wt % austenite $= \dfrac{0.40 - 0.02}{0.80 - 0.02} \times 100\% = 50\%$ ◀

(ii) Wt % proeutectoid ferrite $= \dfrac{0.80 - 0.40}{0.80 - 0.02} \times 100\% = 50\%$ ◀

b. (i) The weight percent proeutectoid ferrite present in the steel just below 723°C will be the same as that just above 723°C, which is 50 percent.

(ii) The weight percent total ferrite and cementite just below 723°C are

$$\text{Wt \% total ferrite} = \frac{6.67 - 0.40}{6.67 - 0.02} \times 100\% = 94.3\%$$

$$\text{Wt \% total cementite} = \frac{0.40 - 0.02}{6.67 - 0.02} \times 100\% = 5.7\%$$

$$\text{Wt \% eutectoid ferrite} = \text{total ferrite} - \text{proeutectoid ferrite}$$

$$= 94.3 - 50 = 44.3\% \blacktriangleleft$$

$$\text{Wt \% eutectoid cementite} = \text{wt \% total cementite} = 5.7\% \blacktriangleleft$$

(No proeutectoid cementite was formed during cooling.)
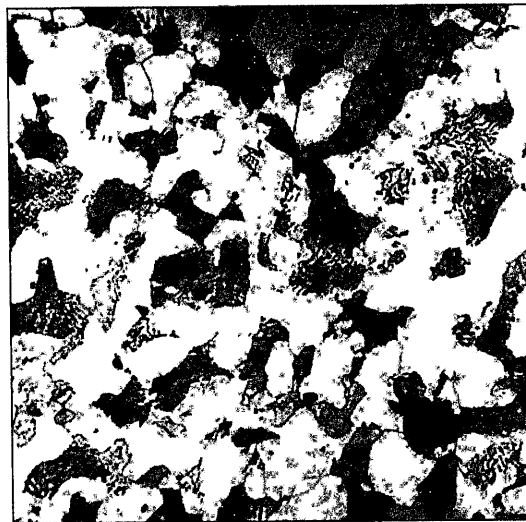
Figure 9.10
Microstructure of a 0.35 percent C hypoeutectoid plain-carbon steel slowly cooled from the austenite region. The white constituent is proeutectoid ferrite; the dark constituent is pearlite. (Etchant: 2% nital; magnification 500×.)
(*After W.F. Smith, "Structure and Properties of Engineering Alloys," 2d ed., McGraw-Hill, 1993, p. 11.*)
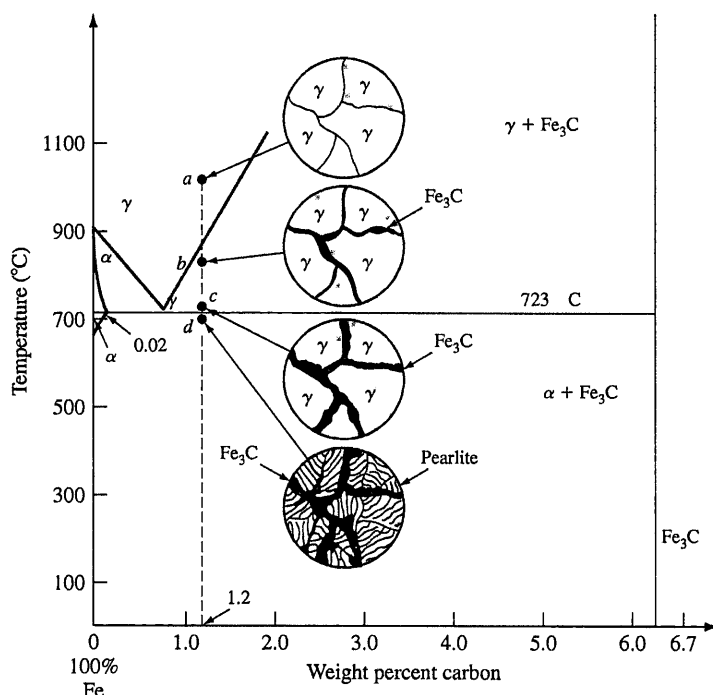
Figure 9.11
Transformation of a 1.2 percent C hypereutectoid plain-carbon
steel with slow cooling.
*(From W.F. Smith, "Structure and Properties of Engineering Alloys," 2d ed.,
McGraw-Hill, 1993, p. 12. Reproduced with permission of The McGraw-Hill
Companies.)*

Hypereutectoid Plain-Carbon Steels   If a sample of a 1.2 percent C plain-
carbon steel (hypereutectoid steel) is heated to about 950°C and held for a suffi-
cient time, its structure will become essentially all austenite (point *a* in Fig. 9.11).
Then, if this steel is cooled very slowly to temperature *b* in Fig. 9.11, **proeutectoid
cementite** will begin to nucleate and grow primarily at the austenite grain bound-
aries. With further slow cooling to point *c* of Fig. 9.11, which is just above 723°C,
more proeutectoid cementite will be formed at the austenite grain boundaries. If
conditions approaching equilibrium are maintained by the slow cooling, the over-
all carbon content of the austenite remaining in the alloy will change from 1.2 to
0.8 percent.

   With still further slow cooling to 723°C or just slightly below this temperature,
the remaining austenite will transform to pearlite by the eutectoid reaction, as indi-
cated at point *d* of Fig. 9.11. The cementite formed by the eutectoid reaction is called
eutectoid cementite to distinguish it from the proeutectoid cementite formed at tem-
peratures above 723°C. Similarly, the ferrite formed by the eutectoid reaction is

Figure 9.12
Microstructure of a 1.2 percent C hypereutectoid steel slowly cooled from the austenite region. In this structure, the proeutectoid cementite appears as the white constituent that has formed at the former austenite grain boundaries. The remaining structure consists of coarse lamellar pearlite. (Etchant: picral; magnification 1000×.)
(*Courtesy of United States Steel Corp.*)

termed *eutectoid ferrite*. Figure 9.12 is an optical micrograph of the structure of a 1.2 percent C hypereutectoid steel that was austenitized and slowly cooled to room temperature.

EXAMPLE PROBLEM 9.3

A hypoeutectoid plain-carbon steel that was slow-cooled from the austenitic region to room temperature contains 9.1 wt % eutectoid ferrite. Assuming no change in structure on cooling from just below the eutectoid temperature to room temperature, what is the carbon content of the steel?

■ **Solution**

Let x = the weight percent carbon of the hypoeutectoid steel. Now we can use the equation that relates the eutectoid ferrite to the total ferrite and the proeutectoid ferrite, which is

$$\text{Eutectoid ferrite} = \text{total ferrite} - \text{proeutectoid ferrite}$$

Using Fig. EP9.3 and the lever rule, we can make the equation.

Figure EP9.3

$$0.091 = \frac{6.67 - x}{6.67 - 0.02} - \frac{0.80 - x}{0.80 - 0.02} = \frac{6.67}{6.65} - \frac{x}{6.65} - \frac{0.80}{0.78} + \frac{x}{0.78}$$

Eutectoid   Total   Proeutectoid
ferrite   ferrite   ferrite

or

$$1.28x - 0.150x = 0.091 - 1.003 + 1.026 = 0.114$$

$$x = \frac{0.114}{1.13} = 0.101\% \text{ C} \blacktriangleleft$$

9.3 HEAT TREATMENT OF PLAIN-CARBON STEELS

By varying the manner in which plain-carbon steels are heated and cooled, different combinations of mechanical properties for steels can be obtained. In this section, we shall examine some of the structural and property changes that take place during some of the important heat treatments given to plain-carbon steels.

9.3.1 Martensite

Formation of Fe-C Martensite by Rapid Quenching   If a sample of a plain-carbon steel in the austenitic condition is rapidly cooled to room temperature by quenching it in water, its structure will be changed from austenite to **martensite.** Martensite in plain-carbon steels is a metastable phase consisting of a supersaturated interstitial solid solution of carbon in body-centered cubic iron or body-centered tetragonal iron (the tetragonality is caused by a slight distortion of the BCC iron unit cell). The temperature,
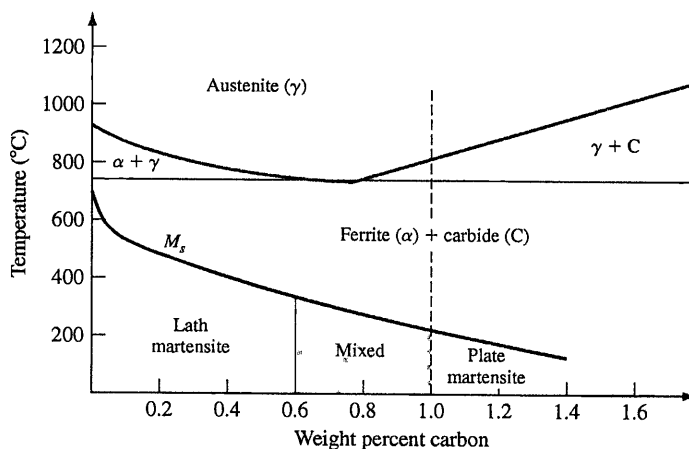
Figure 9.13
Effect of carbon content on the martensite-transformation start temperature, M_s, for iron-carbon alloys.
(*From A.R. Marder and G. Krauss, as presented in "Hardenability Concepts with Applications to Steel," AIME, 1978, p. 238.*)

upon cooling, at which the austenite-to-martensite transformation starts is called the *martensite start, M_s,* temperature, and the temperature at which the transformation finishes is called the *martensite finish, M_f,* temperature. The M_s temperature for Fe-C alloys decreases as the weight percent carbon increases in these alloys, as shown in Fig. 9.13.

Microstructure of Fe-C Martensites The microstructure of martensites in plain-carbon steels depends on the carbon content of the steel. If the steel contains less than about 0.6 percent C, the martensite consists of *domains* of laths of different but limited orientations through a whole domain. The structure within the laths is highly distorted, consisting of regions with high densities of dislocation tangles. Figure 9.14a is an optical micrograph of *lath martensite* in an Fe–0.2% C alloy at 600×, while Fig. 9.15 shows the substructure of lath martensite in this alloy in an electron micrograph at 60,000×.

As the carbon content of the Fe-C martensites is increased to above about 0.6 percent C, a different type of martensite, called *plate martensite,* begins to form. Above about 1 percent C, Fe-C alloys consist entirely of plate martensite. Figure 9.14b is an optical micrograph of plate martensite in an Fe–1.2% C alloy at 600×. The plates in high-carbon Fe-C martensites vary in size and have a fine structure of parallel twins, as shown in Fig. 9.16. The plates are often surrounded by large amounts of untransformed (retained) austenite. Fe-C martensites with carbon contents between about 0.6 and 1.0 percent C have microstructures consisting of both lath- and plate-type martensites.

Structure of Fe-C Martensites on an Atomic Scale The transformation of austenite to martensite in Fe-C alloys (plain-carbon steels) is considered to be *diffusionless*

(a)   (b)
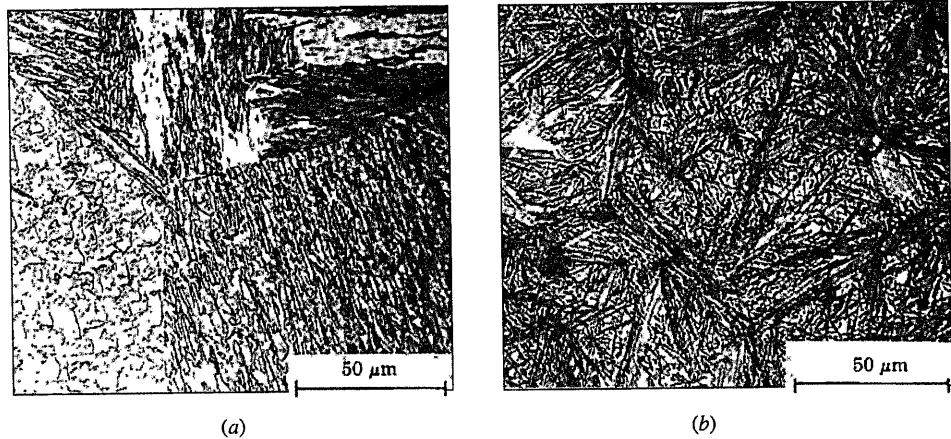
Figure 9.14
Effect of carbon content on the structure of martensite in plain-carbon steels: (a) lath type, (b) plate type. (Etchant: sodium bisulfite; optical micrographs.)
[After A.R. Marder and G. Krauss, Trans. ASM, 60:651(1967). Reprinted with permission of ASM International. All rights reserved. www.asminternational.org.]

Figure 9.15
Structure of lath martensite in an Fe–0.2% C alloy. (Note the parallel alignment of the laths.)
[After A.R. Marder and G. Krauss, Trans. ASM, 60:651 (1967). Reprinted with permission of ASM International. All rights reserved. www.asminternational.org.]

Figure 9.16
Plate martensite showing fine transformation twins.
[After M. Oka and C.M. Wayman, Trans. ASM, 62:370(1969). Reprinted with permission of ASM International. All rights reserved. www.asminternational.org.]

(a) (b) (c)
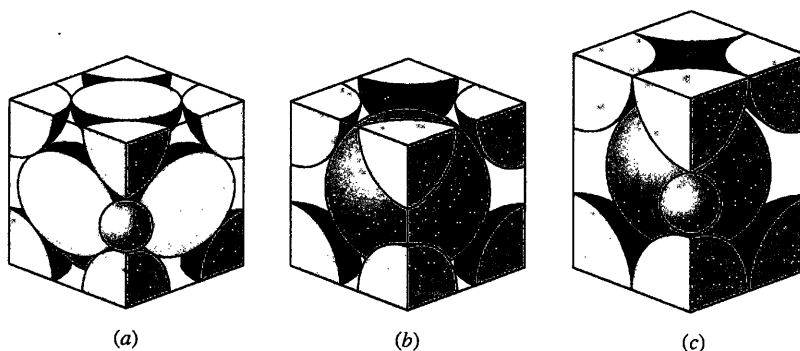
Figure 9.17
(a) FCC γ iron unit cell showing a carbon atom in a large interstitial hole along the cube edge of the cell. (b) BCC α iron unit cell indicating a smaller interstitial hole between cube-edge atoms of the unit cell. (c) BCT (body-centered tetragonal) iron unit cell produced by the distortion of the BCC unit cell by the interstitial carbon atom.
(*From E.R. Parker and V.F. Zackay, "Strong and Ductile Steels," Scientific American, November 1968, p. 42.*)

MatVis

since the transformation takes place so rapidly that the atoms do not have time to intermix. There appears to be no thermal-activation energy barrier to prevent martensite from forming. Also, it is believed that no compositional change in the parent phase takes place after the reaction and that each atom tends to retain its original neighbors. The relative positions of the carbon atoms with respect to the iron atoms are the same in the martensite as they were in the austenite.

For carbon contents in Fe-C martensites of less than about 0.2 percent C, the austenite transforms to a BCC α ferrite crystal structure. As the carbon content of the Fe-C alloys is increased, the BCC structure is distorted into a BCT (*body-centered tetragonal*) crystal structure. The largest interstitial hole in the γ iron FCC crystal structure has a diameter of 0.104 nm (Fig. 9.17a), whereas the largest interstitial hole in the α iron BCC structure has a diameter of 0.072 nm (Fig. 9.17b). Since the carbon atom has a diameter of 0.154 nm, it can be accommodated in interstitial solid solution to a greater extent in the FCC γ iron lattice. When Fe-C martensites with more than about 0.2 percent C are produced by rapid cooling from austenite, the reduced interstitial spacings of the BCC lattice cause the carbon atoms to distort the BCC unit cell along its c axis to accommodate the carbon atoms (Fig. 9.17c). Figure 9.18 shows how the c axis of the Fe-C martensite lattice is elongated as its carbon content increases.

Hardness and Strength of Fe-C Martensites The hardness and strength of Fe-C martensites are directly related to their carbon content and increase as the carbon content is increased (Fig. 9.19). However, ductility and toughness also decrease with increasing carbon content, and so most martensitic plain-carbon steels are tempered by reheating at a temperature below the transformation temperature of 723°C.
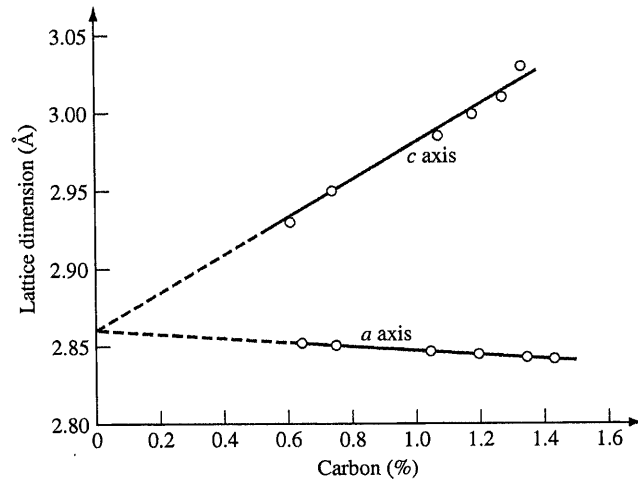
Figure 9.18
Variation of *a* and *c* axes of the Fe-C martensite lattice as a function of carbon content.
(*From p. 36 in E.C. Bain and H.W. Paxton, "Alloying Elements in Steel," 2d ed., American Society for Metals, 1966. Used by permission of ASM International.*)
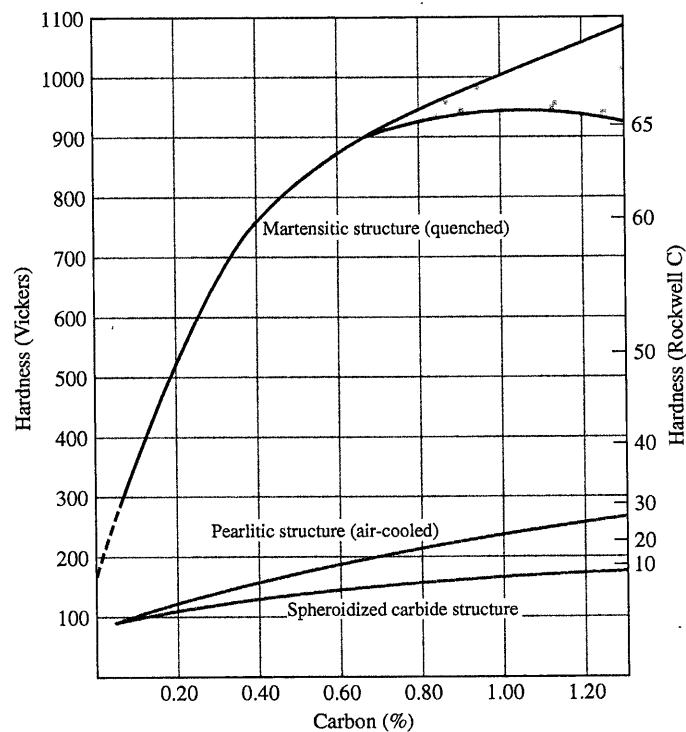
Figure 9.19
Approximate hardness of fully hardened martensitic plain-carbon steel as a function of carbon content. The shaded region indicates some possible loss of hardness due to the formation of retained austenite, which is softer than martensite.
(*From p. 37 in E.C. Bain and H.W. Paxton, "Alloying Elements in Steel," 2d ed., American Society for Metals, 1966. Used by permission of ASM International.*)

CHAPTER 9 Engineering Alloys

Low-carbon Fe-C martensites are strengthened by a high concentration of dislocations being formed (lath martensite) and by interstitial solid-solution strengthening by carbon atoms. The high concentration of dislocations in networks (lath martensite) makes it difficult for other dislocations to move. As the carbon content increases above 0.2 percent, interstitial solid-solution strengthening becomes more important and the BCC iron lattice becomes distorted into tetragonality. However, in high-carbon Fe-C martensites, the numerous twinned interfaces in plate martensite also contribute to the hardness.

9.3.2 Isothermal Decomposition of Austenite

Isothermal Transformation Diagram for a Eutectoid Plain-Carbon Steel In previous sections, the reaction products from the decomposition of austenite of eutectoid plain-carbon steels for very slow and rapid cooling conditions have been described. Let us now consider what reaction products form when austenite of eutectoid steels is rapidly cooled to temperatures below the eutectoid temperature and then *isothermally transformed.*

Isothermal transformation experiments to investigate the microstructural changes for the decomposition of eutectoid austenite can be made by using a number of small samples, each about the size of a dime. The samples are first austenitized in a furnace at a temperature above the eutectoid temperature (Fig. 9.20a). The samples are then rapidly cooled (quenched) in a liquid salt bath at the desired temperature below the eutectoid temperature (Fig. 9.20b). After various time intervals, the samples are removed from the salt bath one at a time and quenched into water at room temperature (Fig. 9.20c). The microstructure after each transformation time can then be examined at room temperature.

Consider the microstructural changes that take place during the isothermal transformation of a eutectoid plain-carbon steel at 705°C, as schematically shown in

Furnace at	Salt bath for	Cold water
temperature	isothermal	quench tank at
above 723°C	transformation at	room temperature
	some temperature	
	below 723°C	
(a)	(b)	(c)
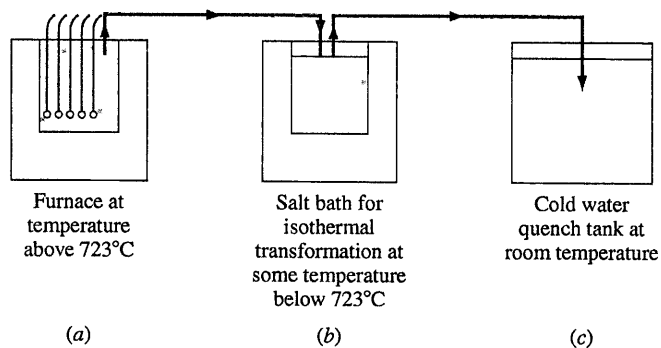
Figure 9.20

Experimental arrangement for determining the microscopic changes that occur during the isothermal transformation of austenite in a eutectoid plain-carbon steel.

(From W.F. Smith, "Structure and Properties of Engineering Alloys," McGraw-Hill, 1981, p. 14. Reproduced with permission of The McGraw-Hill Companies.)
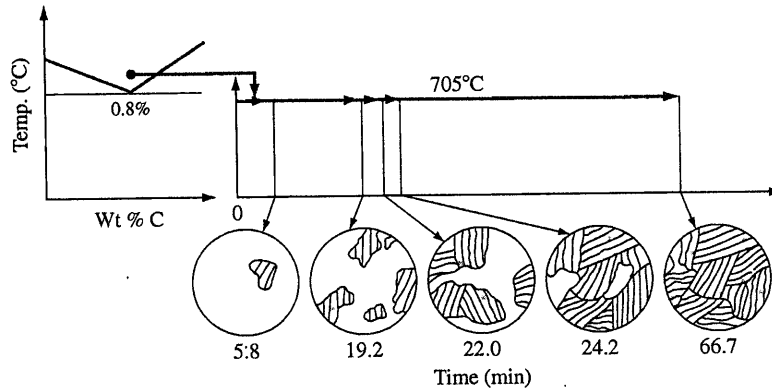
Figure 9.21
Experiment for following the microstructural changes that occur during the isothermal transformation of a eutectoid plain-carbon steel at 705°C. After austenitizing, samples are quenched in a salt bath at 705°C, held for the times indicated, and then quenched in water at room temperature.
(*From W.F. Smith, "Structure and Properties of Engineering Alloys," McGraw-Hill, 1981, p. 14. Reproduced with permission of The McGraw-Hill Companies.*)
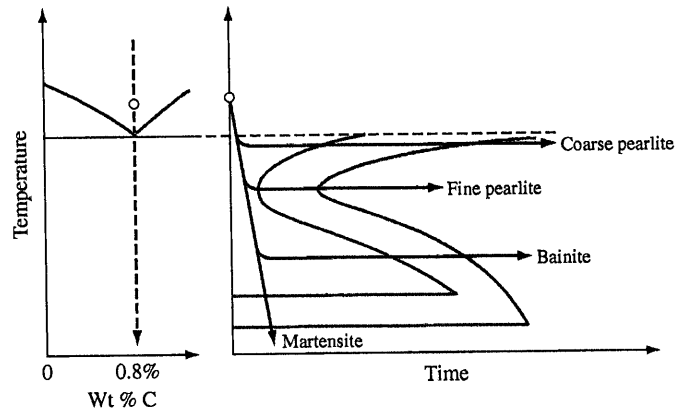
Figure 9.22
Isothermal transformation diagram for a eutectoid plain-carbon steel showing its relationship to the Fe-Fe$_3$C phase diagram.

Fig. 9.21. After being austenitized, the samples are hot-quenched into a salt bath at 705°C. After about 6 min, coarse pearlite has formed to a small extent. After about 67 min, the austenite is completely transformed to coarse pearlite.

By repeating the same procedure for the isothermal transformation of eutectoid steels at progressively lower temperatures, an **isothermal transformation (IT) diagram** can be constructed, as shown schematically in Fig. 9.22 and from experimental

CHAPTER 9 Engineering Alloys
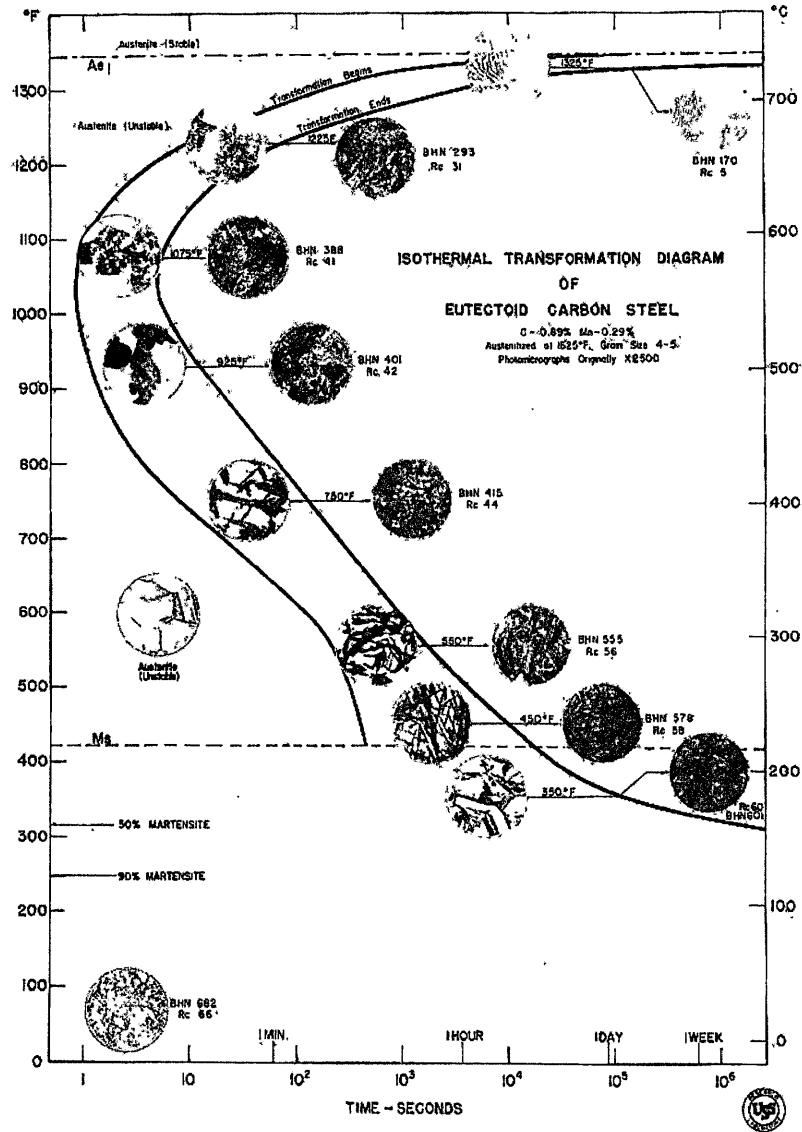
Figure 9.23
Isothermal transformation diagram of a eutectoid steel.
(*Courtesy of United States Steel Corporation.*)

data in Fig. 9.23. The S-shaped curve next to the temperature axis indicates the time necessary for the isothermal transformation of austenite to begin, and the second S curve indicates the time required for the transformation to be completed.

Isothermal transformations of eutectoid steels at temperatures between 723°C and about 550°C produce pearlitic microstructures. As the transformation tempera-

(a)   (b)
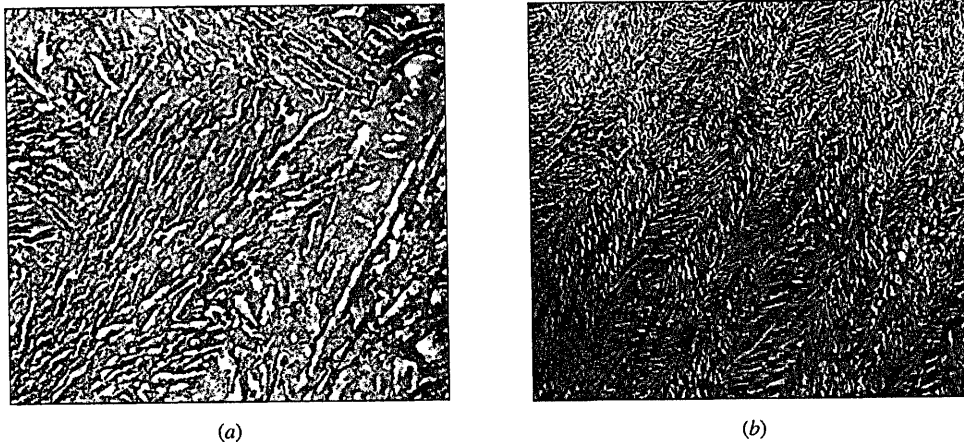
Figure 9.24
(a) Microstructure of upper bainite formed by a complete transformation of a eutectoid steel at 450°C (850°F). (b) Microstructure of lower bainite formed by a complete transformation of a eutectoid steel at 260°C (500°F). The white particles are Fe_3C, and the dark matrix is ferrite. (Electron micrographs, replica-type; magnification 15,000×.)
[After H.E. McGannon (ed.), "The Making, Shaping, and Treating of Steel," 9th ed., United States Steel Corp., 1971.]

ture is decreased in this range, the pearlite changes from a coarse to a fine structure (Fig. 9.23). Rapid quenching (cooling) of a eutectoid steel from temperatures above 723°C, where it is in the austenitic condition, transforms the austenite into martensite, as has been previously discussed.

If eutectoid steels in the austenitic condition are hot-quenched to temperatures in the 550°C to 250°C range and are isothermally transformed, a structure intermediate between pearlite and martensite, called **bainite,**[5] is produced. Bainite in Fe-C alloys can be defined as an austenitic decomposition product that has a *nonlamellar eutectoid structure* of α ferrite and cementite (Fe_3C). For eutectoid plain-carbon steels, a distinction is made between *upper bainite,* which is formed by isothermal transformation at temperatures between about 550°C and 350°C, and *lower bainite,* which is formed between about 350°C and 250°C. Figure 9.24a shows an electron micrograph (replica-type) of the microstructure of upper bainite for a eutectoid plain-carbon steel, and Fig. 9.24b shows one for lower bainite. Upper bainite has large, rodlike cementite regions, whereas lower bainite has much finer cementite particles. As the transformation temperature is decreased, the carbon atoms cannot diffuse as easily, and hence the lower bainite structure has smaller particles of cementite.

---

[5]Bainite is named after E.C. Bain, the American metallurgist who first intensively studied the isothermal transformations of steels. See E.S. Davenport and E.C. Bain, *Trans. AIME,* **90:**117 (1930).

CHAPTER 9 Engineering Alloys

Small, thin pieces of 0.25 mm thick hot-rolled strips of 1080 steel are heated for 1 h at 850°C and then given the heat treatments shown in the following list. Using the isothermal transformation diagram of Fig. 9.23, determine the microstructures of the samples after each heat treatment.

a. Water-quench to room temperature.
b. Hot-quench in molten salt to 690°C and hold 2 h; water-quench.
c. Hot-quench to 610°C and hold 3 min; water-quench.
d. Hot-quench to 580°C and hold 2 s; water-quench.
e. Hot-quench to 450°C and hold 1 h; water-quench.
f. Hot-quench to 300°C and hold 30 min; water-quench.
g. Hot-quench to 300°C and hold 5 h; water quench.

■ **Solution**

The cooling paths are indicated on Fig. EP9.4 and the microstructures obtained are listed as follows:

a. All martensite.
b. All coarse pearlite.
c. All fine pearlite.
d. Approximately 50 percent fine pearlite and 50 percent martensite.
e. All upper bainite.
f. Approximately 50 percent lower bainite and 50 percent martensite.
g. All lower bainite.
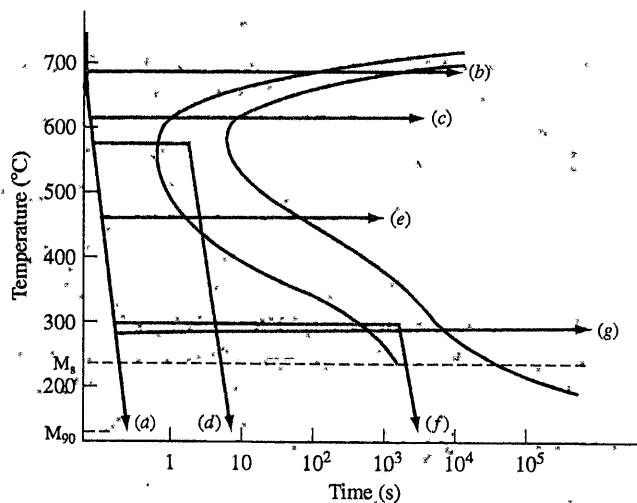
Figure EP9.4
Isothermal transformation diagram for a eutectoid plain-carbon steel indicating various cooling paths.
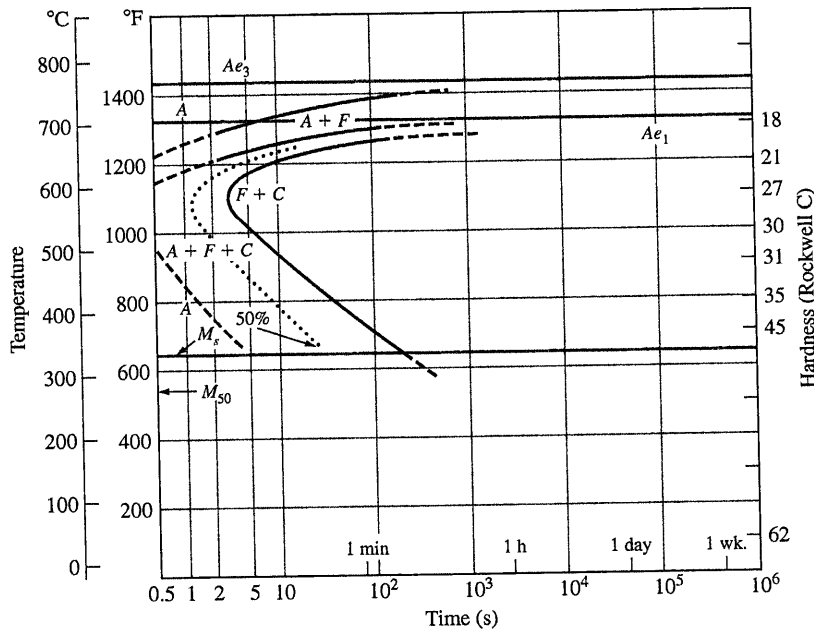
Figure 9.25
Isothermal transformation diagram for a hypoeutectoid steel containing
0.47 percent C and 0.57 percent Mn (austenitizing temperature: 843°C).
[*From R.A. Grange and J.K. Kiefer as adapted in E.C. Bain and H.W. Paxton, "Alloying
Elements in Steel," 2d ed., American Society for Metals, 1966.*]

Isothermal Transformation Diagrams for Noneutectoid Plain-Carbon Steels

Isothermal transformation diagrams have been determined for noneutectoid plain-carbon steels. Figure 9.25 shows an IT diagram for a 0.47 percent hypoeutectoid plain-carbon steel. Several differences are evident between the IT diagram for a noneutectoid plain-carbon steel and the diagram for a eutectoid one (Fig. 9.23). One major difference is that the S curves of the hypoeutectoid steel have been shifted to the left, so that it is not possible to quench this steel from the austenitic region to produce an entirely martensitic structure.

A second major difference is that another transformation line has been added to the upper part of the eutectoid steel IT diagram that indicates the start of the formation of proeutectoid ferrite. Thus, at temperatures between 723°C and about 765°C, only proeutectoid ferrite is produced by isothermal transformation.

Similar IT diagrams have been determined for hypereutectoid plain-carbon steels. However, in this case, the uppermost line of the diagram for these steels is for the start of the formation of proeutectoid cementite.

9.3.3 Continuous-Cooling Transformation Diagram for a Eutectoid Plain-Carbon Steel

In industrial heat-treating operations, in most cases a steel is not isothermally transformed at a temperature above the martensite start temperature but is continuously
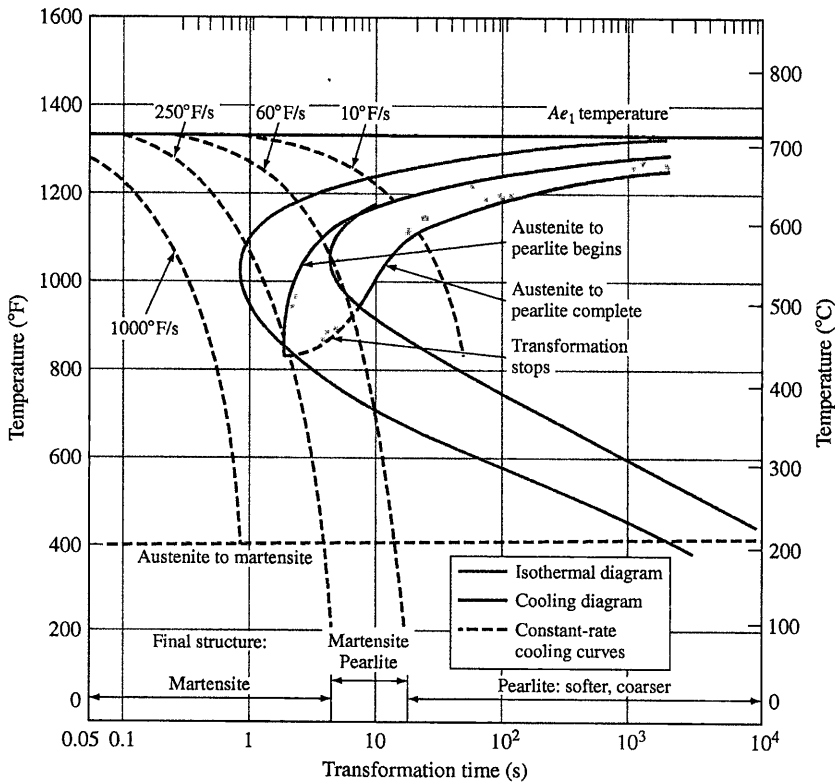
Figure 9.26

Continuous-cooling diagram for a plain-carbon eutectoid steel.

(*After R.A. Grange and J.M. Kiefer as adapted in E.C. Bain and H.W. Paxton, "Alloying Elements in Steel," 2d ed., American Society for Metals, 1966, p. 254.*)

cooled from the austenitic temperature to room temperature. In continuously cooling a plain-carbon steel, the transformation from austenite to pearlite occurs over a range of temperatures rather than at a single isothermal temperature. As a result, the final microstructure after continuous cooling will be complex since the reaction kinetics change over the temperature range in which the transformation takes place. Figure 9.26 shows a **continuous-cooling transformation (CCT) diagram** for a eutectoid plain-carbon steel superimposed over an IT diagram for this steel. The continuous-cooling diagram transformation start and finish lines are shifted to longer times and slightly lower temperatures in relation to the isothermal diagram. Also, there are no transformation lines below about 450°C for the austenite-to-bainite transformation.

Figure 9.27 shows different rates of cooling for thin samples of eutectoid plain-carbon steels cooled continuously from the austenitic region to room temperature. Cooling curve *A* represents very slow cooling, such as would be obtained by shutting off the power of an electric furnace and allowing the steel to cool as the furnace cools. The microstructure in this case would be coarse pearlite. Cooling curve *B* represents
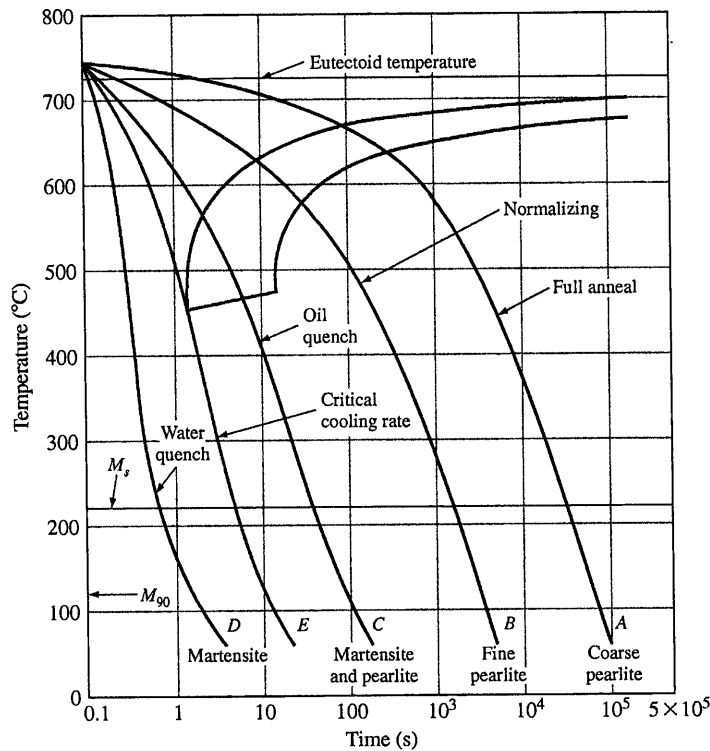
Figure 9.27
Variation in the microstructure of a eutectoid plain-carbon steel
by continuously cooling at different rates.
*(From R.E. Reed-Hill, "Physical Metallurgy Principles," 2d ed., D. Van
Nostrand Co., 1973 © PWS Publishers.)*

more rapid cooling, such as would be obtained by removing an austenitized steel
from a furnace and allowing the steel to cool in still air. A fine pearlite microstructure
is formed in this case.

Cooling curve *C* of Fig. 9.27 starts with the formation of pearlite, but there is
insufficient time to complete the austenite-to-pearlite transformation. The remaining
austenite that does not transform to pearlite at the upper temperatures will transform
to martensite at lower temperatures starting at about 220°C. This type of transfor-
mation, since it takes place in two steps, is called a *split transformation.* The
microstructure of this steel will thus consist of a mixture of pearlite and martensite.
Cooling at a rate faster than curve *E* of Fig. 9.27, which is called the *critical cooling
rate,* will produce a fully hardened martensitic structure.

Continuous-cooling diagrams have been determined for many hypoeutectoid
plain-carbon steels and are more complex since at low temperatures some bainitic
structure is also formed during continuous cooling. The discussion of these diagrams
is beyond the scope of this book.

CHAPTER 9 Engineering Alloys

9.3.4 Annealing and Normalizing of Plain-Carbon Steels

In Chapter 6, the cold-working and annealing processes for metals were discussed, and reference should be made to that section. The two most common types of annealing processes applied to commercial plain-carbon steels are *full annealing* and *process annealing.*

In full annealing, hypoeutectoid and eutectoid steels are heated in the austenite region about 40°C above the austenite-ferrite boundary (Fig. 9.28), held the necessary time at the elevated temperature, and then slowly cooled to room temperature, usually in the furnace in which they were heated. For hypereutectoid steels, it is customary to austenitize in the two-phase austenite plus cementite (Fe$_3$C) region, about 40°C above the eutectoid temperature. The microstructure of hypoeutectoid steels after full annealing consists of proeutectoid ferrite and pearlite (Fig. 9.10).

Process annealing, which is often referred to as a *stress relief,* partially softens cold-worked low-carbon steels by relieving internal stresses from cold working. This treatment, which is usually applied to hypoeutectoid steels with less than 0.3 percent C, is carried out at a temperature below the eutectoid temperature, usually between 550°C and 650°C (Fig. 9.28).

Normalizing is a heat treatment in which the steel is heated in the austenitic region and then cooled in still air. The microstructure of thin sections of normalized
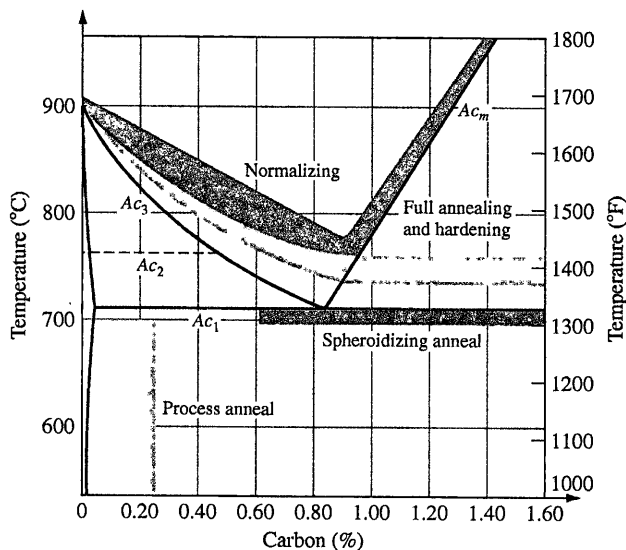
Figure 9.28
Commonly used temperature ranges for annealing plain-carbon steels.
(*From T.G. Digges et al., "Heat treatment and Properties of Iron and Steel," NBS Monograph 88, 1966, p. 10.*)

hypoeutectoid plain-carbon steels consists of proeutectoid ferrite and fine pearlite. The purposes for normalizing vary. Some of these are:

1. To refine the grain structure
2. To increase the strength of the steel (compared to annealed steel)
3. To reduce compositional segregation in castings or forgings and thus provide a more uniform structure

The austenitizing temperature ranges used for normalizing plain-carbon steels are shown in Fig. 9.28. Normalizing is more economical than full annealing since no furnace is required to control the cooling rate of the steel.

9.3.5 Tempering of Plain-Carbon Steels

The Tempering Process   Tempering is the process of heating a martensitic steel at a temperature below the eutectoid transformation temperature to make it softer and more ductile. Figure 9.29 schematically illustrates the customary quenching and tempering process for a **plain-carbon steel.** As shown in Fig. 9.29, the steel is first austenitized and then quenched at a rapid rate to produce martensite and to avoid the transformation of austenite to ferrite and cementite. The steel is then subsequently reheated at a temperature below the eutectoid temperature to soften the martensite by transforming it to a structure of iron carbide particles in a matrix of ferrite.
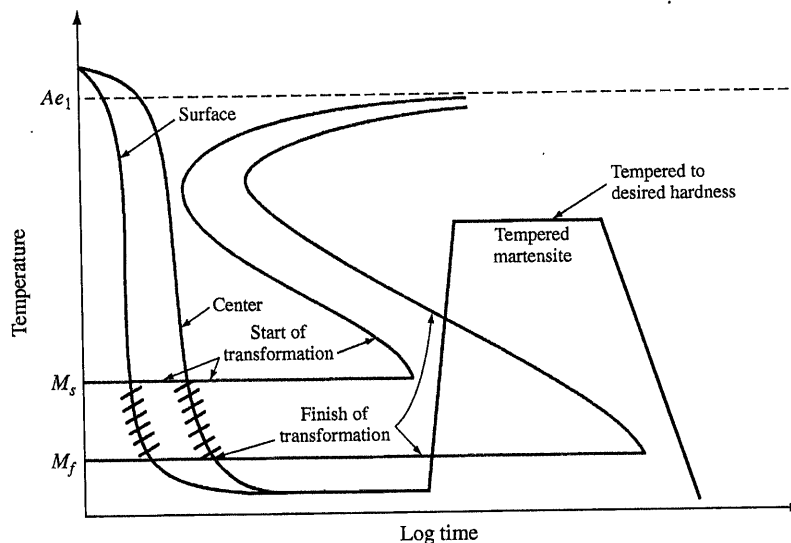
Figure 9.29
Schematic diagram illustrating the customary quenching and tempering process for a plain-carbon steel.
(*From "Suiting the Heat Treatment to the Job," United States Steel Corp., 1968, p. 34. Courtesy of United States Steel Corporation.*)

402   **CHAPTER 9**   Engineering Alloys

Microstructural Changes in Martensite Upon Tempering   Martensite is a metastable structure and decomposes upon reheating. In lath martensites of low-carbon plain-carbon steels, there is a high dislocation density, and these dislocations provide lower-energy sites for carbon atoms than their regular interstitial positions. Thus, when low-carbon martensitic steels are first tempered in the 20°C to 200°C range, the carbon atoms segregate themselves to these lower-energy sites.

For martensitic plain-carbon steels with more than 0.2 percent carbon, the main mode of carbon redistribution at tempering temperatures below 200°C is by precipitation clustering. In this temperature range, a very small-sized precipitate called *epsilon (ε) carbide* forms. The carbide that forms when martensitic steels are tempered from 200°C to 700°C is *cementite, Fe_3C*. When the steels are tempered between 200°C and 300°C, the shape of the precipitate is rodlike (Fig. 9.30). At higher tempering temperatures from 400°C to 700°C, the rodlike carbides coalesce to form sphere-like particles. Tempered martensite that shows the coalesced cementite in the optical microscope is called **spheroidite** (Fig. 9.31).

Figure 9.30
Precipitation of Fe_3C in Fe–0.39% C martensite tempered 1 h at 300°C. (Electron micrograph.)
[*After G.R. Speich and W.C. Leslie, Met. Trans., 31:1043(1972).*]
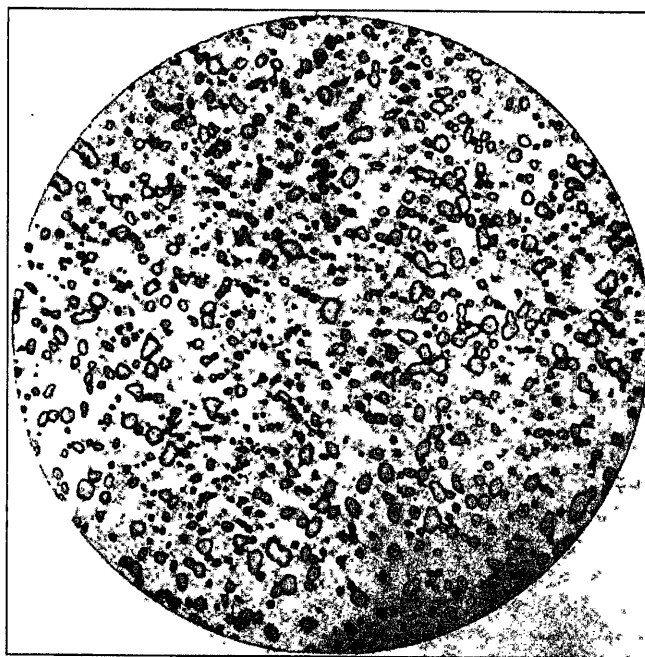
Figure 9.31
Spheroidite in a 1.1 percent C hypereutectoid steel. (Magnification 1000×.)
(*After J. Vilella, E.C. Bain, and H.W. Paxton, "Alloying Elements in Steel," 2d ed., American Society for Metals, 1966, p. 101. Reprinted with permission of ASM International. All rights reserved. www.asminternational.org.*)
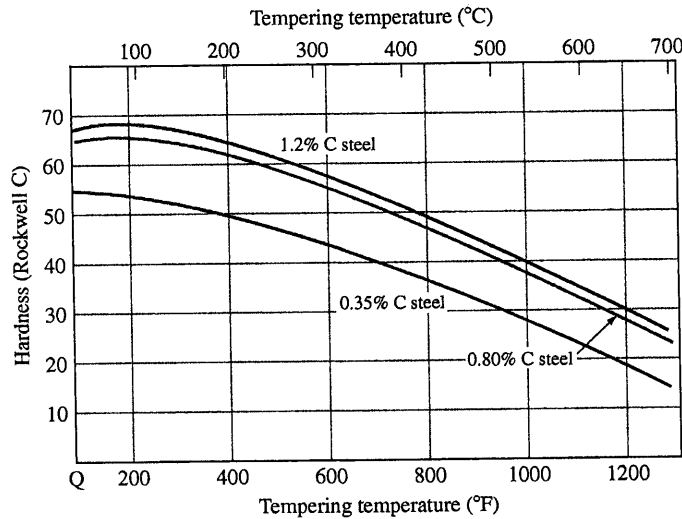
Figure 9.32
Hardness of iron-carbon martensites (0.35 to 1.2 percent C)
tempered 1 h at indicated temperatures.
(*From p. 38 in E.C. Bain and H.W. Paxton, "Alloying Elements in Steel,"
2d ed., American Society for Metals, 1966. Used by permission of
ASM International.*)

Effect of Tempering Temperature on the Hardness of Plain-Carbon Steels
Figure 9.32 shows the effect of increasing tempering temperature on the hardness of
several martensitic plain-carbon steels. Above about 200°C, the hardness gradually
decreases as the temperature is increased up to 700°C. This gradual decrease in hard-
ness of the martensite with increasing temperature is due mainly to the diffusion of
the carbon atoms from their stressed interstitial lattice sites to form second-phase
iron carbide precipitates.

Martempering (Marquenching)   **Martempering (marquenching)** is a modified
quenching procedure used for steels to minimize distortion and cracking that may
develop during uneven cooling of the heat-treated material. The martempering
process consists of (1) austenitizing the steel, (2) quenching it in hot oil or molten
salt at a temperature just slightly above (or slightly below) the M_s temperature,
(3) holding the steel in the quenching medium until the temperature is uniform
throughout and stopping this isothermal treatment before the austenite-to-bainite
transformation begins, and (4) cooling at a moderate rate to room temperature to
prevent large temperature differences. The steel is subsequently tempered by the con-
ventional treatment. Figure 9.33 shows a cooling path for the martempering process.

The structure of the martempered steel is *martensite,* and that of the martem-
pered (marquenched) steel that is subsequently tempered is *tempered martensite.*
Table 9.2 lists some of the mechanical properties of a 0.95 percent C plain-carbon
steel after martempering and tempering along with those obtained by conventional
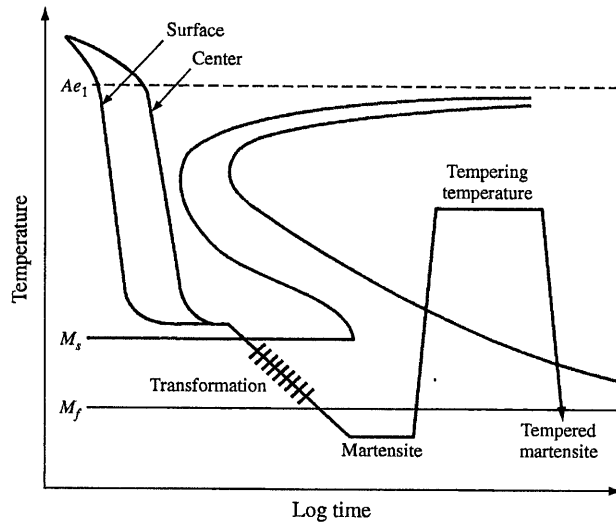
Figure 9.33
Cooling curve for martempering (marquenching)
superimposed on a eutectoid plain-carbon steel IT
diagram. The interrupted quench reduces the stresses
developed in the metal during quenching.
(*From "Metals Handbook," vol. 2, 8th ed., American Society for
Metals, 1964, p. 37. Used by permission of ASM International.*)

Table 9.2 Some mechanical properties (at 20°C) of a 1095 steel developed
by austempering as compared to some other heat treatments

Heat treatment	Rockwell C hardness	Impact (ft · lb)	Elongation in 1 in. (%)
Water-quench and temper	53.0	12	0
Water-quench and temper	52.5	14	0
Martemper and temper	53.0	28	0
Martemper and temper	52.8	24	0
Austemper	52.0	45	11
Austemper	52.5	40	8

Source: "Metals Handbook," vol. 2, 8th ed., American Society for Metals, 1964.

quenching and tempering. The major difference in these two sets of properties is that
the martempered and tempered steel has higher impact energy values. It should be
noted that the term *martempering* is misleading, and a better word for the process
is *marquenching.*

Austempering   **Austempering** is an isothermal heat treatment that produces a bainite
structure in some plain-carbon steels. The process provides an alternative procedure to
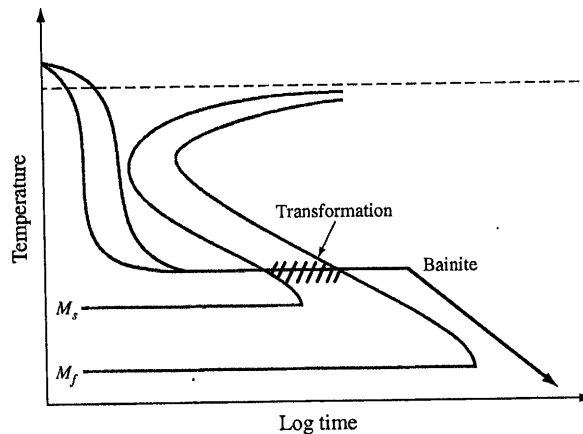
Figure 9.34
Cooling curves for austempering a eutectoid plain-carbon steel. The structure resulting from this treatment is bainite. An advantage of this heat treatment is that tempering is unnecessary. Compare with the customary quenching and tempering process shown in Fig. 9.29. M_s and M_f are the start and finish of martensitic transformation, respectively.
(*From "Suiting the Heat Treatment to the Job," United States Steel Corp., 1968, p. 34. Courtesy of United States Steel Corporation.*)

quenching and tempering for increasing the toughness and ductility of some steels. In the austempering process the steel is first austenitized, then quenched in a molten salt bath at a temperature just above the M_s temperature of the steel, held isothermally to allow the austenite-to-bainite transformation to take place, and then cooled to room temperature in air (Fig. 9.34). The final structure of an austempered eutectoid plain-carbon steel is *bainite*.

The advantages of austempering are (1) improved ductility and impact resistance of certain steels over those values obtained by conventional quenching and tempering (Table 9.2) and (2) decreased distortion of the quenched material. The disadvantages of austempering over quenching and tempering are (1) the need for a special molten salt bath and (2) the fact that the process can be used for only a limited number of steels.

9.3.6 Classification of Plain-Carbon Steels and Typical Mechanical Properties

Plain-carbon steels are most commonly designated by a four-digit AISI-SAE[6] code. The first two digits are 10 and indicate that the steel is a plain-carbon steel. The last

---

[6]AISI stands for the American Iron and Steel Institute, and SAE for the Society for Automotive Engineers.

CHAPTER 9 Engineering Alloys

two digits indicate the nominal carbon content of the steel in hundredths of a percent. For example, the AISI-SAE code number 1030 for a steel indicates that the steel is a plain-carbon steel containing a nominal 0.30 percent carbon. All plain-carbon steels contain manganese as an alloying element to enhance strength. The manganese content of most plain-carbon steels ranges between 0.30 and 0.95 percent. Plain-carbon steels also contain impurities of sulfur, phosphorus, silicon, and some other elements.

Typical mechanical properties of some AISI-SAE type plain-carbon steels are listed in Table 9.3. The very-low-carbon plain-carbon steels have relatively low strengths but very high ductilities. These steels are used for sheet material for forming applications such as fenders and body panels for automobiles. As the carbon content of the plain-carbon steels is increased, the steels become stronger but less ductile. Medium-carbon steels (1020–1040) find application for shafts and gears. High-carbon steels (1060–1095) are used, for example, for springs, die blocks, cutters, and shear blades.

9.4 LOW-ALLOY STEELS

Plain-carbon steels can be used successfully if the strength and other engineering requirements are not too severe. These steels are relatively low in cost but have some limitations, which include the following:

1. Plain-carbon steels cannot be strengthened beyond about 100,000 psi (690 MPa) without a substantial loss in ductility and impact resistance.
2. Large-section thicknesses of plain-carbon steels cannot be produced with a martensitic structure throughout, i.e., they are not deep-hardenable.
3. Plain-carbon steels have low corrosion and oxidation resistance.
4. Medium-carbon plain-carbon steels must be quenched rapidly to obtain a fully martensitic structure. Rapid quenching leads to possible distortion and cracking of the heat-treated part.
5. Plain-carbon steels have poor impact resistance at low temperatures.

    To overcome the deficiencies of plain-carbon steels, alloy steels have been developed that contain alloying elements to improve their properties. Alloy steels in general cost more than plain-carbon steels, but for many applications they are the only materials that can be used to meet engineering requirements. The principal alloying elements added to make alloy steels are manganese, nickel, chromium, molybdenum, and tungsten. Other elements that are sometimes added include vanadium, cobalt, boron, copper, aluminum, lead, titanium, and columbium (niobium).

9.4.1 Classification of Alloy Steels

Alloy steels may contain up to 50 percent of alloying elements and still be considered alloy steels. In this book, low-alloy steels containing from about 1 to 4 percent

Table 9.3 Typical mechanical properties and applications of plain-carbon steels

Alloy AISI-SAE number	Chemical composition (wt %)	Condition	Tensile strength		Yield strength		Elongation (%)	Typical applications
			ksi	MPa	ksi	MPa		
1010	0.10 C, 0.40 Mn	Hot-rolled	40–60	276–414	26–45	179–310	28–47	Sheet and strip for drawing; wire,
		Cold-rolled	42–58	290–400	23–38	159–262	30–45	rod, and nails and screws; concrete reinforcement bar
1020	0.20 C, 0.45 Mn	As rolled	65	448	48	331	36	Steel plate and structural sections; shafts,
		Annealed	57	393	43	297	36	gears
1040	0.40 C, 0.45 Mn	As rolled	90	621	60	414	25	Shafts, studs, high-tensile tubing, gears
		Annealed	75	517	51	352	30	
		Tempered*	116	800	86	593	20	
1060	0.60 C, 0.65 Mn	As rolled	118	814	70	483	17	Spring wire, forging dies, railroad wheels
		Annealed	91	628	54	483	22	
		Tempered*	160	110	113	780	13	
1080	0.80 C, 0.80 Mn	As rolled	140	967	85	586	12	Music wire, helical springs, cold chisels,
		Annealed	89	614	54	373	25	forging die blocks
		Tempered*	189	1304	142	980	12	
1095	0.95 C, 0.40 Mn	As rolled	140	966	83	573	9	Dies, punches, taps, milling cutters,
		Annealed	95	655	55	379	13	shear blades, high-tensile wire
		Tempered*	183	1263	118	814	10	

*Quenched and tempered at 315°C (600°F).

408 **CHAPTER 9** Engineering Alloys

Table 9.4 Principal types of standard alloy steels

13xx	Manganese 1.75
40xx	Molybdenum 0.20 or 0.25; or molybdenum 0.25 and sulfur 0.042
41xx	Chromium 0.50, 0.80, or 0.95, molybdenum 0.12, 0.20, or 0.30
43xx	Nickel 1.83, chromium 0.50 or 0.80, molybdenum 0.25
44xx	Molybdenum 0.53
46xx	Nickel 0.85 or 1.83, molybdenum 0.20 or 0.25
47xx	Nickel 1.05, chromium 0.45, molybdenum 0.20 or 0.35
48xx	Nickel 3.50, molybdenum 0.25
50xx	Chromium 0.40
51xx	Chromium 0.80, 0.88, 0.93, 0.95, or 1.00
51xxx	Chromium 1.03
52xxx	Chromium 1.45
61xx	Chromium 0.60 or 0.95, vanadium 0.13 or min 0.15
86xx	Nickel 0.55, chromium 0.50, molybdenum 0.20
87xx	Nickel 0.55, chromium 0.50, molybdenum 0.25
88xx	Nickel 0.55, chromium 0.50, molybdenum 0.35
92xx	Silicon 2.00; or silicon 1.40 and chromium 0.70
50Bxx*	Chromium 0.28 or 0.50
51Bxx*	Chromium 0.80
81Bxx*	Nickel 0.30, chromium 0.45, molybdenum 0.12
94Bxx*	Nickel 0.45, chromium 0.40, molybdenum 0.12

*B denotes boron steel.

Source: "Alloy Steel: Semifinished; Hot-Rolled and Cold-Finished Bars," American Iron and Steel Institute, 1970.

of alloying elements will be considered alloy steels. These steels are mainly automotive- and construction-type steels and are commonly referred to simply as *alloy steels*.

Alloy steels in the United States are usually designated by the four-digit AISI-SAE system. The first two digits indicate the principal alloying element or groups of elements in the steel, and the last two digits indicate the hundredths of percent of carbon in the steel. Table 9.4 lists the nominal compositions of the principal types of standard alloy steels.

9.4.2 Distribution of Alloying Elements in Alloy Steels

The way in which alloy elements distribute themselves in carbon steels depends primarily on the compound- and carbide-forming tendencies of each element. Table 9.5 summarizes the approximate distribution of most of the alloying elements present in alloy steels.

Nickel dissolves in the α ferrite of the steel since it has less tendency to form carbides than iron. Silicon combines to a limited extent with the oxygen in the steel to form nonmetallic inclusions but otherwise dissolves in the ferrite. Most of the manganese added to carbon steels dissolves in the ferrite. Some of the manganese, however, will form carbides but will usually enter the cementite as $(Fe,Mn)_3C$.

Table 9.5 Approximate distribution of alloying elements in alloy steels*

Element	Dissolved in ferrite	Combined in carbide	Combined as carbide	Compound	Elemental
Nickel	Ni			Ni_3Al	
Silicon	Si			$SiO_2 \cdot M_xO_y$	
Manganese	Mn ⟷ Mn		$(Fe,Mn)_3C$	$MnS; MnO \cdot SiO_2$	
Chromium	Cr ⟷ Cr		$(Fe,Cr_3)C$ Cr_7C_3 $Cr_{23}C_6$		
Molybdenum	Mo ⟷ Mo		Mo_2C		
Tungsten	W ⟷ W		W_2C		
Vanadium	V ⟷ V		V_4C_3		
Titanium	Ti ⟷ Ti		TiC		
Columbium†	Cb ⟷ Cb		CbC		
Aluminum	Al			Al_2O_3; AlN	
Copper	Cu (small amount)				
Lead					Pb

*The arrows indicate the relative tendencies of the elements listed to dissolve in the ferrite or combine in carbides.

†Cb = Nb (niobium).

Source: E.C. Bain and H.W. Paxton, "Alloying Elements in Steel," 2d ed., American Society for Metals, 1966.

Chromium, which has a somewhat stronger carbide-forming tendency than iron, partitions between the ferrite and carbide phases. The distribution of chromium depends on the amount of carbon present and on whether other stronger carbide-forming elements such as titanium and columbium are absent. Tungsten and molybdenum combine with carbon to form carbides if there is sufficient carbon present and if other stronger carbide-forming elements such as titanium and columbium are absent. Vanadium, titanium, and columbium are strong carbide-forming elements and are found in steels mainly as carbides. Aluminum combines with oxygen and nitrogen to form the compounds Al_2O_3 and AlN, respectively.

9.4.3 Effects of Alloying Elements on the Eutectoid Temperature of Steels

The various alloying elements cause the eutectoid temperature of the $Fe-Fe_3C$ phase diagram to be raised or lowered (Fig. 9.35). Manganese and nickel both lower the eutectoid temperature and act as *austenite-stabilizing elements* enlarging the austenitic region of the $Fe-Fe_3C$ phase diagram (Fig. 9.6). In some steels with sufficient amounts of nickel or manganese, the austenitic structure may be obtained at room temperature. The carbide-forming elements such as tungsten, molybdenum, and titanium raise the eutectoid temperature of the $Fe-Fe_3C$ phase diagram to
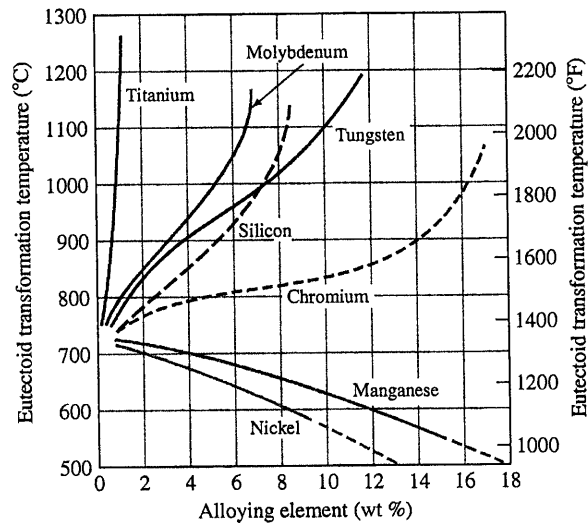
Figure 9.35
The effect of the percentage of alloying elements on the eutectoid temperature of the transformation of austenite to pearlite in the Fe-Fe$_3$C phase diagram.
(From "Metals Handbook," vol. 8, 8th ed., American Society for Metals, 1973, p. 191. Used by permission of ASM International.)

higher values and reduce the austenitic phase field. These elements are called *ferrite-stabilizing elements.*

9.4.4 Hardenability

The **hardenability** of a steel is defined as that property which determines the depth and distribution of hardness induced by quenching from the austenitic condition. The hardenability of a steel depends primarily on (1) the composition of the steel, (2) the austenitic grain size, and (3) the structure of the steel before quenching. Hardenability should not be confused with the *hardness* of a steel, which is its resistance to plastic deformation, usually by indentation.

In industry, hardenability is most commonly measured by the **Jominy hardenability test.** In the Jominy end-quench test, the specimen consists of a cylindrical bar with a 1 in. diameter and 4 in. length and with a $\frac{1}{16}$ in. flange at one end (Fig. 9.36a). Since prior structure has a strong effect on hardenability, the specimen is usually normalized before testing. In the Jominy test, after the sample has been austenitized, it is placed in a fixture, as shown in Fig. 9.36b, and a jet of water is quickly splashed at one end of the specimen. After cooling, two parallel flat surfaces are ground on the opposite sides of the test bar, and Rockwell C
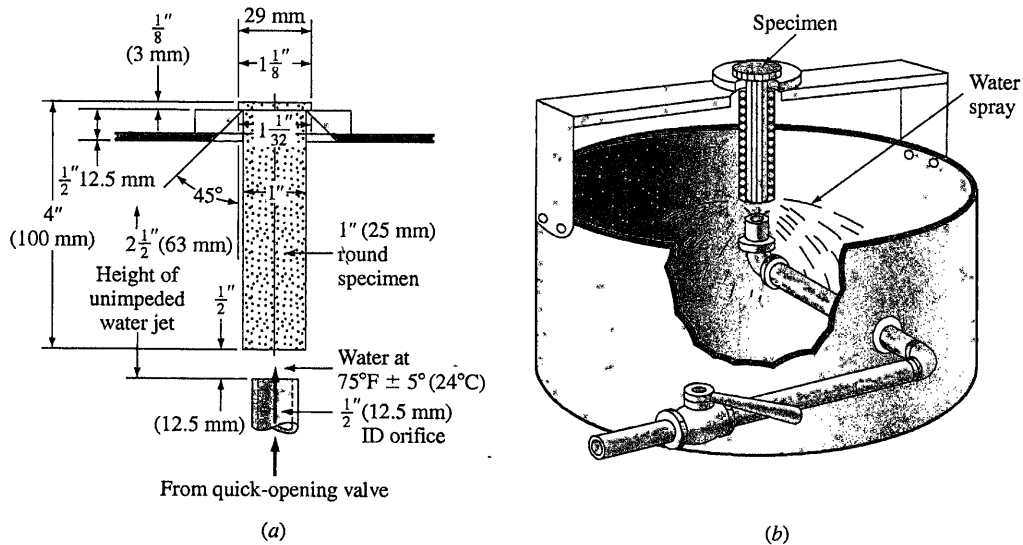
Figure 9.36

(a) Specimen and fixture for end-quench hardenability test.

(After M.A. Grossmann and E.C. Bain, "Principles of Heat Treatment," 5th ed., American Society for Metals, 1964, p. 114.)

(b) Schematic illustration of the end-quench test for hardenability.

[From H.E. McGannon (ed.), "The Making, Shaping, and Treating of Steel," 9th ed., United States Steel, 1971, p. 1099. Courtesy of United States Steel Corporation.]

hardness measurements are made along these surfaces up to 2.5 in. from the quenched end.

Figure 9.37 shows a hardenability plot of Rockwell C hardness versus distance from the quenched end for a 1080 eutectoid plain-carbon steel. This steel has relatively low hardenability since its hardness decreases from a value of RC = 65 at the quenched end of the Jominy bar to RC = 50 at just $\frac{3}{16}$ in. from the quenched end. Thus, thick sections of this steel cannot be made fully martensitic by quenching. Figure 9.37 correlates the end-quench hardenability data with the continuous transformation diagram for the 1080 steel and indicates the microstructural changes that take place along the bar at four distances *A*, *B*, *C*, and *D* from the quenched end.

Hardenability curves for some 0.40 percent C alloy steels are shown in Fig. 9.38. The 4340 alloy steel has exceptionally high hardenability and can be quenched to a hardness of RC = 40 at 2 in. from the quenched end of a Jominy bar. Alloy steels thus are able to be quenched at a slower rate and still maintain relatively high hardness values.

Alloy steels such as the 4340 steel are highly hardenable because, upon cooling from the austenitic region, the decomposition of austenite to ferrite and bainite is delayed and the decomposition of austenite to martensite can be accomplished at
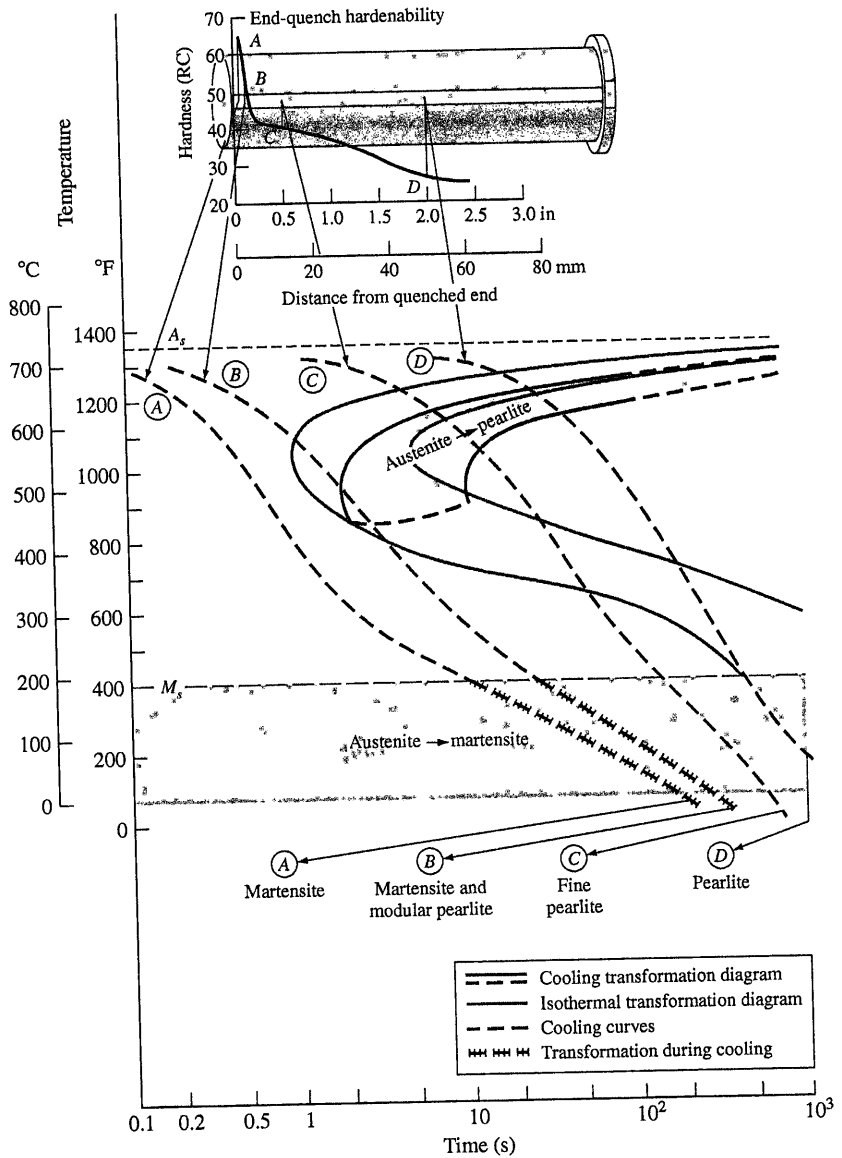
Figure 9.37
Correlation of continuous-cooling transformation diagram and end-quench hardenability test data for eutectoid carbon steel.
(From "Isothermal Transformation Diagrams," United States Steel Corp., 1963, p. 181. Courtesy of United States Steel Corporation.)
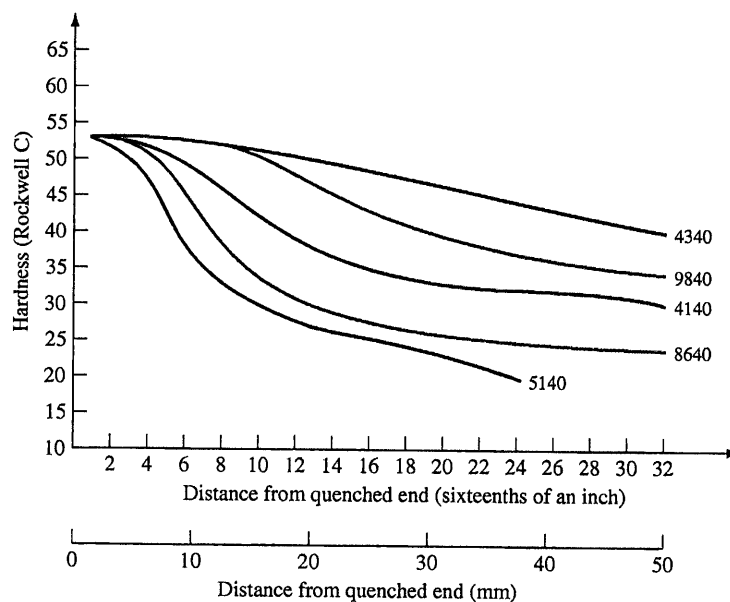
Figure 9.38
Comparative hardenability curves for 0.40 percent C alloy steel.
[*From H.E. McGannon (ed.), "The Making, Shaping, and Treating of Steel," 9th ed., United States Steel Corp., 1971, p. 1139. Courtesy of United States Steel Corporation.*]

slower rates. This delay of the austenite to ferrite plus bainite decomposition is quantitatively shown on the continuous-cooling transformation diagram of Fig. 9.39.

For most carbon and low-alloy steels, a standard quench produces at the same cross-section position common cooling rates along long round steel bars of the same diameter. However, the cooling rates differ (1) for different bar diameters, (2) for different positions in the cross sections of the bars, and (3) for different quenching media. Figure 9.40 shows bar diameter versus cooling rate curves for different cross-section locations within steel bars using quenches of agitated water in agitated oil. These plots can be used to determine the cooling rate and the associated distance from the quenched end of a standard quenched Jominy bar for a selected bar diameter at a particular cross-section location in the bar using a specific quenching medium. These cooling rates and their associated distances from the end of Jominy quenched bars can be used with Jominy plots of surface hardness versus distance from the quenched end for specific steels to determine the hardness of a particular steel at a specific location in the cross section of the steel bar in question. Example Problem 9.5 shows how the plots of Fig. 9.40 can be used to predict the hardness of a steel bar of a given diameter at a specific cross-section location quenched in a given medium. It should be pointed out that the Jominy hardness versus distance from the quenched-end plots are usually plotted as bands of data rather than as lines so that hardnesses obtained from the line curves are actually values in the center of a range of values.
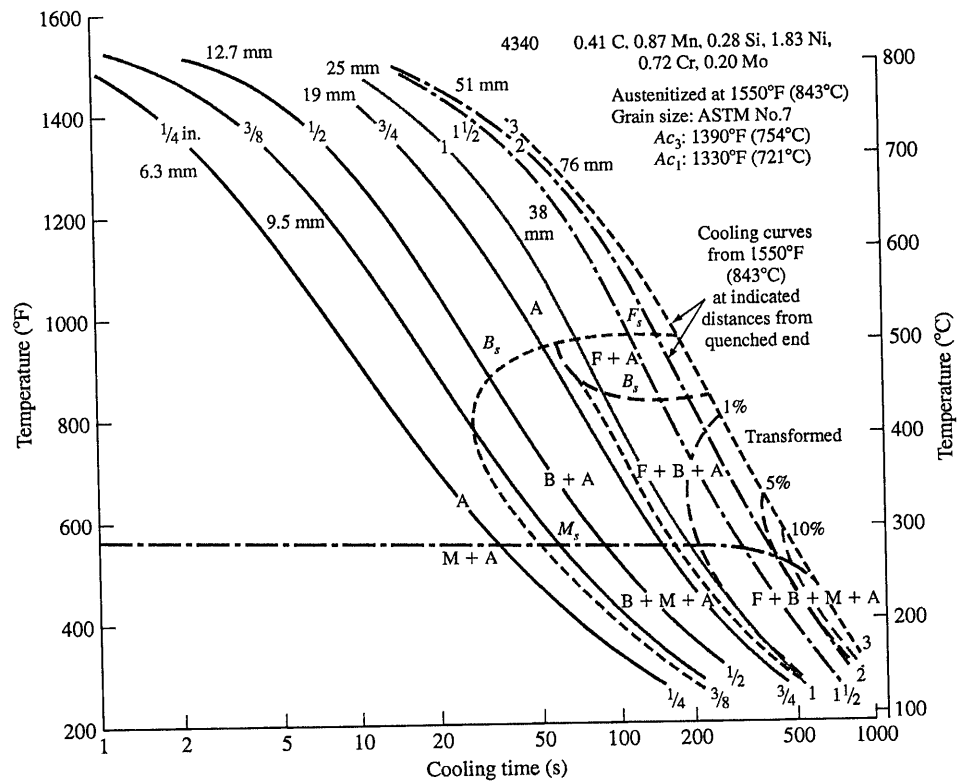
Figure 9.39

Continuous-cooling transformation diagram for AISI 4340 alloy steel. A = austenite, F = ferrite, B = bainite, M = martensite.

(From "Metal Progress," September 1964, p. 106. Used by permission of ASM International.)

EXAMPLE PROBLEM 9.5

An austenitized 40 mm diameter 5140 alloy steel bar is quenched in agitated oil. Predict what the Rockwell C (RC) hardness of this bar will be at (a) its surface and (b) its center.

■ **Solution**

a. Surface of bar. The cooling rate at the surface of the 40 mm steel bar quenched in agitated oil is found from part (ii) of Fig. 9.40 to be comparable to the cooling rate at 8 mm from the end of a standard quenched Jominy bar. Using Fig. 9.38 at 8 mm from the quenched end of the Jominy bar and the curve for the 5140 steel indicates that the hardness of the bar should be about 32 RC.

b. Center of the bar. The cooling rate at the center of the 40 mm diameter bar quenched in oil is found from part (ii) of Fig. 9.40 to be associated with 13 mm from the end of a quenched Jominy bar. The corresponding hardness for this distance from the end of a quenched Jominy bar for the 5140 alloy is found by using Fig. 9.38 to be about 26 RC.
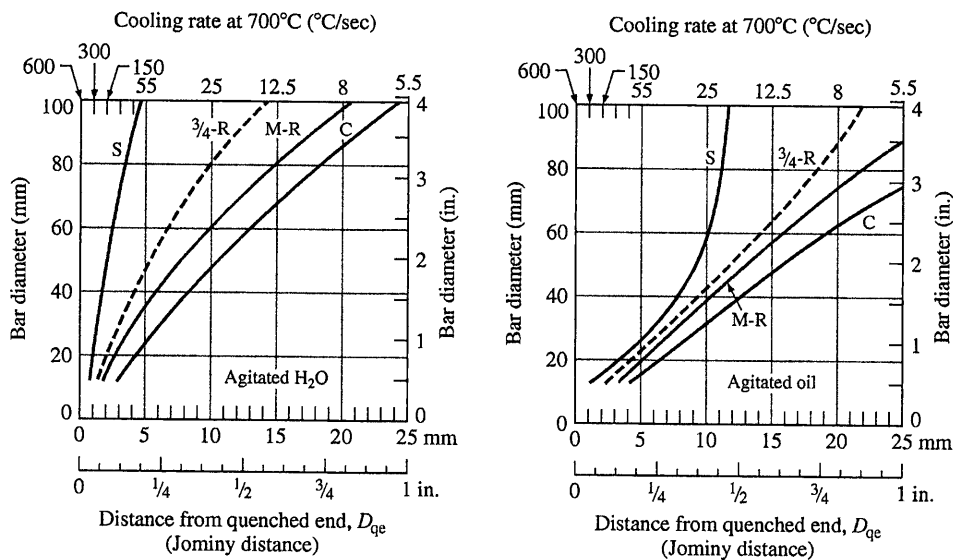
Figure 9.40
Cooling rates in long round steel bars quenched in (i) agitated water and (ii) agitated oil. Top abscissa, cooling rates at 700°C; bottom abscissa, equivalent positions on an end-quenched test bar. (C = center, M-R = midradius, S = surface, dashed line = approximate curve for $\frac{3}{4}$-radius positions on the cross section of bars.)
(*Van Vlack, L.H., "Materials for Engineering: Concepts and Applications," 1st ed., © 1982. Electronically reproduced by permission of Pearson Education, Inc., Upper Saddle River, New Jersey.*)

9.4.5 Typical Mechanical Properties and Applications for Low-Alloy Steels

Table 9.6 lists some typical tensile mechanical properties and applications for some commonly used low-alloy steels. For some strength levels, low-alloy steels have better combinations of strength, toughness, and ductility than plain-carbon steels. However, low-alloy steels cost more and so are used only when necessary. Low-alloy steels are used to a great extent in the manufacture of automobiles and trucks for parts that require superior strength and toughness properties that cannot be obtained from plain-carbon steels. Some typical applications for low-alloy steels in automobiles are shafts, axles, gears, and springs. Low-alloy steels containing about 0.2 percent C are commonly carburized or surface heat-treated to produce a hard, wear-resistant surface while maintaining a tough inner core.

9.5 ALUMINUM ALLOYS

Before discussing some of the important aspects of the structure, properties, and applications of aluminum alloys, let us examine the precipitation-strengthening (hardening) process that is used to increase the strength of many aluminum and other metal alloys.

416   **CHAPTER 9** Engineering Alloys

Table 9.6 Typical mechanical properties and applications of low-alloy steels

Alloy AISI-SAE number	Chemical composition (wt %)	Condition	Tensile strength		Yield strength		Elongation (%)	Typical applications
			ksi	MPa	ksi	MPa		
			Manganese steels					
1340	0.40 C, 1.75 Mn	Annealed	102	704	63	435	20	High-strength bolts
		Tempered*	230	1587	206	1421	12	
			Chromium steels					
5140	0.40 C, 0.80 Cr, 0.80 Mn	Annealed	83	573	43	297	29	Automobile transmission gears
		Tempered*	229	1580	210	1449	10	
5160	0.60 C, 0.80 Cr, 0.90 Mn	Annealed	105	725	40	276	17	Automobile coil and leaf springs
		Tempered*	290	2000	257	1773	9	
			Chromium-molybdenum steels					
4140	0.40 C, 1.0 Cr, 0.9 Mn, 0.20 Mo	Annealed	95	655	61	421	26	Gears for aircraft gas turbine engines, transmissions
		Tempered*	225	1550	208	1433	9	
			Nickel-molybdenum steels					
4620	0.20 C, 1.83 Ni, 0.55 Mn, 0.25 Mo	Annealed	75	517	54	373	31	Transmission gears, chain pins, shafts, roller bearings
		Normalized	83	573	53	366	29	
4820	0.20 C, 3.50 Ni, 0.60 Mn, 0.25 Mo	Annealed	99	683	67	462	22	Gears for steel mill equipment, paper machinery, mining machinery, earth-moving equipment
		Normalized	100	690	70	483	60	
			Nickel (1.83%)-chromium-molybdenum steels					
4340 (E)	0.40 C, 1.83 Ni, 0.90 Mn, 0.80 Cr, 0.20 Mo	Annealed	108	745	68	469	22	Heavy sections, landing gears, truck parts
		Tempered*	250	1725	230	1587	10	
			Nickel (0.55%)-chromium-molybdenum steels					
8620	0.20 C, 0.55 Ni, 0.50 Cr, 0.80 Mn, 0.20 Mo	Annealed	77	531	59	407	31	Transmission gears
		Normalized	92	635	52	359	26	
8650	0.50 C, 0.55 Ni, 0.50 Cr, 0.80 Mn, 0.20 Mo	Annealed	103	710	56	386	22	Small machine axles, shafts
		Tempered*	250	1725	225	1552	10	

*Tempered at 600°F (315°C).

9.5.1 Precipitation Strengthening (Hardening)

Precipitation Strengthening of a Generalized Binary Alloy The object of precipitation strengthening is to create in a heat-treated alloy a dense and fine dispersion of precipitated particles in a matrix of deformable metal. The precipitate particles act as obstacles to dislocation movement and thereby strengthen the heat-treated alloy.

The precipitation-strengthening process can be explained in a general way by referring to the binary phase diagram of metals A and B shown in Fig. 9.41. In order for an alloy system to be able to be precipitation-strengthened for certain alloy compositions, there must be a terminal solid solution that has a decreasing solid solubility as the temperature decreases. The phase diagram of Fig. 9.41 shows this type of decrease in solid solubility in terminal solid solution α in going from point a to point b along the indicated solvus.

Let us now consider the precipitation strengthening of an alloy of composition x_1 of the phase diagram of Fig. 9.41. We choose the alloy composition x_1 since there is a large decrease in the solid solubility of solid solution α in decreasing the temperature from T_2 to T_3. The precipitation-strengthening process involves the following three basic steps:

1. *Solution heat treatment* is the *first step* in the precipitation-strengthening process. Sometimes this treatment is referred to as *solutionizing*. The alloy sample, which may be in the wrought or cast form, is heated to a temperature between the solvus and solidus temperatures and soaked there until a uniform solid-solution structure
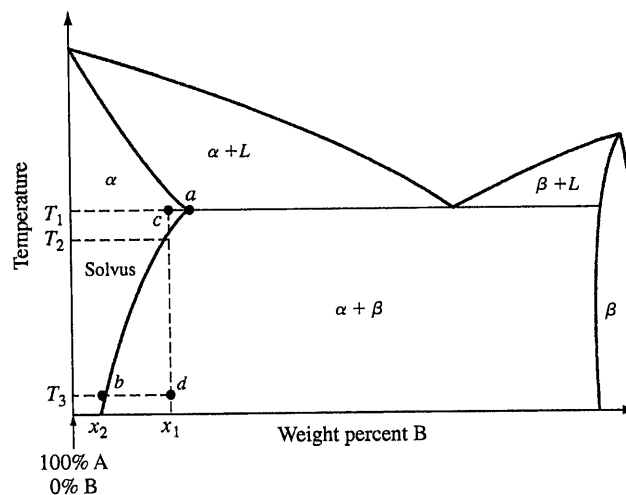
Figure 9.41
Binary phase diagram for two metals A and B having a terminal solid solution α that has a decreasing solid solubility of B in A with decreasing temperature.

is produced. Temperature T_1 at point c of Fig. 9.41 is selected for our alloy x_1 because it lies midway between the solvus and solidus phase boundaries of solid solution α.

2. *Quenching* is the *second step* in the precipitation-strengthening process. The sample is rapidly cooled to a lower temperature, usually room temperature, and the cooling medium is usually water at room temperature. The structure of the alloy sample after water quenching consists of a supersaturated solid solution. The structure of our alloy x_1 after quenching to temperature T_3 at point d of Fig. 9.41 thus consists of a supersaturated solid solution of the α phase.

3. *Aging* is the *third basic step* in the precipitation-strengthening process. Aging the solution heat-treated and quenched alloy sample is necessary so that a finely dispersed precipitate forms. The formation of a finely dispersed precipitate in the alloy is the objective of the precipitation-strengthening process. The fine precipitate in the alloy impedes dislocation movement during deformation by forcing the dislocations to either cut through the precipitated particles or go around them. By restricting dislocation movement during deformation, the alloy is strengthened.

Aging the alloy at room temperature is called *natural aging,* whereas aging at elevated temperatures is called *artificial aging.* Most alloys require artificial aging, and the aging temperature is usually between about 15 and 25 percent of the temperature difference between room temperature and the solution heat-treatment temperature.

Decomposition Products Created by the Aging of the Supersaturated Solid Solution A precipitation-hardenable alloy in the supersaturated solid-solution condition is in a high-energy state, as indicated schematically by energy level 4 of Fig. 9.42. This energy state is relatively unstable, and the alloy tends to seek a lower energy state by the spontaneous decomposition of the supersaturated solid solution into metastable phases or the equilibrium phases. The driving force for the precipitation of metastable phases or the equilibrium phase is the lowering of the energy of the system when these phases form.

When the supersaturated solid solution of the precipitation-hardenable alloy is aged at a relatively low temperature where only a small amount of activation energy is available, clusters of segregated atoms called *precipitation zones,* or *GP zones,*[7] are formed. For the case of our alloy A-B of Fig. 9.41, the zones will be regions enriched with B atoms in a matrix primarily of A atoms. The formation of these zones in the supersaturated solid solution is indicated by the circular sketch at the lower energy level 3 of Fig. 9.42. Upon further aging and if sufficient activation energy is available (as a result of the aging temperature being high enough), the zones develop into or are replaced by a coarser (larger in size) intermediate metastable precipitate, indicated by the circular sketch at the still-lower energy

---

[7]Precipitation zones are sometimes referred to as GP zones, named after the two early scientists Guinier and Preston who first identified these structures by x-ray diffraction analyses.
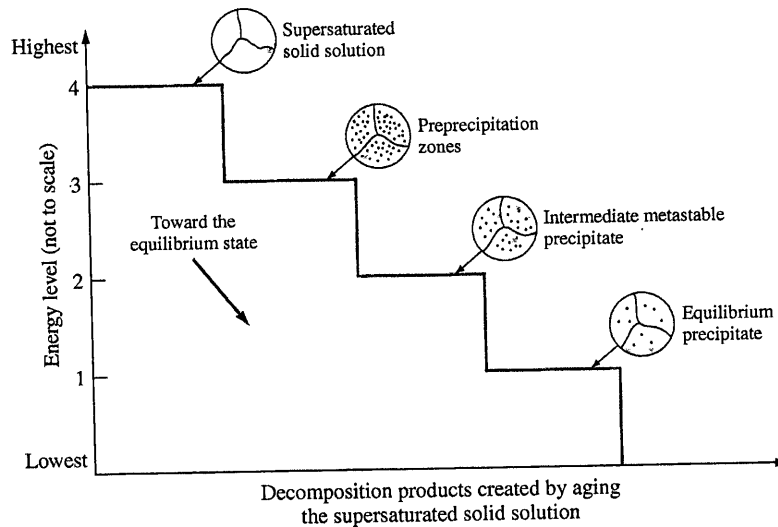
Figure 9.42
Decomposition products created by the aging of a supersaturated
solid solution of a precipitation-hardenable alloy. The highest energy
level is for the supersaturated solid solution, and the lowest energy
level is for the equilibrium precipitate. The alloy can go spontaneously
from a higher energy level to a lower one if there is sufficient
activation energy for the transformation and if the kinetic conditions
are favorable.

level 2. Finally, if aging is continued (usually a higher temperature is necessary)
and if sufficient activation energy is available, the intermediate precipitate is
replaced by the equilibrium precipitate indicated by the even-still-lower energy
level 1 of Fig. 9.42.

**The Effect of Aging Time on the Strength and Hardness of a Precipitation-
Hardenable Alloy that Has Been Solution Heat-Treated and Quenched** The
effect of aging on strengthening a precipitation-hardenable alloy that has been solu-
tion heat-treated and quenched is usually presented as an *aging curve*. The aging
curve is a plot of strength or hardness versus aging time (usually on a logarithmic
scale) at a particular temperature. Figure 9.43 shows a schematic aging curve. At zero
time, the strength of the supersaturated solid solution is indicated on the ordinate
axis of the plot. As the aging time increases, preprecipitation zones form and their
size increases, and the alloy becomes stronger and harder and less ductile (Fig. 9.43).
A maximum strength (peak aged condition) is eventually reached if the aging tem-
perature is sufficiently high, which is usually associated with the formation of an
intermediate metastable precipitate. If aging is continued so that the intermediate
precipitate coalesces and coarsens, the alloy overages and becomes weaker than in
the peak aged condition (Fig. 9.43).
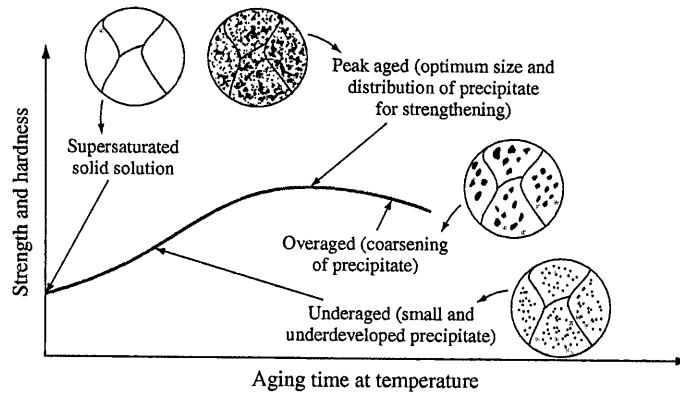
Figure 9.43
Schematic aging curve (strength or hardness versus time) at a particular temperature for a precipitation-hardenable alloy.
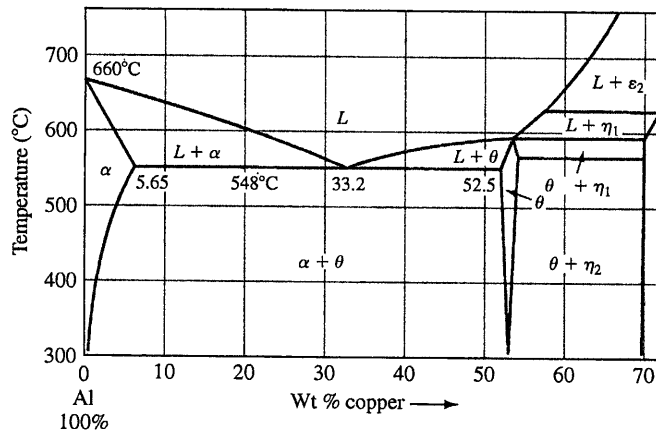
Figure 9.44
Aluminum-rich end of aluminum-copper phase diagram.
[*From K.R. Van Horn (ed.), "Aluminum," vol. 1, American Society for Metals, 1967, p. 372. Used by permission of ASM International.*]

Precipitation Strengthening (Hardening) of an Al–4% Cu Alloy Let us now examine the structure and hardness changes that occur during the precipitation heat treatment of an aluminum–4% copper alloy. The heat-treatment sequence for the precipitation strengthening of this alloy is:

1. Solution heat treatment: the Al–4% Cu alloy is solutionized at about 515°C (see the Al-Cu phase diagram of Fig. 9.44).

2. Quenching: the solution heat-treated alloy is rapidly cooled in water at room temperature.

3. Aging: the alloy after solution heat treatment and quenching is artificially aged in the 130°C to 190°C range.

Structures Formed During the Aging of the Al–4% Cu Alloy   In the precipitation strengthening of Al–4% Cu alloys, five sequential structures can be identified: (1) supersaturated solid-solution α, (2) GP1 zones, (3) GP2 zones (also called θ'' phase), (4) θ' phase, and (5) θ phase, $CuAl_2$. Not all these phases can be produced at all aging temperatures. GP1 and GP2 zones are produced at lower aging temperatures, and θ' and θ phases occur at higher temperatures.

> *GP1 zones.* These preprecipitation zones are formed at lower aging temperatures and are created by copper atoms segregating in the supersaturated solid-solution α. GP1 zones consist of segregated regions in the shape of disks a few atoms thick (0.4 to 0.6 nm) and about 8 to 10 nm in diameter and form on the {100} cubic planes of the matrix. Since the copper atoms have a diameter of about 11 percent less than the aluminum ones, the matrix lattice around the zones is strained tetragonally. GP1 zones are said to be *coherent* with the matrix lattice since the copper atoms just replace aluminum atoms in the lattice (Fig. 9.45). GP1 zones are detected under the electron microscope by the strain fields they create (Fig. 9.46a).

> *GP2 zones (θ'' phase).* These zones also have a tetragonal structure and are coherent with the {100} of the matrix of the Al–4% Cu alloy. Their size ranges from about 1 to 4 nm thick to 10 to 100 nm in diameter as aging proceeds (Fig. 9.46b).

> θ' *phase.* This phase nucleates heterogeneously, especially on dislocations, and is incoherent with the matrix. (An *incoherent precipitate* is one in which the precipitated particle has a distinct crystal structure different from the matrix [Fig. 9.45a]). θ' phase has a tetragonal structure with a thickness of 10 to 150 nm (Fig. 9.46c).

(This type of precipitate has its own structure)

(*a*) Coherent precipitate   (*b*) Incoherent precipitate
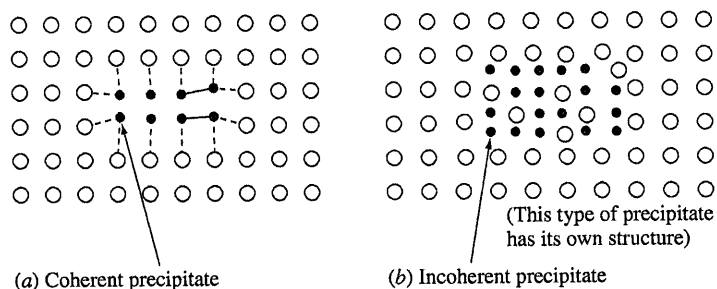
Figure 9.45
Schematic comparison of the nature of (*a*) a coherent precipitate and (*b*) an incoherent precipitate. The coherent precipitate is associated with a high strain energy and low surface energy, and the incoherent one is associated with a low strain energy and high surface energy.

(a)

(b)

(c)
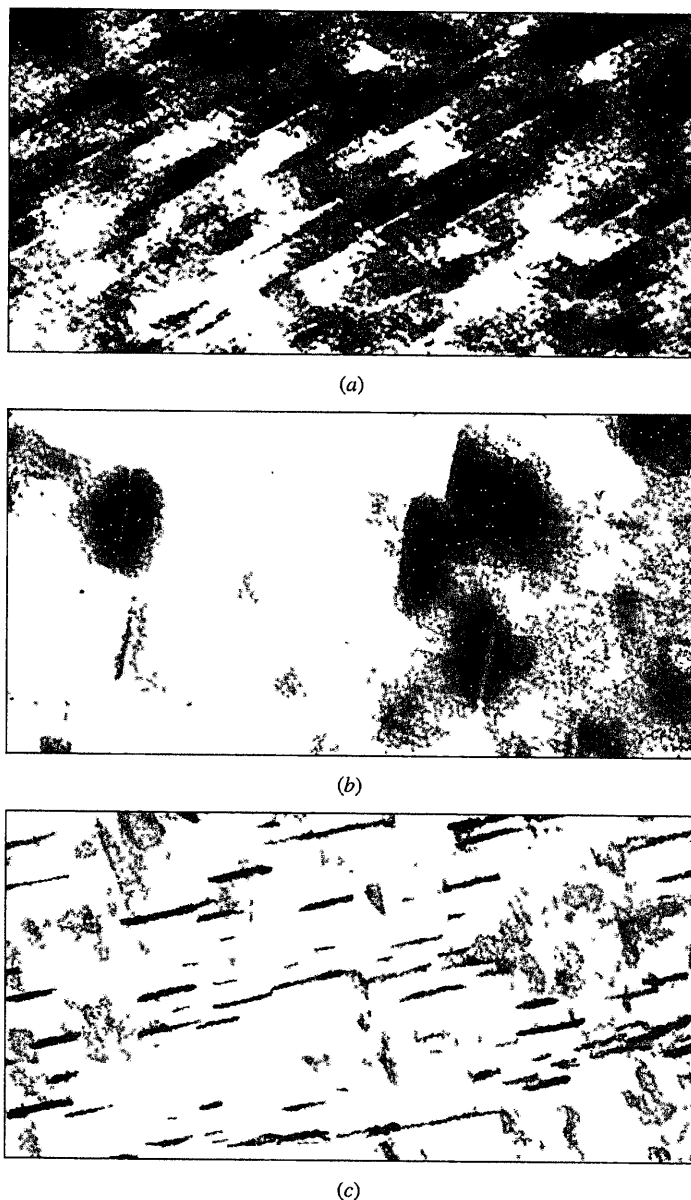
Figure 9.46
Microstructures of aged Al–4% Cu alloys. (a) Al–4% Cu, heated to 540°C, water-quenched, and aged 16 h at 130°C. The GP zones have been formed as disks parallel to the {100} planes of the FCC matrix and at this stage are a few atoms thick and about 100 A in diameter. Only disks lying on one crystallographic orientation are visible. (Electron micrograph; magnification 1,000,000×.) (b) Al–4% Cu, solution-treated at 540°C, quenched in water, and aged for 1 day at 130°C. This thin-foil micrograph shows strain fields due to coherent GP2 zones. The dark regions surrounding the zones are caused by strain fields. (Electron micrograph; magnification 800,000×.) (c) Al–4% Cu alloy solution heat-treated at 540°C, quenched in water, and aged for 3 days at 200°C. This thin-foil micrograph shows the incoherent and metastable phase θ' that forms by heterogeneous nucleation and growth. (Electron micrograph; magnification 25,000×.)
(After J. Nutting and R.G. Baker, "The Microstructure of Metals," Institute of Metals, 1965, pp. 65 and 67.)
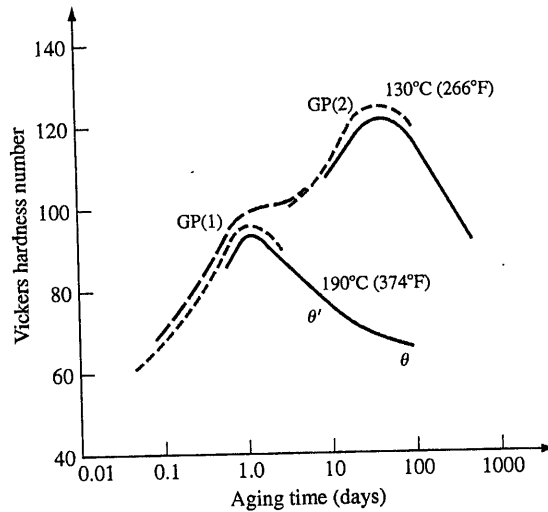
Figure 9.47
Correlation of structures and hardness of Al–4%
Cu alloy aged at 130°C and 190°C.
[From J.M. Silcock, T.J. Heal, and H.K. Hardy as presented
in K.R. Van Horn (ed.), "Aluminum," vol. 1, American
Society for Metals, 1967, p. 123. Used by permission of ASM
International.]

θ *phase.* The equilibrium phase θ is incoherent and has the composition $CuAl_2$. This phase has a BCT structure ($a = 0.607$ nm and $c = 0.487$ nm) and forms from θ' or directly from the matrix.

The general sequence of precipitation in binary aluminum-copper alloys can be represented by

Supersaturated solid solution $\rightarrow$ GP1 zones $\rightarrow$
$$GP2 \text{ zones } (\theta''\text{phase}) \rightarrow \theta' \rightarrow \theta \ (CuAl_2)$$

Correlation of Structures and Hardness in an Al–4% Cu Alloy   The hardness versus aging time curves for an Al–4% Cu alloy aged at 130°C and 190°C are shown in Fig. 9.47. At 130°C, GP1 zones are formed and increase the hardness of the alloy by impeding dislocation movement. Further aging at 130°C creates GP2 zones that increase the hardness still more by making dislocation movement still more difficult. A maximum in hardness is reached with still more aging time at 130°C as θ' forms. Aging beyond the hardness peak dissolves the GP2 zones and coarsens the θ' phase, causing the decrease in the hardness of the alloy. GP1 zones do not form during aging at 190°C in the Al–4% Cu alloy since this temperature is above the GP1 solvus. With long aging times at 190°C, the equilibrium θ phase forms.

424   **CHAPTER 9** Engineering Alloys

EXAMPLE PROBLEM 9.6	Calculate the theoretical weight percent of the θ phase that could be formed at 27°C (room temperature) when a sample of Al–4.50 wt % Cu alloy is very slowly cooled from 548°C. Assume the solid solubility of Cu in Al at 27°C is 0.02 wt % and that the θ phase contains 54.0 wt % Cu.

■ Solution

First, we draw a tie line xy on the Al-Cu phase diagram at 27°C between the α and θ phases, as shown in Fig. EP9.6a. Next, we indicate the 4.5 percent Cu composition point at z. The ratio xz divided by the whole tie line xy (Fig. EP9.6b) gives the weight fraction of the θ phase. Thus,

$$\theta \text{ wt } \% = \frac{4.50 - 0.02}{54.0 - 0.02}(100\%) = \frac{4.48}{53.98}(100\%) = 8.3\% \blacktriangleleft$$
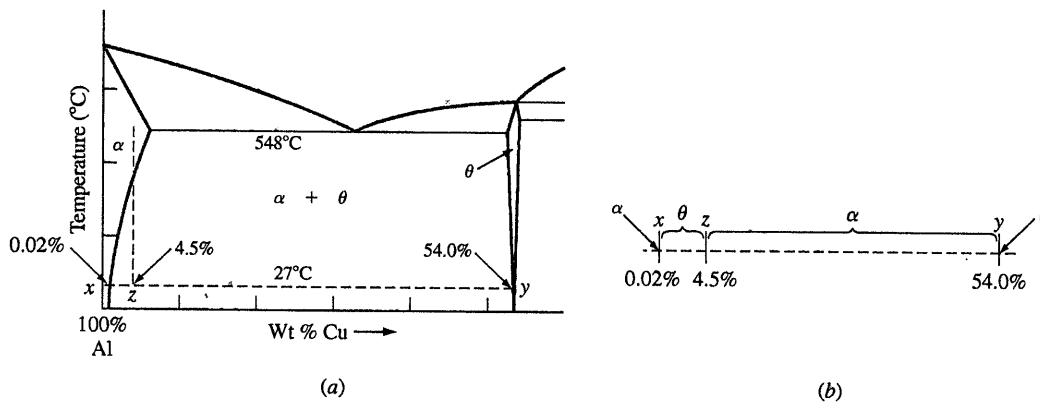
Figure EP9.6
(a) Al-Cu phase diagram with tie line xy indicated on it at 27°C and point z located at 4.5% Cu.
(b) Isolated tie line xy indicating segment xz as representing the weight fraction of the θ phase.

Back Matter

APPENDIX

H

Some Properties of Selected Elements

Element	Symbol	Melting point, °C	Density,* g/cm³	Atomic radius, nm	Crystal structure† (20°C)	Lattice constants 20°C, nm	
						a	c
Aluminum	Al	660	2.70	0.143	FCC	0.40496	
Antimony	Sb	630	6.70	0.138	Rhombohedral	0.45067	
Arsenic	As	817	5.72	0.125	Rhombohedral‡	0.4131	
Barium	Ba	714	3.5	0.217	BCC‡	0.5019	
Beryllium	Be	1278	1.85	0.113	HCP‡	0.22856	0.35832
Boron	B	2030	2.34	0.097	Orthorhombic		
Bromine	Br	−7.2	3.12	0.119	Orthorhombic		
Cadmium	Cd	321	8.65	0.148	HCP‡	0.29788	0.561667
Calcium	Ca	846	1.55	0.197	FCC‡	0.5582	
Carbon (graphite)	C	3550	2.25	0.077	Hexagonal	0.24612	0.67078
Cesium	Cs	28.7	1.87	0.190	BCC		
Chlorine	Cl	−101	1.9	0.099	Tetragonal		
Chromium	Cr	1875	7.19	0.128	BCC‡	0.28846	
Cobalt	Co	1498	8.85	0.125	HCP‡	0.2506	0.4069
Copper	Cu	1083	8.96	0.128	FCC	0.36147	
Fluorine	F	−220	1.3	0.071			
Gallium	Ga	29.8	5.91	0.135	Orthorhombic		
Germanium	Ge	937	5.32	0.139	Diamond cubic	0.56576	
Gold	Au	1063	19.3	0.144	FCC	0.40788	
Helium	He	−270	...	...	HCP		
Hydrogen	H	−259	...	0.046	Hexagonal		
Indium	In	157	7.31	0.162	FC tetragonal	0.45979	0.49467
Iodine	I	114	4.94	0.136	Orthorhombic		
Iridium	Ir	2454	22.4	0.135	FCC	0.38389	
Iron	Fe	1536	7.87	0.124	BCC‡	0.28664	
Lead	Pb	327	11.34	0.175	FCC	0.49502	
Lithium	Li	180	0.53	0.157	BCC	0.35092	

(continued)

APPENDIX II Some Properties of Selected Elements

Element	Symbol	Melting point, °C	Density,* g/cm³	Atomic radius, nm	Crystal structure† (20°C)	Lattice constants 20°C, nm	
						a	c
Magnesium	Mg	650	1.74	0.160	HCP	0.32094	0.52105
Manganese	Mn	1245	7.43	0.118	Cubic‡	0.89139	
Mercury	Hg	−38.4	14.19	0.155	Rhombohedral		
Molybdenum	Mo	2610	10.2	0.140	BCC	0.31468	
Neon	Ne	−248.7	1.45	0.160	FCC		
Nickel	Ni	1453	8.9	0.125	FCC	0.35236	
Niobium	Nb	2415	8.6	0.143	BCC	0.33007	
Nitrogen	N	−240	1.03	0.071	Hexagonal‡		
Osmium	Os	2700	22.57	0.135	HCP	0.27353	0.43191
Oxygen	O	−218	1.43	0.060	Cubic‡		
Palladium	Pd	1552	12.0	0.137	FCC	0.38907	
Phosphorus (white)	P	44.2	1.83	0.110	Cubic‡		
Platinum	Pt	1769	21.4	0.139	FCC	0.39239	
Potassium	K	63.9	0.86	0.238	BCC	0.5344	
Rhenium	Re	3180	21.0	0.138	HCP	0.27609	0.44583
Rhodium	Rh	1966	12.4	0.134	FCC	0.38044	
Ruthenium	Ru	2500	12.2	0.125	HCP	0.27038	0.42816
Scandium	Sc	1539	2.99	0.160	FCC	0.4541	
Silicon	Si	1410	2.34	0.117	Diamond cubic	0.54282	
Silver	Ag	961	10.5	0.144	FCC	0.40856	
Sodium	Na	97.8	0.97	0.192	BCC	0.42906	
Strontium	Sr	76.8	2.60	0.215	FCC‡	0.6087	
Sulfur (yellow)	S	119	2.07	0.104	Orthorhombic		
Tantalum	Ta	2996	16.6	0.143	BCC	0.33026	
Tin	Sn	232	7.30	0.158	Tetragonal‡	0.58311	0.31817
Titanium	Ti	1668	4.51	0.147	HCP‡	0.29504	0.46833
Tungsten	W	3410	19.3	0.141	BCC	0.31648	
Uranium	U	1132	19.0	0.138	Orthorhombic‡	0.2858	0.4955
Vanadium	V	1900	6.1	0.136	BCC	0.3039	
Zinc	Zn	419.5	7.13	0.137	HCP	0.26649	0.49470
Zirconium	Zr	1852	6.49	0.160	HCP‡	0.32312	0.51477

*Density of solid at 20°C.
†b = 0.5877 nm.
‡Other crystal structures exist at other temperatures.

Ionic Radii[1] of the Elements

[1]Ionic radii can vary in different crystals due to many factors.

Atomic number	Element (symbol)	Ion	Ionic radius, nm	Atomic number	Element (symbol)	Ion	Ionic radius, nm
1	H	H^-	0.154	23	V	V^{3+}	0.065
2	He					V^{4+}	0.061
3	Li	Li^+	0.078			V^{5+}	~0.04
4	Be	Be^{2+}	0.034	24	Cr	Cr^{3+}	0.064
5	B	B^{3+}	0.02			Cr^{6+}	0.03–0.04
6	C			C^{4+}	<0.02		
25	Mn	Mn^{2+}	0.091				
7	N	N^{5+}	0.01–0.02			Mn^{3+}	0.070
8	O	O^{2-}	0.132			Mn^{4+}	0.052
9	F	F^-	0.133	26	Fe	Fe^{2+}	0.087
10	Ne					Fe^{3+}	0.067
11	Na	Na^+	0.098	27	Co	Co^{2+}	0.082
12	Mg	Mg^{2+}	0.078			Co^{3+}	0.065
13	Al	Al^{3+}	0.057	28	Ni	Ni^{2+}	0.078
14	Si	Si^{4-}	0.198	29	Cu	Cu^+	0.096
		Si^{4+}	0.039	30	Zn	Zn^{2+}	0.083
15	P	P^{5+}	0.03–0.04	31	Ga	Ga^{3+}	0.062
16	S	S^{2-}	0.174	32	Ge	Ge^{4+}	0.044
		S^{6+}	0.034	33	As	As^{3+}	0.069
17	Cl	Cl^-	0.181			As^{5+}	~0.04
18	Ar			34	Se	Se^{2-}	0.191
19	K	K^+	0.133			Se^{6+}	0.03–0.04
20	Ca	Ca^{2+}	0.106	35	Br	Br^-	0.196
21	Sc	Sc^{2+}	0.083	36	Kr		
22	Ti	Ti^{2+}	0.076	37	Rb	Rb^+	0.149
		Ti^{3+}	0.069	38	Sr	Sr^{2+}	0.127
		Ti^{4+}	0.064				

APPENDIX III Ionic Radii of the Elements

Atomic number	Element (symbol)	Ion	Ionic radius, nm	Atomic number	Element (symbol)	Ion	Ionic radius, nm
39	Y	Y^{3+}	0.106	66	Dy	Dy^{3+}	0.107
40	Zr	Zr^{4+}	0.087	67	Ho	Ho^{3+}	0.105
41	Nb	Nb^{4+}	0.069	68	Er	Er^{3+}	0.104
		Nb^{5+}	0.069	69	Tm	Tm^{3+}	0.104
42	Mo	Mo^{4+}	0.068	70	Yb	Yb^{3+}	0.100
		Mo^{6+}	0.065	71	Lu	Lu^{3+}	0.099
44	Ru	Ru^{4+}	0.065	72	Hf	Hf^{4+}	0.084
45	Rh	Rh^{3+}	0.068	73	Ta	Ta^{5+}	0.068
		Rh^{4+}	0.065	74	W	W^{4+}	0.068
46	Pd	Pd^{2+}	0.050			W^{6+}	0.065
47	Ag	Ag^{+}	0.113	75	Re	Re^{4+}	0.072
48	Cd	Cd^{2+}	0.103	76	Os	Os^{4+}	0.067
49	In	In^{3+}	0.092	77	Ir	Ir^{4+}	0.066
50	Sn	Sn^{4-}	0.215	78	Pt	Pt^{4+}	0.052
		Sn^{4+}	0.074			Pt^{4+}	0.055
51	Sb	Sb^{3+}	0.090	79	Au	Au^{+}	0.137
52	Te	Te^{2-}	0.211	80	Hg	Hg^{2+}	0.112
		Te^{4+}	0.089	81	Tl	Tl^{+}	0.149
53	I	I^{-}	0.220			Tl^{3+}	0.106
		I^{5+}	0.094	82	Pb	Pb^{4-}	0.215
54	Xe					Pb^{2+}	0.132
55	Cs	Cs^{+}	0.165			Pb^{4+}	0.084
56	Ba	Ba^{2+}	0.143	83	Bi	Bi^{3+}	0.120
57	La	La^{3+}	0.122	84	Po		
58	Ce	Ce^{3+}	0.118	85	At		
		Ce^{4+}	0.102	86	Rn		
59	Pr	Pr^{3+}	0.116	87	Fr		
		Pr^{4+}	0.100	88	Ra	Ra^{+}	0.152
60	Nd	Nd^{3+}	0.115	89	Ac		
61	Pm	Pm^{3+}	0.106	90	Th	Th^{4+}	0.110
62	Sm	Sm^{3+}	0.113	91	Pa		
63	Eu	Eu^{3+}	0.113	92	U	U^{4+}	0.105
64	Gd	Gd^{3+}	0.111				
65	Tb	Tb^{3+}	0.109				
		Tb^{4+}	0.089				

*Ionic radii can vary in different crystals due to many factors.

Source: C. J. Smithells (ed.), "Metals Reference Book," 5th ed., Butterworth, 1976.

GLASS TRANSITION TEMPERATURE AND MELTING TEMPERATURE OF SELECTED POLYMERS

Polymer	Glass transition temperature (°C)	Melting temperature (°C)
Nylon 66	50	265
Nylon 12	42	179
Polybutylene terepthalate (PBT)	22	225
Polycarbonate	150	265
Polyetheretherketone (PEEK)	157	374
Polyethylene Terephthalate (PET)	69	265
Polyethylene	−78	100
Acrylonitrile Butadiene Styrene (ABS)	110	105
Polymethyl Methacrylate (PMMA)	38	160
Polypropylene (PP)	−8	176
Polystyrene	100	240
Polytetrafluoroethylene (PTFE)	−20	327
Polyvinyl Chloride (PVC)	87	227
Polyvinyl Ethyl Ether	−43	86
Polyvinyl Fluoride	40	200
Styrene Acrylonitrile	120	120
Cellulose Acetate	190	230
Acrylonitrile	100	317
Polyacetal	−30	183
Polyphenylene Sulfide Molded	118	275
Polysulfone	185	190
Polychloroprene	−50	80
Polydimethyl Siloxane	−123	−40
Polyvinyl Pyrrolidone	86	375
Polyvinylidene Chloride	−18	198

APPENDIX IV

Selected Physical Quantities and Their Units

Quantity	Symbol	Unit	Abbreviation
Length	l	inch	in
		meter	m
Wavelength	λ	meter	m
Mass	m	kilogram	kg
Time	t	second	s
Temperature	T	degree Celsius	°C
		degree Fahrenheit	°F
		Kelvin	K
Frequency	ν	hertz	Hz $[s^{-1}]$
Force	F	newton	N $[kg \cdot m \cdot s^{-2}]$
Stress:			
Tensile	σ	pascal	Pa $[N \cdot m^{-2}]$
Shear	τ	pounds per square inch	lb/in^2 or psi
Energy, work, quantity of heat		joule	J $[N \cdot m]$
Power		watt	W $[J \cdot s^{-1}]$
Current flow	i	ampere	A
Electric charge	q	coulomb	C $[A \cdot s]$
Potential difference, electromotive force	V, E	volt	V
Electric resistance	R	ohm	Ω $[V \cdot A^{-1}]$
Magnetic induction	B	tesla	T $[V \cdot s \cdot m^{-2}]$

1032

APPENDIX IV Selected Physical Quantities and Their Units

Greek Alphabet

Name	Lowercase	Capital	Name	Lowercase	Capital
Alpha	α	A	Nu	ν	N
Beta	β	B	Xi	ξ	Ξ
Gamma	γ	Γ	Omicron	o	O
Delta	δ	Δ	Pi	π	Π
Epsilon	ϵ	E	Rho	ρ	P
Zeta	ζ	Z	Sigma	σ	Σ
Eta	η	H	Tau	τ	T
Theta	θ	Θ	Upsilon	υ	Y
Iota	ι	I	Phi	ϕ	Φ
Kappa	κ	K	Chi	χ	X
Lambda	λ	Λ	Psi	ψ	Ψ
Mu	μ	M	Omega	ω	Ω

SI Unit Prefixes

Multiple	Prefix	Symbol
10^{-12}	pico	p
10^{-9}	nano	n
10^{-6}	micro	μ
10^{-3}	milli	m
10^{-2}	centi	c
10^{-1}	deci	d
10^{1}	deca	da
10^{2}	hecto	h
10^{3}	kilo	k
10^{6}	mega	M
10^{9}	giga	G
10^{12}	tera	T

Example: 1 kilometer = 1 km = 10^3 meters.

Unit Abbreviations

A	ampere
C	Coulomb
°C	degrees Celsius
cm	centimeter
eV	electronic volts
°F	degrees Fahrenheit
ft	foot
g	gram
GPa	gigapascal
in	inch
J	Joule
K	degrees Kelvin
kcal	kilocalorie
kg	kilogram
kJ	kilojoule
ksi	thousands of pounds per square inch
lb	pound
m	meter
min	minute
mm	millimeter
mol	mole
N	Newton
nm	nanometer
MPa	megapascal
P	poise
Pa	Pascal
psi	pounds per square inch
s	second
u	atomic mass unit
V	electronic volts

Periodic Table of the Elements

MAIN–GROUP ELEMENTS

MAIN–GROUP ELEMENTS

Legend:
- ☐ Metals (main-group)
- ■ Metals (transition)
- ▨ Metals (inner transition)
- ▨ Metalloids
- ☐ Nonmetals

TRANSITION ELEMENTS

Period	IA (1)	IIA (2)	IIIB (3)	IVB (4)	VB (5)	VIB (6)	VIIB (7)	VIIIB (8)	VIIIB (9)	VIIIB (10)	IB (11)	IIB (12)	IIIA (13)	IVA (14)	VA (15)	VIA (16)	VIIA (17)	VIIIA (18)
1	1 H 1.008																	2 He 4.003
2	3 Li 6.941	4 Be 9.012											5 B 10.81	6 C 12.01	7 N 14.01	8 O 16.00	9 F 19.00	10 Ne 20.18
3	11 Na 22.99	12 Mg 24.31											13 Al 26.98	14 Si 28.09	15 P 30.97	16 S 32.07	17 Cl 35.45	18 Ar 39.95
4	19 K 39.10	20 Ca 40.08											31 Ga 69.72	32 Ge 72.61	33 As 74.92	34 Se 78.96	35 Br 79.90	36 Kr 83.80
5	37 Rb 85.47	38 Sr 87.62											49 In 114.8	50 Sn 118.7	51 Sb 121.8	52 Te 127.6	53 I 126.9	54 Xe 131.3
6	55 Cs 132.9	56 Ba 137.3											81 Tl 204.4	82 Pb 207.2	83 Bi 209.0	84 Po (209)	85 At (210)	86 Rn (222)
7	87 Fr (223)	88 Ra (226)											113	114 Uuq (285)	115	116 Uuh (289)	117	118 Uuo

INNER TRANSITION ELEMENTS

6	Lanthanides															
7	Actinides															

Source: Davis, M., and Davis, R., *Fundamentals of Chemical Reaction Engineering*, McGraw-Hill, 2003.

Constants

Constant	Symbol	Value
Avogadro's number	N_0	6.023×10^{23} mol^{-1}
Atomic mass unit	u	1.661×10^{-24} g
Electron mass	m_e	9.110×10^{-28} g
Electronic charge (magnitude)	e	1.602×10^{-19} C
Planck's constant	h	6.626×10^{-34} J $\cdot$ s
Velocity of light	c	2.998×10^8 m/s
Gas constant	R	1.987 cal/(mol $\cdot$ K); 8.314 J/(mol $\cdot$ K)
Boltzmann's constant	k	8.620×10^{-5} eV/K
Permittivity constant	ϵ_0	8.854×10^{-12} C^2/(N $\cdot$ m^2)
Permeability constant	μ_0	$4\pi \times 10^{-7}$ T $\cdot$ m/A
Bohr magneton	μ_B	9.274×10^{-24} A $\cdot$ m^2
Faraday	F	9.6485×10^4 C/mol
Gravitational acceleration	g	9.806 m/s
Density of water		1 g/cm^3 = 1 Mg/m^3

Conversion Factors

Length:	1 in = 2.54 cm = 25.4 mm
	1 m = 39.37 in
	1 Å = 10^{-10} m
Mass:	1 lbm (pound-mass) = 453.6 g = 0.4536 kg
	1 kg = 2.204 lbm
Force:	1 N = 0.2248 lbf (pound-force)
	1 lbf = 4.44 N
Stress:	1 Pa = 1 N/m^2
	1 Pa = 0.145×10^{-3} lbf/in^2
	1 lbf/in^2 = 6.89×10^3 Pa
Energy:	1 J = 1 N $\cdot$ m
	1 cal = 4.18 J
	1 eV = 1.60×10^{-19} J
Power:	1 W = 1 J/s
Temperature:	°C = K $-$ 273
	K = °C + 273
	°C = (°F $-$ 32)/1.8
Current:	1 A = 1 C/s
Density:	1 g/cm^3 = 62.4 lbm/ft^3

$\ln x = 2.303 \log_{10} x$